SYNTHETIC CONTROL OF ORDER IN SOLUBLE DIOXYTHIOPHENE POLYMERS

By

CHRISTOPHE R. G. GRENIER

A DISSERTATION PRESENTED TO THE GRADUATE SCHOOL
OF THE UNIVERSITY OF FLORIDA IN PARTIAL FULFILLMENT
OF THE REQUIREMENTS FOR THE DEGREE OF
DOCTOR OF PHILOSOPHY

UNIVERSITY OF FLORIDA

2006

To my family,

ACKNOWLEDGMENTS

I would like to first thank my advisor for his continuous guidance throughout the five years, and a little extra of my Ph.D. studies in Florida. I believe this is a highly challenging time for a young inexperienced researcher growing into a responsible scientific leader, and that appropriate advice is the catalyst of this intellectual growth. In this regard, Prof. John R. Reynolds has always provided the right balance of encouragement, objective criticism, and patience. His insight and advice greatly helped me perform the work discussed in this dissertation. I learned a lot from him. I extend these thanks to my supervisory committee for their support and invaluable discussions: Prof. William R. Dolbier, Prof. Anthony B. Brennan, Prof. Lisa McElwee-White and Prof. Randy S. Duran.

I also owe thanks to Subi George and Prof. “Bert” Meijer whom I was lucky to meet and collaborate with and who have offered me twice their generous hospitality at the Technical University of Eindhoven, The Netherlands. In addition, I am thankful to Dr. Wojciech Pisula, Nok Tsao and Prof. Klaus Müllen from the Max-Planck Institute for Polymer Science in Mainz, Germany, with whom I also had a very productive collaboration and exciting scientific discussions.

I wish to thank my best friends in Gainesville for their unwavering friendship thoughout these five years. Without their support, I would have never made it through these five years: Daniel Serra, Magdalena Swiderska, Emine Boz, Dalia Lopez Colon, Dalianis, Guillermo Mathias, Avni Argun and Pierre-Henry Aubert. I am indebted to

them forever, and I hope to repay them some day, provided I learn how to cook or make better coffee.

I have to thank those friends that have joined me numerous times for coffee break, exercise, lunches and dinner: Ali Cirpan, Ece Unur, Thomas Joncheray, Rachid Matmour, Emilie Galand, Geoffroy and Delphine Sommen, Aleksa Jovanovic, Prof. Pierre Audebert, Dr. Mohammed Bouguettaya and Benoit Lauly.

I would like to also thank people that have greatly helped me scientifically, helped improve my English writing proficiency and with whom I always had interesting conversations: Genay Jones (I will always remember a 3am drive to Waffle House), Aubrey Dyer, Benjamin Reeves (a great mentor to me and a very wise man), Barry Thompson (who has set an unreachable standard for hard-work and scientific excellence), and Nisha Ananthakrishnan, Jeremiah Mwaura, Robert Brookins and Tim Steckler. In addition, special thanks go to Lorraine Williams, Sara Klossner, Tasha Simmons and Gena Borrero for doing all the "little things" without which I could not have had anything done.

I also thank my family, especially my parents, for supporting me during this long time so far away from their home. I know it was a difficult and painful sacrifice for them.

Finally, I want to offer special thoughts to two of my greatest friends departed during the course of my Ph.D. studies: Jean-Baptiste Andrault and Landry Bourely. I miss them both dearly.

TABLE OF CONTENTS

page

LIST OF TABLES

LIST OF FIGURES

Abstract of Dissertation Presented to the Graduate School
of the University of Florida in Partial Fulfillment of the
Requirements for the Degree of Doctor of Philosophy

SYNTHETIC CONTROL OF ORDER IN DIOXYTHIOPHENE POLYMERS

By

Christophe R. G. Grenier

December 2006

Chair: John R. Reynolds
Major Department: Chemistry

The synthesis of electron-rich, highly soluble and processable conjugated poly(3,4-propylenedioxythiophenes) (PProDOTs) is developed. The polymers are substituted with side chains carefully chosen to obtain high solubility while controlling the polymers' physical, optical and electronic properties necessary for the targeted applications. The polymers have been applied to device platforms that probe electrochromism, light-emission and charge-carrier mobilities.

A synthetic methodology to prepare disubstituted poly(3,4-propylenedioxythiophenes) having branched alkyl and alkoxymethyl substituents for electrochromic applications is described . The branched polymers display significantly higher solubility than their linear analogs and are easily processed by spin-coating or spray-casting. The polymers have high electrochromic contrasts, subsecond switching times, and high coloration efficiencies, allowing them to be successfully applied to the construction of highly efficient and fast switching electrochromic devices.

Using enantiomerically pure reagents, chiral alkyl and alkoxymethyl PProDOTs were synthesized. Since few enantiomerically pure reagents are commercially available, an easy, efficient and versatile synthesis was developed to yield new, original chiral polymers. Introduction of side chain chirality allows control of the ordering of the polymer chains, with formation of cholesteric aggregates in poor solvents and the solid state. Solvatochromism and thermochromism experiments coupled with circular dichroism (CD), along with fluorescence and absorption spectroscopy, yield important information on the morphology and self-assembly of the polymer chains from solution to the solid state.

The first synthesis of soluble poly(3,4-phenylenedioxythiophenes) (PPheDOTs) is described. Solubility was induced by introducing substituents at the 4 and 5 positions of the veratrole moiety. Monosubstituted PPheDOTs were found to be poorly soluble, but could be obtained by electrodeposition. On the other hand, disubstituted PPheDOT polymers are soluble. Symmetrically dodecyl substituted PPheDOT$(C_{12})_2$, soluble above 80°C in aromatic and chlorinated solvents, shows a high degree of order in the solid state and is a promising candidate for high mobility and high conductivity applications. Asymmetric, disordered PPheDOT(C_{12})EtHx is soluble at room temperature in most organic solvents. The polymer shows solid state fluorescence and is a promising candidate for light-emitting applications.

CHAPTER 1
INTRODUCTION

1.1. Introduction to Conjugated Polymers

Following the exciting discovery in 1977 of high conductivity in chemically doped polyacetylene, the conjugated polymers (CP) research field has developed exponentially (Figure 1.1). As a result, many other CPs with diverse chemical structures have been investigated. Their exceptional physical, electronic and optical properties have been well characterized and a deep understanding of their incredible properties is now available. In 2000, the importance of the discovery and development of conducting polymers was recognized when the Chemistry Nobel Prize was awarded to Alan Heeger, Hideki Shirakawa and Alan MacDiarmid.

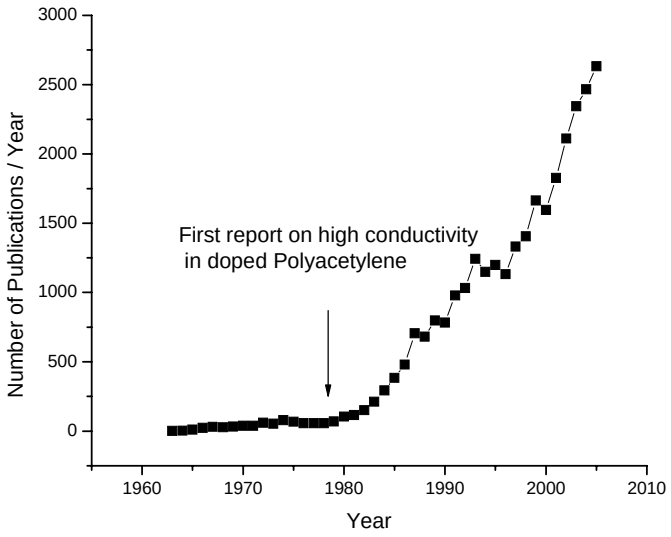

Figure 1-1. Evolution of published work on conducting polymers

As Heeger described, conjugated polymers (often called conducting polymers) "offer a unique combination of properties not available from any other materials."[1] Of special interest is the ability to finely tune their properties through synthetic changes, both at the monomer and polymer level. This enables the use of conducting polymers in many applications such as photovoltaic devices (PVs), electrochromic devices (ECDs), organic field-effect transistors (OFETs), and light-emitting diodes (LEDs). Their performance has improved dramatically leading to their increasing use in commercial applications.

1.2. Electronic Properties of Conjugated Polymers

On a basic level, conjugated polymers are a continuous array of overlapping π-orbitals supported by σ-bond backbone. As long as this array is present, many different backbones can be used. Examples of commonly used π-conjugated polymer structures are given in Figure 1-2.

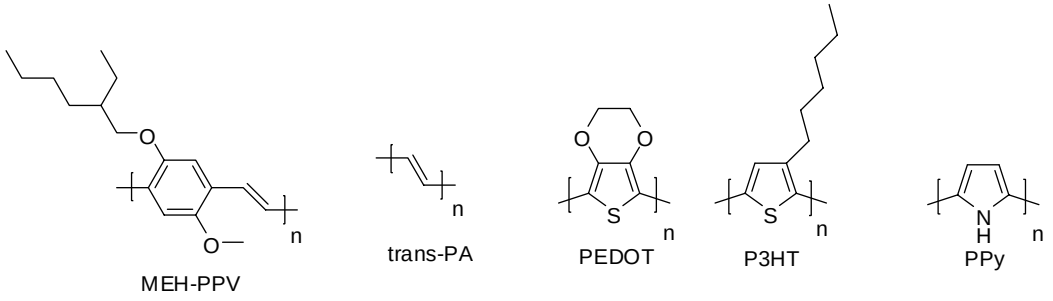

Figure 1-2. Representative structures of conducting polymers. The polymers represented are some of the most used and best performing materials.

To understand the properties of conducting polymers, I will describe polyacetylene. Going from ethylene to 1,3-butadiene, the overall energy of the molecule is stabilized by overlap between the two double bonds. The HOMO is raised, and the LUMO is lowered leading to a smaller HOMO-LUMO gap. By increasing the number of overlapping double bonds, the number of energy levels (occupied and unoccupied) increases, and the

HOMO-LUMO gap is compressed further. As the degree of conjugation grows large, the multiple electronic states are better described by continuous bands. This simple approach can be applied to most conjugated polymers. Complete theoretical calculations giving more precise results have been performed for many conjugated polymers.[2]

Theoretically, if the number of overlapping orbitals becomes infinite, then the band gap is expected to disappear. However, this is not observed due to Peierls distortion. Peierls distortion arises from the interaction between electronic and vibrational states, not taken into account in Hückel theory. This interaction induces the formation of alternating long and short bonds with single and double bond character, and the creation of a band gap.[3] Many other interactions participate in determining the bandgap in conjugated polymers, and will be discussed later. By analogy to inorganic materials, conjugated polymers with typical bandgaps between 1 and 3 eV are semiconducting materials with a conduction band and a valence band.

Poly(acetylene) is a well understood polymer with a degenerate ground state.[4] Two resonance forms of equal energy exist differing only by the order of the single and double bonds (Figure 1-3A).[5] One can switch between phase A and phase B by introducing a radical defect within the chains (Figure 1-3B).This radical defect, called a soliton, is localized over several carbons and has an energy level at mid-gap, occupied by one electron. The electron in the intragap state can be removed to create a positively charged soliton (p-doping), or another electron can be added to create a negatively charged soliton (n-doping) (Figure 1-3C).

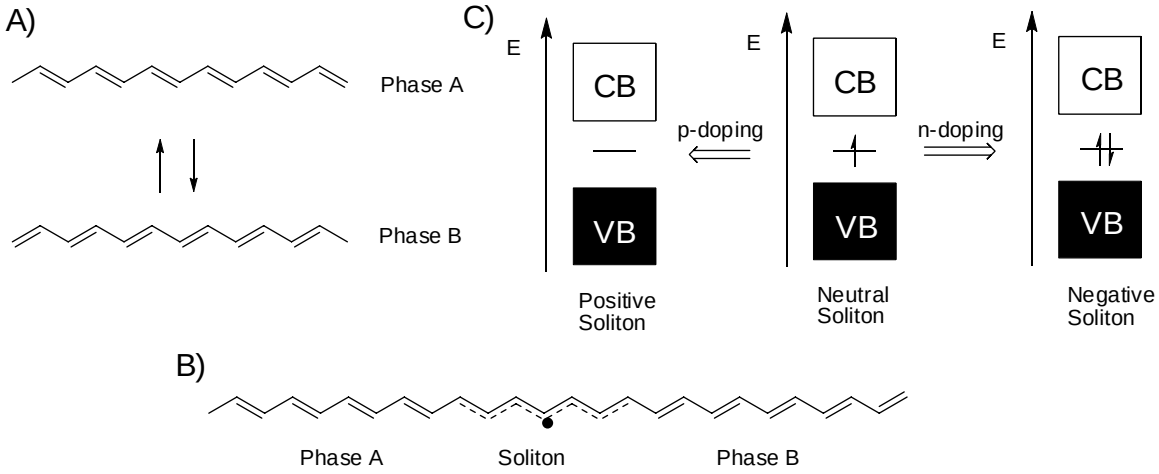

Figure 1-3. Doping in poly(acetylene). (A) The two degenerate forms of poly(acetylene); (B) Self-localized neutral soliton defect in poly(acetylene); (C) p-doping and n-doping in poly(acetylene).

For polymers with a non-degenerate ground state, the picture is slightly different. Two resonance forms exist as in polyacetylene, but with different energies: the most stable is the benzenoid form and the less stable is the quinoid form, (Figure 1-4). Upon doping, either a radical-cation pair, or a radical-anion pair is created. These defects are called polarons and are responsible for conductivity observed at low doping levels. Upon further doping, a second electron can be removed, and a dicationic species is formed, called a bipolaron. At high doping levels, bipolarons are the charge carriers responsible for conductivity. At a hypothetical doping level of 100% (one dopant ion per repeat unit), Bredas et al. have calculated that the intragap states merge with the valence or conduction band giving metallic behavior.[6]

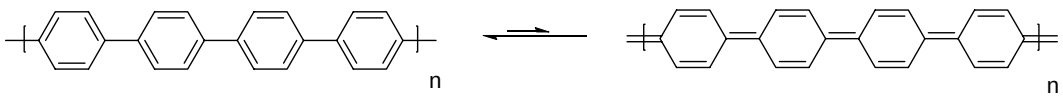

Figure 1-4. The two non-degenerate forms of poly(p-phenylene): aromatic, left and quinoidal, right.

Polarons and bipolarons have specific optical signature. Polaron charge carriers have two characteristic absorptions in the near-IR region, as shown in Figure 1-5 for poly(3,4-(2,2-dimethylpropylene)dioxythiophene) (PProDOT-Me_2), a p-dopable polymer.[7] The first transition corresponds to the transition from the top of the valence band to the single occupied lower intragap state. The second transition is the near-IR transition from the lower intragap state to the higher intragap state. When the chains are oxidized to the bipolaron state, the lower energy intragap state is depleted of its electron, and only the first transition is seen. For degenerate ground state poly(acetylene), only one transition with an onset near half the energy of the bandgap is seen due to solitons, not polarons charge carriers.

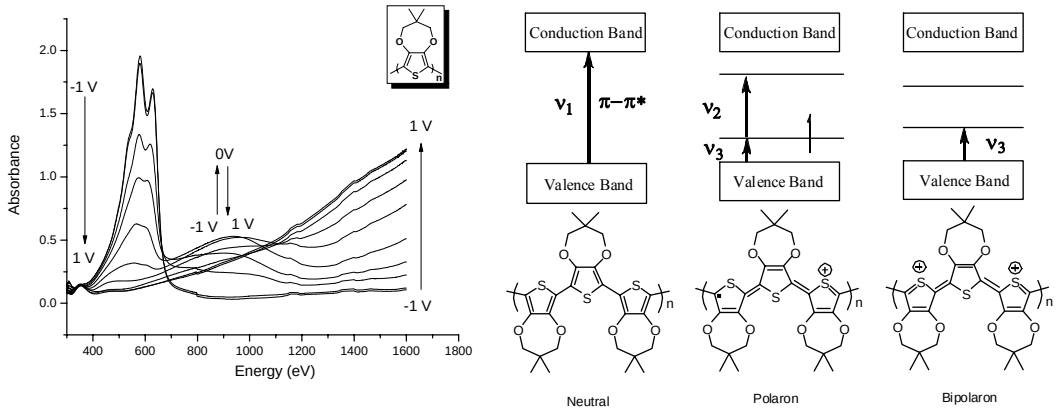

Figure 1-5. Spectroelectrochemistry of PProDOT-Me_2 as a function of applied potential between –1 V and 1V vs. Ag wire in 0.1 M TBAP/ACN. Energy levels, electronic transitions for the neutral and organic structures of polaron, and bipolaron forms of PProDOT-Me_2 with the organic structures are also depicted.

1.3. Doping-induced Properties of Conjugated Polymers

The conjugated polymers can be used in many applications. These applications depend on the mechanism by which the doping is achieved. In this section, I will describe

the different doping mechanisms and introduce applications derived from them. I will not describe the applications in detail but only their working principle.

1.3.1. Chemical Doping

Conjugated polymers can be doped by electron transfer to or from chemical species. Some examples are I_2, and $NOPF_6$ (p-doping), along with Na-naphthalide, and Li (n-doping). Figure 1-6 shows the reversible oxidation of polythiophene by iodine, as well as the irreversible oxidation by $NOPF_6$. In this case, doping charges are compensated by species derived from the oxidizing/reducing agent.

$$(T)_n + 3/2\ ny\ I_2 \longrightarrow [(T)^{+y}(I_3^-)_y]_n$$

$$2(T)_n + 2\ ny\ NOPF_6 \longrightarrow [(T)^{+y}(PF_6^-)_y]_n + nyN_2O_2$$

Figure 1-6. Chemical p-doping by iodine (reversible) and nitrosonium hexafluorophosphate (irreversible) in the case of polythiophene; n refers to the number of repeat units.

Upon careful choice of the dopant ion, high conductivity can be achieved leading to applications of conjugated polymers as anti-static coatings, hole-injecting layers, hole-transport layers and conductive fibers. Because charges with corresponding counterions are introduced during doping, solubility and processability in polar solvent can be obtained. For example, poly(3,4-ethylenedioxythiophene) (PEDOT) doped with bulky poly(styrenesulfonate) (PEDOT:PSS) forms aqueous dispersions in water which can be processed into highly conductive films.[8]

1.3.2. Electrochemical Doping

If a conducting polymer is deposited onto an electrode, and a potential is applied to the electrode, electrons can be added or removed depending on the magnitude of the

potential applied. The polymer is then positively or negatively charged. These charges are compensated by counterions (dopant ions) diffusing into the polymer from the electrolyte solution. If the doped and neutral states are stable, then the electrochemical doping/dedoping is reversible and the polymers are *electroactive*. For many conjugated polymers, the electrochemical oxidation/reduction processes cause a change of optical absorption and, if the changes occur in the visible range, a change of color. This phenomenon is called *electrochromism*. This property can be used in applications such as electrochromic devices (ECDs), "smart" windows, and absorptive/reflective devices.[9,10]

In the case of light-emitting electrochemical cells (LEC), a blend of an emitting conjugated polymer with an ion-transport polymer and an electrolyte salt (for example, MEH-PPV, PEO and lithium trifluoromethanesulfonate) is sandwiched between two metal electrodes (Figure 1-7).[11]

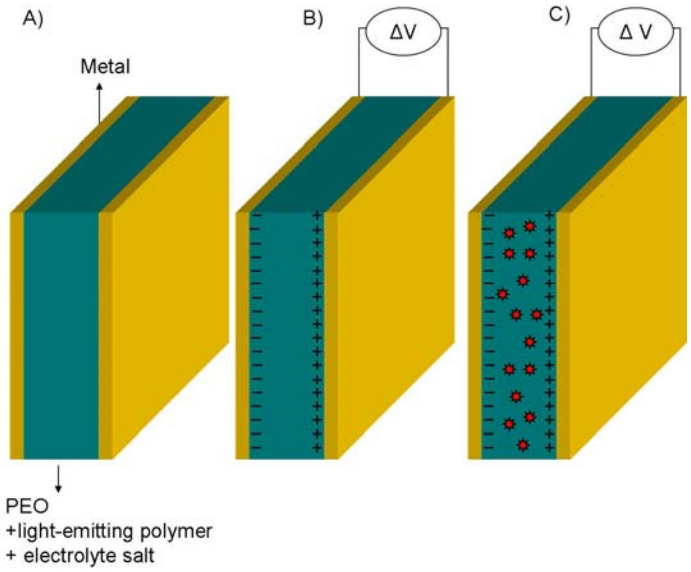

Figure 1-7. Schematic representation of a LEC device. A) LEC device with no voltage applied; B) LEC device shortly after application of a voltage bias showing electrochemical doping at the interfaces; C) LEC device after diffusion of the charge carrier in the material bulk and recombination, leading to light-emission.

When a sufficient voltage is applied to the polymer, holes and electrons are injected at the cathode and anode creating p-type and n-type charge carriers, which are compensated by counterions from the solid electrolyte. A front of charge carriers moves from each electrode to the center under the influence of the electric field applied between the electrodes. Eventually, the hole and electron recombine, forming an excimer which relaxes to the ground state by emission of light (Figure 1-7C).

1.3.3. Fluorescence and Photochemical Charge Transfer

When light is absorbed by a conjugated polymer, an electron is promoted from the valence band to the conduction band. Normally, these excited states would recombine and return to the ground state yielding their excess energy by fluorescence, phosphorescence or non-radiative decay. Another process is energy transfer to an acceptor. If an electric field is applied, or if an electron-accepting or electron-donating species (with appropriate HOMO and LUMO levels) is nearby, then charge separation of the two charge carriers may also occur. This is the general idea behind photovoltaic devices, where the sunlight energy is collected and converted into electrical power. A complete literature review on photovoltaics was recently written in the Reynolds group.[27c]

1.3.4. Interfacial Doping

Interfacial doping is similar to electrochemical charge injection, but lacks charges compensation by electrolyte. This is seen in organic field-effect transistors. As shown in Figure 1-7, a typical OFET is made of two electrodes (source and drain) separated from a third electrode (the gate) by a semiconducting layer coated on dielectric material. When a voltage is applied at the gate, the dielectric material behaves like a capacitor and charges build at the gate electrode. Opposite charges build at the conjugated polymer/dielectric

material interface. Figure 1-8 shows the example of a p-dopable material. As p-doped sites appear, current flows from the source to the drain. As the gate voltage is increased, the current rises as the number of charge carriers increase.

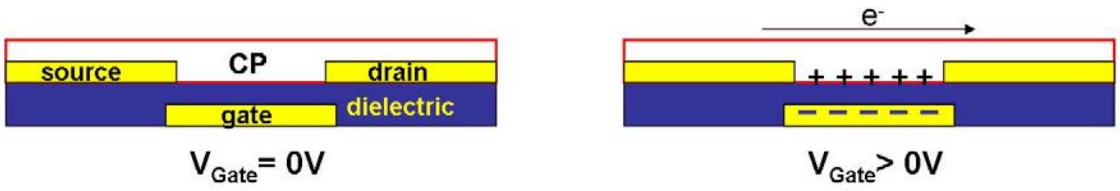

Figure 1-8. Schematic diagram of a thin film transistor. The semi-conducting material is a p-dopable material.

Since current is directly proportional to the charge mobility of the material, the thin film transistor configuration can be used to measure hole or electron mobilities. An important point is that other methods can be used to measure mobilities, yielding different values due to their different configurations.[12] These methods include hole-only devices or time-of-flight measurements. In hole-only devices, the p-dopable semi-conducting material is sandwiched between two electrodes. At the cathode, a low work function metal creates a large barrier for electron injection. The result is that the mobile charges circulating in the device are only holes, not electrons. Another essential difference is that the two electrode configurations probe the bulk material, whereas the gate-source-drain configuration probes only the mobility of a thin layer at the dielectric-semiconductor interface. Therefore, one must consider carefully how the mobilities were obtained when comparing mobility values.

In organic light-emitting diodes (OLEDs), electrons and holes are injected at electrodes interfaces into a conjugated polymer by applying a given voltage between two electrodes. Contrary to the LEC configuration, no electrolyte is present, and the

electrodes must match the HOMO and LUMO levels to allow easy charge injection. The remaining concepts are essentially identical.

1.4. Improving Active Material Performance

In this part, I will examine selected applications to see what properties are necessary to obtain high performance, focusing on the active materials. Still, device engineering plays a significant role in improving the efficiency of conjugated polymer devices. I will later discuss how synthetic changes in CPs can achieve these desired properties. Each application requires specific structural changes to obtain maximum performance. This is the advantage of CPs and their unique synthetic versatility.

1.4.1. OFETs

As described previously, the efficiency of organic field-effect transistors depends mainly on the charge mobility of the semiconducting material. In conjugated polymers, the charge mobility is limited by the ability of charge carriers to hop between neighboring localized states on polymer chains. With this, a high degree of interchain order is required in the polymer. As a result, conjugated polymers with a typically high amorphous content yield lower mobilities than small molecules. To obtain high mobility, polymers with a high degree of crystallinity and long range order must be synthesized. P3HT, a semi-crystalline polymer, has led to p-type mobilities up to 0.1-0.2 $cm^2 V^{-1} s^{-1}$.[13] The crystalline regions consist of lamellar organized interchain stacks, possessing a high degree of interchain interaction. For most ordered films, it is believed that there is two-dimensional interchain charge transport. More recent work on liquid crystalline polymer yield the highest mobility reported to date with a value of 0.7 $cm^2 V^{-1} s^{-1}$.[14]

To some extent, the mobility can be increased by careful deposition of the films. In P3HT, the polymer can be processed easily from solution. The conditions of processing

(solvent, temperature, concentration, etc.) can be tuned to obtain the highest amount of order within the polymer films.[15] But this method requires a soluble polymer. Most conjugated polymers, due to π-stacking interactions, are insoluble.

The mobility is also dependent on the molecular weight. Studies show that increased molecular weights lead to dramatically higher mobilities.[16,17] This can be explained by higher planarity of the polymer chains leading to increased interchain order and the ability of charge carriers to travel further along the chains before hopping to neighboring chains. [16] Other authors have argued that the improvement observed with increasing molecular weight is due to a difference in morphology. The higher molecular weight polymers form large interconnected domains while the lower molecular weight polymers forms small crystalline domains separated by the amorphous matrix.[17]

It was also shown that impurities or defects must be avoided. For example, partial doping, although it leads to higher mobilities, is detrimental to field-effect transistors as it yields poor "On-Off" ratios, meaning that even when no voltage is present at the gate the transistor still conducts current.

1.4.2. Photovoltaic Application

To be a commercially interesting alternative to inorganic materials, it is estimated that a power-conversion efficiency of at least 10% is required for photovoltaic devices.[18] Much work has already been performed in the last few years towards this objective. Power-conversion efficiencies up to 3-5% have now been obtained.[19] However, it is clear that new concepts and new materials are needed to improve this value even further.

Several factors can be tuned synthetically to increase photovoltaic power-conversion efficiency. 1) The absorption of photons can be improved. The polymers used so far have too high bandgap and most of the solar energy is not absorbed. Therefore, a

low band-gap polymer able to absorb the intense NIR emission (700 nm, 1.4 eV) of the sun must be synthesized. Blends of conjugated polymers can also be used to broaden the absorption profile of the devices.[20] 2) Increase the interfacial surface area. This has already been accomplished by replacing the bilayer device configuration with a bicontinuous bulk heterogenous junction configuration in donor-acceptor photovoltaic devices. In bulk heterojunction devices, both donor and acceptor are intimately mixed, resulting in a significant improvement of the efficiency.[21] Further improvement can be obtained by decreasing the domain size in the blend layers. However, the domain size must be large enough so that recombination is prevented and the charges are carried efficiently to the electrodes. It is estimated that an exciton can travel an average of 10 nm before returning to the ground state implying an optimum distance of 20 nm for the size of the layers, so that the acceptor is within reach of all excitons generated in the donor materials. This morphology control can possibly be obtained in block copolymers. By maintaining a low polydispersity, controlling the nature and size of the blocks, precise control of the morphology is achieved. 3) Control of the active materials' HOMO and LUMO levels is essential. As fullerene and its derivatives have proven to be the best acceptors, I will look only at the donor HOMO and LUMO levels. Control of the LUMO level plays a decisive role in the charge separation process. It is estimated that the value of the donor HOMO must be at least 0.3 eV above the LUMO of the fullerene LUMO level to enable efficient charge separation by overcoming the exciton binding energy.[22] The HOMO of the donor is important too, as it is believed to control the open-circuit voltage and the power-conversion efficiency.[18] 4) In addition, the materials used in photovoltaic devices must have high mobility values. High electron and hole mobilities

will afford fast transport of charges to the electrodes and avoid recombination. Low mobility of either holes or electrons will result in an increase of the series resistance, decreasing the current generated by the device.[19] Therefore, a material having significant interchain interactions and some crystallinity should improve the charge transport in the photovoltaic cells.

1.4.3. Polymer Electroluminescent Diodes (PLEDs)

Essential to PLEDs is to control the bandgap. By modifying the bandgap, albeit is possible to change the color emitted by the polymer. Obtaining blue, red and green emitting polymers opens the way for full-color display applications. In Figure 1-9, several conjugated polymer along with their emitted colors are introduced. These materials afford access to every color required for display applications.

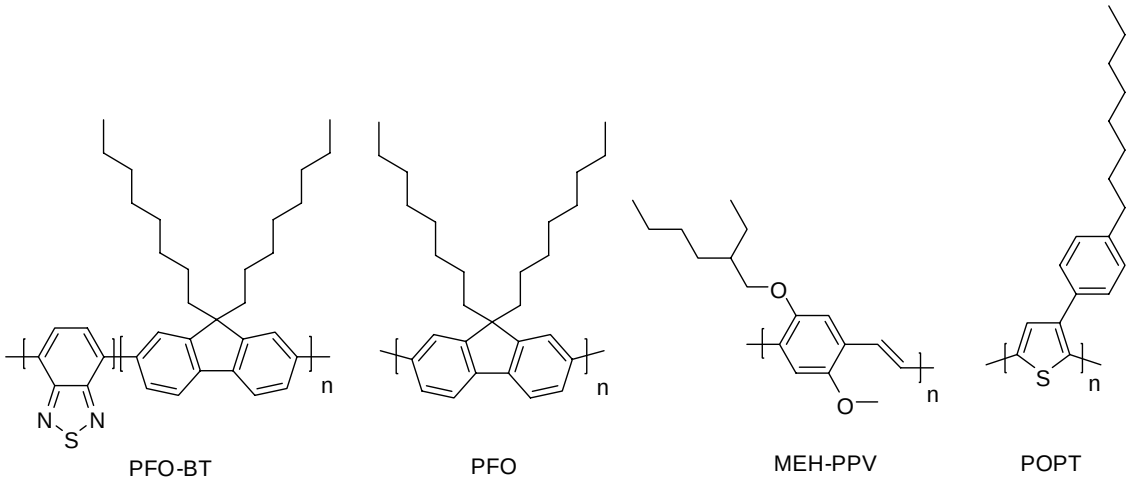

Figure 1-9. Representative luminescence colors of some conjugated polymers.

Netherveless, if any colors can be obtained, the efficiency of the light-emission process and the brightness are not satisfying. Part of the limited efficiency comes from a theoretical limit inherent to the electroluminescence process in conjugated polymers. In PLEDs, electrons and holes are injected at both electrodes. When an electron-hole pair is

formed, simple spin-statistics predicts that 25% of the excited states are singlet states, and 75% are triplet states. It is believed that 25% percent is the theoretical maximum efficiency achievable in polymer light-emitting diodes. However, more recent theoretical studies have since suggested that this might not apply to all polymers.[22]

To estimate the efficiency of the emission once a singlet excited state is formed, it is necessary to look at the photoluminescence quantum efficiency. Film photoluminescence quantum yield, the ratio of the amount of emitted photons to the absorbed photons, gives us a good gauge of whether a polymer is a good candidate for OLED applications. The quantum yield is highly dependent on the extent of interchain interactions. After recombination the presence of π-stacking interactions in conjugated polymers leads to efficient interchain energy transfer to non-emissive, low energy traps. The excitation energy is thus lost through non-radiative decay. In highly ordered materials, although the *solution* quantum yields are often very high, the *film* quantum yields are very low. To obtain higher quantum yield values, interchain interactions must be prevented. Poly(2- methoxy-5-(2-ethylhexyl)oxy-paraphenylenevinylene) (MEH-PPV), shown in Figure 1-9 is one of the most efficient polymers reported to date in PLEDs. It displays high quantum yield in the solid-state due to several factors: 1) presence of bulky and flexible 2-ethylhexyloxy side chains, 2) main chain disorder due to the presence of both syn and trans substituted double bonds, 3) interchain disorder induced by the asymmetry of the monomer with methyloxy and ethylhexyloxy side chains, and 4) presence of tetrahedral defects due to incomplete conversion from the saturated precursor to the unsaturated polymer.

Low mobilities are an advantage as charges spend more time within the active layer and chances of recombination increase. But the mobilities of electrons and holes also need to be balanced so that recombination occurs within the active materials, not at the electrode interface. This is difficult as there are few polymers having similar electron and hole mobilities. Introducing additional layers at the electrodes to transport or block charges solves the problem. Solubility of the polymers is of course required for inexpensive, easy processing of the polymers.

1.4.4. Electrochromic Devices

As mentioned before, the redox process in electrochemical devices is very different as counterions balance the doped states. This implies that for efficient switching of an electrochromic device, the dopant ion must be able to penetrate the polymer film efficiently and the electrons must be able to move from the electrode inside the polymer films.[23] Highly ordered polymers dope slowly since they possess crystalline regions, where the dopant ions cannot penetrate easily. Amorphous materials are therefore excellent candidates for these applications. However, some interchain interactions are necessary for electron transport between the electrode and the polymer bulk. PEDOT, used in electrochromic windows, switches from a dark blue absorptive color to a highly transmissive sky blue color with a switching speed of ~2s. This is much shorter than most inorganic electrochromic materials. Increasing amorphous domains and decreasing interchain interactions is expected to improve switching speeds. This should increase the doping level resulting in better contrast between neutral and doped state.[24]

Moreover, the control of both the neutral and oxidized state colors must be obtained. By tuning the bandgap, a variety of colors are now available.[25] Large bandgap polymers, with absorptions in the UV region of the electromagnetic spectrum, are clear in

the neutral state but colored in the doped state, as polaron and bipolaron intragap optical transitions are shifted to lower energies in the visible spectrum range. Polymers with absorptions in the visible region will display a bathochromic shift in the doped state and can be colorless. This is the case for PProDOT-Me_2 and PEDOT, which absorb in the red and have a dark blue color in the neutral state. When doped, the polymers absorb in the infra-red and are mostly transparent.

Polymer solubility is also essential for inexpensive processing, as electrochemical polymerization is problematic when considering large area applications.

1.5. Synthetic Control in Conjugated Polymers

This section will highlight how synthetic changes can affect the properties of conjugated polymers.

Discussing bandgap modification through synthetic changes, Roncali has shown that the bandgap is determined by the sum of several contributions: Peirls distortion (or bond-length alternation (BLA)), substituents effects, intrachain interactions, interchain interactions and resonance effects.[26] A donor-acceptor contribution can be added to provide a more complete description, as this effect does not obviously fit in the above. It must be noted that all contributions are connected and that tuning the individual contributions will result in changing the others.

All the parameters described above are not only defining the bandgap value, but also the properties of the conjugated polymers. In this section, only the substituents effects, and inter- and intrachain interactions will be detailed as they are most relevant to the work presented in this dissertation. More information on donor-acceptor systems can be found elsewhere.[27]

1.5.1. Substituent Effects

By introducing substituents on the conjugated polymer backbone, HOMO and LUMO levels can be controlled precisely. By attaching electron-donating or electron-withdrawing chains in direct conjugation with the conjugated backbone, the HOMO and LUMO will be increased and decreased, respectively. Poly(3,4-alkylenedioxythiophenes) (PXDOTs) are examples of a donor substituent effect. By introducing the oxygen at the 3- and 4- positions of the thiophene, π-donation of the lone pairs into the thiophene ring occurs. As a result, the HOMO level is raised (-4.1 eV for neutral PEDOT, -5.3eV for P3HT) and the bandgap is decreased (1.6 eV for PEDOT, 2.35eV for P3HT). PXDOTs are therefore much easier to oxidize than polythiophenes and a bathochromic shift is observed in their absorption spectrum (polymers are more blue). If electron-withdrawing species are introduced in conjugation with the conjugated backbone, the result is a lower LUMO level and a smaller bandgap. The oxygens have also an inductive electron-withdrawing effect but it is overwhelmed by the resonance donating effect. But if a methylene spacer is introduced between the backbone and the oxygen, then the resonance effect no longer occurs. The inductive effect is dominant and the oxidation potential is raised. Compared to poly(thiophenes), it was shown that poly(3-alkyloxymethylthiophenes) have 100mV higher oxidation potential, corresponding to 0.1 eV lower HOMO levels.[28]

1.5.2. Intrachain Interactions

When the backbone of a conducting polymer is twisted out of planarity, the π orbital overlap decreases, resulting in a decrease of the effective conjugation length.[29] The bandgap will be much higher in twisted polymers than in planar polymers. This leads to blue-shifted absorption and emission spectra.

Internal twisting has a dramatic effect on conductivity and charge transport in the solid state. With increased twisting, intrachain charge transport along polymer chains will decrease strongly. This results also in changes in interchain ordering which is highly dependent on the individual chains conformations. Normally, polymers chains with a strongly twisted backbone cannot order easily in the solid state. One exception is possible where the twisting is *regular* leading to a formation of a helical structure.[30]

Polyfluorenes and polycarbazoles are good examples of highly twisted materials. They are transparent in the neutral state, and emit blue light. Steric repulsions from neighboring hydrogens on adjacent aryl rings prevent a planar conformation. Since interchain ordering is strongly hindered, these two polymers are excellent candidates for light-emitting applications having high fluorescence quantum yield efficiencies.[31] In addition, these polymers are cathodically coloring polymers. When oxidized, they absorb in the visible range and are colored. When neutral, the polymers are highly transmissive, as they mostly absorb UV radiations. Drawbacks of these polymers include high turn-on voltages in PLEDs, high oxidation potential in electrolytes, and problems of degradation over time leading to color changes.

Another striking example of the importance of intrachain order is found in poly(3-alkylthiophenes). The monomer is not symmetric and can lead to Head-to-Tail (HT), Head-to-Head (HH) and Tail-to-Tail (TT) arrangements during polymerization (Figure 1-10A). When the polymer is obtained from electropolymerization (see chapter 2) or $FeCl_3$ mediated chemical polymerization, the polymer is regiorandom and contains significant amounts of HH and TT couplings. This creates steric interactions between every other thiophene unit, as shown in Figure 1-10B, forcing twisting of the conjugated backbone.

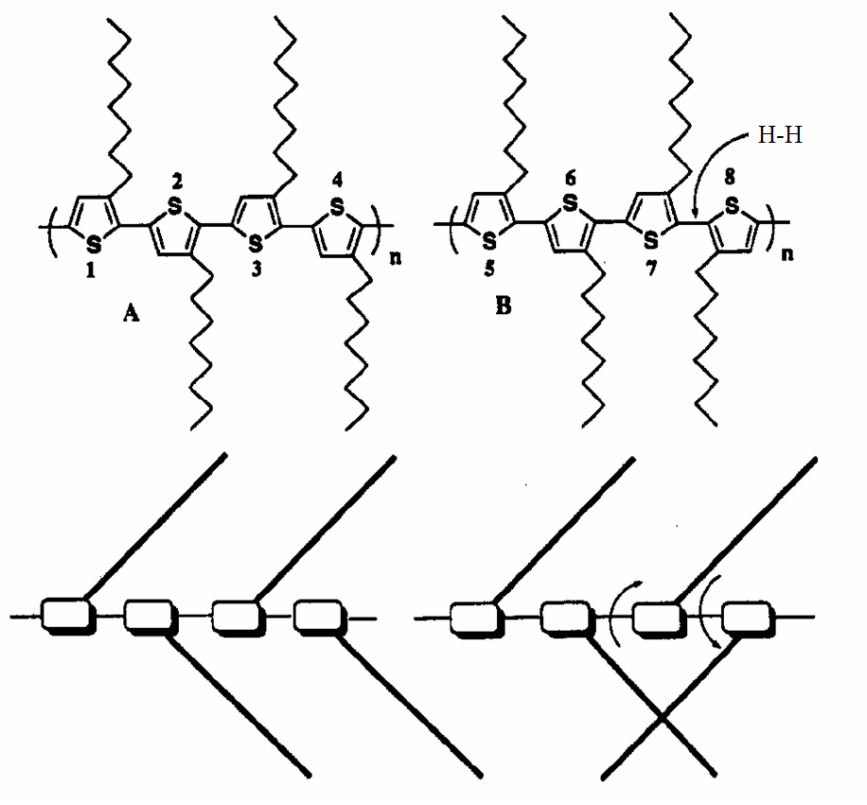

Figure 1-10. Effect of structural regularity on poly(3-octylthiophene) chain conformation. (A) Regioregular P3OT; (B) Regioirregular P3OT; twisting arises from steric interaction at the H-H site. Adapted from ref. 32.

This torsion results in low interchain interactions, low mobilities and low conductivities. On the other hand, if the polymer is obtained by Rieke polymerization or Grignard metathesis polymerization, then a high degree of regioregularity (HT >95%) is obtained.[32] These polymers can adopt a planar conformation with higher conjugation lengths. The planarity enables a high degree of interchain interactions in the solid state, leading to an increase of conductivity and mobility of several orders of magnitude.[33] In solution, the regioregular samples absorption displays a bathochromic shift (20-30 nm), indicating a more planar (rod-like) conformation and longer conjugation length.[34] This is much less than the shift observed in the solid state (140 nm), which implies that alkyl poly(thiophene) chains have a significant degree of conformational freedom in solution,

and therefore display smaller regioregularity dependence. Because of the increased planarity, P3ATs are strongly colored in the neutral states, with a bandgap around 2.3 eV. When oxidized, the absorption is shifted to longer wavelengths and the polymer is blue colored.

Intrachain twisting also leads to changes in emission colors. Figure 1-11 shows a series of different substituted polythiophenes with their emission colors.[39] Disubstitution of thiophene leads to a high degree of twisting arising from steric repulsions between side chains on adjacent thiophenes, and also steric interactions between side chains and the large sulfur atom. The polymers then have shorter conjugation lengths, and their emission shifts to higher energy (blue-shift) as the twisting increases.

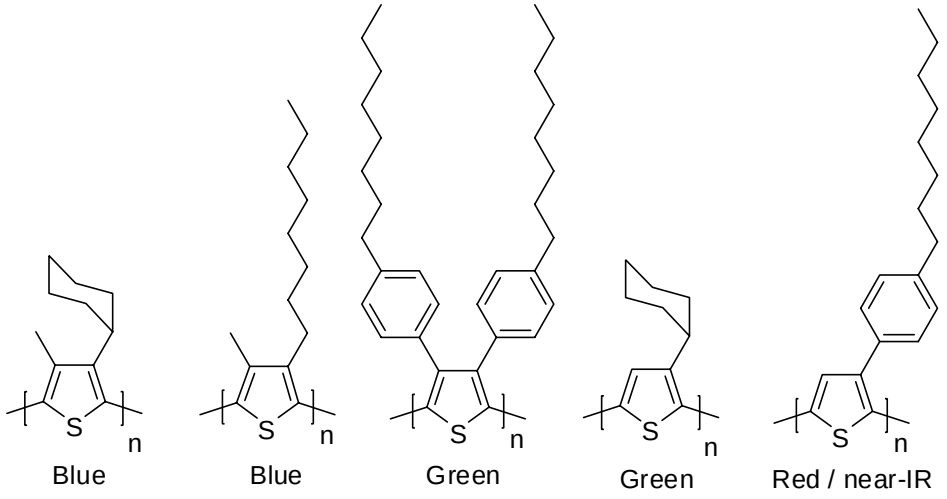

Figure 1-11. Color tuning of film luminescence though intrachain twisting. The driving force is steric repulsion between bulky groups.

1.5.3. Interchain Interactions

As seen above, intrachain planarity favors interchain interactions. Another important parameter is the regularity of the chains. In poly(*m*-phenylene) polymers, strong intermolecular order is observed despite that the chains having a helical, nonplanar backbone.[30] The same regularity in the side chains is needed to allow interchain order.

The density and the nature of side chains also play a role in the solid state ordering of the chains, as shown by Wegner et al. on substituted poly(*p*-phenyleneterephthalate) rigid-rod polymers.[35] When a high density of identical side chain is used, the polymer yields two-dimensional lamellar packing. When a spacer without side chains is used between terephthalic units bearing linear alkyl side chains, the side chains on neighboring lamellar stacks are interdigitated. With higher side chain density, interdigitation is not possible.

The packing described above is general to rigid-rod polymers and applies to most regioregular conjugated polymers. Winokur et al. demonstrated that poly(3-hexylthiophenes) form non-interdigitated stacks.[36] The side chains are essential to the solid state packing as in planar alkyl polythiophenes, side chains extend into the plane of the backbone, and do not present any hindrance to the chains stacking. Since the tendency of the side chains to crystallize increases with the number of carbons, more order is observed in poly(thiophenes) with longer side chains. This leads to significant improvements in conductivity.[33]

Introduction of bulky groups instead of linear considerably decrease the interchain interactions, as steric hindrance is introduced in the stacking direction. Poly(3-(2S-methylbutyl)thiophene) displays much lower mobility (10^{-3} $cm^2V^{-1}s^{-1}$), even though the branched group is small.[37] By introducing larger branching, interchain interactions can be decreased further. This has proved a very efficient method for the synthesis of highly luminescent polythiophenes.[39,71] The presence of the heavy sulfur atom helps inter-system crossing to the triplet state, resulting in limited solution fluorescence quantum yields (0.2-0.4).[38] A much bigger issue is that poly(thiophenes) have a high degree of interchain order in the solid state resulting in low film quantum yields. By introducing

steric bulk in the side chains, interchain interactions are strongly decreased and the photoluminescence quantum yield can be greatly improved (Figure 1-12).[39] Poly(3-(2,5-dioctylphenyl)thiophene), which has the phenyl ring perpendicular to the poly(thiophene) backbone, has a high film quantum yield of 0.24 (0.37 in $CHCl_3$).

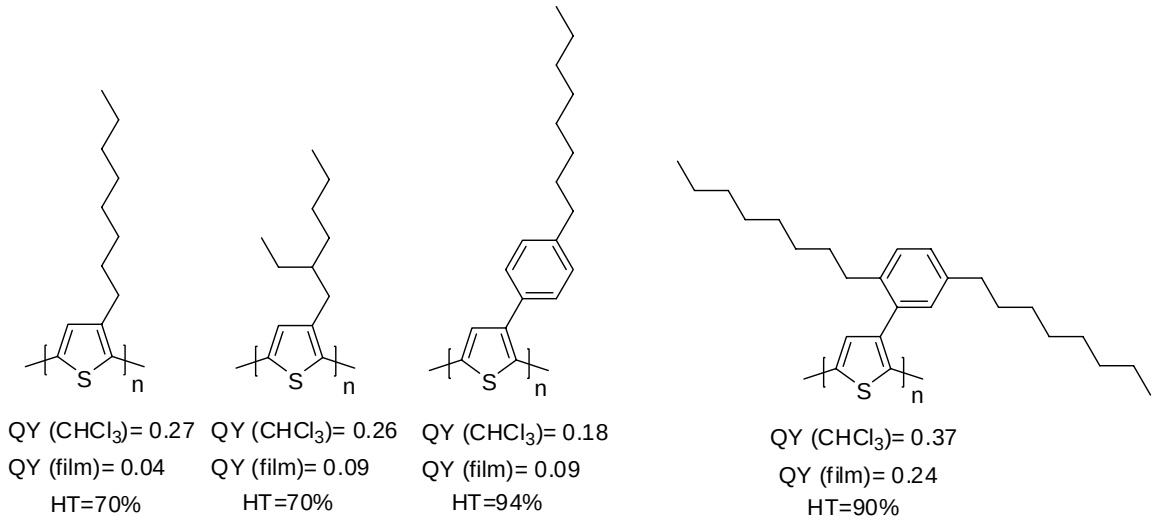

Figure 1-12. Fluorescence quantum yield dependence on substituents bulk. Both solution and film fluorescence quantum yield are provided. The regioregularity is provided as some polymers have limited HT content, which might result in higher film quantum yield. All polymers are red-emitters. Adapted from ref. 39.

Interchain interactions also have a strong effect on the bandgap and the absorption/emission properties of conjugated polymers. Strong π-stacking interactions lead to significant shifts of the bandgap. The shift depends heavily on the relative orientation of neighboring chains, as shown in Figure 1-13.[40,41] For H-aggregates, formed when two chromophores are in cofacial arrangement, the transition from the ground state to the lower level of the excited state is forbidden but the transition from the ground state to the upper level is allowed, leading to a blue-shifted absorption. For the same reason, the emission for such aggregates is expected to be strongly quenched. [42] For J-aggregates, formed when two chromophores are in a staggered ("brick-work") arrangement, there is a

bathochromic shift, as the transition from the ground state to the upper level of the dimer excited state is forbidden and the transition from the ground state to the lower level is allowed. In this type of aggregate, strong emission is seen.[43] A third type of aggregate, where each chromophores is tilted relative to its neighbors, leads to little or no shift of the absorption since both transitions to the excited state are allowed. Only if the Davydov splitting is large enough, it is possible to observe splitting in the absorbance spectrum.

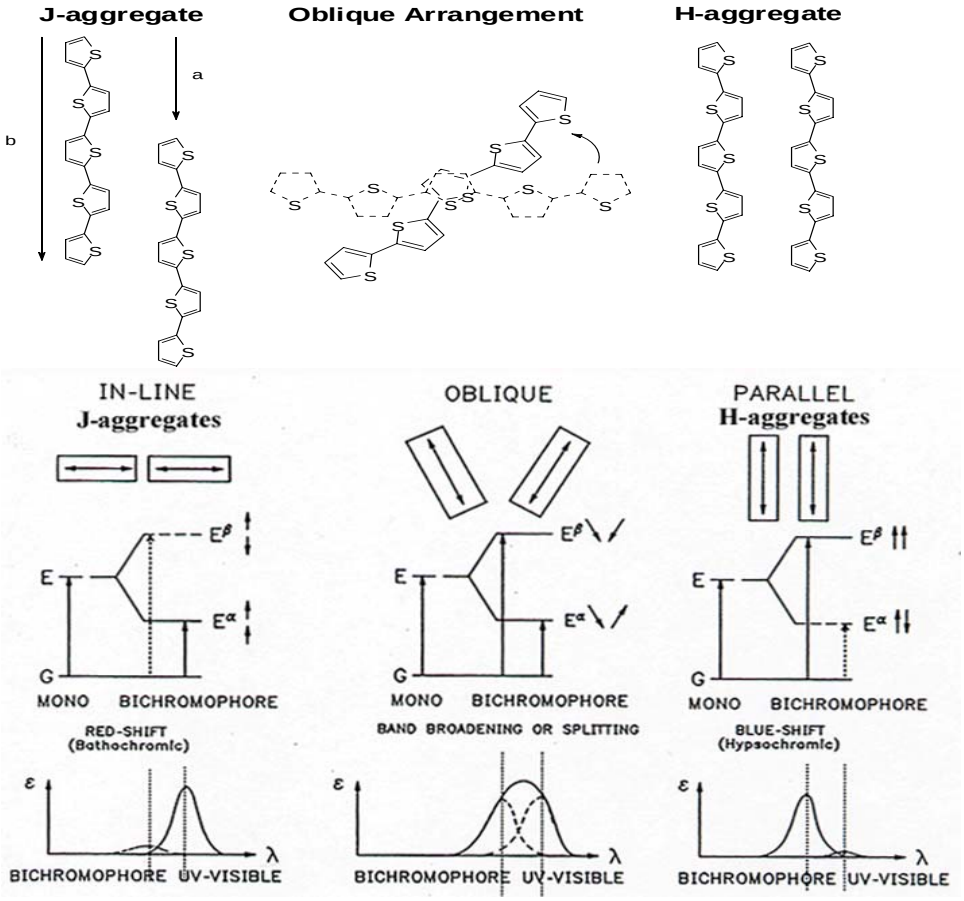

Figure 1-13. Davydov splitting in interchain aggregates. The resulting energy levels and absorption spectrum are also shown. Solid Lines: allowed transition; dashed lines: forbidden transitions. Adapted from reference 77.

Oblique chromophores arrangement has been reported by Swager et al.[44] Using a poly(phenylene ethynylene) (PPE) copolymer with alternated pentiptycene and chiral

dimethyloctyl side chains, they showed that the film fluorescence quantum yield is 0.65, one of the highest reported to date.

1.6. Towards Soluble Conjugated Polymers

Unsubstituted polythiophene, polypyrrole, polyphenylene and other CPs are insoluble, intractable and infusible. This makes them practically useless for most applications. On the other hand, soluble organic conjugated polymers can be spray-coated, spin-coated, or even printed. Obtaining solubility in conjugated polymers is, however, a difficult task due to their propensity to form interchain π-stacks. The individual π-π interactions are weak, but they add up to a strong interaction. To induce solubility, it is necessary to decrease interchain interactions, and to make the solvent-polymer interactions more favorable. Substituents increase the entropy of the polymer chains, and increase the solvent-polymer interactions. By selecting polar or ionic substituents (oligoethers chains, phosphate, carboxylate, sulfonate, ammonium, etc.), solubility in polar solvents (including water) can be achieved.[45] With nonpolar substituents (alkyl chains for example) solubility in organic solvents can be obtained. Bulky substituents create a larger increase in entropy, and prevent a close chain packing. But as discussed earlier, this will decrease mobility and conductivity of the materials. For applications where high mobility or conductivity is required, substitution with linear substituents is then a better approach. Another possibility is to introduce regioirregularity in the backbone or induce intrachain twisting but this often leads to decreased interchain interactions. It is therefore important to consider the application when choosing which method will be the most appropriate to obtain solubility.

Soluble polymers can be obtained through a wide variety of polymerization methods.[46] The most used is $FeCl_3$ polymerization. It directly uses the

electropolymerizable monomer and does not require further functionalization. The polymerization mechanism proceeds through formation of the radical cation of the monomer that propagates through coupling with other monomer units. The polymer is obtained in the oxidized state, and reduction of the polymer back to the neutral state as well as removal of the iron catalyst is difficult. Also, the high reactivity of the cation radical leads to numerous side reactions (in the case of alkyl poly(thiophene)s crosslinking through the 3 position of thiophene can occur), leading to high polydispersity. In addition, this method yields highly regioirregular polymers. By using metal-mediated polymerization, side reactions can be eliminated. The process requires functionalization of the monomer with halogen or organometallic groups (organomagnesium, organotin or organoborates). Introduction of the metal catalyst yields the neutral polymer, removing the chemical reduction step. Regioregularity can be obtained if the functionality of the monomer, catalyst and reaction conditions are well chosen. Figure 1-14 presents polymerization conditions leading to regioregular polymers. One drawback of this polymerization conditions is that they require cryogenic conditions. A new method developed by the McCullough group, Grignard Metathesis (GriM) polymerization removes that constraint, providing a simple and convenient way to prepare regioregular, neutral conjugated polymers.[32,33,46,47,48,49,85] It requires preparation and purification of a dibrominated analog of the electropolymerizable monomer. For the polymerization step, the halogenated monomer is reacted with one equivalent of methylmagnesium bromide, converting one bromine to an organomagnesium functionality. After the conversion is complete, a coupling catalyst such as Ni(II)dpppCl$_2$ is introduced, leading to a fast polymerization.

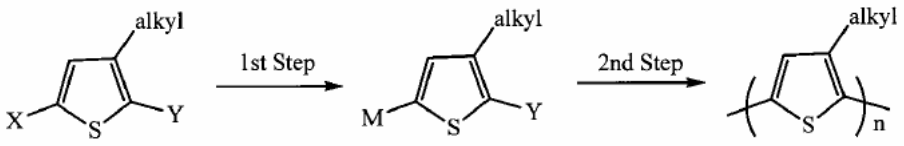

Method	X	Y	1st Step	M	2nd Step
1 [a]	-H	-Br	1) LDA, THF, -78°C 2) $MgBr_2 \cdot OEt_2$, -78°C to rt	-MgBr	$Ni(dppp)Cl_2$
2 [b]	-Br	-Br	1) Zn*	-ZnCl	$Ni(dppe)Cl_2$ [c]
3	-H	-I	1) LDA, THF, -78°C 2) Bu_3Sn-Cl, -78°C	$-SnBu_3$	$[Pd(Ph_3)_4]$
4	-H	-I	1) LDA, THF, -40°C 2) $B(OMe)_3$, -78°C 3) H^+ 4) R-OH, Na_2SO_4	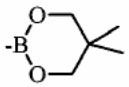	$Pd(OAc)_2$, K_2CO_3 THF, EtOH, H_2O

[a] yields 60-75%, Mw=20K-40K, PDI=1.12-1.4. [b] yields 67-82%, Mw=37K-49K, PDI=1.13-1.48. [c] dppe = diphenylphosphinoethane.

Figure 1-14. Polymerization method leading to regioregular Poly(3-alkylthiophene)s. Adapted from reference 47j.

The mechanism of the reaction is still under investigation. It may proceed through a chain growth process (Figure 1-14).[48] During initiation and reduction of the Ni(II) catalyst to Ni(0), the Ni(0) forms an associated pair with the coupling product. Following a cycle of oxidative addition, transmetalation and reductive elimination, a monomer unit is added to the chain, and the associated pair is reformed. This implies that the polymerization is controlled not by stoichiometry of bromide to organomagnesium functionalities as would be expected in a condensation polymerization, but by the monomer to catalyst concentration ratio. The McCullough group also demonstrated that Grignard Metathesis is a "quasi-living" polymerization, with the chain end remaining active at the end of the polymerization process,[49] allowing for the functionalization of the chain ends and the synthesis of block copolymers.

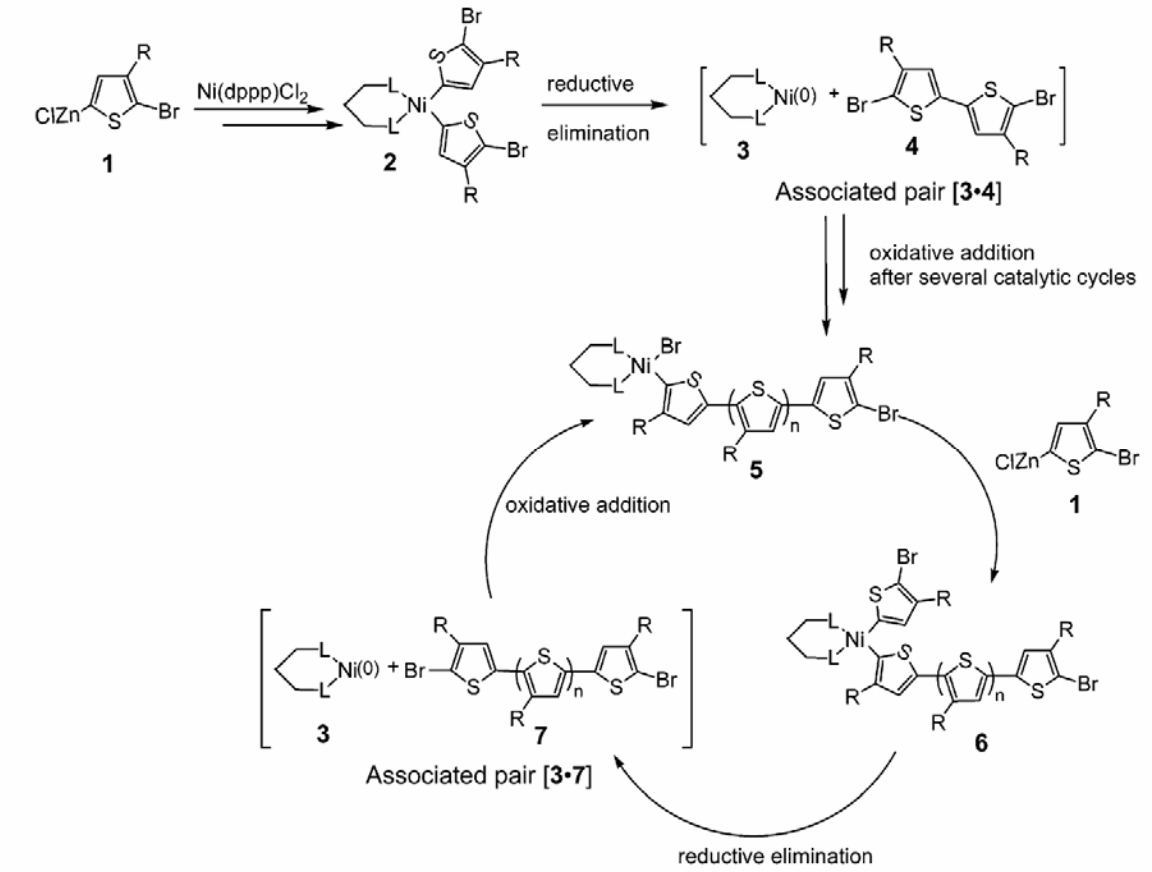

Figure 1-15. Proposed chain growth mechanism for Grignard Metathesis Polymerization. Adapted from ref 48.

Grignard metathesis is therefore a very promising method for obtaining tailored block copolymers with controlled morphology, crucial in photovoltaic devices and light-emitting applications. However, it must be pointed out that chain termination still occurs at high conversion, and the polymerization is therefore not yet "controlled". The polydispersity, although quite low, is still much higher than anionic or cationic living polymerizations. It is also not obvious that the study for poly(3-hexylthiophene) can be transferred to other monomers such as more electron-poor or electron-rich monomers, or that the molecular weights can be obtained reproducibly. Much work must still be carried out to achieve true living polymerization but initial reports so far are truly exciting.

In this dissertation, after giving a general experimental overview in Chapter 2 and a detailed introduction to dioxythiophene-based polymers in Chapter 3, I will discuss how electrochromic properties of disubstituted poly(3,4-propylenedioxythiophenes) (PProDOT) are greatly improved by introducing branched substituents that decrease interchain interactions and yield more amorphous polymers. The branched alkyl substituted PProDOTs, presented in Chapter 3, yield polymers that self-assemble during processing and give ordered aggregates of stacked chains. Alkoxy substituted PProDOTs, described in Chapter 4, yield more disordered aggregates. This leads to Chapter 5 which describes the synthesis and properties of chiral branched PProDOTs along with the use of circular dichroism (CD) to investigate the aggregation and ordering behavior in PProDOTs. Finally, Chapter 6 shows the synthesis and properties of the first soluble poly(3,4-phenylenedioxythiophene)s (PPheDOTs). Regiosymmetric didodecyl PPheDOTs with linear substituents have a high degree of order and provide an excellent platform for the development of high mobility and high conductivity materials, while asymmetric disubstituted PPheDOTs containing dodecyl and ethylhexyl substituents are highly disordered and provide an excellent platform for the development of light-emitting materials.

CHAPTER 2
EXPERIMENTAL METHODS

In Chapter 1, the theory and concepts which control the chemistry and properties behind conjugated polymers were presented. Some areas where CPs find applications and what can be done synthetically to improve the performance of the materials were also described. In this chapter, all of the experimental methods used to characterize the structure as well as the electronic and optical properties of the molecules and polymers presented in this dissertation will be introduced.

2.1. General Synthetic Methods

All chemical and solvents were purchased from Aldrich or Acros and used without further purification unless otherwise noted. Dry THF and dry diethyl ether were obtained by distillation from Na/benzophenone ketyl. Dry dichloromethane and dry acetonitrile were obtained by distillation from CaH_2. All reactions were performed under argon atmosphere using standard Schlenk techniques. Detailed synthesis of each compound presented in this dissertation can be found at the end of each chapter.

2.2. Molecular Characterization

All the new molecules presented in this dissertation were structurally characterized by ^{1}H NMR and ^{13}C NMR, High Resolution Mass Spectrometry. ^{1}H, ^{13}C NMR were obtained from a Gemini 300 FT-NMR, Mercury 300 FT-NMR, or VXR 300 FT-NMR. HRMS was obtained on a Finnigan MAT 95Q mass spectrometer. The purity was evaluated using elemental analysis carried out by the elemental service at the University of Florida (C, H, N) or Robertson Microlit Laboratories, Michigan (C, H, N, S, Br). IR

spectroscopy was also used for functional group identification and was recorded on a Perkin-Elmer Spectrum One FT-IR spectrophotometer.

2.3. Electrochemical Characterization

Monomer electrochemistry, polymer electrodeposition and polymer electrochemistry were performed using a standard three electrodes configuration: a platinum button working electrode (area= 0.02 cm^2), a platinum foil counter-electrode (S~1 cm2>>0.02 cm^2) and a silver wire pseudo-reference (Figure 2-1). The potential is applied from an EG&G Potentiostat/Galvanostat 273A. The Pt counter-electrode was cleaned by Bunsen-burner flaming. The silver quasi-reference was polished using sand paper. The Pt button working electrode was cleaned by rubbing gently with a kimwipe wetted with toluene. The silver wire was systematically calibrated with a ferrocene solution following experiments. To determine with precision the monomer and polymer oxidation potential, an immediate calibration with ferrocene is performed following each experiment. A solution of 0.1M tetrabutylammonium perchlorate (TBAP, prepared from tetrabutylammonium bromide and perchloric acid solution, recrystallized in methanol) in dry acetonitrile (from CaH2) was used as electrolyte.

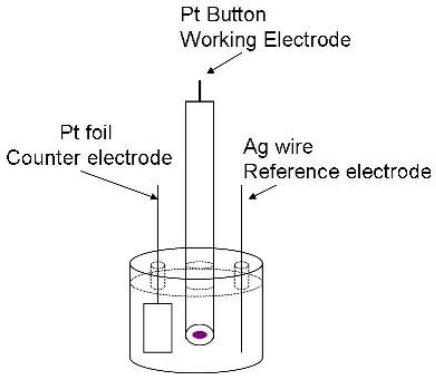

Figure 2-1. Three electrodes (Pt button, large Pt foil counter, Ag wire reference) electrochemical setup.

2.4. Polymer Characterization

2.4.1. Structural Characterization

The polymers were characterized by ^{1}H NMR, ^{13}C NMR (if polymer soluble), and elemental analysis. Due to the fast relaxation from the polymers, up to 20,000 scans were often needed. Either $CDCl_3$ or C_6D_6 was used depending on the polymers solubility. GPC was performed on two 300 x 7.5 mm Polymer Laboratories PL Gel 5 μM mixed-C columns with a 2996 photodiode array detector at the λ_{max} of the polymer solution. A constant flow rate of 1 mL/min was used. Molecular weights were obtained relative to polystyrene standards. Polymer solutions (0.5 mg/mL) were prepared in THF and filtered through a 450 nm GPC filter before injection. In the case of PPheDOT$(C_{12})_2$ described in Chapter 7, which is only soluble in chlorinated or aromatic solvent above 80°C, the NMR was carried out in 1,1,2,2-tetrachloroethane-d_2 at 120°C. GPC analysis on PPheDOT$(C_{12})_2$ (Chapter 6) was carried out by Dr Steve Eyles at the University of Massachusetts, Amherst. It was performed on a PL220 high temperature GPC (Polymer Laboratories, Inc., Amherst MA). The sample was injected at 5 mg/mL concentration using 1,2,4-trichlorobenzene at 135 °C, 1 mL/min as mobile phase. Separation was achieved using a set of four Polymer Labs Mixed A columns (7.5 x 300 mm). The polymer was detected by differential refractive index. Molecular weights were obtained relative to polystyrene standards.

2.4.2. Thermal Characterization

All polymers were characterized by thermogravimetric (TGA) and differential scanning calorimetry (DSC) analysis. TGA was carried out on a Perkin-Elmer TGA7 thermogravimetric analyzer. DSC was carried out on a TA Instrument DSC Q1000 calorimeter.

2.4.3. Morphology Characterization

This work was carried out in collaboration with Dr Wojciech Pisula, Nok Tsao and Pr Klaus Mullen of the Max Planck Institute for Polymer Science, Mainz, Germany. The 2D-WAXS experiments were performed by means of a rotating anode (Rigaku 18 kW) X-ray beam with a pinhole collimation and a 2D Siemens detector. A double graphite monochromator for the Cu-Kα radiation (λ=0.154 nm) was used. For this experiment, fibers were extruded using a home-built mini-extruder.[50] A photograph of a poly(paraphenyleneethynylene) extruded fiber can be found in the literature.[51]

AFM work was done in collaboration with Thomas Joncheray. AFM imaging was carried out in tapping mode with a Nanoscope III AFM (Digital Instruments, Inc., Santa Barbara, CA) using silicon probes (Nanosensor dimensions: T = 3.8-4.5μm, W = 26-27 μm, L = 128 μm). The images were processed with a second-order flattening routine.

2.4.4. Solution Optical Characterization

Polymer solutions were prepared using spectrophotometric grade solvents. New bottles were used, especially with chlorinated solvents, as old bottles develop acidity leading to oxidation of the polymers. All absorption spectra were obtained using a Varian Cary 500 scan UV-vis-NIR spectrophotometer. Thermochromism studies were performed using a SPV 1*1 Varian Cary dual-cell Peltier accessory.

Solution fluorescence spectra of the polymers and fluorescence solvatochromism were recorded on a Fluorolog 3. Solution fluorescence quantum yields were measured relative to a standard. The standard was chosen by analyzing the absorbance and fluorescence spectra of many possible candidates listed on the Oregon Medical Laser Center website under the Alphabetical Index of Photochem CAD Spectra.[52] Either

Rhodamine 6G (ethanol, λ_{ex}=480 nm, Φ_f= 0.95) or sulforhodamine (ethanol, λ_{ex}=550 nm, Φ_f= 0.9) were found appropriate as standard, depending on the absorption spectrum of the specific polymer considered. The integration time and the slits (excitation and emission) were respectively set at 0.5s and 2mm. When doing a quantum yield measurement, it is necessary to record the standard and the fluorescence with the same slits and integration value. The slit size should be increased if the fluorescence signal is low and noisy. However, the signal intensity at λ_{max} should always be kept well under 10^7 counts s^{-1}, as the response of the detector is not proportional to the emission intensity at such high value, resulting in large errors in quantum yields. Integration time can be increased to improve the signal-to-noise ratio (it does not change the signal intensity though). Only spectrophotometric grade solvents were used. Unless specified, absorption of the samples was kept under 0.1 (at λ_{max}) to prevent intermolecular quenching due to aggregation excessive concentration. The following equation was used to calculate the solution fluorescence quantum yield:

Equation 2-1:
$$\Phi_{sample} = \Phi_{standard} \times \frac{(1-10^{-A_{standard}})}{(1-10^{-A_{sample}})} \times \frac{(n^2_{sample})}{(n^2_{standard})} \times \frac{(I_{sample})}{(I_{standard})}$$

A is the absorbance at the excitation wavelength, n is the refractive index of the solvent used to take the fluorescence spectrum, and I is the number of emitted photons (obtained by integrating the fluorescence spectrum).

2.4.5. Solution Processing Techniques

The processing of conjugated polymers from solution is an extremely important step in their characterization and application. Different methods are available that lead to various film qualities, control of thickness, and different ease of processing. In this

section, a description of the processing techniques used in this dissertation is given: drop-casting, spin-coating and spray-coating.

2.4.5.1. Drop-casting

Drop-casting is the easiest technique to make a film. But it is also the technique leading to the poorest film quality. The polymer solutions are generally deposited on polar materials (mica, glass, ITO, and most metals). The wettability of the polymer solutions on polar substrates is very low, as all polymers presented in this dissertation are hydrophobic. As a result, the solution tends to concentrate at specific spots and poor film quality is obtained. To improve film quality, it is possible to use a razor blade to spread the solution on the surface as the solvent dries up but the resulting films still have poor quality. The concentration used is usually 5mg/mL in toluene.

2.4.5.2. Spin-coating

Spin-coating leads to the best film quality of all the film deposition techniques. In this method, a substrate is placed in the middle of the spin-coater and vacuum is applied underneath. The polymer solution is deposited with a pipette all over the surface of the substrate. The substrate is then rotated at the desired rate and after solvent evaporation, a uniform film is formed on the surface.

Many factors contribute to the quality of the spin-coated films, as well as the thickness of the deposited layer. The main factors are rotation speed, solvent, evaporation rate, concentration of the polymer solution and polymer molecular weight. Below is the AFM of a spin-coated film on glass.

For AFM imaging, a concentration of 0.2 mg/mL was used. The best solvent, leading to the most ordering was found to be ortho-dichlorobenzene for all polymers. The spin-coating rate used was 2000 rpm. This typically led to the formation of homogenous

monolayer thick films. For film fluorescence, thicker films are needed, so a higher concentration of 5-10 mg/mL was used, with a spin-coating rate between 1000-2000 rpm. Toluene was used as the solvent since it is a good solvent for all of the polymers analyzed for film fluorescence in this dissertation. To increase film thickness, higher solution concentrations or lower spin rates can be used, but using excessive concentration or too low a spin-rate can lead to polymer aggregation, which leads to poor film quality.

Spin-coating is the preferred method for making LEDs, LECs or OFETs where high film quality is a requirement. Drawbacks of the methods include the loss of materials since most of the deposited solution is ejected off the subtrate (it is possible to recover part of this lost material but it is very tedious), the fact that only thin films (<300 nm) can be deposited and that a symmetrical substrate must be used (disc, square). Also, the method is hard to apply to large surface areas.

2.4.5.3. Spray-coating

The spray-coating method is a very practical method to form uniform films on any kind of surface and applicable to large surface areas. In this method, the polymer solution is placed in a reservoir cup of a spray-brush (Aztek A470), and sprayed through a nozzle using compressed air. The resulting films are very homogenous to the eyes as seen in Figure 2-2. However, a closer look by profilometry reveals that the roughness is much higher than observed in spin-coated films, although it is clear that the films are fully covered. Thick films (1-2μm) can be obtained through this method. If the conditions are well controlled, the solvent evaporates rapidly and does not have enough time to dissolve the lower deposited layers. These conditions are pressure (it was found 12 psi to be appropriate for our films), polymer concentration (often 5mg/mL, but higher concentration must be used for low molecular weights polymers), solvent (highest quality

films with toluene for all polymers studied) and distance from the substrate (at least 10-20 cm distance from the substrate is needed, to allow the dispersion of thin droplets from the spray-brush nozzle). For colored films, the film thickness can be simply controlled by eye during spray-coating, as 50nm differences in film thickness are easily seen.

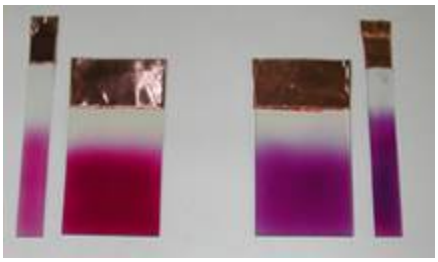

Figure 2-2. Spray-coated films of PProDOT-$(CH_2O(2\text{-ethylhexyl}))_2$ and PProDOT-$(CH_2OC_{18}H_{37})_2$. Films are sprayed from a 5mg/mL solution in toluene at an air pressure of 12 psi.

This is a method of choice for electrochromism characterization and electrochromic devices.

2.4.6. Film Fluorescence Characterization

Film quantum yield were obtained using a PTI MOD A1010 white light illumination and an Instruments SA, Inc. monochromator. The light from the source or fluorescence was collected using an ORIEL 70451 integrating sphere and a Spectrum-One CCD detector. The fluorescence quantum yield is then calculated following a published method.[53]

2.4.7. Spectroelectrochemical Characterization

The properties of conjugated polymers, as discussed earlier depend heavily on the redox state. The spectroelectrochemistry experiment (see Chapter 1) is used to monitor the variation of optical spectrum with applied potential. This experiment follows the fundamental optical changes of a polymer as a function of the doping levels, as described in Chapter one. The films' absorption spectra were obtained using a Varian Cary 500

scan UV-vis-NIR spectrophotometer. The optical bandgap is obtained from the onset of the neutral polymer π-π^* transition. A three electrode setup connected to an EG&G Potentiostat/Galvanostat 273 was used to change the potential applied to the films.

Another measurement, allowing one to follow the color with doping, is in-situ colorimetry analysis.[54] According to the Yxy color system developed by the Commission Internationale de l'Eclairage (CIE) in 1931, the color is defined by its chromaticity (x,y) and by its luminance (Y). These parameters were defined based on the "standard observer", meaning that they were designed based on how colors are perceived by an average of multiple people. The luminance parameter Y can be thought to be the brightness of a color as perceived by the human eye. For example, white is perceived as a very bright color where grey is perceived as less bright, although they have the same chromaticity. The chromaticity is defined by the two parameters x and y, which characterized the color itself, independently of its brightness. They represent two variables defining the color perceived and are a mathematical combination of what is detected by the three receptors present in our eyes (often refered to as blue, green, red receptors), each detecting a range of the visible light wavelength.

In this dissertation, x,y and Y values were recorded by a Minolta Chromameter CS-100. Y is given in Cd/m^2 (x,y have no units). Sample was illuminated from behind using a D50 (500K) light source. A background measurement was recorded using a blank ITO slide in the appropriate electrolyte solution in a quartz cuvette. The colorimetry was recorded using the following settings: calibration set at "PRESET", measuring mode set at "Abs". And response set at "SLOW". These settings must be used as other settings will lead to erroneous data. All films (except PPheDOT$(C_{12})_2$) used in

spectroelectrochemistry, luminance and CE experiments were prepared by spray-coating onto Indium Tin Oxide (ITO) coated glass slides (Delta Technologies, 8-12 Ω/□). PPheDOT(C_{12})$_2$ films were prepared by drop-casting on ITO-coated glass slides from a hot (100°C) solution in xylenes, as it is insoluble at room temperature and cannot be spray-coated.

Another useful tool in electrochromic materials characterization is the composite coloration efficiency.[24] In this measurement, the transmittance of the film at λ_{max} and the charge injected into the film are recorded as a function of time during a potential step from a potential where the polymer is fully neutral to a potential where the polymer is fully oxidized. As shown in Figure 2-3 for PProDOTMe$_2$, as the potential is stepped from -0.5V to 1.2V, the transmittance at 585 nm increases strongly as the polymer is oxidized and the visible π-π^* optical transition is bleached, reaching a plateau when it is fully oxidized. The time required to obtain 95% of the optimum contrast is taken as the *switching time* of the polymer and is a critical parameter to characterize a material designed for an electrochromic application. The coloration efficiency is calculated from the following equations:

Equation 2.2: $\Delta OD = \log[T(\text{ox at } 95\%)/T_{red}]$

Equation 2.3: $CE = \Delta OD/Qd$

Q_d is the charge required to obtain 95% of the total optical contrast. T(ox at 95%) is the film transmittance at 95% of the total contrast. T_{red} is the film transmittance in the neutral state.

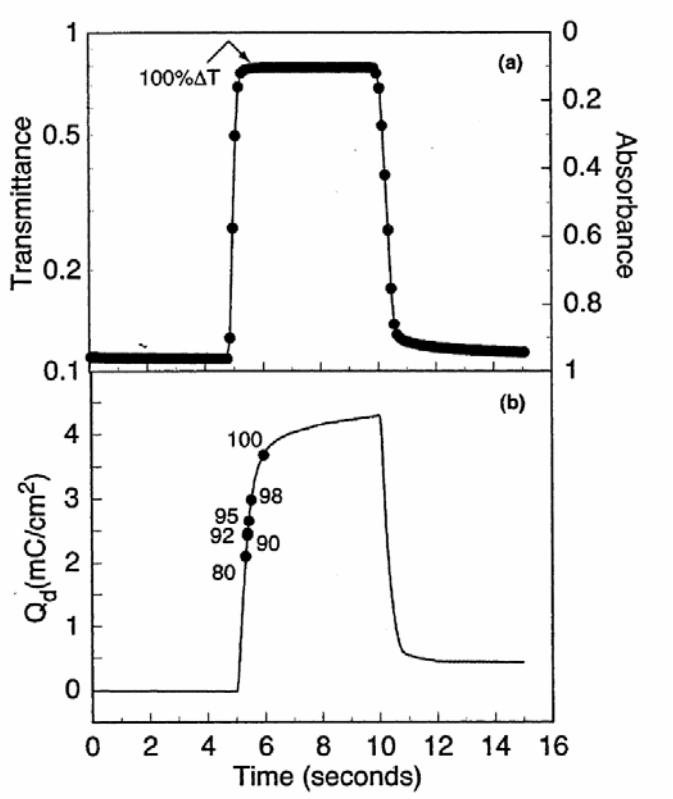

Figure 2-3. Time evolution of transmittance and injected charge for an electropolymerized film of PProDOT-Me_2. Adapted from ref. 24.

The CE value provides a practical way of comparing color change charge efficiency between different materials. For example, our research group showed that PEDOT, PProDOT and PProDOT-Me_2 have increasing CE values: 183 cm^2/C, 255cm^2/C, 375cm^2/C.[64] This trend correlates well with PProDOTs having a higher contrast than PEDOT (51% Δ%T at λ_{max} of 585 nm for PEDOT, 63% Δ%T at λ_{max} of 578 nm for PProDOT, 72% Δ%T at λ_{max} of 585 nm for PProDOTMe_2). PProDOTs also requires less charge to obtain full doping of the polymer. This is explained by PEDOT having more ordered, packed morphology than PProDOT, as the more flexible seven-membered ring provides steric hindrance to chain packing and allows for easier penetration of the dopant ion. Substitution of the seven-membered ring with methyl groups hinders interchain interaction. This could result in more capacitive contributions

to the current (not contributing to polymer doping) for PEDOT, than PProDOT and PProDOT-Me_2.

2.4.8. Circular Dichroism

The method will be discussed in details in Chapter 5 concerning chiral PProDOTs. CD spectra were measured on a JASCO J-815 CD spectrometer, with a Peltier Temperature Programmer model JASCO PTC-348WI.

2.4.9. Conductivity Measurements

In this work, most conductivity values were measured using the four-point probe method. The experimental setup is shown in Figure 2-4.

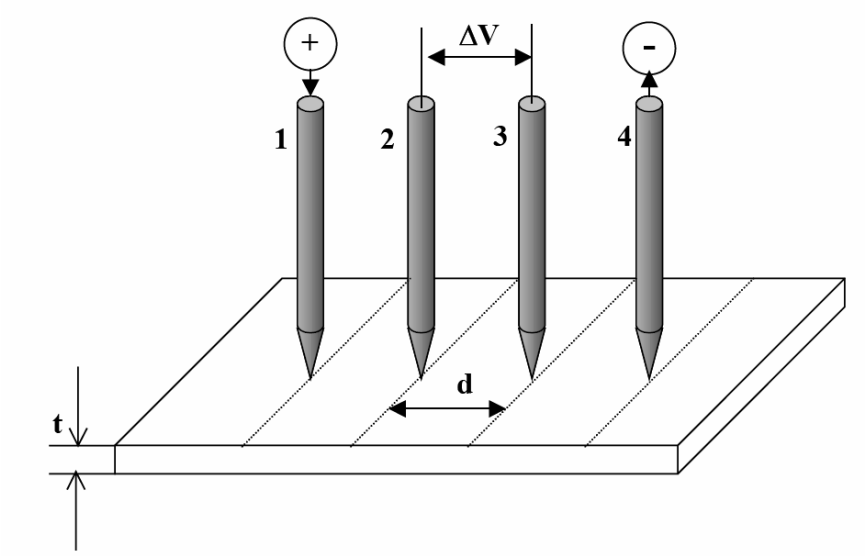

Figure 2-4. Four-point probe conductivity method.

This method has several advantages. If the voltmeter has a high impedance, then problem of contact resistance met in two points measurements is avoided. This method also allows the conductivity to be measured at several locations in the films. An average measurement is then obtained, which is useful since the presence of cracks or morphology defects will alter the measured conductivity. This cannot be done in methods

involving thermal evaporation of metal electrodes onto the film, used for PPheDOT(C_{12})$_2$.

The films used for this measurement were all spray-coated onto glass slides (1 square inch), except for PPheDOT(C_{12})$_2$ which cannot be spay-coated (a procedure is described later for this polymer). The spray-coated films were exposed to iodine vapor in an iodine chamber overnight and then quickly brought to the Signatone S-301-4 four-point probe apparatus for conductivity measurement. As seen in Figure 2-5, a constant current I (between 1μA and 100 μA) is applied between electrode 1 and 4 using a Keithley 224 current generator (voltage threshold was set at 30 V, intensity threshold was set at 5×10^{-3} A), and the voltage drop between electrodes 2 and 3 (ΔV) was monitored using a Keithley 197 voltammeter. After obtaining the film thickness t from a Sloan Dektak 3030 profilometer, the conductivity is then calculated by the following equation:

Equation 2.4: $\rho = (\Delta V/I)\,(t\,\pi\,/\ln 2)\,F$

where F(t/d) is a correction factor approaching zero when $t \ll d$.[55] Since all the films used in our study are very thin compared to the distance between electrodes, $F \approx 1$.

If the electrodes make good contact with the oxidized polymer, the $V_{threshold}$ light on the current generator should be solid. If a poor contact is made with the films (caused by holes, cracks in the film between the electrodes) then the $V_{threshold}$ light will blink. To verify that a valid conductivity measurement will be obtained, the voltage drop is monitored as the applied current is modified. If the conductivity measurement is good, the voltage drop change is directly proportional to the current change (Ohm's law). For every measurement, the voltage drop and film thickness were measured at several locations and an average value is then calculated, yielding an average value of

conductivity for the polymer film. Usually, the current applied to electrodes 1 and 4 is set at 100 μA. However, it was discovered that for the lower conductivity films, the voltage needed to obtain this current quickly rose above the threshold of 30V after the four-point probe is applied on the film. In this case, the current was decreased to down to 10 μA or 1-2 μA.

In the case of PPheDOT$(C_{12})_2$, films could not be spray-coated. Spin-coating from hot toluene solutions (100 °C) afforded homogenous thin films. Four gold electrodes were thermally evaporated onto the spin-cast films (Figure 2-5). Copper wires were soldered to the 4 electrodes and connected to the current generator and voltmeter described above for the 4 point conductivity measurement. The films were placed in a specially designed chamber, and sealed under vacuum. Bromine was introduced through a septum via syringe and the voltage drop was measured. After measurement of the film thickness, conductivity was calculated using Equation 2.4.

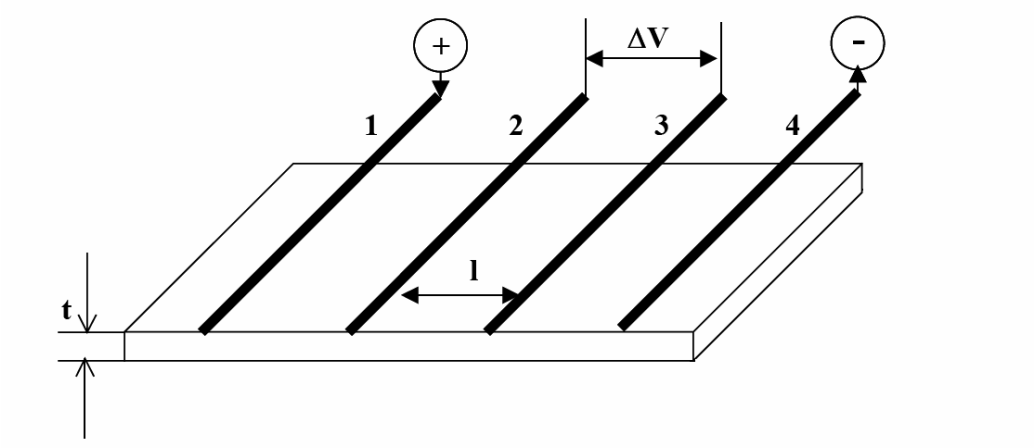

Figure 2-5. Four-point conductivity measurement. Gold electrodes are thermally evaporated on spin-coated polymer film.

CHAPTER 3
SYNTHETIC CONTROL OF ORDER IN BRANCHED ALKYL POLY(3,4-PROPYLENEDIOXYTHIOPHENES) (PPRODOT-R2)

3.1. Introduction

Chapter 1 described the properties of soluble alkyl poly(thiophene)s. These polymers have good solubilities, but high oxidation potentials. By introducing two electron-donating oxygens onto the 3- and 4-positions of the thiophene ring, the oxidation potential is considerably lowered, and the polymers become stable in their oxidized state. It also prevents crosslinking at the 3-and 4- positions of the thiophene ring, as observed in alkyl poly(thiophene)s. Poly(3,4-ethylenedioxythiophene) (PEDOT) is an electron-rich, highly conductive polymer that has been used in many applications, including anti-static coatings, capacitors, and "smart windows".[56] PEDOT has conductivities up to 200-500 S cm^{-1} in the oxidized form.[8] The polymer is highly insoluble because of the high degree of interchain interactions due to a more planar intrachain conformation. This was shown by studies on EDOT oligomers and theoretical calculations.[57] Multiple factors contribute to the planarization of the backbone: mesomeric effect induced by the electron-donating oxygens, low steric interactions between the sulfur atom and the small oxygen atoms (much smaller than methylene), and attractive sulfur-oxygen interactions.[58] Also, the two alkoxy substituents are tied together in the six-membered ring. The ring structure is critical since poly(3,4-dialkoxythiophenes) have been shown to exhibit much lower conductivities,[59] attributed to the flexibility of the alkoxy substituents generating intrachain steric repulsion between substituents on adjacent thiophenes. As discussed

earlier, this steric repulsion results in intrachain twisting and decreased interchain interactions.

Substitution of the six-membered rings of PEDOT with linear tetradecyl alkyl chain induces solubility in organic solvent.[60] Shorter linear alkyl chains (C_1-C_{10}) do not create sufficient steric hindrance to overcome the π-stacking, leading to insoluble polymers. The introduction of such long linear alkyl chains does not disturb the packing of the chains. This is a bit surprising given as inter and intrachain would be expected (the polymer is regioirregular) side chain repulsion. Theoretical calculations in our group by Alejandro Perdomo (in collaboration with the Bredas research group) show the six-membered ring adopts a twisted chair conformation, in which the substituent lies in an equatorial position within the polythiophene backbone plane (Figure 3-1).

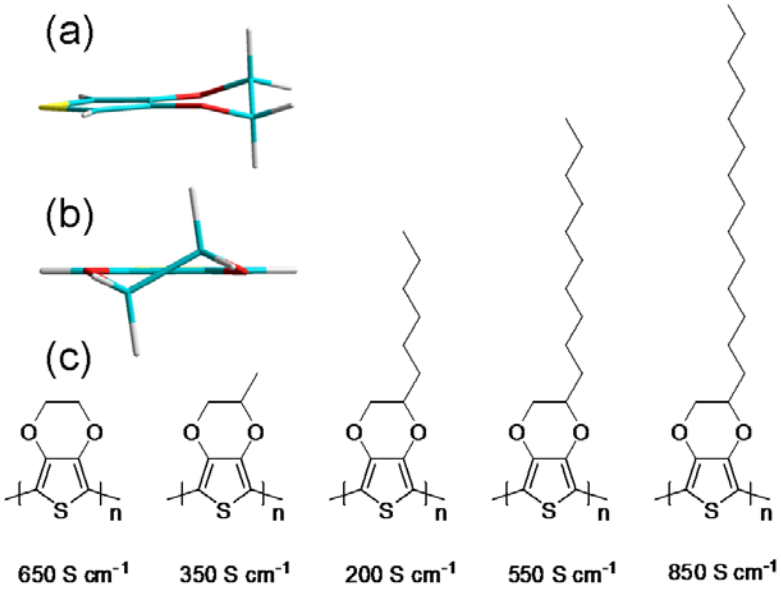

Figure 3-1. Conformational and substituents effects on 3,4-ethylenedioxythiophenes. (a) side view and (b) back view of EDOT in the "twisted" conformation, calculated to be the most stable conformer using ANNEALING method as implemented in AMPAC and optimized at the B3LYP/6-31G* level of theory. (c) Structures and conductivities for a series of alkylated PEDOTs. The conductivities were all obtained by in-situ conductivity on electropolymerized films.[62]

As a result, crystallization of the long linear alkyl chains yields an improvement of the stacking of the polymer chains and allows for higher conductivities.[61] With shorter chains that do not order easily, the regioirregularity of the side chains dominates and lower conductivities are observed compared to PEDOT.[62] This trend is also illustrated in Figure 3-1. One drawback of neutral PEDOT based polymers is their instability to ambient conditions (air, light and water). The polymers easily oxidize in air and degrade over time. This is different with the neutral form of the poly(3,4-propylenedioxythiophenes) (PProDOT) based polymers. Although the only difference lies in the presence of the larger 7-membered ring in place of the six-membered ring, PProDOTs are much more stable to ambient conditions and can be stored in air for extended periods of time without oxidizing. Theoretical calculations (by Alejandro Perdomo) show that this increased stability may originate from the greater flexibility of the seven-membered ring with two stable conformations: the "twisted" conformation, similar to PEDOT (both in conformation and in energy), and a lower energy chair type conformation (Figure 3-2). The predominant form depends heavily on the substitution of the seven-membered ring. X-ray crystal structure on crystalline ProDOT derivatives have confirmed the existence of these two conformers.[63] To induce solubility, alkyl chains can be introduced at the 2-position of the propylene bridge. This substitution leads to a regiosymmetric monomer; therefore regioregularity of the side chains in the polymer is induced. Also, interactions between substituents of adjacent thiophenes are minimized at this position. Early attempts using methyl (PProDOT-Me_2) and ethyl (PProDOT-Et_2) substituents yielded insoluble polymers.[24,64] Electropolymerized films of PProDOT-Me_2,

PProDOT-Et_2 displayed enhanced properties, with higher coloration efficiency, and shorter switching times than PProDOT and PEDOT

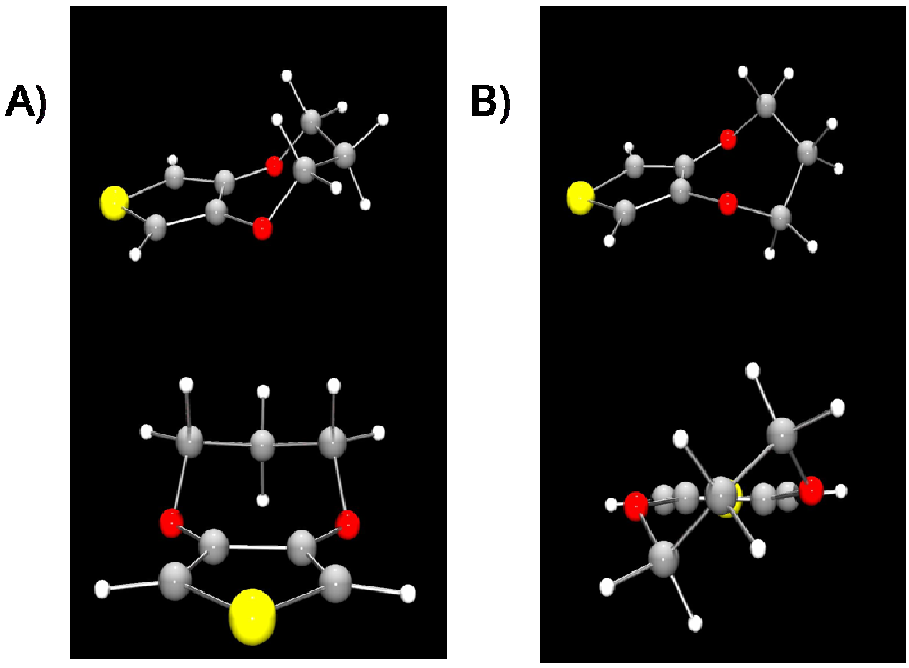

Figure 3-2. Two most stable conformations of ProDOT. A) The "*chair*" conformation; B) The "*twisted*" conformation. Calculations were performed using ANNEALING method as implemented in AMPAC. Each conformer found was subsequently optimized at the B3LYP/6-31G* level of theory. Hydrogens are white; carbons are grey; oxygens are red; sulfurs are yellow.

To induce solubility, longer alkyl chains were required. The synthesis of PProDOT-Bu_2 indeed provided the first soluble PProDOT,[63a] but the solubility was limited to the lower molecular weight fractions (M_n= 3000 g mol^{-1}). To further increase the solubility, the first approach employed was to increase the length of the linear alkyl side chains. The second was to introduce steric bulk and branched substituents. In this chapter are introduced PProDOTs symmetrically substituted with various branched alkyl groups and the effect of substitution on the properties of the conjugated polymers is discussed thoroughly. The family of polymers synthesized and described in this Chapter is shown in Figure 3-3.

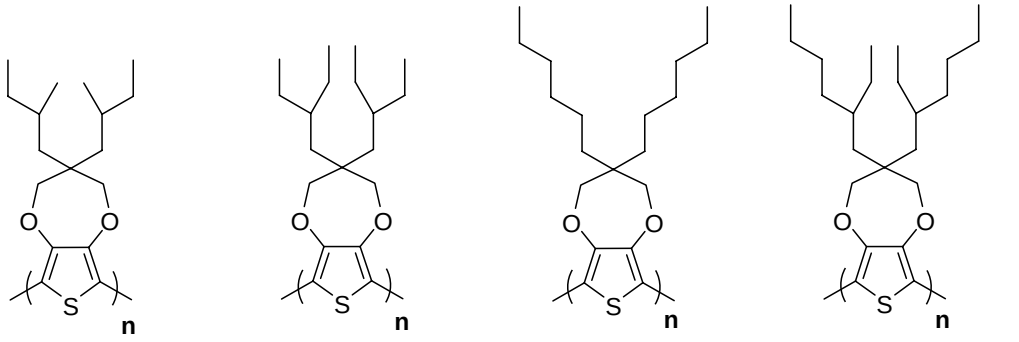

Figure 3-3. Family of branched dialkyl PProDOTs. PProDOT-Hexyl$_2$ was synthesized for comparison and discussion of branching effects.

3.2. Electropolymerized PProDOT-R$_2$

3.2.1. Electropolymerizable Monomer Synthesis

The electropolymerizable monomers were synthesized by transetherification of 3,4-dimethoxythiophene and 2,2-dialkyl-propane-1,3-diol, as shown in Figure 3-4. All diols used in this dissertation were synthesized by malonic ester synthesis followed by lithium aluminum hydride reduction as indicated in Figure 3-4.[65] The synthesis is easily scalable and the starting materials are inexpensive. In the case of 2,2-dihexylpropane-1,3-diol, the synthesis was scaled up to a several hundred grams scale in a collaborative work with Benjamin Reeves and Barry Thompson. The key intermediate, 3,4-dimethoxythiophene, was prepared from a copper-mediated Ullmann ether reaction of 3,4-dibromothiophene. The preparation of 3,4-dibromothiophene from thiophene is also included since much of the 3,4-dibromothiophene used for this dissertation work was obtained by this method. This product is now commercially available at a competitive price, avoiding large scale, tedious and potentially dangerous steps. These steps include tetrabromination of thiophene (with a large amount of HBr released), followed treatment of

tetrabromothiophene with either two equivalents of n-butyllithium or Zn metal in acetic acid.

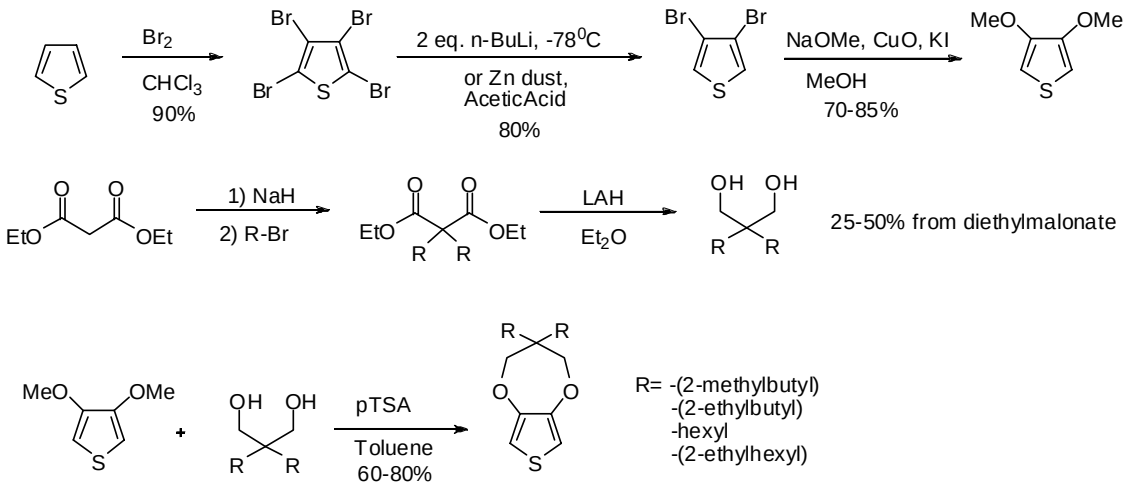

Figure 3-4. Synthesis of electropolymerizable alkyl substituted ProDOTs. Branched 2-methylbutyl and 2-ethylhexyl derivatives are prepared from racemic reagents.

3.2.2. Electrodeposition and Electrochemistry

After thorough purification of the electropolymerizable monomers, polymer films were electrodeposited onto platinum button electrodes. As seen in Table 3-1, the monomer oxidation depends little on the substitution.

Table 3-1. ProDOT-R_2 monomer oxidation onset and peak potentials. Scan-rate is 50 mV/s.

R	E_{onset} (V)	E_{peak} (V)
-butyl	0.99 V	1.10 V
-hexyl	0.97 V	1.11 V
-2-methylbutyl	0.88 V	1.08 V
-2-ethylbutyl	0.98 V	1.11 V
-2-ethylhexyl	1.03 V	1.11 V

All onsets of oxidation or peak potentials are within a range of less than 100mV from each other, consistent with the fact that the substituents are remote from the dioxythiophene ring and do not affect significantly the electronic properties of the thiophenes. All PProDOT-R_2 polymers are easily electrodeposited in a polar,

electrochemically stable solvent such as acetonitrile. The monomers used in this study are soluble in this solvent, but the polymers are not, allowing a smooth deposition of films with various thicknesses. Figure 3-5 illustrates the deposition of a PProDOT-(2-ethylhexyl)$_2$ film on a platinum button.

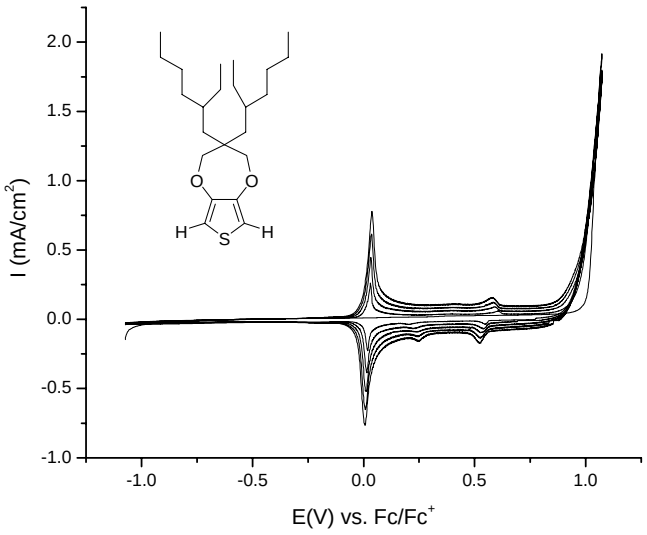

Figure 3-5. Electrodeposition of PProDOT-(2-ethylhexyl)$_2$ on platinum button electrode. The film was deposited from a 0.01M monomer solution in 0.1M TBAP/ACN, at a scan rate of 50 mV/s.

After deposition of the polymers from each of the monomers, the films were rinsed and studied in monomer-free 0.1M TBAP/ACN solution. In contrast to the monomer oxidation, significant differences are observed in polymer oxidation as the side chains are modified. Figure 3-6 presents the overlayed cyclic voltammetry of all PProDOT-R$_2$ polymers studied. In the butyl substituted series, as methyl and ethyl branching are introduced on the 2-position of the butyl side chains, the oxidation peaks are shifted to higher oxidation potentials. In addition, the redox waves become narrower as steric bulk is introduced. In the hexyl series, the same trend is observed going from PProDOT-Hexyl$_2$ to PProDOT-(2-ethylhexyl)$_2$. As the chains with the stronger interchain

interactions are expected to have lower oxidation potential, this trend is consistent with decreased interchain interactions as the steric bulk of substituents increases. The narrowing of the redox waves may possibly be explained by the increasing open morphology of the polymer films as steric bulk is increased.

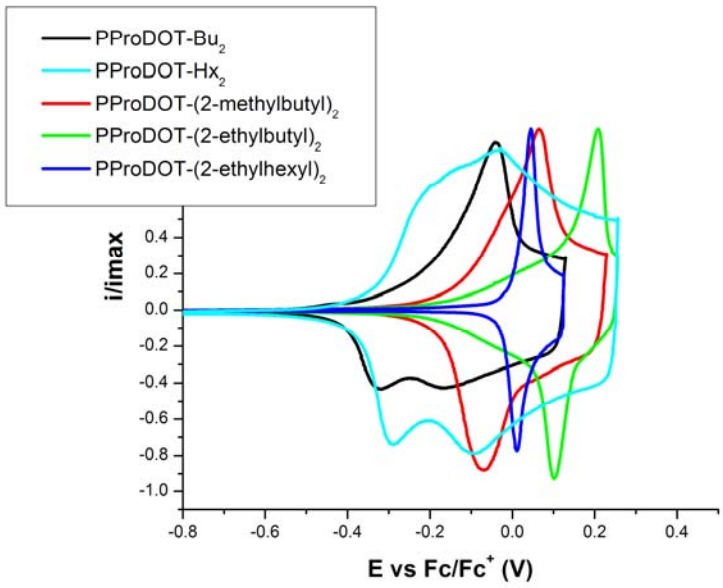

Figure 3-6. Polymer oxidation in the PProDOT-R_2 series. All the polymers were deposited by cyclic voltammetry at 50mV/s scan rate from 0.01M monomer solution in 0.1M TBAP/ACN. The polymer oxidation curves were recorded in monomer-free electrolyte at 50mV/s.

Comparing the oxidation curves of PProDOT-(2-ethylhexyl)$_2$ and PProDOT-(2-ethylbutyl)$_2$, it seems that although the steric bulk of ethylhexyl is greater than ethylbutyl, PProDOT-(2-ethylbutyl)$_2$ has the higher oxidation potential. Examining the onset of polymer oxidation, PProDOT-(2-ethylhexyl)$_2$ has a higher onset potential, consistent with a decrease of interchain interactions. The higher oxidation peak for PProDOT-(2-ethylbutyl)$_2$ is explained by considering the penetration of dopant ions into the polymer film. We speculate that cyclic voltammetry is not only probing thermodynamic behavior of the polymer but also the kinetic diffusion of the dopant ion inside the polymer film. In

the lower potential region of the oxidation wave, the oxidation of the polymer is thermodynamically controlled and the chains with the lowest oxidation potentials will oxidize first. At higher potential the current is limited by the penetration of the dopant ions into the film, which is diffusion limited. In the case of PProDOT-(2-ethylhexyl)$_2$, the bulkier side chains provide more distance between chain stacks (different from the interchain π-stacking distance) and the diffusion of the dopant ion is easier, resulting in a lower peak potential.

3.3. Chemically Polymerized Soluble PProDOT-R_2

3.3.1. Synthesis and Polymer Characterization

After bromination of the electropolymerizable monomer, the polymer is prepared by Grignard Metathesis polymerization (Figure 3-7).[47] In this method, the chemically polymerizable monomer is reacted in THF at reflux temperature with one equivalent of methylmagnesium bromide (titrated by a published method[66]). After the halogen-metal exchange is complete, Ni(dppp)Cl_2 is added in one portion, initiating the polymerization. Within a few seconds, the yellow color of the catalyst turns red or purple as polymer is formed. The polymerization is complete a few hours following introduction of the catalyst.

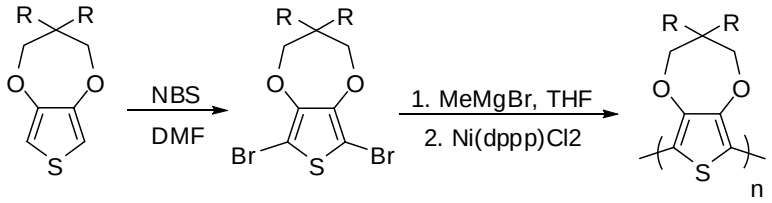

Figure 3-7. Grignard Metathesis polymerization of soluble PProDOT-R_2.

After purification by Soxhlet extraction in MeOH (to remove magnesium salts, polar impurities) and Soxhlet extraction with hexanes (to remove low molecular weight

polymer), the polymer is extracted with dichloromethane, chloroform or toluene. All polymers show high solubility in many organic solvents (e.g. toluene, chloroform, THF). Proton and carbon NMR confirmed the structure (see Experimental Section). Molecular weights were estimated by GPC analysis in THF and are shown in Table 3-2. PProDOT-Hx_2 could be obtained in 5-10 g quantity, demonstrating that the synthesis is scalable.

Table 3-2. Molecular weight analysis of GriM polymerized PProDOT-R_2. Molecular weights are estimated vs. polystyrene standards.

	M_n (g mol^{-1})	X_n	M_w (g mol^{-1})	PDI
Butyl	6,000	22	n/a	n/a
Hexyl	27,000	83	47,600	1.73
2-methylbutyl	17,000	57	40,000	1.76
2-ethylhexyl	43,000	113	62,600	1.6

It is important to point out that the number-average molecular weight is well above the effective conjugation length, and the optical and electronic properties are saturated. Figure 3-8 shows the evolution of UV-Vis absorption spectrum as it is eluted out of the GPC columns. Up to a number-average molecular weight of 5,700 g mol^{-1}, there is a significant shift of the λ_{max}. Above this molecular weight, the maxima of absorption remain constant, suggesting an effective conjugation length of ca. 15 repeat units.

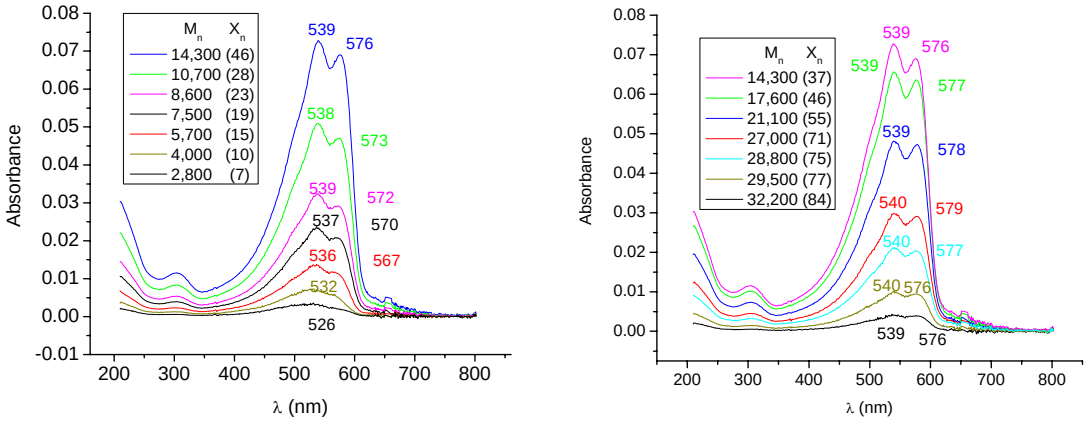

Figure 3-8. Evolution of UV-Vis absorption spectrum with molecular weight for PProDOT(2-ethylhexyl)$_2$. Number-average molecular weights are estimated vs. polystyrene standards.

The thermal properties of the bulk polymers were studied by TGA and DSC analysis. TGA indicates that the polymers have good thermal stability, reaching 5% weight loss at ca. 350°C. For each polymer, the weight loss corresponds to the loss of the 2,2-dialkylpropyl unit. DSC analysis revealed no transition in the -150 to 250°C range suggesting the polymers are amorphous, as expected from introducing bulky branched substituents.

3.3.2. Solution Properties

The solution properties were studied by UV-Vis absorbance and fluorescence spectroscopy. Figure 3-9 shows the spectra for PProDOT-Hexyl$_2$ and PProDOT(2-ethylhexyl)$_2$.

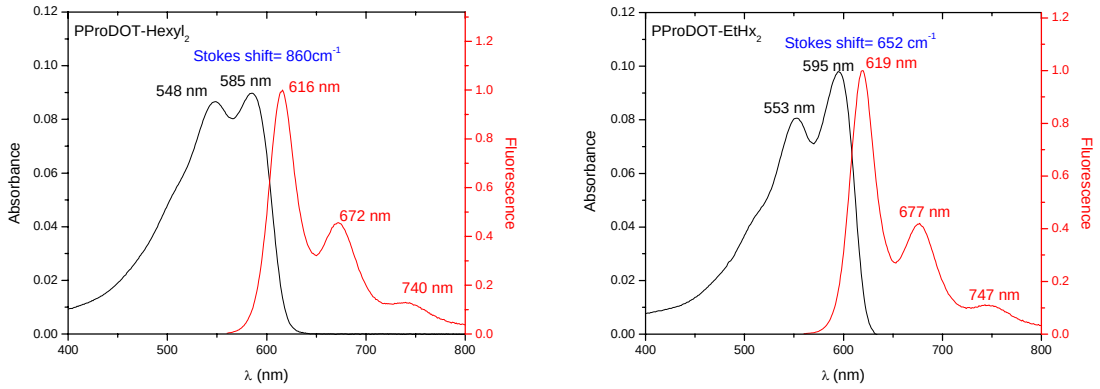

Figure 3-9. Absorption and photoluminescence spectrum of PProDOT-Hexyl$_2$ and PProDOT(2-ethylhexyl)$_2$. The polymers were excited at 550 nm.

The striking features of the solution optical properties are the presence of well-resolved vibronic features, and the small stokes shifts (<700 cm^{-1}). Some controversy still exists on the origin of vibronic coupling and whether it is an interchain or intrachain phenomenon as reviewed in our research group.[67] Overall, there is overwhelming support that vibronic features in CPs absorption and emission spectra arise from the coupling of electronic absorption with vibrational modes of the polymer backbone and have an

intramolecular origin.[69] In the spectra shown above, the polymer solutions are diluted but still have well-resolved vibronic features, also suggesting an intramolecular, not intermolecular origin of vibronic coupling. This was confirmed by dilution studies showing no dependence of the peak wavelengths on the absorption on concentration.

As described by Bredas et al.,[69] vibronic coupling depends on the respective geometries of the ground and excited state (Figure 3-10). In a molecule where ground state and excited state have identical geometries, such coupling is forbidden. The result is that a single identical peak should be observed for absorption and emission. But when the ground state and the excited state geometries are different, then vibronic coupling can be seen.[68]

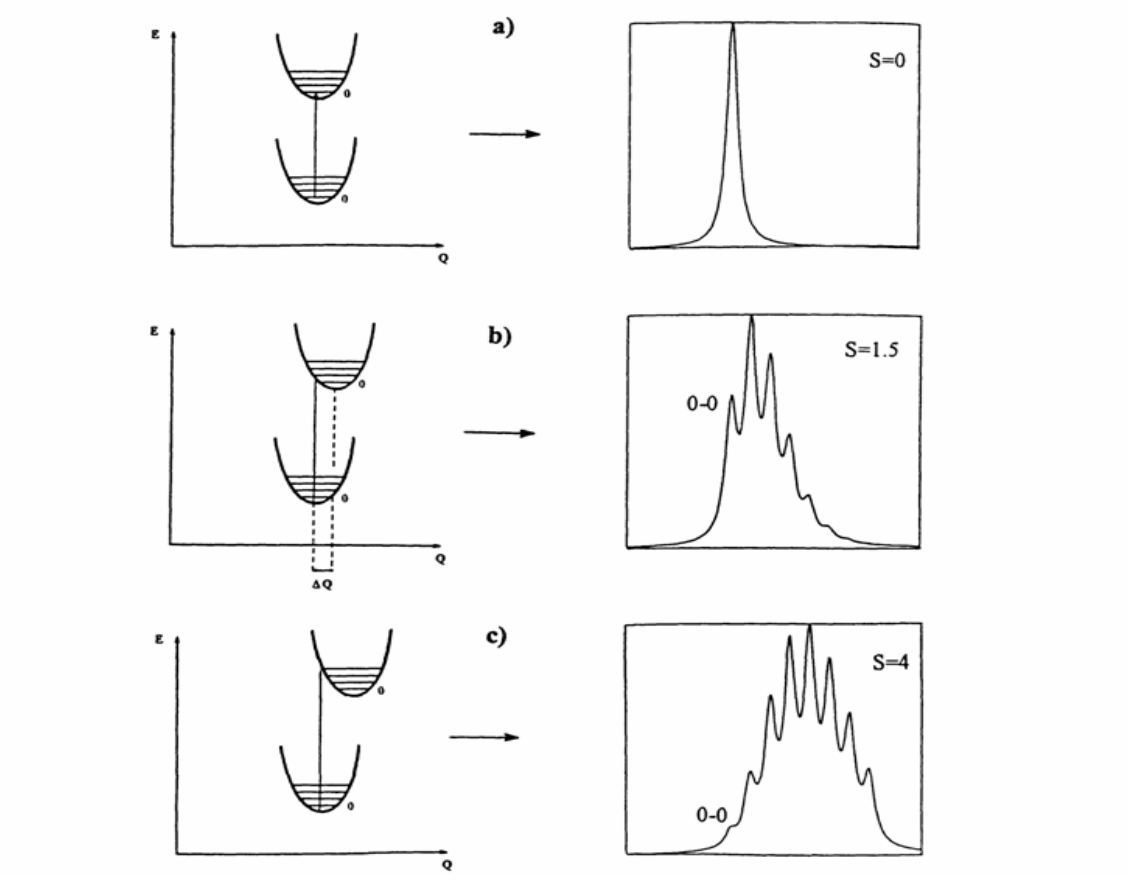

Figure 3-10. Evolution of absorption spectrum with increasing distortion between the ground state and the excited state. Adapted from ref. 69.

According to Kasha's rule,[70] the fluorescence will occur from the lowest vibrational state of the excited state resulting in a bathochromic shift of the emission compared to the absorption. This is the origin of the Stokes shift, defined as the energy difference between the energy at the maximum of absorption and the energy at the maximum of emission. The larger the Stokes shift, the more distortion exists between the ground and the excited states. As a quinoidal planar form is predicted in the excited state, it follows that a small Stokes shift indicates a planar arrangement of the chain in the ground state.

In the case of PProDOT-R_2 polymers, the presence of two clear vibronic peaks in absorption and three in emission, assigned to the 0-0, 0-1 and 0-2 (only in emission) vibronic transitions, along with a small Stokes shift indicate a small displacement of geometry between the ground and the first excited state along with a planar conformation of the chains. In poly(3-alkylthiophene)s, which have much higher intrachain conformational flexibility in solution, the absorption is broad and featureless and the Stokes shift is much higher at 5500 cm^{-1}.[71] Table 3-3 shows the solution properties for all alkyl substituted PProDOTs studied here.

Table 3-3. Optical properties of alkyl substituted PProDOTs in toluene solution. Also indicated is the relative intensity of the vibronic bands.

R	**λ_{max} absorption (nm)**	**λ_{max} emission (nm)**	**Stokes Shift (cm^{-1})**	**Φsol.[a]**
Hexyl	585 (*1*), 548 (*0.96*)	616 (*1*), 672 (*0.46*), 740 (*0.13*)	860	0.35
2-methylbutyl	602 (*1*), 556 (*0.74*)	621 (*1*), 677 (*0.40*), 746 (*0.10*)	482	0.36
2-ethylhexyl	595 (*1*), 553 (*0.82*)	619 (*1*), 677 (*0.44*), 747 (*0.11*)	652	0.37

(a) Quantum yield was calculated using sulforhodamine excited at 550 nm as standard.

From the solution optical data above, it is clear that branched substituted PProDOTs have a more planar backbone and less conformational freedom than linear substituted PProDOTs, as indicated by a smaller Stokes shift and more resolved vibronic

features. As expected, such differences are not seen in the fluorescence spectrum as there is vibrational relaxation to the more stable, planar quinoidal conformation before emission. The quantum yield remains mostly unaffected by the increasing steric bulk, suggesting interchain interactions are not involved in toluene solution and that the chains are molecularly dissolved.

3.3.3. Optoelectronic Properties of Solution Processed Films

To characterize the optical properties of the PProDOT-R_2 polymers in the solid state, films were spray-cast from toluene solution. The solutions were all red-colored. For branched alkyl polymers, as the solvent dried out on the substrate, the red color changed to a blue-purple color in the solid state. The corresponding absorption spectrum, shown in Figure 3-11 for PProDOT(2-methylbutyl)$_2$, shows a 20 nm bathochromic shift in absorption between the toluene solution and the film as cast, indicating that the polymer chains order during solvent evaporation and that there is significant interchain interactions between polymer chains in the solid state. The vibronic coupling of the spray-coated films becomes more resolved, consistent with planarization of the chains induced by the aggregation process. When the films are oxidized and reneutralized electrochemically, no further changes of optical absorption are observed.

PProDOT-Hx_2 behaves differently. The red color of the solution is maintained in the film state. As seen in Figure 3-11, the absorption spectra of solution and spray-coated films have identical λ_{max}. This indicates that the polymer chains retain a solution conformation upon casting. The broader absorption of the film state suggests that aggregation does occur, but that the aggregates are ill-defined. Upon redox switching of PProDOT-Hx_2 spray-coated films, the color changes to blue-purple and the absorption spectrum undergoes a 20 nm bathochromic shift. This behavior was also observed in

PProDOT-Bu_2.[63a] The absorption shift is attributed to a doping-induced rearrangement of the polymer chains. In the oxidized state, the chains adopt the more planar quinoidal structure, forcing intrachain but also interchain rearrangements. These changes are preserved upon reduction to the neutral polymer and no further shift is observed upon further redox cycles.

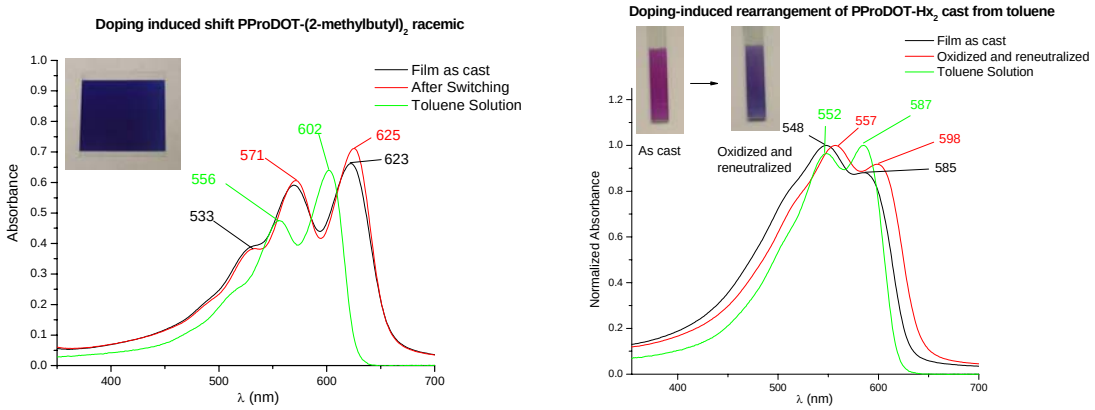

Figure 3-11. Doping/Casting induced rearrangement in linear vs. branched alkyl substituted PProDOTs. (left) PProDOT(2-methylbutyl)$_2$; (right) PProDOT-Hx_2.

A possible explanation for the different behavior is that PProDOT-Hx_2, is that the linear substituted seven-membered ring can adopt both chair and twisted conformations discussed above. This is supported by X-ray structures carried out on BisProDOT-$(Et)_2$, presented in Figure 3-12, and also theoretical calculations predicting a very small difference of energy between the two conformers, in favor of the chair conformation.[63a] In the case of branched substituents, theoretical calculations predict the twisted (more planar) conformer to be significantly lower in energy than the chair conformer. As a result, the branched polymer chains would have a much higher planarity and regularity. This would favor strong interchain interactions and spontaneous organization during

casting. In the case of PProDOT-Hx_2, the irregular distribution of the two conformers within a polymer chain is expected to prevent efficient packing in the solid state.

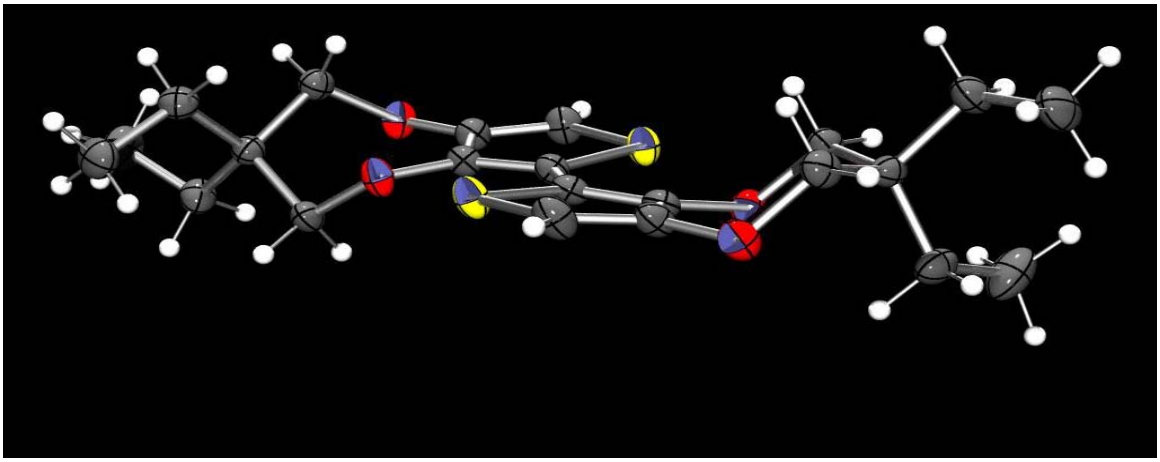

Figure 3-12. X-ray crystal structure of BisProDOT-Et_2 showing that a mixture of chair and twisted conformations are present.[7] Theoretical calculation (A. Perdomo) shows the difference of energy between the two conformers to be less than 2.5kJ/mole (k_BT at room temperature).

As demonstrated from the solution properties, the linear substituted PProDOTs are more twisted than branched PProDOTs. This intrachain twisted conformation is expected to easily hinder solid state packing and can also explain why linear PProDOTs form disordered aggregates. Oxidation during electrochemical switching will force a more planar conformation. Also, some authors suggest that in the oxidized state, π-dimers might form to stabilize the polaron and bipolaron state.[72] These two effects would allow the reordering observed during switching. Table 3-4 displays the absorption maximum for all polymers freshly cast from toluene, and following electrochemical doping.

Table 3-4. Solution, cast films and electrochemically oxidized and reneutralized films absorption properties (a) (sh)= shoulder

R=	**λ_{max} (nm)**	**E_g (eV)**	**λ_{max} (cast) (nm)**	**E_g (eV) (cast)**	**λ_{max} (nm) (switched)**	**E_g (eV) (redox)**
Hexyl	552, 585	2.01	548, 585	1.97	576	1.85
2-methylbutyl	602, 556, 517 (sh)[a]	1.98	623, 571, 533	1.88	625, 572, 533	1.88
2-ethylhexyl	552, 595	1.99	612, 559, 525	1.94	618, 564, 523	1.93

Films spray-cast onto ITO were studied by spectroelectrochemistry. The behavior is highly dependent on the type of substituents. As the steric bulk is increased, the optical changes with increasing potential become more abrupt. PProDOT-Hx_2 switches within 600mV potential increase, but PProDOT(2-methylbutyl)$_2$ and PProDOT(2-ethylhexyl)$_2$ switch within 350mV and 250mV, respectively (Figure 3-13). It was also observed that the absorption of PProDOT-Hx_2 does not exhibit a well defined vibronic structure, in contrast to the branched derivatives indicating that the hexyl polymer retains conformational disorder in the solid state, even following doping-induced rearrangement. Consistent with electrochemical results suggesting decreasing interchain interactions with steric bulk, the bandgap is increased from 1.85 eV for the hexyl polymer to 1.92eV for the ethylhexyl polymer.

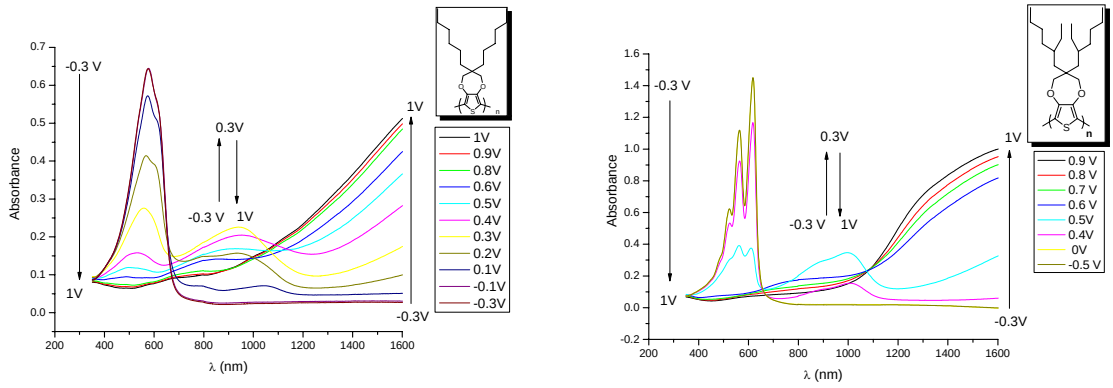

Figure 3-13. Spectroelectrochemistry experiment for PProDOT-Hx_2 (left) and PProDOT-(2-ethylhexyl)$_2$ (right) in 0.1M TBAP/ACN.

This trend is also reflected in the potential dependence of the luminance seen in Figure 3-14. The luminance of PProDOT-Hx_2 changes gradually (600mV) but the luminance of the branched polymers varies abruptly (<300mV). To compare the polymers electrochromic efficiency, coloration efficiency experiments were carried out on the polymers. The results are summed up in Table 3-5. All spray-cast alkyl substituted

PProDOTs films display high color contrast, but the charge required to achieve 95% of this contrast is higher in the linear polymers than the branched polymers, yielding higher coloration efficiencies for the branched polymers. This can be explained by the amorphous character of the branched polymers, with the bulky substituents providing more open volume for the dopant ions to penetrate the films, effectively decreasing the amount of capacitive currents contributions to the overall current during the polymers oxidation.

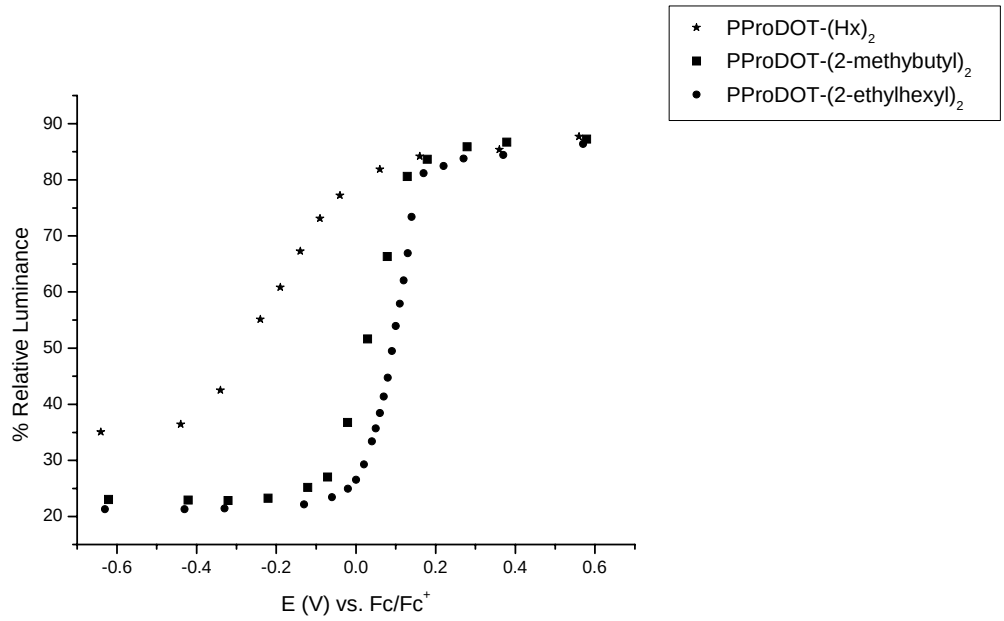

Figure 3-14. Luminance change with applied potential. All films were spray-coated from toluene solution switched between -0.5V and 1V to eliminate any doping-induced rearrangement effect. All films were ~150-200 nm thick as determined by profilometry.

Table 3-5. Coloration Efficiency study on PProDOT-R_2 spray-coated films.

Substituent	**Switching Time (s)**	**ΔY (%)**	**ΔT (%)**	**ΔOD**	**Qd (mC/cm^2)**	**CE (cm^2/C)**
Hexyl	0.37	58	65	0.52	0.61	850
2-methylbutyl	0.40	64	70	0.6	0.38	1020
2-ethylhexyl	0.73	70	79	N/A	0.87	1050

3.3.4. Conductivity Measurements

The conductivity of spray-coated PProDOT-R_2 polymer films was determined by the four-point probe method and the experimental parameters are reported in Table 3-6.. The measurements are taken as an average of multiple locations of the films, and reproducibility was checked by measuring conductivity on several films, leading to statistically consistent results.

Table 3-6. Conductivity measurements on spray-coated films gas phase doped with iodine. Measurements are average values of at least two films, taken at multiple locations of the films.

R=	**I (μA)**	**ΔV (mV)**	**Average Thickness (nm)**	**σ (S cm^{-1})**
Hexyl	N/A	N/A	N/A	5-10
2-methylbutyl	100	203, 185	286, 251	3.8, 4.2
2-ethylhexyl	10	300, 194	222, 234	0.3, 0.5

The conductivity decreases by an order of magnitude with increasing steric bulk, going from hexyl to the ethylhexyl side chains. The methyl butyl derivative surprisingly gives a similar conductivity to the linear hexyl substituted polymer. This can be explained by considering both inter and intrachain interactions. PProDOT-(2-methylbutyl)$_2$ has less interchain interactions but has a more planar chain conformation. It is therefore expected to have lower interchain charge transport through the polymer stacks than PProDOT-Hx_2, but higher intrachain charge transport along the polymer chains. Also, as discussed for the polymer electrochemistry, the inter-stack distance is expected to be shorter in the butyl polymers corresponding to a higher charge transport and conductivity between stacks. Overall, introducing larger substituents prevents efficient charge transport in the bulk material. This is the drawback of using branched substituents instead of longer alkyl chains to induce solubility.

3.4. High Performance Electrochromic Devices

Because of the properties described above, the dialkyl substituted PProDOTs, and in particular the branched compounds, seem ideal materials for high contrast electrochromic materials. This section describes the application of these polymers in an absorptive/reflective electrochromic device. The devices made with PProDOT-R_2 were prepared by Aubrey Dyer and Harun Turkcu. Figure 3-15 gives a schematic representation of the device construction.

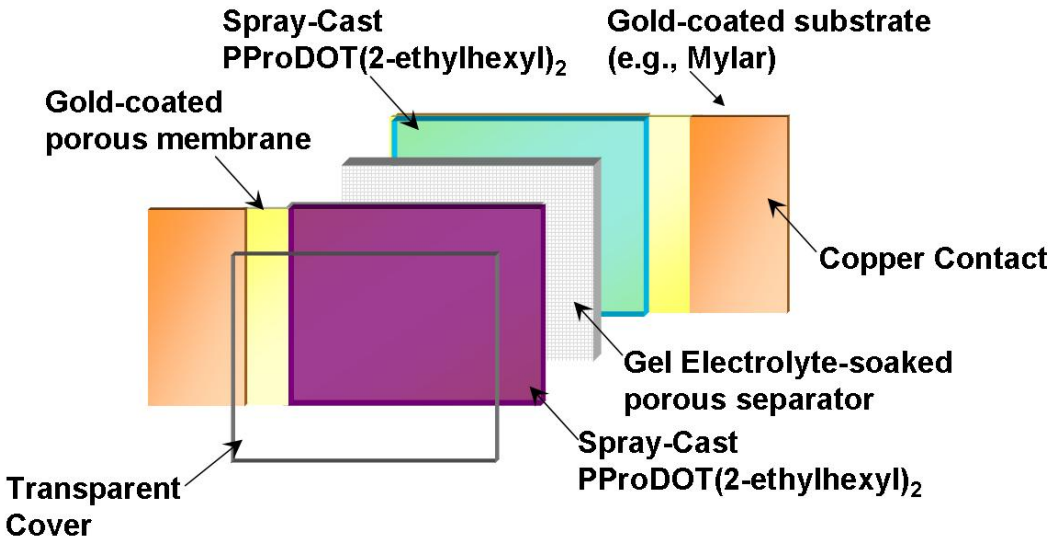

Figure 3-15. Schematic representation of a reflective/absorptive EC device using spray-coated PProDOT(2-ethylhexyl)$_2$ as the active and storage layer.

A porous gold membrane is coated with an electrochromic polymer (spray-coated PProDOT(2-ethylhexyl)$_2$), which constitutes the active layer of the device. The polymer is oxidized electrochemically prior to building the device. The device is assembled by placing the coated membrane on another layer of electrochromic polymer coated with gel electrolyte serving as a charge storage layer. Upon applying a negative bias to the device, the active polymer layer is reduced to the neutral form, and the device is absorptive to

visible light but highly reflective to NIR light, as shown in Figure 3-16.

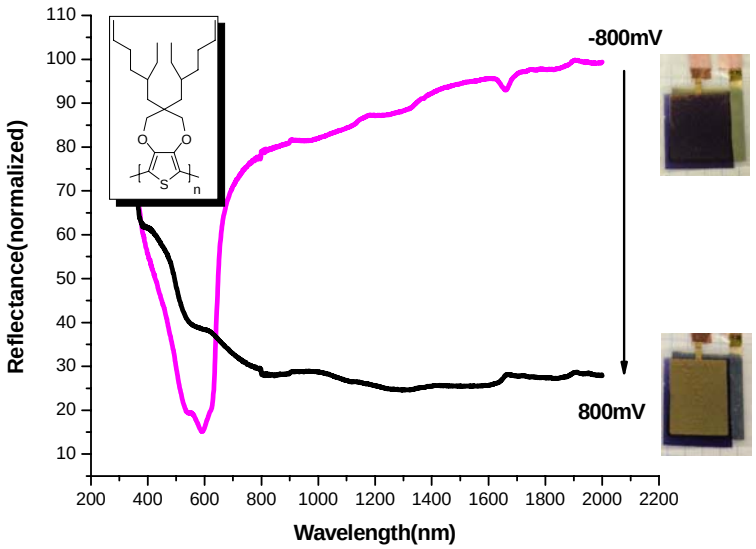

Figure 3-16. Reflectance plot for a reflective/absorptive EC device using spray-coated PProDOT(2-ethylhexyl)$_2$ as the active and storage layer.

3.5. Conclusion

A series of soluble, regiosymmetrically substituted branched alkyl PProDOTs were synthesized by Grignard Metathesis. Introduction of branching results in significant improvement in solubility and electrochromic properties, leading to faster switching rates, higher contrasts and significantly higher coloration efficiencies. The improvement is attributed mainly to a decrease of interchain interactions promoted by the bulkiness of the branched substituents, resulting in the highest coloration efficiencies, but also the lowest conductivities for PProDOT-(2-ethylhexyl)$_2$ polymer. In addition, the branched polymers display unusual spectroelectrochemical properties, with most optical changes obtained in a narrow optical window (<350mV), in contrast to linear substituted polymers, requiring much larger potential increase (>600mV). This behavior is attributed

to a more open morphology of the polymer films substituted with the bulky side chains, allowing easier penetration of dopant ions.

The introduction of branched alkyl substituents also affects the intrachain conformation of the chains. Optical absorption studies on solutions indicate small Stokes shift, well-resolved vibronic features with a dominant 0-0 transition, pointing to a mostly planar conformation of the polymer chains. The chains planarity allows easy interchain ordering of the polymer chains in the solid state, evidenced from the large bathochromic shift in absorption and a significant change of color observed during spray-casting of the polymers.

In Chapter 5, the synthesis of chiral equivalents of these polymers will be described. These polymers can be studied using chiroptical techniques which are powerful tools to examine interchain and intrachain interactions, affording better understanding on how the branched substituents affect the electrochromic properties.

3.6. Chapter Synthetic Details

3,4-dimethoxythiophene: In a 250 mL 3-neck round bottom flask equipped with a reflux condenser 6.2 g (0.27 mol) of sodium was slowly dissolved in 90 mL of methanol under argon. Then 4.2 g (0.053 mol) of CuO, 0.9 g (0.0053 mol) of KI, and 13 g (0.053 mol) of 3,4-dibromothiophene were added. The black mixture was refluxed for 3 days. 0.9 g (0.0053 mol) of KI was added and the mixture was refluxed for an additional 24 hours. The dark mixture was cooled, filtered through Büchner, diluted with 150 mL of water, and extracted 3 times with ether. The combined ether layers were washed with water and dried with magnesium sulfate. The ether was removed under vacuum, and the crude product was purified by vacuum distillation (80-82 °C / 1.0 mm Hg), (lit. 59-65 °C

/ 0.5 mm Hg) to yield 5.0 g (65 %) of product. ^{1}H NMR (300 MHz, $CDCl_3$) δ 6.2 (s, 2H), 3.8 (s, 6H).

General Procedure for the synthesis of alkylated diethyl malonate: In a 5 L flame dried 3 neck round bottom flask equipped with an argon inlet, a condenser, and an addition funnel were combined 2L of dry THF, 3.5 mol of alkyl bromide (3eq), and 3.5 mol of NaH. The flask was cooled to 0 °C and 1.15 mol of freshly distilled diethyl malonate was added dropwise through the addition funnel. When the addition of the malonate was completed, the mixture was refluxed overnight. The flask was then cooled at 0 °C and the remaining sodium hydride was quenched by adding water dropwise. The mixture was then poured into brine (2 L), extracted two times with ether, and washed with brine. The solvent and the alkyl bromide were removed under vacuum. The crude oil obtained was then used in the next step without further purification.

General Procedure for the synthesis of diols: In a 5 L flame dried 3 neck round bottom flask equipped with an argon inlet, a condenser, and an addition funnel, were combined 2 L of dry ethyl ether and 1.7 mol of $LiAlH_4$ powder. The crude dialkyl malonate (1.13 mol) was added dropwise at 0 °C. When the addition was completed, the mixture was allowed to warm to room temperature. The reaction mixture was stirred under argon for 20 hr. The excess $LiAlH_4$ was SLOWLY quenched with one liter of 1M HCl at 0°C. The aqueous phase was extracted with 2×500 mL ether and the combined organic phases were washed with water (4×500 mL). The organic phase was dried with magnesium sulfate and the solvent was evaporated under vacuum. The resulting product is purified by column chromatography (90% DCM/10% acetonitrile, product revealed

with vanillin dip as black spots). After purification, yield obtained is 25-50% for branched derivatives, 65-80% for the linear derivatives.

2,2-Dihexylpropane-1,3-diol: White crystalline solid. ^{1}H NMR (300 MHz, $CDCl_3$) δ 3.59 (d, 4H, *J*= 5.3 Hz), 2.39 (t, 2H, *J*= 5.3 Hz), 1.40-1.10 (m, 20H), 0.90 (t, 6H, *J*= 7.3 Hz); ^{13}C NMR (75 MHz, $CDCl_3$) δ 69.7, 41.2, 32.0, 31.1, 30,5, 29.9, 23.1, 22.9, 14.3; HRMS calculated for $C_{15}H_{32}O_2$: 245.2481 Found: 245.2475 Elemental Anal. Calcd for $C_{15}H_{32}O_2$: C 73.71; H 14.20. Found: C 74.12; H 14.18.

2,2-Bis-(2-methylbutyl)-propane-1,3-diol: white amorphous solid. ^{1}H NMR (300 MHz, $CDCl_3$) δ 0.73-0.97 (m, 12H), 1.05-1.26 (m, 4H), 1.26-1.51 (m, 6H), 2.21-2.32 (br, 2H), 3.51-3.66 (br, 4H); ^{13}C NMR (75 MHz, $CDCl_3$) δ 11.73, 21.92, 29.56, 32.21, 39.18, 42.82, 70.21.

2,2-Bis-(2-ethylhexyl)-propane-1,3-diol: clear oil. ^{1}H NMR (300 MHz, $CDCl_3$) δ 3.65 (s, 4H), 2.41 (s, 2H), 1.40-1.10 (m, 22H), 0.95-0.80 (m, 12H); ^{13}C NMR (75 MHz, $CDCl_3$) δ 70.1, 42.8, 37.1, 34.9, 33.7, 29.0, 27.9, 23.4, 14.4, 10.8 HRMS Calcd for $C_{19}H_{41}O_2$ $(M+H)^+$ 301.3106 Found 301.3103; Elemental Anal. Calcd for $C_{19}H_{40}O_2$ C 75.94; H 13.42. Found C 75.95 H 12.35.

General procedure for the transetherification of 3,4-dimethoxythiophene with diols: 21 mmol of 3,4-dimethoxythiophene, 22 mmol of diol, 2.1 mmol of *p*-toluenesulfonic acid, and 200 mL toluene were combined in a 500 mL flask equipped with a soxhlet extractor with type 4A molecular sieves or $CaCl_2$ in a cellulose thimble. The solution was refluxed overnight. The reaction mixture was cooled and washed once with water. The toluene was removed under vacuum, and the crude product was purified by column chromatography on silica gel with 3:2 hexanes / methylene chloride.

3,3-Dihexyl-3,4-dihydro-2*H*-thieno[3,4-*b*][1,4]dioxepine (ProDOT(Hx)$_2$): clear oil (95 % yield); ^{1}H NMR (300 MHz, $CDCl_3$) δ 6.42 (s, 2H), 3.88 (s, 4H), 1.45-1.20 (m, 20 H), 0.95-0.82 (m, 6H). ^{13}C NMR (75 MHz, $CDCl_3$) δ 149.9, 104.9, 77.8, 43.9, 32.0, 32.0, 30.4, 23.0, 22.9, 14.3. HRMS calculated for $C_{19}H_{32}O_2S$: 324.2123 Found: 324.2120. Elemental Anal. Calcd for $C_{19}H_{32}O_2S$: C 70.32; H 9.94; S 9.88 Found: C 70.48; H 10.48; S 9.78.

3,3-bis(2-methylbutyl)-3,4-dihydro-2*H*-thieno[3,4-*b*][1,4]dioxepine (ProDOT(2-methylbutyl)$_2$): clear oil (70% yield); ^{1}H NMR (300 MHz, $CDCl_3$) δ 0.77-1.01 (m, 12H), 1.07-1.63 (m, 10H), 3.79-4.05 (m, 4H), 6.42 (s, 2H); ^{13}C NMR (75 MHz, $CDCl_3$) δ11.69, 22.06, 22.08, 29.66, 29.68, 32.17, 32.21, 40.85, 40.88, 45.57, 78.24, 78.35, 78.39, 104.65, 149.92.

3,3-Bis-(2-ethylbutyl)-3,4-dihydro-2*H*-thieno[3,4-*b*][1,4]dioxepine (ProDOT(2-ethylbutyl)$_2$): The crude oil obtained was purified by column chromatography (3:2) hexanes/dichloromethane followed by another column using 3:1 hexanes/dichloromethane to afford a clear oil (66% yield). ^{1}H NMR (300MHz, $CDCl_3$) δ 0.78-0.95 (t, 12H), 1.21-1.47 (m, 14H), 3.93 (s, 4H), 6.42 (s, 2H); ^{13}C NMR (75MHz, $CDCl_3$) δ 10.94, 27.57, 35.17, 38.23, 45.44, 77.98, 104.66, 149.97.

3,3-Bis-(2-ethylhexyl)-3,4-dihydro-2*H*-thieno[3,4-*b*][1,4]dioxepine (ProDOT(2-ethylhexyl)$_2$): The crude oil obtained was purified by column chromatography (3:2) hexanes/dichloromethane followed by another column using 3:1 hexanes/dichloromethane to afford 6.0 g of clear oil (57%). ^{1}H NMR (300MHz, $CDCl_3$) δ 6.43 (s, 2H), 3.93 (s, 4H), 1.2-1.5 (m, 22H), 0.75-1.0 (m, 12H); ^{13}C NMR (75MHz, $CDCl_3$) δ 150.0, 104.61, 78.0 (t), 45.5, 38.7, 35.0, 33.8, 29.0, 28.0, 23.3, 14.4, 10.8.;

HRMS Calcd for $C_{23}H_{40}O_2S$ 380.2749. Found 380.2753; HRMS calculated for $C_{23}H_{40}O_2S$: 380.2749 Found: 380.2753. Elemental Anal. Calcd for $C_{23}H_{40}O_2S$: C 72.58; H 10.59; O 8.41; S 8.42. Found: C 72.78; H 10.30; O 8.68; S 8.24.

General procedure for the bromination of ProDOT-R_2: In a 2-neck 250 mL round bottom flask filled with 80 mL chloroform, 1.5g (2.1 mmol) of ProDOT was added and the solution was bubbled under argon for 60 minutes. Then 1.12 g (6.24 mmols) *N*-bromosuccinimde was added and the solution was stirred for 20 hr. After completion, the solvent was removed by rotary evaporation under reduced pressure and the resulting residue was purified by column chromatography on SiO_2 with (4:1) hexanes/dichloromethane .

6,8-Dibromo-3,3-Dihexyl-3,4-dihydro-2*H*-thieno[3,4-*b*][1,4]dioxepine (ProDOT(Hx)$_2$Br$_2$): clear oil obtained (91% yield).^{1}H NMR (300MHz, $CDCl_3$) δ 3.93 (s, 4H), 1.45-1.15 (m, 20H), 0.90 (t, 6H, *J*= 7.0 Hz); ^{13}C NMR (75MHz, $CDCl_3$) δ 147.4, 104.8, 90.8, 78.3, 44.2, 31.9, 30.3, 22.9, 14.3; HRMS calculated for $C_{19}H_{30}O_2SBr_2$: 480.0333 Found: 480.0334. Elemental Anal. Calcd for $C_{19}H_{30}O_2SBr_2$: C 47.31; H 6.27; S 6.65; Br 33.13. Found: C 47.83; H 6.79; S 6.88; Br 32.79.

6,8-Dibromo-3,3-bis(2-methylbutyl)-3,4-dihydro-2*H*-thieno[3,4-*b*][1,4]dioxepine (ProDOT(2-methylbutyl)$_2$Br$_2$): product obtained as a clear oil (86%).^{1}H NMR (300MHz, $CDCl_3$) δ 0.8-1.0 (m, 12H), 1.08-1.27 (m, 2H), 1.27-1.59 (m, 8H), 3.86-4.10 (m, 4H); ^{13}C NMR (75MHz, $CDCl_3$) δ 11.67, 21.93, 21.96, 29.67, 29.70, 32.08, 32.13, 40.81, 40.83, 40.85, 45.87, 78.98, 79.07, 79.11, 90.64, 147.31.

6,8-Dibromo-3,3-Bis-(2-ethylbutyl)-3,4-dihydro-2*H*-thieno[3,4-*b*][1,4]dioxepine (ProDOT(2-ethylbutyl)$_2$Br$_2$): The crude oil obtained was purified by column

chromatography (4:1) hexanes/dichloromethane to afford 1.2 g of clear oil (81%). ^{1}H NMR (300MHz, $CDCl_3$) δ 0.77-0.92 (t, 12H), 1.2-1.45 (m, 14H), 4.0 (s, 4H); ^{13}C NMR (75MHz, $CDCl_3$) δ 10.92, 27.48, 35.19, 38.27, 45.72, 78.59, 90.65, 147.30; HRMS Calcd for $C_{23}H_{38}O_2SBr_2$ 483.0386. Found 483.0380; Elemental Anal. Calcd for $C_{19}H_{30}O_2SBr_2$: C 47.31; H 6.27 Found: C 47.43; H 6.40.

6,8-Dibromo-3,3-Bis-(2-ethylhexyl)-3,4-dihydro-2*H*-thieno[3,4-*b*][1,4]dioxepine (ProDOT(EtHx)$_2$Br$_2$): The crude oil obtained was purified by column chromatography (4:1) hexanes/dichloromethane to afford a clear oil (80 %). ^{1}H NMR (300MHz, $CDCl_3$) δ 4.00 (s, 4H), 1.15-1.5 (m, 22H), 0.8-1.0 (m, 12H); ^{13}C NMR (75MHz, $CDCl_3$) δ 147.3, 90.5, 78.6, 45.8, 38.8, 35.0, 29.0, 28.0, 23.3, 14.4, 10.8; HRMS Calcd for $C_{23}H_{38}O_2SBr_2$ 538.0940. Found 538.0944; Elemental Anal. Calcd for $C_{23}H_{38}O_2SBr_2$: C 51.31; H 7.11; S 5.96 Found: C 51.28; H 7.00; S 6.04.

General Procedure for Grignard metathesis polymerization of ProDOT-R$_2$Br$_2$: In a flame dried 250 mL round bottom flask, dry THF (150 mL) and 3.0 g (0.34 mmol) of ProDOT(R)$_2$Br$_2$ was added under argon. Then methyl magnesium bromide (3.75 mL, 3.45 mmol, 0.918 M) was slowly added by syringe. The mixture was then refluxed for 2 hrs. After, the flask was cooled and Ni(dppp)Cl_2 (18.4 mg, 0.0341 mmol) was added and the reaction was heated at reflux overnight under argon. The solution was then cooled and the polymer was precipitated by pouring the solution in 400 mL methanol. The dark purple solid was purified by soxhlet extraction with methanol for 24 hr, hexanes for 48 hr, and finally chloroform for 24 hr. The chloroform was evaporated under reduced pressure to afford purple solid.

Poly(3,3-Dihexyl-3,4-dihydro-2*H*-thieno[3,4-*b*][1,4]dioxepine) (PProDOT(Hexyl)$_2$): shiny brown solid obtained (66 %). ^{1}H NMR (300 MHz, $CDCl_3$) δ 3.95 (bs, 4H), 1.62-1.2 (m, 20H), 0.97-0.80 (m, 6H); ^{13}C (75 MHz, benzene-d_6) δ 146.4, 115.3, 78.0, 44.3, 32.6, 31.0, 23.5, 14.8; Elemental Anal. Calcd for $(C_{19}H_{30}O_2S)_{164}HBr$: C 70.65; H 9.38; S 9.91, Br 0.15 Found: C 69.87; H 9.99; S 9.52; Br 0.15; Ni <0.01. GPC analysis: M_n= 38,100, M_w=65,900 PDI=1.73.

Poly(3,3-bis(2-methylbutyl)$_2$-3,4-dihydro-2*H*-thieno[3,4-*b*][1,4]dioxepine) (PProDOT(2-methylbutyl)$_2$): shiny brown solid obtained (60%). ^{1}H NMR (300 MHz, $CDCl_3$) δ 0.82-1.16 (br, 12H), 1.16-1.3 (br, 4H), 1.3-1.5 (br, 4H), 1.5-1.65 (br, 2H), 3.9-4.15 (br, 4H); ^{13}C (75 MHz, benzene-d_6) δ 12.15, 22.61, 30.10, 32.67, 32.77, 41.22, 45.93, 78.72, 114.98, 145.87; GPC analysis: M_n=17,000, M_w=30,000 PDI= 1.76.

CHAPTER 4
SYNTHETIC CONTROL OF ORDER IN BRANCHED ALKOXYMETHYL POLY(3,4-PROPYLENEDIOXYTHIOPHENES) (PPRODOT-$(CH_2OR)_2$)

4.1. Introduction

The previous chapter demonstrated that increasing the steric bulk in branched alkyl PProDOT polymers, these having all carbon based substituents, results in a decrease of π-stacking interactions and possibly an increase of the distance between π-stacks as well. This leads to polymers with higher solubility in organic solvents, higher contrast and fast switching electrochromic devices due to the fast diffusion of dopant ions into the polymer films being facilitated. To enhance the polymer solubility and further optimize the electrochromic properties, alkoxymethyl spacers were placed between the 2- position of the ProDOT propylene bridge and the branched alkyl side chains to provide ether linked substituents. The presence of this spacer in the side chains will provide more steric hindrance and prevent ordering due to the conformational flexibility of the alkoxy chains. Combined with the steric bulk of the branched side chains should lead to a strong decrease in interchain interactions, and more disorder in solution and solid state. On the other hand, as the branching groups are further away from the seven-membered ring and have more flexibility than the rigid alkyl group, less effect of the branching group on the ring conformation could be expected, leading to important intrachain and interchain changes. Figure 4-1 displays the structures described and studied in this Chapter. PProDOT-$(CH_2OC_{18}H_{37})_2$, synthesized by Ben Reeves, is used to demonstrate the differences between branched and linear polymers.

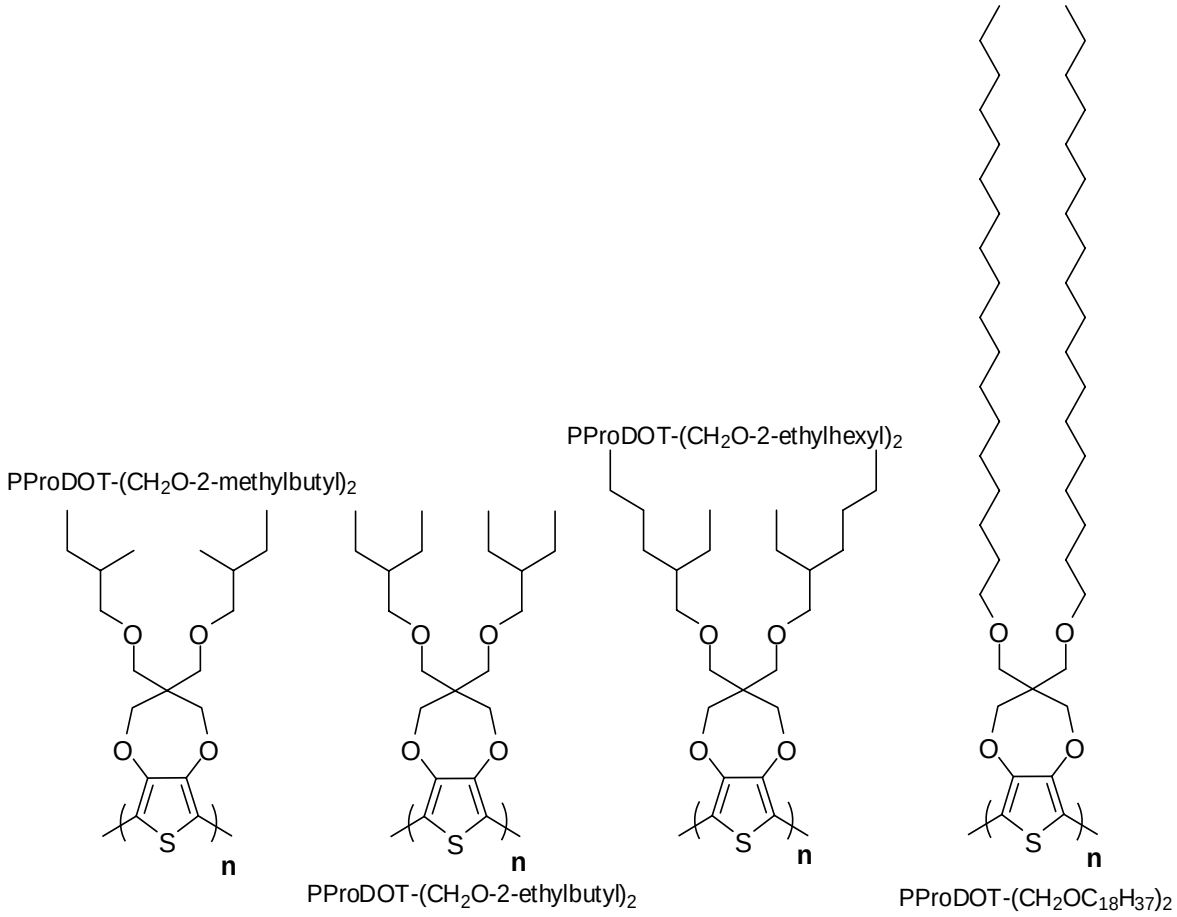

Figure 4-1. Family of branched dialkoxymethyl substituted PProDOTs. PProDOT-$(CH_2OC_{18}H_{37})_2$ was synthesized by Ben Reeves and will be used for comparison and discussion of branching effects.

4.2. Electropolymerized PProDOT-$(CH_2OR)_2$

4.2.1. Electropolymerizable Monomer Synthesis

An advantage of the synthesis of dialkoxymethyl substituted ProDOTs, compared to the alkyl substituted polymers, is their ease of synthesis. As shown in Figure 4-2, the substituents are placed in the last step of the synthesis using a simple Williamson etherification between the corresponding alcohol and PProDOT-$(CH_2Br)_2$. PProDOT-$(CH_2Br)_2$ is prepared by transetherification between 3,4-dimethoxythiophene and 2,2-bis(bromomethyl)-propane-1,3-diol, both commercially available. The alkyl substituted

ProDOTs, described in Chapter 3 are more difficult to synthesize, as the disubstituted 2,2-propane-1,3-diol must be prepared. On the contrary, many linear and branched alcohols are commercially available. Also, in the case of branched derivatives, the diol synthesis has a low overall yield, which is a problem when the starting materials are expensive or difficult to obtain.

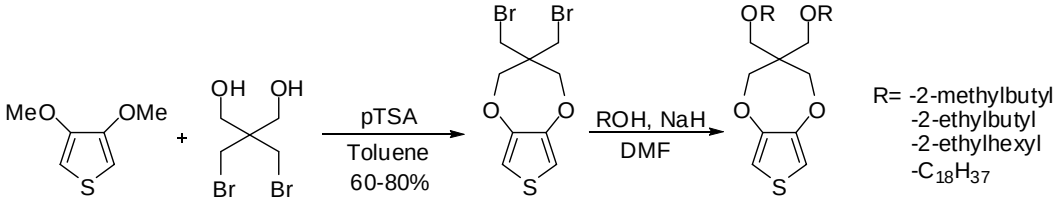

Figure 4-2. Synthesis of electropolymerizable alkoxymethyl substituted ProDOTs. Branched 2-methylbutyl and 2-ethylhexyl derivatives are prepared from racemic reagents.

4.2.2. Electrodeposition and Electrochemistry

The alkoxymethyl substituted ProDOT electropolymerizable monomers were electrodeposited on a platinum button from a 0.01M monomer solution in 0.1M TBAP/ACN. Figure 4-3 shows the electrodeposition of PProDOT-(CH_2O-2-ethylhexyl)$_2$.

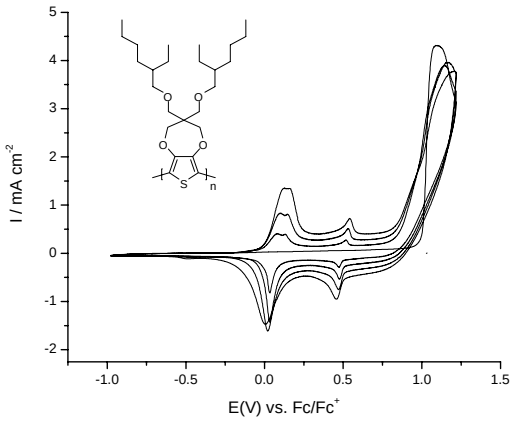

Figure 4-3. Electrodeposition of PProDOT(CH_2O-2-ethylhexyl)$_2$ on Pt Button. The film was deposited from a 0.01M monomer solution in 0.1M TBAP/ACN, at a scan rate of 50 mV/s.

After electrodeposition on platinum button electrodes, the polymers oxidations in monomer-free electrolyte were compared (Figure 4-4). A similar trend to the alkyl derivatives was observed, where increasing the steric bulk of the side chains results in an increase of the onset and peak oxidation potentials. This shift is consistent with less interchain interactions when the substituents are bulkier. Again, as seen with the alkyl substituted PProDOT, the ethylhexyloxymethyl derivative has a lower peak oxidation potential than PProDOT-$(CH_2O$-2-ethylbutyl$)_2$, although the ethylhexyloxy chains are bulkier. This behavior might be explained by easier diffusion of the dopant ions between polymer stacks.

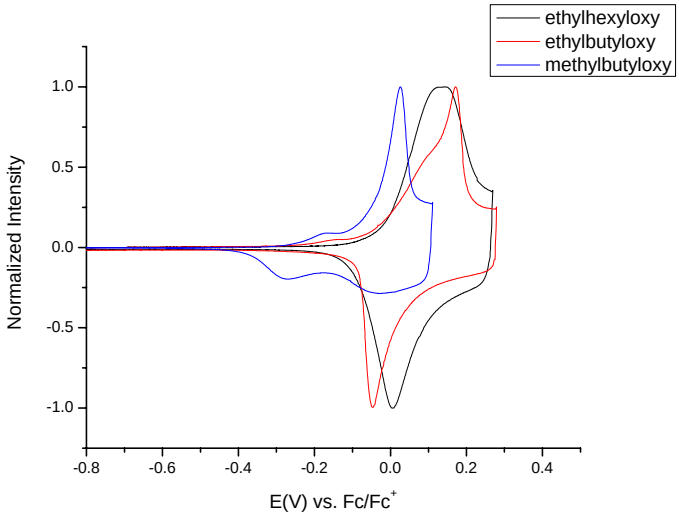

Figure 4-4. Polymer oxidation in the PProDOT-$(CH_2OR)_2$ series. All the polymers were deposited by cyclic voltammetry at 50mV/s scan rate from 0.01M monomer solution in 0.1M TBAP/ACN. The polymer oxidation curves were recorded in monomer-free electrolyte at 50mV/s.

Table 4-1 compares the polymer oxidation values of the PProDOT-R_2 and PProDOT-$(CH_2OR)_2$ series. Overall, introduction of the oxygens does not seem to have a strong effect on the polymer oxidation, except in the case of the methyl branched polymers. PProDOT-(2-methylbutyloxymethyl)$_2$ has a significantly poorer reversibility in

oxidation than PProDOT-(2-methylbutyl)$_2$. In the case of the bigger branching ethyl group, the oxidation peaks are all quasi-reversible. This trend indicates that the branching groups are mainly responsible for the increase in polymer oxidation due to steric bulk. The introduction of the oxymethyl spacer seems to have a minor effect, especially with small branching groups, where a broad two-peak reduction suggests different chain conformations or aggregates exist in the oxidized state.

Table 4-1. Comparison of alkyl and alkoxymethyl substituted PProDOTs polymer oxidation. Potentials are vs. Fc/Fc^+.

PProDOT Substituents	**E_{onset} monomer**	**$E_{1/2}$ (mV) Polymer**	**ΔE_p (mV) Polymer**	**$I_{[ox],\,p}$ / $I_{[red],\,p}$ Polymer**
Butyl	0.99 V	-65 (-180[a])	129 (281)	2.15
Hexyl	0.97 V	-66(-165 [a])	54 (252)	1.12
2-methylbutyl	0.88 V	-3	135	1.14
2-methylbutyloxymethyl	1.02V	0 (-269)	50 (295)	3.51
2-ethylbutyl	0.98 V	155	107	1
2-ethylbutyloxymethyl	0.97V	52	124	1
2-ethylhexyl	1.03 V	28	34	1.3
2-ethylhexyloxymethyl	1.01V	75	139	1

4.3. Chemically Polymerized Soluble PProDOT-($CH_2OR)_2$

4.3.1. Synthesis and Polymer Characterization

After bromination of the electrochemically polymerizable monomer with N-bromosuccinimide, the soluble polymers were obtained by Grignard Metathesis (Figure 4-5).

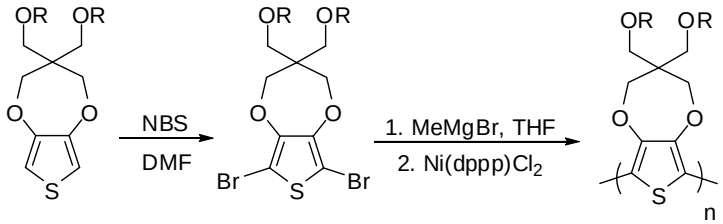

Figure 4-5. Polymerization of PProDOT-($CH_2OR)_2$ by Grignard Metathesis.

After purification by Soxhlet extraction with MeOH and hexanes, the polymers were extracted with chloroform, and obtained as shiny brown solids after solvent

evaporation. The polymers are highly soluble in chloroform, toluene, and THF. For PProDOT-(CH_2O-2-methylbutyl)$_2$, heat was required to obtain dissolution of the polymer chains. The polymer chains remained in solution but a change of color from red to purple suggests aggregation might occur as the solutions are cooled to room temperature. The polymer structures were confirmed by ^1H and ^{13}C NMR. GPC analysis of the polymers show molecular weights between 10,000 and 20,000 g mol^{-1} (Table 4-2), corresponding to a molecular structure of more than 30 repeating units.

Table 4-2. Molecular weight analysis of GriM polymerized PProDOT-(CH_2OR)$_2$. The molecular weights are determined vs. polystyrene standards.

R	M_n (g mol^{-1})	X_n	M_w (g mol^{-1})	PDI
CH_2O-2-methylbutyl	N/A	N/A	N/A	N/A
CH_2O-2-ethylbutyl	12,400	33	17,500	1.4
CH_2O-2-ethylhexyl	13,000	30	22,200	1.7

4.3.2. Solution properties

The solution properties were studied by UV-Vis absorbance and fluorescence spectroscopy. Figure 4-6 shows the spectrum for PProDOT-(CH_2O-2-methylbutyl)$_2$ and PProDOT-(CH_2O-2-ethylhexyl)$_2$ in xylenes solutions.

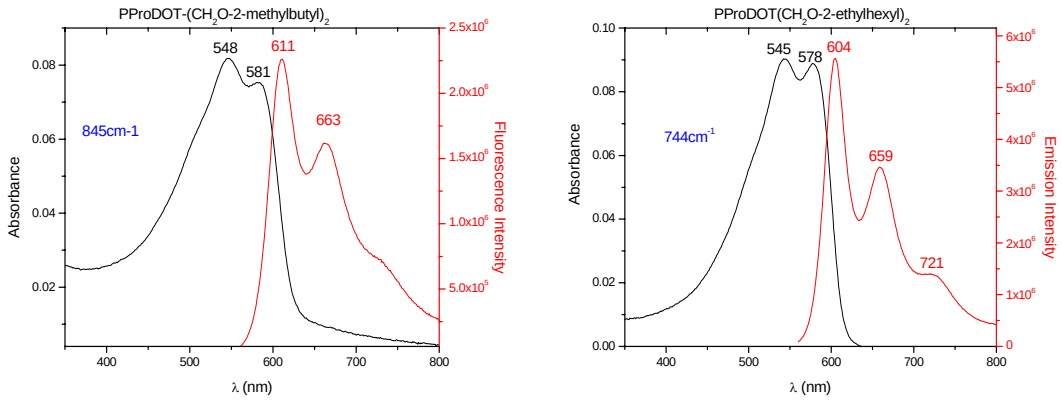

Figure 4-6. Absorption and photoluminescence spectrum of PProDOT(CH_2O-2-methylbutyl)$_2$ and PProDOT(CH_2O-2-ethylhexyl)$_2$. For fluorescence, λ_{ex}=550nm.

UV-Vis absorption and fluorescence results for PProDOT(CH_2O-2-methylbutyl)$_2$, PProDOT(CH_2O-2-ethylbutyl)$_2$ and PProDOT(CH_2O-2-ethylhexyl)$_2$ are summarized in Table 4-3. The alkoxymethyl substituted polymers have clear vibronic features, attributed to the 0-0 and 0-1 vibrational transitions. The 0-1 vibronic transition is the dominant vibronic feature, in contrast with branched alkyl substituted PProDOTs, where the 0-0 transition is dominant. In PProDOT-Hx_2, the two vibronic transitions have similar intensities. As described in Figure 3-12, stronger higher energy vibronic transitions for alkoxymethyl substituted polymers (and PProDOT-Hx_2) suggest these polymers have more intrachain conformational disorder.

Table 4-3. Optical properties of alkoxymethyl substituted PProDOTs in toluene solution. Also indicated in parenthese is the relative intensity of the vibronic bands

R	λ_{max} absorption (nm)	λ_{max} emission (nm)	Stokes Shift (cm^{-1})	Φsol.[a]
2-methylbutyl	548 (*1*), 581 (*0.92*)	611 (*1*), 663 (*0.71*)	845	0.18
2-ethylbutyl	545 (*1*), 584 (*0.99*)	605 (*1*), 658 (*0.55*), 721 (*0.17*)	595	0.37
2-ethylhexyl	545 (*1*), 578 (*0.98*)	604 (*1*), 659 (*0.62*), 721 (0.25)	744	0.34

(a) Quantum yield was calculated using sulforhodamine excited at 550 nm as standard.

PProDOT(CH_2O-2-ethylbutyl)$_2$ and PProDOT(CH_2O-2-ethylhexyl)$_2$ in solution have quantum yields of 0.34 and 0.37, similar to values obtained for PProDOT-R_2. The minimal dependence of the quantum yields on the polymer structure suggests that interchain interactions are not involved and the chains are molecularly dissolved. If interchain interactions were involved in solution, significant differences of quantum yields would be expected as interchain distance varies with steric bulk. PProDOT-(CH_2O-2-methylbutyl)$_2$, on the other hand, has a lower quantum yield of 0.18. The decreased quantum yield is consistent with interchain quenching in solution as the polymer has low solubility at room temperature and required heating to dissolve. Another possible explanation is that the more twisted polymer conformation allows for intrachain

folding. Intrachain quenching between chromophores within a single chain will lead to energy transfer to traps, leading to a decrease in quantum yield.

4.3.3. Optoelectronic Properties of Solution Processed Films

Films were spray-cast from either toluene or chloroform solution (5mg/ mL, 12 psi) onto ITO-coated glass slides. Absorbance was recorded after casting and following redox switching of the films. Results for the alkoxymethyl substituted PProDOTs are presented in Table 4-4, and in Figure 4-7 for PProDOT(CH_2O-2-methylbutyl)$_2$ and PProDOT-(CH_2O-2-ethylhexyl)$_2$.

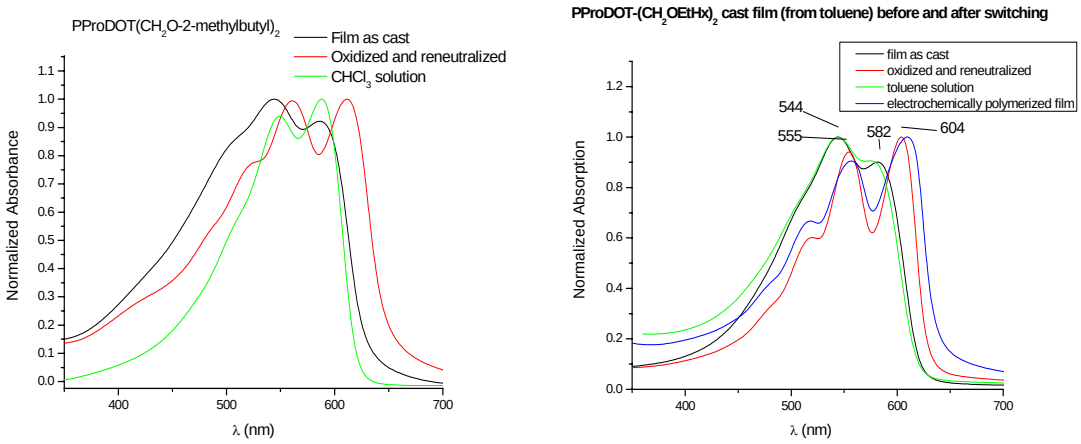

Figure 4-7. Doping/Casting induced rearrangement in linear vs. branched alkyl substituted PProDOTs. (left) PProDOT(CH_2O-2-methylbutyl)$_2$; (right) PProDOT-(CH_2O-2-ethylhexyl)$_2$.

The behavior of PProDOT-(CH_2O-2-ethylhexyl)$_2$ and PProDOT-(CH_2O-2-ethylbutyl)$_2$ is similar to the one observed in PProDOT-Hx_2. Upon casting, the polymer films retain a solution conformation, as they have similar absorption spectrum. PProDOT(CH_2O-2-methylbutyl)$_2$ spray-cast film, although its absorbance maxima are identical for both cast film and solution, has a broader absorption spectrum dominated by the 0-1 vibronic transition, different from chloroform solution where the 0-0 vibronic

features dominate. This suggests that the polymer forms disordered aggregates with limited interchain interactions and that the individual chains are highly twisted.

Upon switching the polymer film electrochemically, the absorption spectra of the spray-cast films undergo a bathochromic shift, the optical bandgap is lowered, and the vibronic features become better resolved. The well-resolved vibronic structure supports a planar intrachain conformation of the polymer chains, which can also explain the absorption bathochromic shift and lower bandgap. An increase of interchain interactions after redox switching is also likely, as the planarity favor interchain ordering of the polymer chains.

Table 4-4. Optical properties of PProDOT(CH_2O-2-alkyloxymethyl)$_2$ polymers in solution, films as cast and films following electrochemical oxidation/reneutralization cycle.

R=	**λ_{max} (toluene)**	**E_g (Toluene)**	**λ_{max} (cast)**	**E_g (cast)**	**λ_{max} (switched)**	**E_g (switched)**
2-methylbutyl	588, 549	2.0	586, 544	1.96	612, 561, 528 (sh)	1.91
2-ethylbutyl	579, 545	2.01	581, 544	1.98	607, 556, 520	1.95
2-ethylhexyl	575, 544	2.01	582, 544	2.0	604, 555, 520	1.97

The spray-cast films were then analyzed by spectroelectrochemistry. For the branched ethylhexyloxymethyl polymer, shown in Figure 4-8, a similar effect to the branched alkyl analogs is observed, with sharp optical changes as the potential is increased. For PProDOT-(CH_2O-2-ethylhexyl)$_2$, most optical changes are obtained with less than 150 mV potential increase. This is sharper than the ethylhexyl alkyl substituted polymer, possibly indicating a synergistic effect between the steric bulk from the ethyl branching group and the flexibility provided by introduction of the oxygens. In contrast the linear octadecyloxymethyl substituted polymer, also shown in Figure 4-8, switches

gradually and requires 600mV potential increase to obtain similar optical changes. These differences can be rationalized in terms of morphology of the polymer films. In the case of the octadecyloxy methyl substituted polymer, crystallization of the side chains, evidenced by melting and crystallizations transitions in the DSC thermal analysis, hinders the penetration of the dopant ions inside the polymer film.[73] In the case of the bulky substituents, the interchain and interstack distance increase, leaving more space for the dopant ions to penetrate.

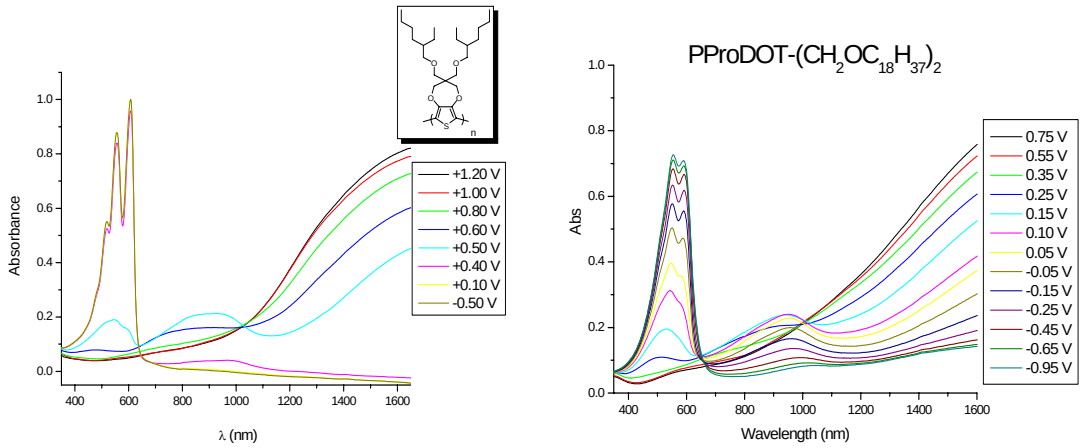

Figure 4-8. Spectroelectrochemistry experiment for PProDOT-(CH_2O-2-ethylhexyl)$_2$ (left) and PProDOT-($CH_2OC_{18}H_{37}$)$_2$ (right).

Luminance studies on spray-cast films confirm the trend observed in the spectroelectrochemistry experiment. Figure 4-9 shows the overlayed luminance plot as a function of potential of alkoxymethyl PProDOT polymers. The alkyl substituted PProDOT-(2-ethylhexyl)$_2$ is added for comparison. As expected, as the steric bulk is increased by introducing larger branching, the optical changes with potential are sharper. This demonstrates that the branching group is responsible for these unusual optical changes. The introduction of alkoxy in place of alkyl substituents seems to reinforce this

effect as the ethylhexyloxymethyl polymer display sharper optical changes than the ethylhexyl polymer.

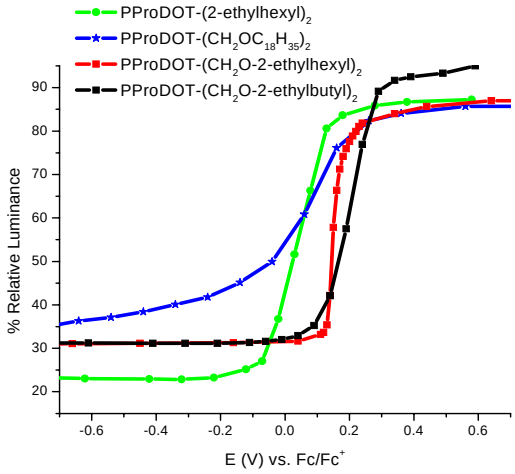

Figure 4-9. Luminance change vs. applied potential in PProDOT($CH_2OR)_2$ polymers. All films were spray-coated from toluene solution switched between -0.5V and 1V to eliminate any doping-induced rearrangement effect. All films were ~150-200 nm thick as determined by profilometry.

To evaluate the efficiency of the electrochromic transition, coloration efficiency experiments on the spray-cast films were carried out (Table 4-5).

Table 4-5. Coloration Efficiency of PProDOT-($CH_2OR)_2$ films sprayed on ITO-coated glass slides.

Substituent	**Switching Time (s)[a]**	**ΔT (%)**	**ΔOD**	**Qd (mC/cm^2)**	**CE (cm^2/C)**
2-methylbutyl	0.7	72	1.1	1.2	923
2-ethylbutyl	0.4	70	0.8	0.65	1240
2-ethylhexyl	0.6	80	1.12	0.9	1235

[a] time to achieve 95% of total color contrast; [b] color contrast between fully oxidized and neutral states; [c] $\log(T_{ox}(95\%)/T_{red})$

The results indicate that as the branching size increases, the coloration efficiency increases as well. PProDOT-(CH_2O-2-methylbutyl)$_2$, compared to PProDOT-(CH_2O-2-ethylhexyl)$_2$, requires more charges to obtain a similar change of optical density. The switching time is also smaller for ethylhexyl polymer. The increasing coloration

efficiency trend can therefore be explained by the increased interchain and interstacks distance, allowing more efficient penetration of the dopant ions into the polymer films.

4.3.4. Conductivity Measurement

The conductivity of spray-coated PProDOT-CH_2OR_2 polymer films was determined by the four-point probe method. The measurements are taken as an average of multiple locations of the films, and reproducibility was checked by measuring conductivity on several films, leading to consistent results. The value obtained for the alkoxymethyl substituted PProDOTs are given in Table 4-6, along with the voltage drop obtained for a constant intensity applied to the doped spray-coated films. The conductivity decreases sharply with increasing size of the branching group. Interestingly, increasing the size of the main chain from butyl to hexyl does not appear to affect significantly the film conductivity.[63a] This correlates well with our assumption that the branching size, not the main chain size, is controlling the interchain distance.

Table 4-6. Conductivity measurement for PProDOT$(CH_2OR)_2$ spray-coated films. Films were gas phased doped for 12 hours in an iodine chamber prior to measuring conductivity.

R=	**I (μV) [a]**	**ΔV (mV) [b]**	**Thickness[c](nm)**	**σ (S cm^{-1})**
2-ethylbutyloxymethyl	2	83	658	0.08
2-ethylhexyloxymethyl	1	246	367	0.07
2-ethylhexyl	10	300, 194	222, 234	0.3, 0.5
2-methylbutyloxymethyl	10	148, 165	233, 246	0.54, 0.64
2-methylbutyl	100	203, 185	286, 251	3.8, 4.2
Hexyl	N/A	N/A	N/A	5-10

(a) Intensity setting; (b) Average voltage drop; (c) Average thickness obtained by profilometry.

Comparing the properties of alkyl and alkoxy polymers, the conductivity of the alkoxymethyl substituted polymers is one order of magnitude lower than their alkyl analogs. Given the electronic and optical results presented above, a possible explanation is that the alkoxymethyl substituted polymers have a higher degree of intrachain and

interchain disorder. Further studies on the chiral equivalents of these polymers, presented in Chapter 5, will provide additional data supporting it. The lower conductivities of branched polymers are further evidence that the coloration efficiency of these polymers is limited by the diffusion of dopant ion into the films, not the electronic conductivity.

4.4. High Performance Electrochromic Devices

Figure 4-10 shows a schematic representation of the construction of a dual-window electrochromic device.

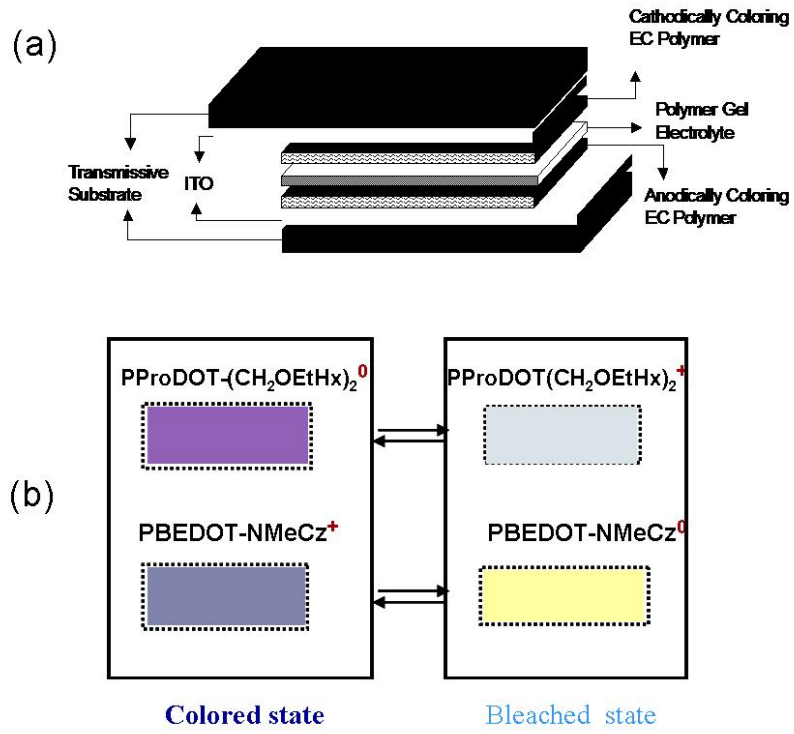

Figure 4-10. Electrochemical device using spray-coated PProDOT(CH_2O_2-ethylhexyl)$_2$ as the anodically coloring polymer and Poly(BisEDOT-N-methylcarbazole) electropolymerized film as the cathodically coloring polymer. (a) Schematic diagram of the dual-window electrochromic device; (b) Polymer colors for an applied bias of -1V (colored state) and +1V (bleached state).

The electrochromic device is built from two ITO-coated glass slides, one coated with an anodically coloring polymer (in our case spray-cast PProDOT-($CH_2OEtHx)_2$) and a second coated with an electrochemically oxidized, cathodically coloring polymer (in

this work, the polymer used is (Poly(BisEDOT-N-methylcarbazole)). The two ITO slides are then combined, facing each other, with a layer of gel electrolyte. When a negative bias (-1V) is applied to the device both polymers are colored, giving a dark absorptive color to the film (Figure 4-10). When a positive potential of +1V is applied then PProDOT-$(CH_2OEtHx)_2$) is fully oxidized in its highly transmissive, sky blue color state while Poly(BisEDOT-N-methylcarbazole)$_2$ is reduced to its neutral, highly transmissive yellow color state. As presented in Figure 4-11, PProDOT$(CH_2O$-2-ethylhexyl$)_2$ yields an electrochromic device with high luminance contrast and high coloration efficiency (4800 cm^2/C). The device can be fully switched up to rates of 2Hz.

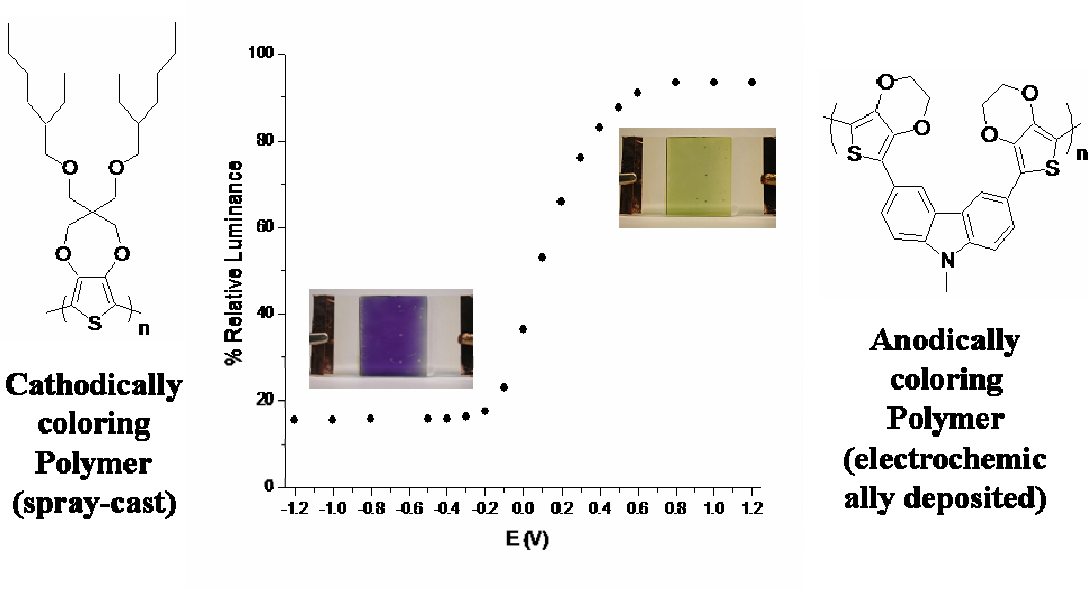

Figure 4-11. Luminance plot of a dual-window EC device using spray-coated PProDOT($(CH_2O$-2-ethylhexyl$)_2$) as the anodically coloring polymer and electrolpolymerized Poly(BisEDOT-N-methylcarbazole) as the anodically coloring polymer.

Similar devices, using a spray-coated PProDOT$(CH_2O$-$C_{18}H_{37})_2$, led to CE values of only 1300 $cm^2\ C^{-1}$. This work was carried out by Ali Cirpan and Avni Argun. It demonstrates nicely the difference of properties obtained between branched and long linear alkyl chains, both displaying high solubility.

4.5 Conclusion

Soluble PProDOTs, symmetrically substituted with flexible, ether-linked branched alkyl groups, were synthesized by Grignard Metathesis. Similarly to the alkyl substituted polymers studied in Chapter 4, increasing the branching size leads to shorter switching times, higher coloration efficiencies, higher oxidation potentials but lower conductivities. In spectroelectrochemistry and luminance experiments, abrupt optical changes with increasing potentials are also observed but the changes occur in a much narrower potential window (<150mV). In addition, upon spray-casting, the polymer chains retain a "solution" conformation, suggesting little interchain order is present in the films. This behavior can be explained by increased intrachain torsion of the polymer chains, preventing self-assembly in the solid state and leading to a more open morphology of the polymer chains. By oxidizing and reneutralizing the polymer films, a significant bathochromic shift is observed, corresponding to intrachain and possibly interchain rearrangement of the polymer chains.

As mentioned in Chapter 3, further studies using chiral equivalents of the alkoxy substituted PProDOTs will be described in Chapter 5 and provide substantial information on the interchain and intrachain interactions of the polymer chains in solution and in the solid state.

4.6. Chapter Synthetic Details

3,3-Bis(bromomethyl)-3,4-dihydro-*2H*-thieno[3,4-*b*][1,4]dioxepine (ProDOT-($CH_2Br)_2$): The intermediate was obtained by transetherification, as described in the experimental section of Chapter 3. The product is a white crystalline solid obtained (73 %). mp 66-68 °C. ^{1}H NMR (300 MHz, $CDCl_3$) δ 6.49 (s, 2H), 4.10 (s, 4H), 3.61 (s, 4H); ^{13}C NMR (75 MHz, $CDCl_3$) δ 148.5, 105.7, 74.1, 46.1, 34.4. HRMS calculated for

$C_9H_{10}O_2Br_2S$: 339.8768 Found: 339.8820. Elemental Anal. Calcd for $C_9H_{10}O_2Br_2S$: C 31.60; H 2.95; S 9.37 Found: C 31.83; H 2.99; S 9.20.

General procedure for the Williamson etherification of ProDOT($CH_2Br)_2$: A 250 mL flame dried round bottom flask filled with 50 mL of DMF, 8.7 mmols of alcohol (3eq), and 17.5 mmols of NaH (6eq) was heated at 110 °C overnight. Then 2.92 mmols of ProDOT($CH_2Br)_2$ was added and the reaction continued at 110 °C for another 24 hr. After completion, the flask was cooled and added to 200 mL brine and extracted 3 times with ethyl ether. The organic layer was then washed 3 times with water, dried over magnesium sulfate, and the solvent was removed by rotary evaporation under reduced pressure. The resulting orange oil was purified by column chromatography (3:2 hexanes, methylene chloride).

3,3-Bis-(2-methylbutyloxymethyl)-3,4-dihydro-2H-thieno[3,4-b][1,4]dioxepine (ProDOT(CH_2O-2-methylbutyl)$_2$): The crude oil obtained was purified by column chromatography affording a clear oil (91%). ^{1}H NMR (300 MHz, $CDCl_3$) δ 0.81-0.93 (m, 12H), 1.02-1.20 (m, 2H), 1.32-1.48 (m, 2H), 1.51-1.69 (m, 2H), 3.11-3.28 (m, 4H), 3.42-3.5 (m, 4H), 3.99 (s, 4H); ^{13}C NMR (75 MHz, $CDCl_3$) δ 11.57, 16.80, 26.42, 35.08, 48.08, 69.91, 73.94, 76.96, 105.21, 149.90. HRMS calculated for $C_{25}H_{44}O_4S$: 356.2021 Found 356.2048. Elemental Anal. Calcd for $C_{25}H_{44}O_4S$: C 64.01; H 9.50 Found: C 64.03; H 9.05.

3,3-Bis-(2-ethylbutyloxymethyl)-3,4-dihydro-2H-thieno[3,4-b][1,4]dioxepine (ProDOT(CH_2O-2-ethylbutyl)$_2$): Purification by column chromatography (CH_2Cl_2) to afford a clear oil (88%). ^{1}H NMR (300 MHz, $CDCl_3$) δ 0.79-0.94 (t, 12H), 1.20-1.50 (m, 10H), 3.29 (d, 4H, J=5.96Hz), 3.47 (s, 4H), 4.01 (s, 4H); ^{13}C NMR (75 MHz, $CDCl_3$) δ

11.40, 23.68, 41.34, 48.06, 69.99, 73.97, 74.05, 105.16, 149.88. HRMS calculated for $C_{25}H_{44}O_4S$: 384.2334 Found: 384.2328. Elemental Anal. Calcd for $C_{25}H_{44}O_4S$: C 65.59; H 9.44 Found: C 65.66; H 9.66.

3,3-Bis-(2-ethyl-hexyloxymethyl)-3,4-dihydro-2H-thieno[3,4-b][1,4]dioxepine (ProDOT(CH_2OEtHex)$_2$): The crude oil obtained was purified by column chromatography to afford a clear oil (70 %). ^{1}H NMR (300 MHz, $CDCl_3$) δ 6.42 (s,4H), 3.98 (s, 4H), 3.44 (s, 4H), 3.25 (d, 4H), 1.2-1.6 (m, 18H), 0.8-1.0 (m, 12H); ^{13}C NMR (75 MHz, $CDCl_3$) δ, 149.7, 104.9, 74.3, 73.8, 69.8, 47.9, 39.6, 30.7, 29.1, 24.0, 23.1, 14.1, 11.1. HRMS calculated for $C_{25}H_{44}O_4S$: 440.2960 Found: 440.2964. Elemental Anal. Calcd for $C_{25}H_{44}O_4S$: C 68.14; H 10.06; S 7.28. Found: C 68.17; H 10.39; S 7.26.

General procedure for the bromination of ProDOTs: In a 2-neck 250 mL round bottom flask filled with 80 mL DMF, 1.5g (2.1 mmol) of ProDOT was added and the solution was bubbled under argon for 60 minutes. Then 1.12 g (6.24 mmols) of *N*-bromosuccinimide was added and the solution was stirred for 20 hr. After completion, the solvent was removed by rotary evaporation under reduced pressure and the resulting residue was purified by column chromatography on SiO_2 with (4:1) hexanes/dichloromethane as eluent.

6,8-Dibromo-3,3-bis-(2-methylbutyloxymethyl)-3,4-dihydro-2H-thieno[3,4-b][1,4]dioxepine (ProDOT(CH_2O-2-methylbutyl)$_2$Br$_2$): The crude oil obtained was purified by column chromatography (4:1) hexanes/dichloromethane to afford 1.3 g of product (90%).^{1}H NMR (300 MHz, $CDCl_3$) δ 0.83-0.93 (m, 12H), 0.99-1.20 (m, 2H), 1.29-1.47 (m, 2H), 1.53-1.66 (m, 2H), 3.11-3.27 (m, 4H), 3.43-3.52 (m, 4H), 4.09 (m,

4H); ^{13}C NMR (300MHz, $CDCl_3$) δ 11.59, 16.81, 26.42, 35.11, 69.80, 74.52, 76.81, 91.12, 149.45; HRMS Calcd for $C_{25}H_{42}O_4SBr_2$ 514.0232. Found 514.0227.

6,8-Dibromo-3,3-bis-(2-ethylbutyloxymethyl)-3,4-dihydro-2H-thieno[3,4-b][1,4]dioxepine (ProDOT(CH_2O-2-ethylbutyl)$_2Br_2$): The crude oil obtained was purified by column chromatography (4:1) hexanes/dichloromethane to afford 0.990g of product (92%). ^{1}H NMR (300MHz, $CDCl_3$) δ 0.79-0.92 (t, 12), 1.15-1.5 (m, 6H), 3.29 (d, 4H, 5.4Hz), 3.49 (s, 4H), 4.08 (s, 4H); ^{13}C NMR (300MHz, $CDCl_3$) δ 11.41, 23.68, 41.35, 48.18, 69.91, 74.07, 74.55, 91.00, 147.19. Elemental Anal. Calcd for $C_{25}H_{42}O_4SBr_2$: C 46.85; H 6.32 Found: C 46.85; H 6.42.

6,8-Dibromo-3,3-bis-(2-ethyl-hexyloxymethyl)-3,4-dihydro-2H-thieno[3,4-b][1,4]dioxepine (ProDOT(CH_2OEtHx)$_2Br_2$): The crude oil obtained was purified by column chromatography (4:1) hexanes/dichloromethane to afford a clear oil (98 %). ^{1}H NMR (300MHz, $CDCl_3$) δ 4.09 (s, 4H), 3.49 (s, 4H), 3.28 (d, 4H), 1.2-1.6 (m, 18H), 0.8-1.0 (m, 12H); ^{13}C NMR (300MHz, $CDCl_3$) δ147.2, 91.0, 74.6, 70.0, 48.2, 39.9, 30.9, 29.4, 24.2, 23.3, 14.4, 11.4; HRMS Calcd for $C_{25}H_{42}O_4SBr_2$ 596.1171. Found 596.1161; Elemental Anal. Calcd for $C_{25}H_{42}O_4SBr_2$: C 50.17; H 7.07; S 5.36. Found: C 50.43; H 7.09; S 5.16.

General Procedure for Grignard metathesis polymerization of ProDOT($CH_2OR)_2Br_2$: In a flame dried 250 mL round bottom flask, dry THF (150 mL) and 3.0 g (0.34 mmol) of ProDOT$(R)_2Br_2$ was added under argon. Then methyl magnesium bromide (3.75 mL, 3.45 mmol, 0.918 M) was slowly added by syringe. The mixture was then refluxed for 2 hr. The flask was cooled and Ni(dppp)Cl_2 (18.4 mg, 0.0341 mmol) was added and the reaction was heated at reflux overnight under argon.

The solution was then cooled and the polymer was precipitated by pouring the solution in 400 mL methanol. The dark purple solid was purified by soxhlet extraction with methanol for 24 hr, hexanes for 48 hr, and finally chloroform for 24 hr. The chloroform was evaporated under reduced pressure to afford a dark shiny solid.

Poly(3,3-bis-(2-methylbutyloxymethyl)-3,4-dihydro-2H-thieno[3,4-b][1,4]dioxepine) (PProDOT(CH_2O-2-methylbutyl)$_2$): 0.47g of purple solid obtained (68%). ^{1}H NMR (300 MHz, benzene-d_6) δ 0.68-0.97 (br, 12H), 1-1.24 (br, 2H), 1.24-1.47 (m, 2H), 1.47-1.69 (m, 2H), 2.87-3.27 (br doublet, 4H), 3.37-3.74 (br, 4H), 3.96-4.7 (br, 4H); ^{13}C (75 MHz, benzene-d_6) δ 11.24, 16.77, 26.55, 35.22, 70.61, 77.11.

Poly(3,3-bis-(2-ethyl-hexyloxymethyl)-3,4-dihydro-2H-thieno[3,4-b][1,4]dioxepine) (PProDOT(CH_2O-2-ethylbutyl)$_2$): 0.310g of purple solid obtained (%). ^{1}H NMR (300 MHz, benzene-d_6) δ 0.85-1.07 (br, 12H), 1.28-1.56 (bs, 10H), 3.24-3.32 (br, 4H), 3.43-3.67 (br, 4H), 4.1-4.4 (br, 4H); ^{13}C (75 MHz, benzene-d_6) δ 11.91, 24.43, 30.6, 41.9, 48.62, 70.90, 74.24, 75.15, 115.47, 146.20**;** GPC analysis: M_n= 12,400, M_w= 17,500, PDI=1.4.

Poly(3,3-bis-(2-ethyl-hexyloxymethyl)-3,4-dihydro-2H-thieno[3,4-b][1,4]dioxepine) (PProDOT(CH_2OEtHx)$_2$): 0.350 g of purple solid obtained (93 %). ^{1}H NMR (300 MHz, benzene-d_6) δ 4.25 (br, 4H), 3.58 (br, 4H), 3.25 (br, 4H), 1.62- 1.30 (br, 22H), 1.09-0.99 (m, 12H); ^{13}C (75 MHz, benzene-d_6) δ 146.2, 115.3, 75.1, 74.8, 71.0, 48.7, 40.4, 31.6, 30.0, 25.0, 24.0, 14.9, 11.9**;** GPC analysis: M_n= 21,400, M_w= 36,100 PDI=1.72.

CHAPTER 5
CHIRAL SUBSTITUTED POLY(3,4-PROPYLENEDIOXYTHIOPHENES)

5.1. Introduction

5.1.1. CD Spectroscopy

It is essential to control the ordering of π-conjugated molecules from their assembly at the mesoscopic level to their applications at the macroscopic level. Many tools, recently reviewed by the Meijer group, are available to control the assembly process of π-conjuguated systems.[74] One of these tools is the introduction of chiral substituents, which strongly influence the self-assembly of molecules, often leading to intra or intermolecular chiral assemblies. Such chiral assemblies can be analyzed by chiroptical techniques. One of them, circular dichroism (CD), is commonly used to analyze the secondary and tertiary structures of proteins and biomolecules such as the α-helix, β-helix or β-sheet, each having a specific CD signature.[75] CD is also a highly sensitive technique as small changes of conformation in the chiral assemblies will induce changes in the CD signal. As a result, there is a strong dependence of CD on temperature while in solution, solvent and concentration also affect the CD signal.

In a CD spectrophotometer, plane polarized light, which is the sum of left and right circularly polarized light of equal amplitudes with a phase difference of 180°,[76] passes through a sample in solution or a cast film on a transparent substrate. If the sample is CD active, then either the left or the right polarized light will be preferentially absorbed. This is circular dichroism. As a result of the preferential absorption of one circularly polarized light radiation, recombination no longer gives planar polarized light but elliptically

polarized light, as seen in Figure 5-1. The variation of the elliptical angle θ as a fuction of wavelength yields the CD spectrum. This spectrum is equivalent to the regular absorption spectrum, where the absorption of unpolarized light is followed with wavelength.

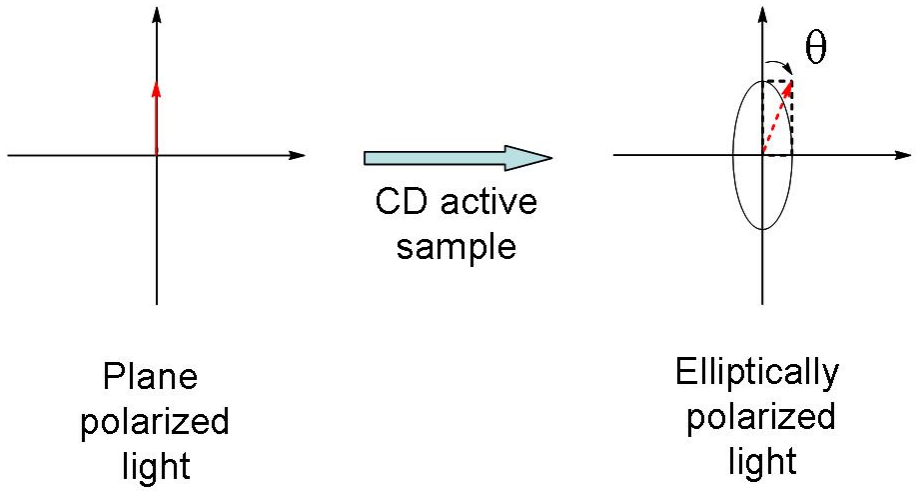

Figure 5-1. CD spectroscopy principle. θ is the value measured by the spectrophotometer.

Like absorbance, the CD signal is directly proportional to the concentration of the sample. Concentration-independent Δε and anisotropy factor g (Δε/ε) are sometimes reported and are calculated by:

$$\Delta\varepsilon = \frac{\theta(m\deg)}{32980 * C}(M^{-1}cm^{-1})$$

$$g = \frac{\Delta\varepsilon}{\varepsilon} = \frac{\theta(m\deg)}{A \times 32980}$$

where θ is elliptical angle, ε and A are the extinction coefficient and the absorbance at a given wavelength.

To observe a CD signal, absorbing chromophores must either be chiral or possess a helical arrangement. Both their electrical and magnetic transitions dipoles must also be different from zero. This is different than unpolarized absorption, where only the electrical transition dipole must be different than zero and helical order is not required. In

the case of exciton-coupled chromophores in a chiral oblique arrangement, described in Chapter 1 and Figure 5-2, both optical transitions are electrically and magnetically allowed, and a CD signal is observed. Exciton-coupling theory predicts that the transitions corresponding to the two Davydov energy levels have opposite rotations, leading to a bisignate CD signal.[77] Exciton-coupled J-aggregates or H-aggregates, on the other hand, have optical transitions which are magnetically forbidden, and no CD signal can be observed.

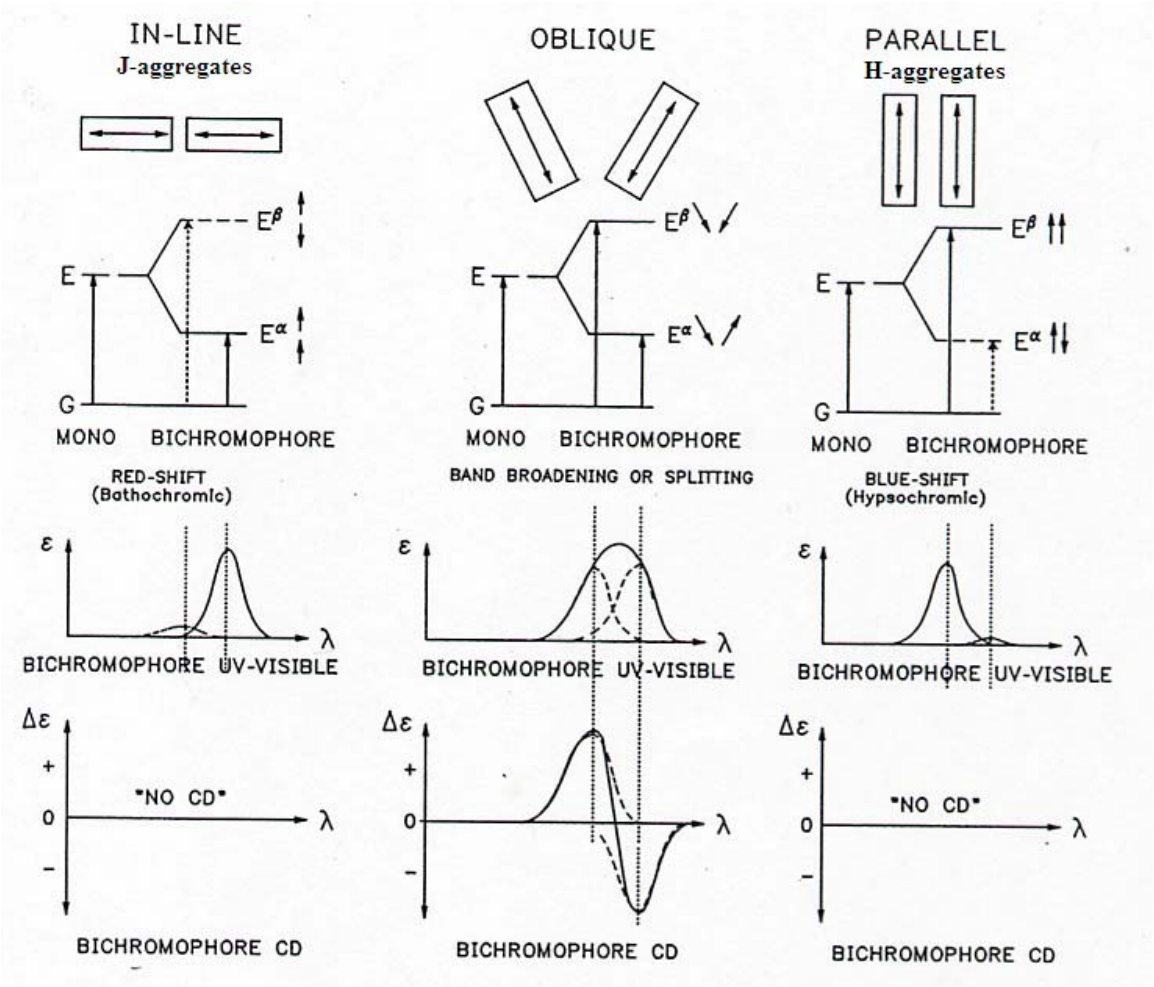

Figure 5-2. CD signal of exciton-coupled chromophores with varying chromophores arrangement. Adapted from ref. 77.

In exciton-coupled chromophores, the CD signal amplitude is at a maximum when interacting chromophores are at projection angle of 70°. The signal is also proportional to

the square of the extinction coefficient ε, and proportional to the square of the chromophores distance.[77]

5.1.2. Applications of Chiral Polymers and CD Spectroscopy

Many applications utilizing the unique properties of chiral polymers have been studied. As the chiral polymers often emit circularly polarized light, circularly polarized light-emitting devices have been studied.[78] These polymers are also interesting candidates for non-linear optics as the chiral aggregates are non-centrosymmetric.[79] In addition, the chiral polymers have been utilized in chiral membranes and sensors.[80]

However, most authors utilize chiral conjugated molecules and polymers as a unique tool to understand and control the self-assembly. This is important as film processing conditions, chain conformations, and film morphology have been shown to strongly influence the performance of π-conjugated materials in devices.[81, 13] By synthesizing chiral equivalents of the polymers and studying them via circular dichroism, information on conformation and organization of the polymer chains from solution to the solid state can be extracted. This was elegantly demonstrated by Swager in chiral substituted poly(p-phenyleneethynylene) (PPE).[82] Analysis of these polymers by CD, absorption and fluorescence spectroscopy demonstrated that, when dissolved in varying good solvent/ poor solvent mixtures, different type aggregates are formed, some having unusually high fluorescence. Other works have shown that the polymer chains conformation and their organization in solution and solid state are greatly modified by tuning solvent, temperature or film processing conditions.[83]

5.1.3. Thermochromism/Solvatochromism in Chiral Substituted Polymers

Thermochromism has long been used to study conformational changes of polymer chains with temperature. In substituted poly(thiophenes), important changes of color are

observed with temperature both in solution and in the solid state. When cooled, solutions of substituted polythiophenes undergo a progressive bathochromic shift and vibronic features appear. There is often presence of an isosbestic point, showing that two distinct forms are in equilibrium. At longer times aggregation and precipitation often occur. The mechanism of this thermochromic transition, even today, is the center of great debate. Some authors have argued that the phenomenon is interchain related, while others argued it is intrachain in origin. The intrachain mechanism was first proposed by Heeger on the basis that dilution do not result in significant optical changes.[84] The aggregation is then seen as a result of the intrachain planarity, favoring strong interchain interactions. In this mechanism, the thermochromic transition is attributed to a rod-coil transition within the polymer chains with the presence of ordered regions (rod-like) and disordered regions (coiled-like). The interchain mechanism proposes that the thermochromic transition arises from equilibrium between aggregated chains in suspension and molecularly dissolved chains.[85] A recent study using a dendrimer capped oligothiophene support that mechanism.[86] It suggests that intrachain changes only play a pre-organization role in the change of optical absorption with temperature. Leclerc and his group later demonstrated that thermochromism in substituted polythiophenes is highly dependent on the substitution and regioregularity.[84b] With a regioirregular backbone, or when substituents prevent the polymer chains from adopting a planar conformation, neither isosbestic point, nor appearance of vibronic coupling are observed.

By using chiral polythiophenes and CD spectroscopy, Meijer et al. showed that interchain interactions such as those illustrated in Figure 5-3 play a crucial role in the thermochromism process, as demonstrated by the appearance of a strong bisignate CD

signal corresponding to the π- π* optical transition when the solutions were cooled to low temperatures.[87] The CD signal was attributed to Davydov exciton coupling between chains involved in cholesteric aggregates.

Chiral aggregation could also be induced by solvatochromism. In chloroform, a good solvent for the chiral polythiophenes, no CD signal is observed as the polymer chains are molecularly dissolved. As methanol, a poor solvent of the polymer, is added, a bisignate CD signal is observed, indicating presence of interchain helical aggregates.

The chiral aggregates were also formed in the solid state, as evidenced by the presence of a CD signal in films cast from chloroform. The films emitted circularly polarized light, suggesting that the chiral aggregates are maintained in the excited state.

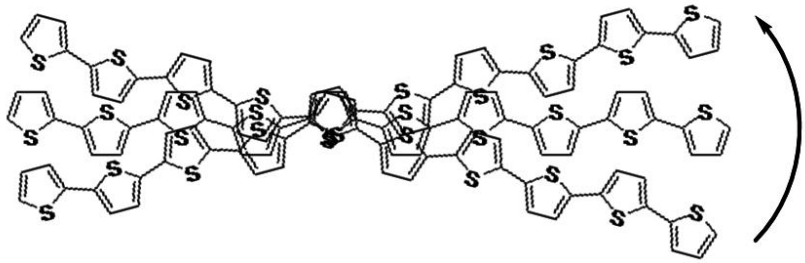

Figure 5-3. Cholesteric packing in aggregated chiral poly(thiophenes). Only the polythiophene backbone is displayed.

5.1.3. Chiral Substituted PProDOTs

In Chapter 3 and 4, the focus was on the unique properties of branched dialkyl and dialkoxymethyl substituted PProDOTs. Their applications as highly efficient electrochromic materials were also described, with high contrasts and subsecond switching times. Most of these branched substituents are chiral chains, but were obtained from racemic reagents, resulting in polymers with a random distribution of R and S chiral centers. In this chapter, the synthesis and properties of fully chiral polymers, shown in Figure 5-4, obtained from enantiomerically pure reagents are described. The polymers

were studied by fluorescence, absorption and circular dichroism. In addition, a unique, versatile synthesis yielding enantiomerically pure chiral substituents is presented. These substituents were utilized in the synthesis of unique chiral polymers.

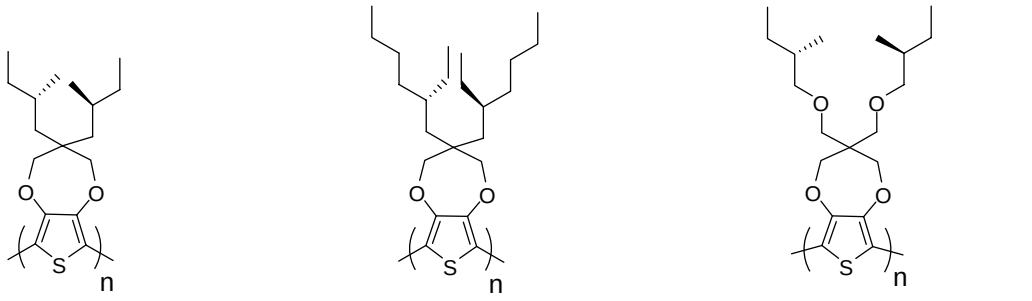

Figure 5-4. New soluble Chiral PProDOTs polymers obtained by Grignard Metathesis

5.2. Synthesis of PProDOT-Based Chiral Polymers

5.2.1 New Chiral Reagents Synthesis

As shown in the previous two chapters, substitution with branched alkyl chains is a highly effective method for inducing solubility in otherwise insoluble conjugated polymers (CPs) and improving electrochromic properties. PProDOT-(2-ethylhexyl)$_2$ and PProDOT-(CH_2O-2-ethylhexyl)$_2$ yielded the highest contrast and highest coloration efficiency of the PProDOTs series. PProDOTs substituted with linear substituents yield materials with much lower performance. It was also observed that the two polymers undergo a very sharp optical transition in luminance and absorption spectrum as a function of increasing potentials. Another 2-ethylhexyl substituted polymer, poly(2-methoxy, 5-(2-ethylhexyloxy),1,4-phenylenevinylene) (MEH-PPV), is one of the most studied and efficient polymers in light-emitting and photovoltaic applications.[88] In that work, it is therefore of high interest to synthesize chiral ethylhexyl substituted polymers. But to date, only one conjugated polymer with chiral 2-ethylhexyl side chains, poly(9.9-(bis((R)-2-ethylhexyl)fluorene-2,7-diyl) has been reported.[89] The chiral substituents were

obtained by enzymatic catalysis but the method gives low yields (10%) and the substrates that can be used, as well as the products that can be obtained with this method, are limited. Often, only one enantiomer is accessible. In this work, 2S-ethylhexanol was synthesized by enantioselective alkylation of an acylated pseudo-ephedrine, as detailed in Figure 5-5, modifying a procedure outlined by Myers et al..[90] The enantiomeric excess of the alcohol was determined to be 96% by GC of the Mosher ester derivative. This route uses inexpensive materials, gives high yield and can be easily scaled up. Both enantiomeric products can be obtained by using either of the two inexpensive enantiomeric d- and l-pseudoephedrines. In addition, it utilizes a flexible method allowing the efficient synthesis of many different chiral primary alcohols with variable substituents on the α position along with other derivatives including chiral acids, acyl chlorides, and aldehydes.

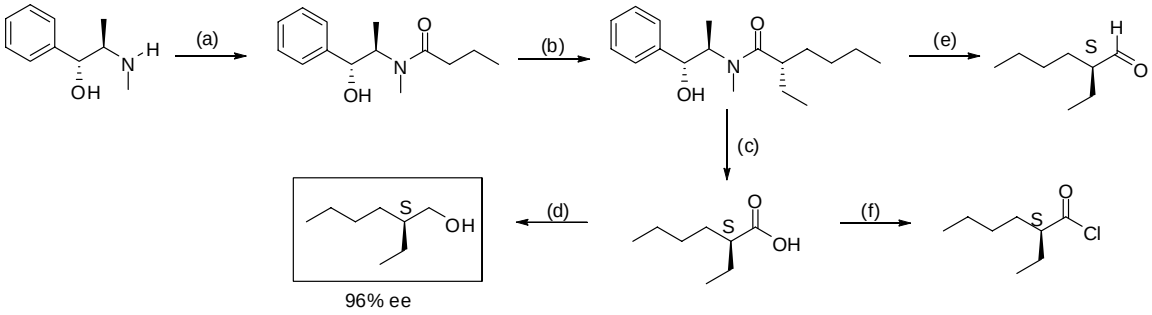

Figure 5-5. Synthesis of 2S-ethylhexyl substituents using a pseudoephedrine chiral auxiliary. (a) butyric anhydride, RT, THF, 23°C; (b) LDA, 6 eq. LiCl, -78°C, 1 hr→0°C, 15min→23°C, 5 min then butyliodide, 30 min, 0°C; (c) 18N H_2SO_4, dioxane, reflux; (d) $LiAlH_4$, Et_2O, reflux;(e) $LiAlH(OEt)_3$, THF; (f) $SOCl_2$, DCM, reflux.

5.2.2 Electrochemically Polymerizable Monomer and Electrodeposition

The electropolymerizable monomers were obtained through the same synthetic methods described in Chapter 3 and 4 for the racemic polymers except for a slight change in the synthesis of the chiral alkyl PProDOTs. The alkyl bromides used in the malonic

ester synthesis were replaced by tosylated alcohols, as 2S-methylbutyl alcohol is less expensive than 2S-methylbutylbromide and the 2S-ethylhexyltosylate is easily obtained from the alcohol obtained through the synthetic method presented above. Purification of the tosylate is also easier, as ethylhexylbromide is highly volatile.

Electrodeposited films of the chiral polymers were studied by electrochemistry. As seen in Figures 5-6, PProDOT-(2-methylbutyl)$_2$ and PProDOT-(2S-methylbutyl)$_2$ have similar half-wave and onset potentials, suggesting that the introduction of chiral side chains does not change the macroscopic properties.

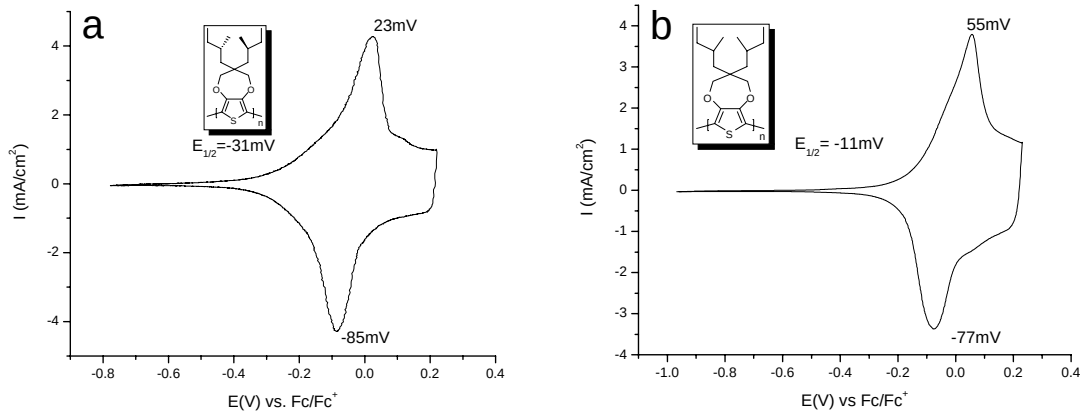

Figure 5-6. Cyclic voltammetry of electrodeposited PProDOT((2S)-methylbutyl)$_2$ and PProDOT((2S)methylbutyl)$_2$. Scan rate is 50mV/s. Potential are reported against Fc/Fc$^+$.

Following Grignard metathesis, PProDOT((2S)-methylbutyl)$_2$, PProDOT(CH_2O-(2S)-methylbutyl)$_2$ and PProDOT((2S-ethylhexyl)$_2$) were obtained as shiny brown solids. After Soxhlet purification with methanol and hexanes, PProDOT((2S)-methylbutyl)$_2$ was extracted with dichloromethane. A fraction of this polymer remained in the Soxhlet thimble, but was successfully extracted with chloroform. As expected, GPC results, detailed in Figure 5-1, indicate that the fraction soluble in dichloromethane has a lower molecular weight than the chloroform fraction. PProDOT(CH_2O-2S-methylbutyl)$_2$ was

insoluble in dichloromethane, but was successfully extracted with chloroform. For PProDOT-(2S-ethylhexyl)$_2$, the polymer was soluble in both dichloromethane and chloroform. GPC analysis revealed a similar molecular weight distribution than the highest molecular weight fraction of PProDOT((2S)-methylbutyl)$_2$, showing that the larger branched substituents yield significantly higher solubility.

Table 5-1. GPC data for chiral substituted PProDOTs. Molecular weights are versus polystyrene standards.

Substituents	**M_n**	**M_w**	**DPI**	**X_n**	**Solubility**
2S-methylbutyl	5,400	8,400	1.5	18	DCM, $CHCl_3$
	8,400	13,800	1.6	28	$CHCl_3$
2S-ethylhexyl	8,700	14,200	1.6	22	DCM, $CHCl_3$
2S-methylbutyloxymethyl	18,900	32,000	1.7	53	$CHCl_3$

After spray-casting of the polymers onto ITO-coated glass slides, the optoelectronic properties of the films were analyzed. Spectroelectrochemistry experiments, carried out on PProDOT-(2-methylbutyl)$_2$ and PProDOT-(2S-methylbutyl)$_2$ spray-cast films, indicate that the maxima of absorption and the vibronic features vary little between the racemic and chiral polymers as displayed in Figure 5-7. Also, for both PProDOT-(2S-methylbutyl)$_2$ and its racemic analog, most optical changes are obtained within only a 350 mV potential increase.

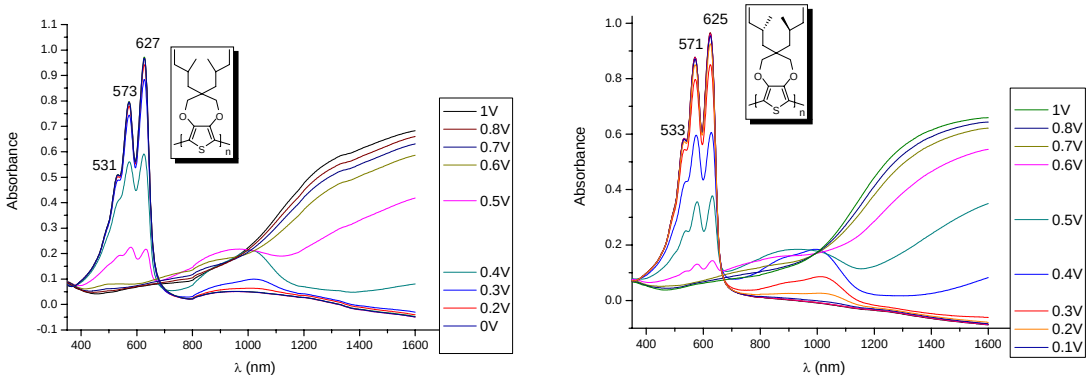

Figure 5-7. Comparison of PProDOT-((2S)methylbutyl)$_2$ and PProDOT-((2S)methylbutyl)$_2$ spectroelectrochemistry. Both films were spray-cast from toluene.

For PProDOT-((2S)-ethylhexyl)$_2$ and PProDOT-(CH_2O-(2S)-methylbutyl)$_2$, the polymer properties are also comparable to the racemic polymers (Table 5-2).

Table 5-2. Comparison of chiral and racemic PProDOTs polymers.

	PProDOT-(2-ethylhexyl)$_2$		**PProDOT-(CH_2O-2-methylbutyl)$_2$**	
	Racemic	**Chiral**	**Racemic**	**Chiral**
$E_{p,a}$ (mV)[a]	45	89	26	N/A
$E_{p,c}$ (mV)[a]	11	43	-29 (-269)	N/A
λ_{max} cast film[b] (nm)	618, 564, 523	617, 564, 524	612, 561, 528	615, 564, 529
Eg[a]	1.93	1.92	1.91	1.91
Conductivity[c] (S cm^{-1})	0.4	N/A	0.6	0.8

(a) Electrodeposited films Potential vs. Fc/Fc^+; (b) Neutral films spray-coated on ITO after electrochemical switching; (c) Films gas phase doped with iodine.

Although the macroscopic properties indicate clearly no significant dependence on the chirality, circular dichroism spectroscopy indicates significant differences in their ordering behavior.

5.3. Chiral Ordering in Chiral PProDOTs

5.3.1. Optical Properties in "Good" Solvent Solutions

The thermochromism of the chiral polymers was studied in xylenes, a good solvent of the polymer. The absorption thermochromism for PProDOT-(CH_2O-2S-methylbutyl)$_2$ in xylenes is shown in Figure 5-8a. As the temperature is raised, a gradual blue-shift of the absorption is observed and the vibronic features progressively disappear. The decrease is bigger for the 0-0 transition than the 0-1 transition, leading to a dominant 0-1 vibration above 45°C. No clear isosbestic point can be seen in the temperature range studied. When the absorbance at 591nm is followed with temperature, a linear variation is observed, as shown in the inset of Figure 5-8a. As it was shown that interchain and intrachain mechanisms display different temperature dependence, the linear variation of

the optical maximum suggests either an intrachain or interchain-only mechanism for the thermochromism of PProDOT-(CH_2O-2S-methylbutyl)$_2$.[86] The other PProDOTs (chiral or racemic) display a similar behavior when dissolved in a good solvent. When the polymers are dissolved in more polar solvents such as chloroform (ε= 4.8) or ortho-dichlorobenzene (ε= 9.9), a bathochromic shift is observed, as seen in Figure 5-8b. The vibronic features are identical and the shift therefore cannot be due to changes in the intrachain conformation of the polymer chains. The shift is rather due to an increased stabilization of the polarized excited state by the more polar solvents.

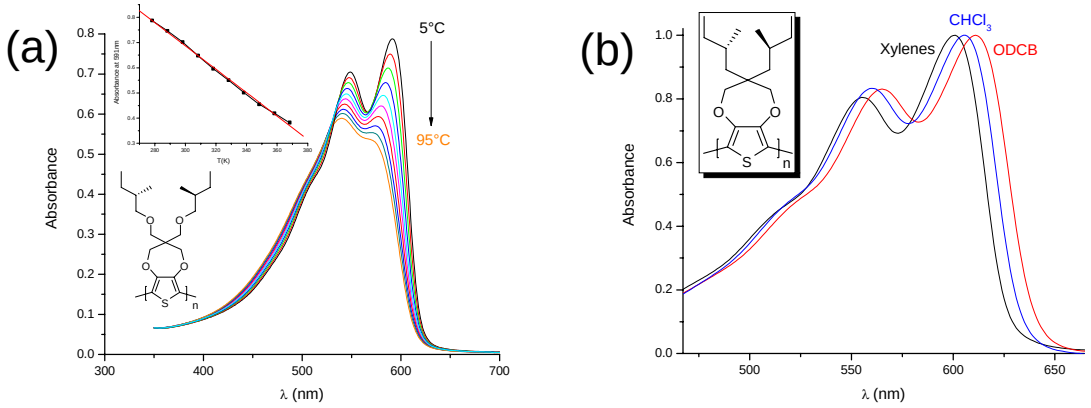

Figure 5-8. Temperature dependence of PProDOT(CH_2O-2S-methylbutyl)$_2$ in xylenes solution.

To eliminate the possibility that interchain interactions are involved in the thermochromic transition of PProDOTs in good solvent solutions, the solutions were examined by fluorescence and circular dichroism spectroscopy. As shown in Figure 5-9 for PProDOT-(2S-ethylhexyl)$_2$, the fluorescence decreases and is blue-shifted with increasing temperature. A possible explanation for the decreased fluorescence is that the number of photons absorbed decrease at the excitation wavelength (λ_{exc}=550 nm). Closely inspecting at the absorption, a decrease in absorption is indeed seen, but is much smaller than the decrease in fluorescence intensity. It follows that the decreased

absorption at the excitation wavelength cannot account for the weaker emission. Such decrease of emission also demonstrates that interchain quenching cannot be involved in the pure solvent solutions, as interchain interaction would break up as the temperature is increased, leading to an increase in fluorescence intensity. Moreover, CD analysis carried out on xylenes solutions reveals no CD signal, and dilution experiments indicate no shift in absorption spectrum, confirming the absence of interchain interactions. As a result, thermochromism and vibronic features in PProDOTs, dissolved in good solvent solutions, are attributed to *intrachain* interactions only.

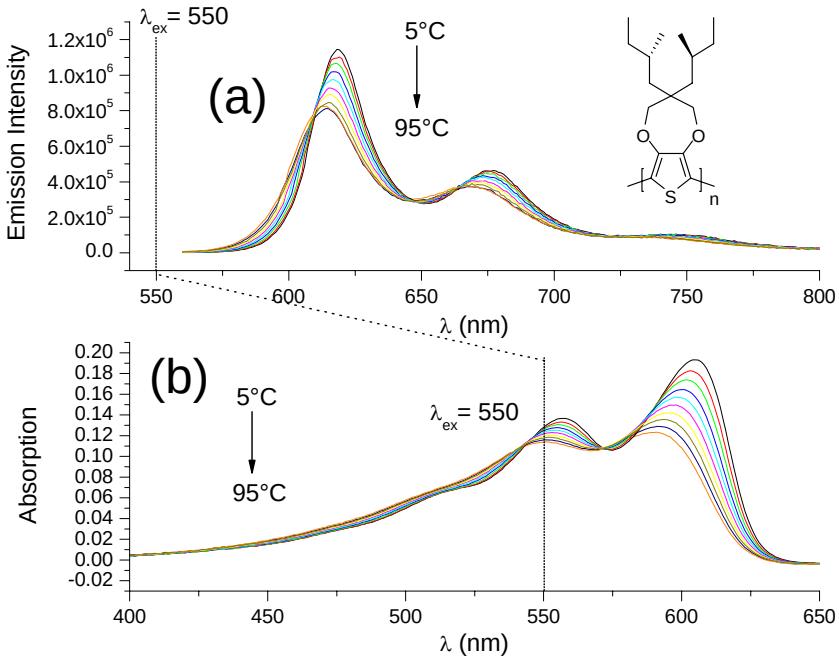

Figure 5-9. Thermochromism of PProDOT((2S)-methylbutyl)$_2$ in xylenes solution. (a) Fluorescence spectrum with excitation at 550nm; (b) Absorbance spectrum.

5.3.2. Solvatochromism Effects in PProDOTs Solutions

When the chiral polymers are dissolved in good solvent (xylenes, ortho-dichlorobenzene, chloroform, THF) / poor solvent (methanol, DMF) mixtures, their

optical properties are drastically affected. Figure 5-10 illustrates the effect of adding DMF to a xylenes solution of PProDOT(2S-methylbutyl)$_2$ on the absorption, emission and circular dichroism spectra. At low DMF content (≤30%), the absorbance remains constant, no CD signal is observed and the fluorescence intensity decreases slightly. These observations indicate that no aggregation has occurred. The decreased fluorescence intensity could possibly be explained by the energy gap law, predicting that rate of non-radiative decay increases as the difference of energy between the ground and excited state. As the DMF content is increased, the polarity of the solvent mixture increases, resulting in a stabilization of the excited state, as shown earlier in Figure 5-8. The stabilization is expected to result in an increase of non-radiative decay, as predicted by the energy gap law. This behavior is observed up to a 70/30 xylenes/DMF ratio. At a ratio of 60/40, abrupt optical changes are observed. The absorption spectrum undergoes a 20nm bathochromic shift, the emission is strongly quenched and a well-defined CD signal appears. These changes correspond to an aggregation of the polymer chains, with highly efficient interchain quenching of the photoluminescence. As shown in Figure 5-10c and Figure 5-10d, the CD signal is bisignate and matches with the first derivative of the absorption, fully consistent with Davydov exciton splitting.[87,91] The CD signal is reminiscent of the signal observed in aggregated poly(3,4-bis((S)-2-methylbutoxy)thiophene), suggesting that PProDOT((2S)-methylbutyl)$_2$ forms cholesteric interchain aggregates in poor solvent mixtures. The maximum anisotropy factor is $g_{max}=1.6\times10^{-2}$ at 642 nm and is close to the values reported for poly(3,4-bis((S)-2-methylbutoxy)thiophene).[87] PProDOT((2S)-ethylhexyl)$_2$ displays a similar behavior to PProDOT((2S)-methylbutyl)$_2$ in xylenes/DMF mixtures. At a 60/40 ratio, aggregation

again occurs, leading to a sharp decrease in fluorescence, a bathochromic shift in absorption and the appearance of a bisignate CD signal. The maximum anisotropy factor of the CD signal is $g_{max}= 2.4\times10^{-2}$, comparable to the chiral methylbutyl analog.

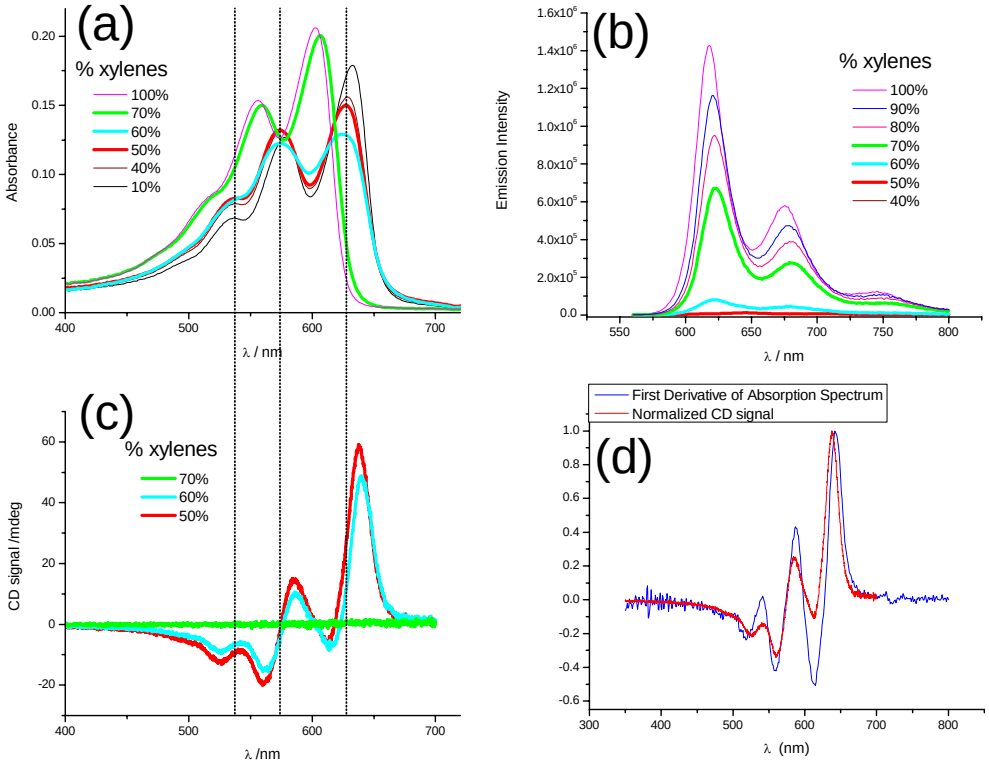

Figure 5-10. Optical properties of PProDOT((2S)-methylbutyl)$_2$ solutions in Xylenes/DMF mixtures (C= 8.6×10^{-6}M). (a) absorption spectra; (b) photoluminescence spectra, λ_{exc}=550nm; (c) CD spectra; (d) comparison between CD spectrum and first derivative of the absorbance of a 30/70 xylenes/DMF solution.

The alkoxymethyl substituted PProDOT(CH_2-O-2S-methylbutyl)$_2$, however, behaves differently. When poor solvent is added to a xylenes solution of PProDOT(CH_2-O-2S-methylbutyl)$_2$, although a clear red shift is observed at a 60/40 xylenes/DMF ratio indicating aggregation of the polymer chains, no CD signal is observed. Possible explanations for the absence of CD signal are:

1. Alkoxymethyl substituted polymers chains have a more distorted backbone. (see Chapter 4).
2. ProDOT seven-membered ring conformational flexibility between "chair" and "twisted" conformations (see Chapter 3) hinder polymer chains self-assembly.
3. The chiral centers are too remote from the conjugated backbone to induce preferential helical order.
4. The flexibility of the alkoxymethyl prevents ordering of the chiral side chains.

The two last explanations are unlikely as previous studies in chiral poly(3-alkylthiophenes) show that introducing alkyl or alkoxy spacers do not prevent the formation of chiral aggregates.[92]

5.3.3. Thermochromism in PProDOTs Aggregated Solutions

Thermochromism was carried out on PProDOT(2S-ethylhexyl)$_2$ polymer solutions dissolved in various xylenes/DMF solvent mixtures. The evolution of the optical properties with temperature was probed with CD, fluorescence and absorption spectroscopy. For each solvent composition, the absorbance at the λ_{max} of the 5°C spectrum is followed with temperature, as observed in Figure 5-11. In pure xylenes, a linear trend is observed within the temperature range probed (Figure 5-11a), as already seen with PProDOT((CH$_2$O-(2S)-methylbutyl)$_2$. The linear trend is also observed for the 10/90 xylenes/DMF solutions (Figure 5-11d). These results suggest that a single mechanism operates in the thermochromic changes.[86] For the 50/50 and 40/60 xylenes/DMF solutions (Figures 5-11b and 5-11c), the maximum of absorption also varies linearly, but there is a clear change of slope between 40 and 60°C for the 50/50 solution and between 60 and 70°C for the 40/60 solution. The CD intensity, followed at 616 nm, decreases for both solutions with increasing temperature indicating that aggregates progressively break up and chains become molecularly dissolved (Figure 5-14a and 5-14b). At temperatures close to the change of slope in absorption, the CD becomes zero, indicating the polymer chains become molecularly dissolved and that

further changes in absorption are due only to intrachain interactions. The interchain breakup temperature highly depends on the xylenes/DMF ratio, as increasing the DMF content leads to higher interchain breakup temperatures. At higher DMF content than 60%, the aggregates cannot be fully reversed within the temperature experimentally accessible (0-100°C).

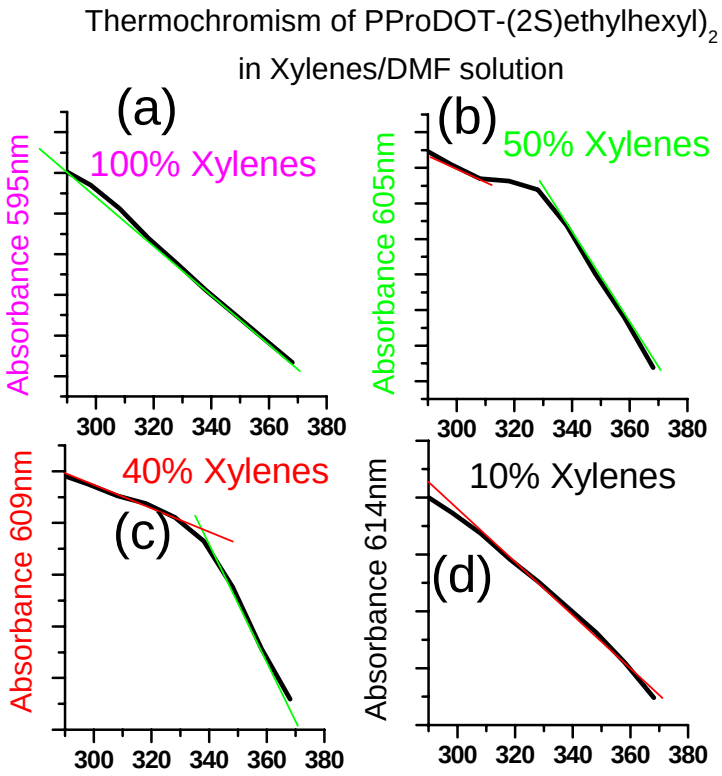

Figure 5-11. Thermochromism of PProDOT((2S)ethylhexyl)$_2$ in xylenes/DMF mixtures. The λ_{max} at of the absorption spectrum at 5°C is followed with temperature in: (a) 100% xylenes; (b) 50/50 xylenes/DMF; (c) 40/60 xylenes/DMF (d) 90/10 xylenes/DMF.

Looking at the fluorescence spectra for 50/50 xylenes/DMF solutions of PProDOT(2S-ethylhexyl)$_2$ and PProDOT(2S-methylbutyl)$_2$, a strong increase in fluorescence is observed as the temperature is increased (Figure 5-12). For PProDOT(2S-ethylhexyl)$_2$, the fluorescence increases until 70°C, as aggregates progressively breakup,

shown by the decrease in CD intensity. Above this temperature, the fluorescence levels off, likely to what is observed in the pure xylenes solutions, indicating that, as expected, no interchain interaction remains and the optical changes above 70°C are only due to intrachain interactions. For PProDOT(2S-methylbutyl)$_2$, there is a continual increase in fluorescence even up to 90°C (upper temperature limited by water chiller).

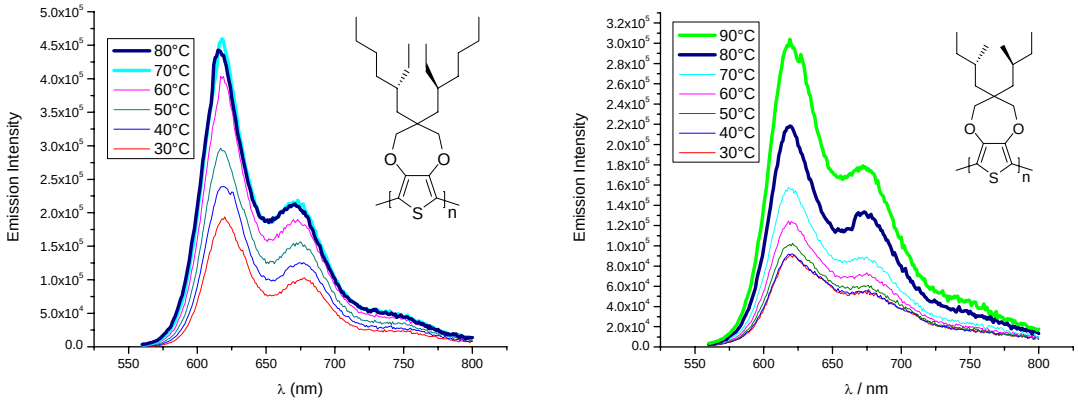

Figure 5-12. Fluorescence thermochromism of 50/50 xylenes/DMF PProDOT((2S)methylbutyl)$_2$ and PProDOT((2S)ethylhexyl)$_2$.

The results above show two different mechanisms are responsible for the thermochromic changes. In good solvent solutions or thermoreversible aggregates solutions above the interchain breakup temperature, intrachain distortions are responsible for the optical changes with temperature. On the other hand, in thermo-irreversible aggregates or thermoreversible aggregates studied below the interchain breakup temperature, interchain interactions are playing a large role in the optical changes, as shown by the progressive decrease of the CD intensity at 616nm.

As seen in Figure 5-13, the absorption spectrum at 95°C of the thermoreversible PProDOT(2S-ethylhexyl)$_2$ 50/50 xylenes/DMF aggregated solution is almost identical to the absorption in pure xylenes at 95°C, showing that intrachain interactions also play a role in the thermochromic changes.

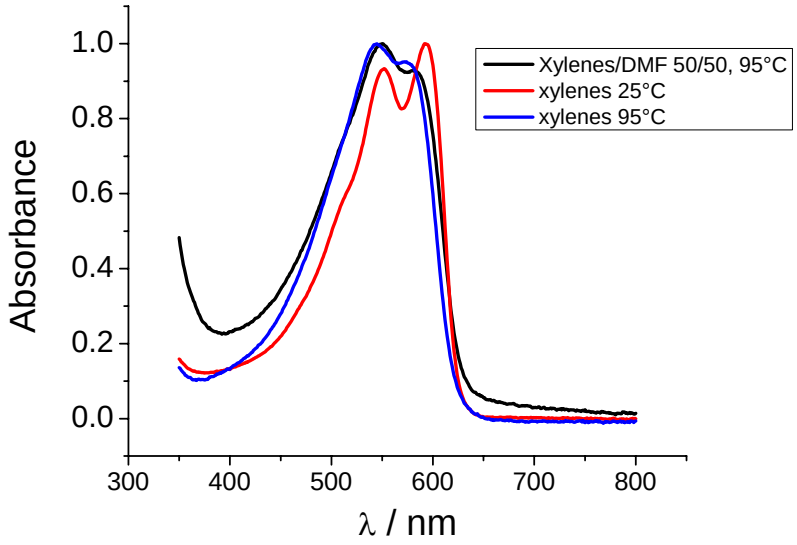

Figure 5-13. UV-Vis absorption of a 50/50 xylenes/DMF aggregated solution at 95°C. Comparison with pure xylenes solution at 95°C and 25°C.

By cooling slowly (12°C/hr) the 50/50 xylenes/DMF solution from the molecularly dissolved state, the aggregates reform with a significant hysteresis as shown in Figure 5-14a, as the CD intensity at 616nm only reappears at a temperature of ca. 40°C. At room temperature, after slow cooling treatment, the CD intensity at 616nm is fully recovered, but the CD signal shape is different, as displayed in Figure 5-15a. The CD signal of the slowly cooled solution indicates that new, thermodynamically stable chiral aggregates form. Such dependence on the cooling rate was observed in oligothiophenes as well.[93] The hysteresis depends strongly on the xylenes/DMF ratio. At a 40/60 xylenes/DMF ratio, only part of the CD intensity at 616 nm, as presented in Figure 5-14b, is recovered and the corresponding CD signal is also significantly modified. A possible explanation for the lower CD intensity, illustrated in Figures 5-14c and 5-14d, is that in the case of the 40/60 xylenes/DMF ratio, the chiral aggregates reform at a much higher temperature than the 50/50 solution. At such higher temperature, the intrachain conformation is expected to be more twisted, hindering the chains self-assembly. The absorbance spectra

after slow cooling are fully consistent with this assumption, as the maximum of absorption is blue shifted for the 40/60 xylenes/DMF solution compared to the 50/50 xylenes/DMF solution. In addition, the 0-1 vibronic transition becomes dominant for the 40/60 xylenes/DMF solution, characteristic of a more twisted intrachain conformation.

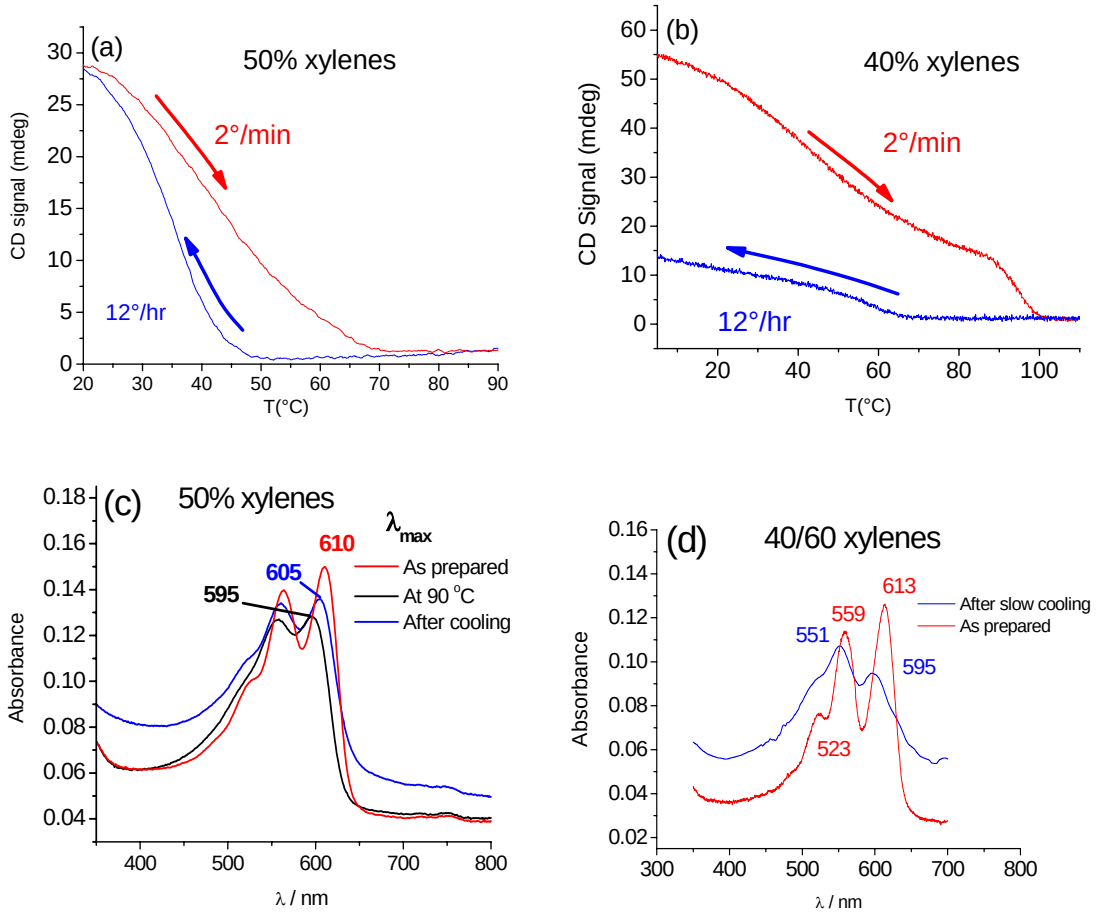

Figure 5-14. Evolution of absorption spectrum of 40/60 and 50/50 xylenes/DMF PProDOT-((2S)ethylhexyl)$_2$ solution following heating/slow cooling cycle. (a) CD signal, 50% xylenes; (b) CD signal, 40% xylenes; (c) UV-Vis absorption, CD signal, 50% xylenes; (d) UV-Vis absorption, CD signal, 40% xylenes.

Thermoreversibility was not observed in PProDOT((2S-methylbutyl)$_2$ solutions. Figure 5-15 compares the CD signals for PProDOT-((2S)-methylbutyl)$_2$ and PProDOT-((2S)ethylhexyl)$_2$ dissolved in 50/50 xylenes/DMF as a function of temperature. As the temperature is increased up to 100°C for PProDOT((2S-methylbutyl)$_2$, the CD signal is

decreased but still present. This observation is consistent with increased π-stacking interactions. (Figure 5-15d). Upon slow cooling of the hot solutions, a hysteresis in CD spectrum is also seen (Figures 5-15c and 5-15d).

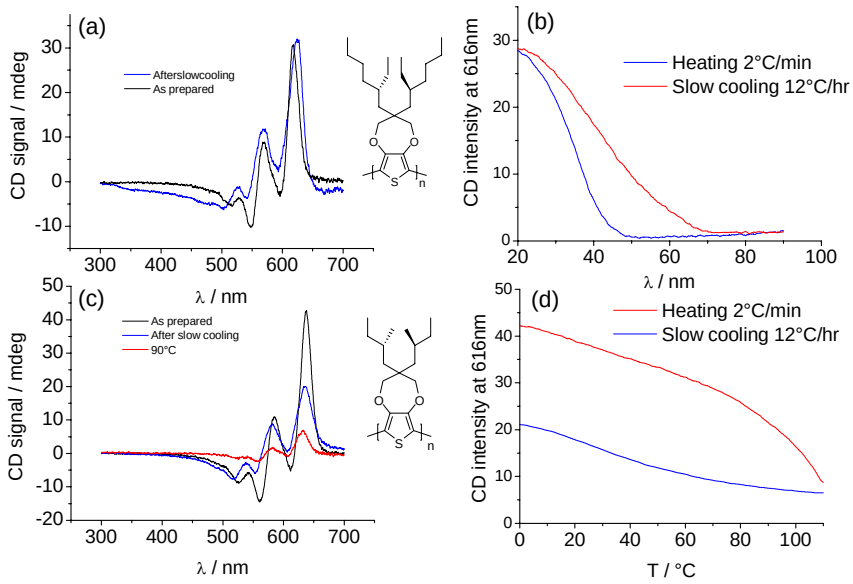

Figure 5-15. Polymer optical properties evolution during heating/slow cooling cycle. PProDOT(2S)-ethylhexyl)$_2$ 50/50 xylenes/DMF (a) CD spectrum "as prepared" and after slow cooling, (b) evolution of the CD signal at 616nm with temperature; PProDOT(2S)-methylbutyl)$_2$ 50/50 xylenes/DMF; (c) CD spectrum "as prepared", at 90°C and after slow cooling, (d) evolution of the CD signal at 616nm with temperature.

5.3.4. Chiral Order in Spray-cast Films

Films were spray-cast from toluene solution onto ITO-coated glass slides and analyzed by CD and absorption spectroscopy. The chiral branched alkyl PProDOTs both yield CD signals. The shape of the CD signal for spray-cast PProDOT-(2S-methylbutyl)$_2$ is similar to the solution aggregates, but the maximum anisotropy factor value is slightly lower with $g_{max} = 0.7\times10^{-2}$ at 637nm, possibly indicating that the aggregates are more disordered than in aggregated solution.

PProDOT-(2S-ethylhexyl)$_2$ yields a much higher CD signal, leading to an anisotropy factor comparable to its aggregated solutions with $g_{max} = 2.9\times10^{-2}$ at 627 nm. Remarkably, the shape of the CD signal is identical to the CD signal observed for the slowly cooled polymer solution, and is attributed to the formation of thermodynamically stable aggregates. Figure 5-16 shows the evolution of the absorption and CD spectra during a gas phase iodine doping/ hydrazine vapor reneutralization cycle. Upon exposure to iodine, the film CD signal is dramatically changed. The UV-Vis spectrum indicates the polymer film is fully oxidized to the bipolaron state (Figure 5-16b). The corresponding CD signal (Figure 5-16a), seen in the visible range of the absorption spectrum, is much less intense and blue shifted compared to the neutral film. This suggests that undoped chromophores with short conjugation lengths remain in the film and, more importantly, that the polymer chains retain a chiral orientation in the doped state. Similar observation were made in chiral poly(dithieno[3,2-b:2',3'-d]pyrroles).[94] A negative CD signal is also observed between 700 nm and 900 nm (Inset of Figure 5-16a), suggesting the bipolaron band is CD active. Such results are quite unique as the presence of CD activity in the bipolaron state has not been reported, mostly due to limitations of CD spectrophotometers in the near-IR region, where the bipolaron band absorbs. Upon exposure of the films to hydrazine vapor, the neutral polymer CD signal is fully recovered, demonstrating the stability of the chiral aggregates upon oxidation and the absence of doping-induced rearrangements. Studies on chiral poly(3-alkylthiophenes), on the other hand, showed that doping/dedoping cycles often result in significant CD signal changes.[95] After two days, the UV-vis and CD spectra of the cast films were examined again. The results indicate the polymer was dedoped to the polaron state, as noted by the

presence of the characteristic absorption peak centered at 950 nm. No CD signal is observed for this band showing the polaron absorption is not CD active.

Conversely to the aggregated solution study, significant differences between the first derivative of the absorption spectrum and the CD spectrum are observed. As seen in Figure 5-16, the wavelengths corresponding to the CD signal maxima now coincide with the wavelengths of the absorption spectrum maxima. Such behavior was not observed in chiral alkyl poly(thiophenes), as the CD signals for both aggregated solutions and films match the first derivative of the absorption spectra.[87]

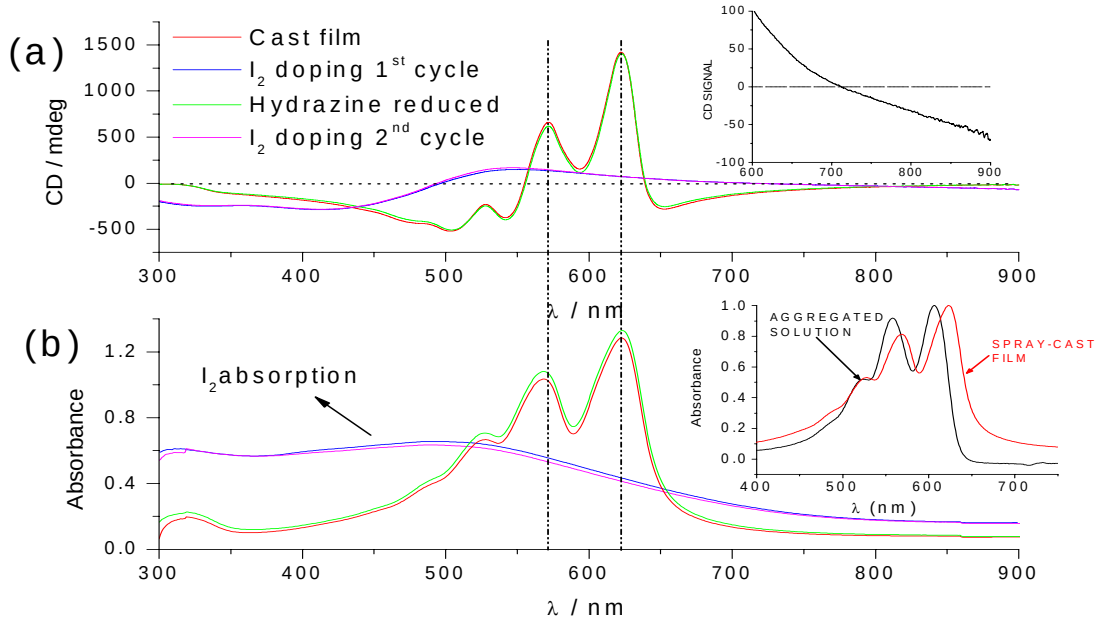

Figure 5-16. Absorption and CD signal for PProDOT-((2S)-ethylhexyl)$_2$) spray-coated films. (a) CD signal with doping/dedoping cycle. Inset shows a magnification of the 600-900nm region. (b) Absorption with doping/dedoping cycle. Inset shows a comparison of the absorption of a 30/70 xylenes/DMF aggregated solution to the spray-cast film absorption.

Given that the CD signals of the films and aggregated solutions are very close to one another, the difference between the CD signal of PProDOT((2S)-ethylhexyl)$_2$ in the

film state and the first derivative of the absorption spectrum could be explained from the difference of absorption spectra which are shifted 20 nm from one another (Inset, Figure 5-16b). This would suggest that achiral aggregates, absorbing on the low energy side of the optical transition (550-750nm), are also formed during film casting. However, a more likely explanation is that a new type of chiral aggregates is formed during casting. This possibility is supported by the high CD signals observed for this polymer, and also the stability of the CD signal to oxidation/reneutralization cycles. Recent results by Swager also indicate that multiple aggregates can form in the solid state depending on the processing conditions.[83a]

PProDOT(CH_2O-2S-methylbutyl)$_2$, spray-coated from a $CHCl_3$ solution on ITO, yields no CD signal, as seen in Figure 5-17. Upon electrochemical doping, a CD signal appears. The CD signal is quite weak and its shape is not well-defined, showing that the aggregates, although more ordered than the fresh cast film, remain disordered. The formation of chiral aggregates after an oxidation/reneutralization cycle demonstrates that, in addition to the doping-induced intrachain rearrangements created by the formation of the more planar quinoidal form in the oxidized state, interchain rearrangements occur. It also suggests that the disorder of the aggregates in alkoxy substituted PProDOTs originates from intrachain torsion of the chains in solution. This assumption is consistent with studies from Verbiest et al. on chiral poly(3,7-dimethyloctyloxythiophene) with varying degrees of regioregularity showing that regioregular samples, having much higher intrachain planarity (see Chapter 1), give much higher CD signal in the film state.[96] Regioirregular samples, having a more twisted backbone, were found to give no CD signal.

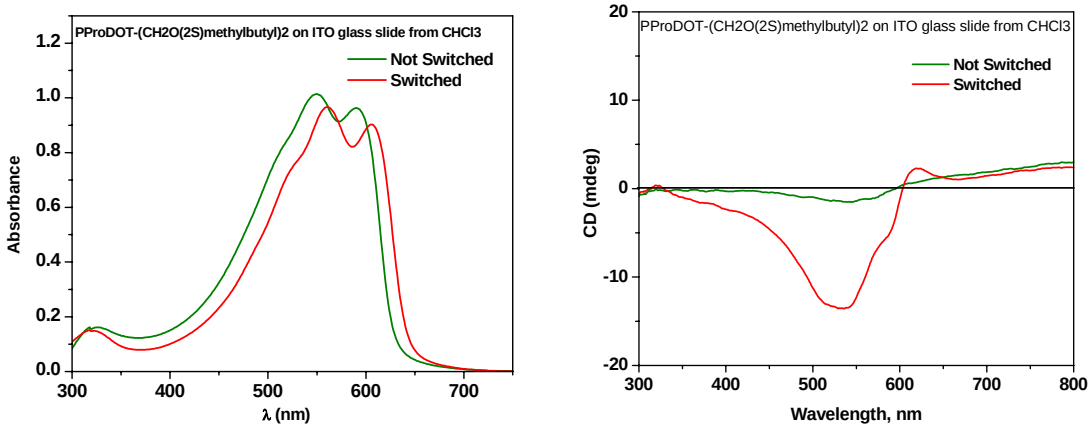

Figure 5-17. CD signal of chiral PProDOT(CH_2O-2-methyl)$_2$ spray-cast films. (left) UV absorption spectra; (right) CD signal.

5.4. Conclusion

Three regiosymmetric, soluble chiral polymers, PProDOT(CH_2O-2S-methylbutyl)$_2$, PProDOT(2S-methylbutyl)$_2$ and PProDOT(2S-ethylhexyl)$_2$ were synthesized by Grignard Metathesis. The synthesis of the latter polymer was made possible by a new synthesis of chiral 2S-ethylhexanol. The synthesis is simple, scalable, extremely versatile and should prove useful to many researchers in the field of soluble π-conjugated polymers. Using UV-Vis absorption, fluorescence and circular dichroism spectroscopy, a clear distinction between the role of inter and intrachain interactions in thermochromism and solvatochromism of ProDOT-based polymers was obtained. The alkyl substituted chiral polymers were found to form cholesteric aggregates similar to chiral substituted polythiophenes. Remarkably, the chiral aggregates in solution were found to be thermoreversible for PProDOT((2S)ethylhexyl)$_2$ but not for PProDOT(CH_2O-2S-methylbutyl)$_2$. This behavior is consistent with decreased π-stacking interchain interactions arising from introduction of the larger ethylhexyl substituents. In the solid

state, the polymers seem to form new chiral aggregates, stable to oxidation/reneutralization cycles, giving rise to intense CD signals. On the other hand, the ether linked , PProDOT(CH_2O-2S-methylbutyl)$_2$ does not form chiral aggregates in solution or in freshly cast films. Some limited chiral aggregation occurs upon oxidation and reneutralization cycle, indicated by the apparition of a weak, ill-defined CD signal. This behavior is attributed to intrachain torsion of the ether linked polymer preventing self-assembly of the molecules into helically ordered structures.

5.5. General Synthetic Details

Lithium chloride was dried under 0.1 mmHg vacuum at 150°C overnight. Dry THF, ether, toluene were obtained by distillation from Na/benzophenone ketyl. Dry diisopropylamine, hexane and ethyl acetate were obtained by distillation from CaH_2. Dry dimethylformamide was obtained by distillation from $MgSO_4$. n-BuLi was titrated with N-pivaloyl-o-benzylaniline.

(1R,2R)-pseudoephedrinepropionamide. In a flame-dried 500 mL round bottom flask (1R,2R)-(-)-pseudoephedrine (10g, 60.6 mmol, 1 eq.) was dissolved in 200 mL of dry THF. The flask was equipped with a pressure-equalizing addition funnel equipped with an argon inlet containing butyric anhydride (10.25g, 64.85 mmol, 1.07eq.). The reaction flask was placed in a water bath (25°C), and the anhydride was added dropwise over 15 minutes. The solution was stirred for one hour, after which the excess anhydride was quenched by slow addition of saturated sodium bicarbonate (300 mL). The product was extracted with ethyl acetate (3×200 mL) and washed with water (2×100 mL water). After drying the organic phase with magnesium sulfate, the solvent was removed under vacuum to yield a white solid. Recrystallization was accomplished in toluene to yield 12.3 g of white needle like crystals (86%). ^{1}H NMR (C_6D_6, 300 MHz) 0.61 (d), 0.82 (t),

0.98 (t), 1.55-1.67 (m), 1.74-1.88 (m), 2.1 (s), 2.45 (m), 2.84 (s), 3.74-3.86 (m), 4.06 (d), 4.25-4.42 (m), 4.52-4.62 (t), 4.98-5.18 (br), 7.00-7.42 (m); ^{13}C NMR ($CDCl_3$, 75 MHz) 14.135, 14.711, 15.539, 18.628, 18.979, 33.234, 35.867, 36. 498, 58.924, 75.686, 126.539, 127.087, 127.774, 128.511, 128.869, 142.676, 175.645 (NMR are complex because of the amide geometrical isomerism); HRMS $[M+H]^+$ calcd. 236.1650, found 236.1662.

(1R,2R)-pseudoephedrine-2S-ethylhexanamide. A flame-dried, 1L 3-neck flask equipped with an argon inlet was charged with dry lithium chloride (13.98 g, 330mmol), dry diisopropylamine (17.47 mL) (distilled from CaH_2) and 60 mL dry THF. After cooling at -78°C, nBuLi (51.5 mL, 2.23M, 115 mmol) was added via syringe over 15 min time. The reaction was warmed at 0°C for 5 min and cooled back to -78°C. (1R,2R)-(-)-pseudoephedrine, cooled at 0°C, was transferred by cannula into the reaction over 15 min. The reaction is stirred at -78°C for one hour, 0°C for 15 min 5 min at 25°C and then cooled down to 0°C where butyliodide (15.35 g, 83.31 mmol) was added dropwise. After 15 min, 5 mL of saturated ammonium chloride was added and the reaction was poured in 500 mL saturated ammonium chloride. The aqueous phase was extracted with ethyl acetate (3×250 mL). After washing with water (250 mL) the organic phase was dried over magnesium sulfate and the solvent was removed under vacuum, to yield a slight yellow viscous oil. The product was purified by column chromatography on silica gel (eluent: hexanes/ethylacetate (1/1)) and obtained as a colorless viscous oil (10g, 71%). ^1H NMR (C_6D_6, 300MHz) 0.72-0.76 (d), 0.8-1.25 (m), 2.61-2.83 (m), 2.1-2.23 (m), 2.3-2.36 (s), 2.65-2.72 (br), 2.92-2.94 (s), 4.1-4.25 (br), 4.45-4.62 (t), 5.2-5.4 (br), 7.04-7.38 (m); ^{13}C NMR (C_6D_6, 75 MHz) 12.43, 14.56, 14.91, 23.60, 26.83, 30.27, 33.06, 33.34, 44.34,

58.54, 60.92, 75.81, 76.72, 127.04, 127.64, 144.35, 178.20 (NMR are complex because of the amide geometrical isomerism); HRMS $[M+H]^+$ calcd. 292.2277, Found 292.2280.

2S-ethylhexylhexanoic acid. A 250 mL round-bottom flask was charged with (1R,2R)-pseudoephedrine-2S-ethylhexanamide (7g, 24mmol), sulfuric acid (45 mL, 18N) and dioxane (45 mL). The mixture was refluxed for one hour. After cooling to 25°C, the pH was brought to >10 by slow addition of 50% aqueous sodium hydroxide. The mixture was extracted with dichloromethane (2×100 mL). The aqueous phase was acidified to pH 1 and extracted again with dichloromethane (3×100 mL) to collect the product. After drying of the organic phase, the solvent is evaporated under vacuum (15°C, 20 mmHg) to obtain the product as a slightly yellow oil (2.4g, 70%). ^{1}H NMR ($CDCl_3$, 300MHz) 0.8-1.0 (m, 6H), 1.25-1.4 (m, 4H), 1.42-1.75 (m, 4H), 2.2-2.35 (m, 1H), 11-12 (br, 1H); ^{13}C NMR ($CDCl_3$, 75MHz) 11.98, 14.13, 22.86, 25.41, 29.75, 31.69, 47.31, 67.28, 182.93; HRMS calcd. $[M+H]^+$ 145.1231; exp. 145.1245; IR (C=O); $[\alpha]_D$ (C=1.3g/100 mL, acetone)= +10.0°.

2S-ethylhexanal. In a flame-dried 100 mL schlenk flask under argon atmosphere, lithium aluminum hydride (0.68g, 17.9 mmol) was suspended in 40 mL dry hexane. The flask was cooled to 0°C where dry ethyl acetate (2.3g, 26.1 mmol) was added very slowly over 90 minutes. After cooling the resulting suspension -78°C, a solution of (1R,2R)-pseudoephedrine-2S-ethylhexanamide (2.2g, 7.9 mmol) in 30 mL THF was transferred via cannula over 10 min. The reaction is then warmed to 0°C and stirred at this temperature for one hour. The solution is then transferred via cannula into a three neck round-bottom flask containing trifluoroacetic acid (7 mL, 90 mmol) in 100 mL of 1N HCl solution. After 5 min, the solution is transferred in 300 mL 1N HCl and extracted

with ethyl acetate (3×100 mL). The organic phase was washed with saturated sodium bicarbonate solution (2×100 mL). After drying with magnesium sulfate, the solvent is removed under vacuum (15°C, 20 mmHg) to give a yellow-brown oil. The product was purified by column chromatography on silica gel (eluent: hexanes/ethyl acetate 9/1, product revealed using 2,4-dinitrophenylhydrazine dip as bright yellow spots) to yield 2S-ethylhexanal as a slightly yellow oil (290mg, 30% yield). ^{1}H NMR ($CDCl_3$, 300MHz) 0.75-0.9 (m, 6H), 1.14-1.65 (m, 8H), 2.04-2.18 (m, 1H), 9.5 (d, 1H, J=3Hz). ^{13}C NMR ($CDCl_3$, 75 MHz) 11.68, 14.10, 22.08, 22.99, 28.38, 29.44, 53.64, 205.92; HRMS $[M+H]^+$ calcd. 129.1282 found 129.1290.

2S-ethylhexanoyl chloride. In a flame-dried 250 mL round-bottom flask under argon atmosphere 2S-ethylhexanoic acid (500mgs, 3.4mmol) was dissolved in dry dichloromethane. Thionyl chloride (3.2g, 27mmol, 8eq.) was added in one portion. The reaction was equipped with a condenser and reflux under argon overnight. The solvent and the excess thionyl chloride were removed under rotary evaporation, yielding the product as a slightly yellow-orange oil (510 mgs, 92% yield). ^{1}H NMR ($CDCl_3$, 300MHz) 0.78-0.95 (m, 6H), 1.18-1.26 (m, 4H), 1.43-1.8 (m, 4H), 2.58-2.7 (m,1H); ^{13}C NMR ($CDCl_3$, 75MHz) 11.53, 14.02, 22.70, 25.33, 29.27, 31.49, 58.95; $[\alpha]_D$ (C=1.2g/100 mL, acetone)= +7.4°.

Synthesis of 2S-ethylhexanol. In a flame-dried 3-neck flask equipped with a condenser and an argon inlet, Lithium aluminum hydride (1.74g, 46 mmol, 3 eq.) was dispersed in 100 mL of dry diethyl ether. A solution of 2S-ethylhexanoic acid (2.2g, 15.2mmol) in 50 mL of diethyl ether is added via cannula to the $LiAlH_4$ suspension. The reaction was then refluxed for one hour. After cooling the solution at 0°C, the excess

hydride was quenched (dropwise) by addition of water. When the hydride was quenched, 100 mL of water is added and the two phases were separated. The aqueous phase was further extracted with diethyl ether (2×100 mL). The combined organic fractions were washed with 1M HCl (100 mL), and water (2×100 mL). After drying with magnesium sulfate, the solvent was evaporated (20mmHg, 15°C) and the product was recovered as a transparent oil. ^{1}H NMR ($CDCl_3$, 300MHz) 0.8-1.05 (m, 6H), 1.05-1.45 (m, 9H), 3.45-3.65 (br, 2H); ^{13}C NMR ($CDCl_3$, 75MHz) 11.31, 14.30, 23.30, 23.56, 29.33, 30.34, 42.19, 65.55. $[\alpha]_D$ (C=1.2g/100 mL, acetone)= +3.1°. To determine the enantiomeric excess, the chiral alcohol was derivatizated with Mosher's reagent. Chiral 2S-ethylhexanol (20mgs, 0.15 mmol) was dissolved in 1 mL CCl_4 and R-(+)-α-methoxy-α-trifluoromethylphenylacetic acid chloride (50mgs, 0.2 mmol) was added. The reaction was stirred for 48hrs and water (10 mL) was added. After extraction with diethylether (2*10 mL), the organic phase was dried with magnesium sulfate and evaporated under reduced pressure. The resulting product was analyzed by GC to determine the enantiomeric excess of the alcohol (Chirasil-Dex CB column, 0.25mm×25cm). ee= 96%; Retention time: 23.9 min (corresponding to the minor R enantiomer of the alcohol, derivatized with Mosher's reagent) and 24.13 min (corresponding to the major S enantiomer of the alcohol derivatized with Mosher's reagent).

2S-ethylhexyltosylate: In a 100 mL round bottom flask was dissolved 2S-ethylhexanol (2.2g, 17 mmol) in 25 mL pyridine. Tosyl chloride (6.84g, 36mmol, 2eq.) was added in one portion. The reaction was stirred overnight at room temperature. Water (100 mL) and diethyl ether were added to the reaction. After separation of the two phases, the aqueous phase was further extracted with diethyl ether (2×50 mL). The

combined organic fractions were washed with water. The organic phase was dried with magnesium sulfate and the solvent was removed under vacuum to yield a yellow oil. The product was purified by column chromatography (Hexanes/dichloromethane) to yield a slightly yellow, viscous oil (4.1g, 85%); ^{1}H NMR ($CDCl_3$, 300MHz) 0.76-0.88 (m, 6H), 1.05-1.18 (m, 8H), 1.5-1.6 (m, 1H), 2.43 (s, 3H), 3.85-3.98 (m, 2H), 7.36 (d, 2H), 7.8 (d,2H); ^{13}C NMR ($CDCl_3$, 75MHz) 10.97, 14.18, 21.85, 23.05, 23.46, 28.87, 30.02, 39.28, 72.73, 128.12, 129.97.

2,2-((2S)-ethylhexyl)-propane-1,3-diol. In a 100 mL flame-dried 3-neck round bottom flask equipped with an argon inlet, a condenser, and an addition funnel were combined 30 mL of dry DMF, 2S-ethylhexyltosylate (4g, 14mmol, 2.5 eq.). After cooling at 0 °C, NaH (60% dispersion, 0.67g, 16.8mmol, 3eq) was added . The flask was maintained at 0 °C and freshly distilled diethyl malonate (0.9g, 5.6 mmol, 1eq.) in 20 mL dry DMF was added dropwise through the addition funnel. When the addition of the malonate was completed the mixture was heated to 100°C for three days. The flask was then cooled at 0 °C and the remaining sodium hydride was quenched by adding water dropwise. The mixture was then poured into water (200 mL), extracted with ether (2×100 mL), and washed with brine (100 mL). The solvent was removed under vacuum yielding a viscous oil. In a flame-dried 3 neck-flask, equipped with an argon inlet, a condenser and an addition funnel, lithium aluminum hydride (0.64g, 17mmol, 3eq.) was dispersed in 100 mL of dry diethyl ether. A solution of the dialkylated malonate in 50 mL of diethyl ether was added dropwise to the hydride dispersion. The addition funnel was removed and the reaction was refluxed for one hour. After cooling the solution at 0°C, the excess hydride was quenched (dropwise) by addition of water. When the hydride was quenched,

100 mL of water is added and the two phases were separated. The aqueous phase was further extracted with diethyl ether (2×100 mL). The combined organic fractions were washed with 1M HCl (100 mL), and water (2×100 mL). After drying with magnesium sulfate, the solvent was evaporated and the product was recovered as brown oil. The product was purified by column chromatography to yield a white solid (550 mgs, 33% yield). ^{1}H NMR ($CDCl_3$, 300MHz) 0.78-0.94 (m, 12H), 1.15-1.42 (m, 22H), 2.58 (s, 2H), 3.63 (s, 4H); ^{13}C NMR ($CDCl_3$, 75MHz) 10.79, 14.38, 23.35, 27.86, 29.04, 33.73, 34.94, 37.17, 42.81, 70.00. $[\alpha]_D$ (C=2.7g/100 mL, acetone)= -10.0°.

3,3-bis((S)-2-ethylhexyl)-3,4-dihydro-2H-thieno[3,4-b][1,4]dioxepine (ProDOT((2S)-ethylhexyl)$_2$). 3,4-dimethoxythiophene (0.24mgs, 1.69mmol), 2,2-((2S)-ethylhexyl)-propane-1,3-diol (500mgs, 1.67mmol), *p*-toluenesulfonic acid (32mgs, 0.17mmol) with 50 mL of dry toluene were combined in a 100 mL flask equipped with a soxhlet extractor with $CaCl_2$ molecular sieves in a cellulose thimble. The solution was refluxed overnight. The reaction mixture was cooled and 5 mL triethyl amine is added. Ether (100 mL) is added and the organic solution is washed once with water (100 mL). The solvent was removed under vacuum, and the crude product was purified by column chromatography on silica gel with 4:1 hexanes/methylene chloride, to yield the pure product as a clear viscous oil (440mgs, 70%). ^{1}H NMR ($CDCl_3$, 300MHz) 0.75-0.92 (m, 12H), 1.15-1.5 (m, 22H), 3.92 (s, 4H), 6.42 (s, 2H); ^{13}C NMR ($CDCl_3$, 75MHz) 10.82, 14.38, 23.34, 28.02, 29.02, 33.87, 35.09, 38.79, 45.56, 78.07, 104.60, 149.99.

6,8-dibromo-3,3-bis((S)-2-ethylhexyl)-3,4-dihydro-2H-thieno[3,4-b][1,4]dioxepine (ProDOT((2S)-ethylhexyl)$_2$-Br$_2$). ProDOT((2S-ethylhexyl)$_2$ (420 mgs, 1.1mmol, 1eq.) was dissolved in 100 mL dry DMF in a 250 mL round-bottom flask. The

solvent was degassed by bubbling argon in the solution for one hour. N-bromosuccinimide (500mgs, 2.8mmol, 2.5eq.) was added in one portion, and the reaction was stirred under argon overnight, at room temperature. Water (200 mL) was added to the reaction and the aqueous phase was extracted with diethylether (3×100 mL). The organic phase was washed with water (3×100 mL), dried with magnesium sulfate. After solvent evaporation, the resulting oil was purified by column chromatography on silica gel (hexanes/dichloromethane 4/1) to afford ProDOT((2S)-ethylhexyl)$_2$-Br$_2$ as a clear, colorless viscous oil (512mgs, 86% yield). ^{1}H NMR ($CDCl_3$, 300MHz) 0.78-0.96 (m, 12H), 1.17-1.46 (m, 22H), 3.99 (s, 4H); ^{13}C NMR ($CDCl_3$, 75MHz) 10.81, 14.38, 23.32, 27.97, 29.01, 33.93, 35.01, 38.88, 45.81, 78.61, 90.54, 147.30; HRMS $[M]^+$ Calcd. 536.1028 Found 536.0990

Poly(3,3-bis((S)-2-ethylhexyl)-3,4-dihydro-2H-thieno[3,4-b][1,4]dioxepine) (PProDOT((2S)-ethylhexyl)$_2$). To a two-neck round bottom flask equipped with a condenser and an argon inlet, ProDOT((2S)-ethylhexyl)$_2$Br$_2$ (440mgs, 0.82mmol, 1eq.) was dissolved in 25 mL of dry THF. Methylmagnesium bromide (0.85mL, C=0.96M, 0.82 mmol, 1eq.) was added via syringe. The reaction was refluxed for one hour, after which Ni(dppp)Cl_2 (9mgs, 0.016mmol, 0.02 eq.) was added. After a few seconds, the solution turned bright red. The reaction was refluxed overnight, and then allowed to cool to room temperature. The polymer was precipitated in 200 mL of MeOH and filtered through a soxhlet thimble. The polymer was purified by Sohlet Extraction with MeOH (24hrs) then Hexanes (24hrs). It was then extracted with $CHCl_3$, to yield after rotary evaporation 180 mgs of shiny-brown colored solid. GPC (THF, 25°C) M_n= 8,700 g mol^{-1}, M_n= 14,200 g mol^{-1}, PDI=1.6; ^{1}H NMR (300MHz, $CDCl_3$) 0.75-0.92 (br, 12H), 1.12-1.63

(br, 22H), 3.8-4.3 (br, 4H); ^{13}C NMR (75MHz, $CDCl_3$) 10.91, 14.44, 23.44, 27.80, 28.98, 33.88, 35.22, 38.65, 45.66, 78.16, 115.75, 144.93.

2S-methylbutyltosylate: In a 100 mL round bottom flask was dissolved 2S-methylbutanol (5g, 57 mmol) in 100 mL pyridine. Tosyl chloride (21.6g, 113mmol, 2eq.) was added in one portion. The reaction was stirred overnight at room temperature. Water (300 mL) and diethyl ether were added to the reaction. After separation of the two phases, the aqueous phase was further extracted with diethyl ether (2×150 mL). The combined organic fractions were washed with water. The organic phase was dried with magnesium sulfate and the solvent was removed under vacuum to yield a yellow oil. The product was purified by column chromatography (Hexanes/dichloromethane) to yield a clear viscous oil (11.9g, 92%); ^{1}H NMR ($CDCl_3$, 300MHz) 0.78-0.92 (m, 6H), 1.04-1.23 (m, 1H), 1.3-1.46 (m, 1H), 1.62-1.78 (m, 1H), 2.44 (s, 3H), 3.77 (m, 2H), 7.35 (d,2H), 7.77 (d, 2H); ^{13}C NMR ($CDCl_3$, 75MHz) 10.97, 14.18, 21.85, 23.05, 23.46, 28.87, 30.02, 39.28, 72.73, 128.12, 129.97.

2,2-((2S)-methylbutyl)-propane-1,3-diol. In a 100 mL flame-dried 3-neck round bottom flask equipped with an argon inlet, a condenser, and an addition funnel were combined 100 mL of dry DMF, 2S-ethylhexyltosylate (11g, 49mmol, 2.5 eq.). After cooling at 0 °C, NaH (60% dispersion, 2.34g, 58.4mmol, 3eq) was added. The flask was maintained at 0 °C and freshly distilled diethyl malonate (3.14g, 19.6 mmol, 1eq.) in 50 mL dry DMF was added dropwise through the addition funnel. When the addition of the malonate was completed the mixture was heated to 100°C for three days. The flask was then cooled at 0 °C and the remaining sodium hydride was quenched by adding water dropwise. The mixture was then poured into water (500 mL), extracted with ether (3×200

mL), and washed with brine (200 mL). The solvent was removed under vacuum yielding a viscous oil, used without further purification. In a flame-dried 3 neck-flask, equipped with an argon inlet, a condenser and an addition funnel, lithium aluminum hydride (2.24g, 17mmol, 3eq.) was dispersed in 300 mL of dry diethyl ether. A solution of the dialkylated malonate in 150 mL of diethyl ether was added dropwise to the hydride dispersion. The addition funnel was removed and the reaction was refluxed for one hour. After cooling the solution at 0°C, the excess hydride was quenched (dropwise) by addition of water. When the hydride was quenched, 300 mL of water is added and the two phases were separated. The aqueous phase was further extracted with diethyl ether (3×200 mL). The combined organic fractions were washed with 1M HCl (200 mL), and water (2×200 mL). After drying with magnesium sulfate, the solvent was evaporated and the product was recovered as yellow oil. The product was purified by column chromatography to yield a white solid (1.3 g, 31% yield). ^{1}H NMR ($CDCl_3$, 300MHz) 0.82-0.95 (m, 12H), 1.08-1.53 (m, 10H), 2.54 (t, 2H), 3.62 (d, 4H); ^{13}C NMR ($CDCl_3$, 75MHz) 11.70, 21.91, 29.55, 32.20, 39.19, 42.81, 70.13; HRMS $[M+H]^+$ Calcd. 217.2168 Found 217.2178.

3,3-bis((2S-methylbutyl)-3,4-dihydro-2H-thieno[3,4-b][1,4]dioxepine (ProDOT((2S)-methylbutyl)$_2$). 3,4-dimethoxythiophene (0.66mgs, 4.62mmol), 2,2-((2S)-methylbutyl)-propane-1,3-diol (1g, 4.62mmol), *p*-toluenesulfonic acid (32mgs, 0.46mmol) with 250mL of dry toluene were combined in a 500 mL flask equipped with a soxhlet extractor with $CaCl_2$ molecular sieves in a cellulose thimble. The solution was refluxed overnight. The reaction mixture was cooled and 5 mL triethyl amine is added. Ether (300 mL) is added and the organic solution is washed once with water (200 mL).

The solvent was removed under vacuum, and the crude product was purified by column chromatography on silica gel with 4:1 hexanes/methylene chloride, to yield the pure product as a clear viscous oil (1.08mgs, 79%). ^{1}H NMR ($CDCl_3$, 300MHz) 0.88 (t, 6H), 0.95 (d, 6H), 1.22-1.57 (m, 10H), 3.92 (m, 4H), 6.41 (s, 2H); ^{13}C NMR ($CDCl_3$, 75MHz) 11.67, 22.09, 29.71, 32.24, 40.98, 45.61, 78.36, 104.63, 149.96. HRMS $[M]^+$ Calcd. 296.1810 Found 296.1798.

6,8-dibromo-3,3-bis(2S-methylbutyl)-3,4-dihydro-2H-thieno[3,4-b][1,4]dioxepine (ProDOT((2S)-methylbutyl)$_2$-Br$_2$) ProDOT((2S-methylbutyl)$_2$ (0.8g, 2.7 mmol, 1eq.) was dissolved in 250 mL dry DMF in a 500 mL round-bottom flask. The solvent was degassed by bubbling argon in the solution for one hour. N-bromosuccinimide (1.2g, 6.8mmol, 2.5eq.) was added in one portion, and the reaction was stirred under argon overnight, at room temperature. Water (500 mL) was added to the reaction and the aqueous phase was extracted with diethylether (3×200 mL). The organic phase was washed with water (3×200 mL), and dried with magnesium sulfate. After solvent evaporation, the resulting oil was purified by column chromatography on silica gel (hexanes/dichloromethane 4/1) to afford ProDOT((2S)-methylbutyl)$_2$-Br$_2$ as a clear, colorless viscous oil (1.1gs, 90% yield). ^{1}H NMR ($CDCl_3$, 300MHz) 0.89 (t, 6H), 0.95 (d, 6H), 1.12-1.54 (m, 10H), 3.99 (s, 4H); ^{13}C NMR ($CDCl_3$, 75MHz) 11.63, 21.96, 29.67, 32.12, 40.83, 45.84, 79.00, 90.64, 147.30; HRMS $[M]^+$ Calcd. 452.0021 Found 452.0015.

Poly(3,3-bis((2S-methylbutyl)-3,4-dihydro-2H-thieno[3,4-b][1,4]dioxepine) (PProDOT((2S)-methylbutyl)$_2$). To a two-neck round bottom flask equipped with a condenser and an argon inlet, ProDOT((2S)-methylbutyl)$_2$Br$_2$ (0.95g, 2.1mmol, 1eq.) was

dissolved in 25 mL of dry THF. Methylmagnesium bromide (1.95 mL, C=1.07M, 2.1 mmol, 1eq.) was added via syringe. The reaction was refluxed for two hours, after which Ni(dppp)Cl_2 (23mgs, 0.042mmol, 0.02 eq.) was added. After a few seconds, the solution turned bright red. The reaction was refluxed overnight, and then allowed to cool to room temperature. The polymer was precipitated in 200 mL of MeOH and filtered through a soxhlet thimble. The polymer was purified by Soxhlet extraction with MeOH (24hrs) then Hexanes (24hrs). It was then extracted with $CHCl_3$, to yield after rotary evaporation 460 mgs of shiny-brown colored solid. GPC (THF, 25°C) M_n= 8,400 g mol^{-1}, M_n= 13,800 g mol^{-1}, PDI=1.6; ^{1}H NMR (300MHz, C_6D_6) 0.7-0.95 (br, 6H), 0.95-1.07 (br, 6H), 1.07-1.27 (br, 2H), 1.27-1.65 (br, 8H), 3.65-4.3 (br, 4H); ^{13}C NMR (75MHz, C_6D_6) 12.15, 22.63, 30.09, 32.77, 41.24, 45.95, 78.65, 114.97, 145.89.

3,3-Bis-(2S-methylbutyloxymethyl)-3,4-dihydro-2H-thieno[3,4-b][1,4]dioxepine (ProDOT(CH_2O-2S-methylbutyl)$_2$). A 250 mL flame dried round bottom flask filled with 60 mL of DMF, 23.4 mmols of alcohol (4eq), and 23.4 mmols of NaH (4eq) was heated at 110 °C overnight. Then 5.85 mmols of ProDOT($CH_2Br)_2$ was added and the reaction continued at 110 °C for another 24 hr. After completion, the flask was cooled and added to 200 mL brine and extracted 3 times with ethyl ether. The organic layer was then washed 3 times with water, dried over magnesium sulfate, and the solvent was removed by rotary evaporation under reduced pressure. The resulting orange oil was purified by column chromatography (3:2 hexanes, methylene chloride).The crude oil obtained was purified by column chromatography (CH_2Cl_2) to afford 2.1g of clear oil (95%). ^{1}H NMR (300 MHz, $CDCl_3$) δ 0.81-0.91 (m, 12H), 1.01-1.21 (m, 2H), 1.33-1.48 (m, 2H), 1.55-1.68 (m, 2H), 3.14-3.29 (m, 4H), 3.45-3.53 (m, 4H), 4.09 (s, 4H); ^{13}C

NMR (75 MHz, $CDCl_3$) δ 11.80, 17.05, 26.68, 35.36, 48.36, 70.21, 74.20, 77.88, 105.42, 150.15. HRMS calculated for $C_{25}H_{44}O_4S$: 356.2021 Found 356.2026. Elemental Anal. Calcd for $C_{25}H_{44}O_4S$: C 64.01; H 9.05; S 8.99 Found: C 64.04; H 9.41; S 8.78.

6,8-Dibromo-3,3-bis-(2-methylbutyloxymethyl)-3,4-dihydro-2H-thieno[3,4-b][1,4]dioxepine (ProDOT(CH_2O-2-methylbutyl)$_2Br_2$) ProDOT(CH_2O-(2S-methylbutyl)$_2$ (2.8g, 7.9 mmol, 1eq.) was dissolved in 250 mL dry DMF in a 500 mL round-bottom flask. The solvent was degassed by bubbling argon in the solution for one hour. N-bromosuccinimide (3.5g, 20mmol, 2.5eq.) was added in one portion, and the reaction was stirred under argon overnight, at room temperature. Water (500 mL) was added to the reaction and the aqueous phase was extracted with diethylether (3×200 mL). The organic phase was washed with water (3×200 mL), and dried with magnesium sulfate. After solvent evaporation, the resulting oil was purified by column chromatography on silica gel (hexanes/dichloromethane 4/1) to afford ProDOT(CH_2O-(2S)-methylbutyl)$_2$-Br_2 as a clear, colorless viscous oil (3.5gs, 86% yield).^{1}H NMR (300 MHz, $CDCl_3$) δ 0.84-0.91 (m, 12H), 1.04-1.21 (m, 2H), 1.33-1.48 (m, 2H), 1.55-1.69 (m, 2H), 3.13-3.29 (m, 4H), 3.44-3.53 (m, 4H), 4.09 (m, 4H); ^{13}C NMR (300MHz, $CDCl_3$) δ 11.57, 16.83, 26.45, 35.14, 69.86, 74.52, 77.01, 91.11, 147.27; HRMS Calcd for $C_{25}H_{42}O_4SBr_2$ 514.0232. Found 514.0226; Elemental Anal. Calcd for $C_{25}H_{42}O_4SBr_2$: C 44.37; H 5.88; S 6.23; Br 31.07 Found: C 44.46; H 6.16; S 6.08; Br 30.84.

Poly(3,3-bis-(2S-methylbutyloxymethyl)-3,4-dihydro-2H-thieno[3,4-b][1,4]dioxepine) (PProDOT(CH_2O-2S-methylbutyl)$_2$. To a two-neck round bottom flask equipped with a condenser and an argon inlet, ProDOT(CH_2O-(2S)-methylbutyl)$_2Br_2$ (0.82g, 1.6 mmol, 1eq.) was dissolved in 25 mL of dry THF.

Methylmagnesium bromide (1.45 mL, C=1.1M, 2.1 mmol, 1eq.) was added via syringe. The reaction was refluxed for two hours, after which Ni(dppp)Cl_2 (15mgs, 0.032mmol, 0.02 eq.) was added. After a few seconds, the solution turned bright red. The reaction was refluxed overnight, and then allowed to cool to room temperature. The polymer was precipitated in 200 mL of MeOH and filtered through a soxhlet thimble. The polymer was purified by Soxhlet extraction with MeOH (24hrs) then Hexanes (24hrs). It was then extracted with $CHCl_3$, to yield after rotary evaporation 450 mgs of shiny-brown colored solid.g of purple solid obtained (80%). ^{1}H NMR (300 MHz, benzene-d_6) δ 0.82-1.07 (br, 12H),1.1-1.27 (br, 2H), 1.34-1.53 (br, 2H), 1.55-1.72 (br, 2H), 3.04-3.26 (br doublet, 4H), 3.46-3.64(br singlet, 4H), 4.1-4.35 (br singlet, 4H); ^{13}C (75 MHz, benzene-d_6) δ 11.93, 17.37, 27.07, 35.69, 70.8, 75.21, 77.7.

CHAPTER 6
SOLUBLE POLY(3,4-PHENYLENEDIOXYTHIOPHENES)

6.1. Introduction

As discussed earlier, regioregular poly(3-alkylthiophene)s provide some of the best performing semiconducting polymeric materials and are increasingly finding use in device applications which include organic field-effect transistors,[13,17c,88,97] and photovoltaics[98,19], where their high degree of order yields high charge carrier mobilities. The more easily oxidized poly(3,4-ethylenedioxythiophene) (PEDOT) has been used as the active material in electrochromic devices, anti-static coatings and capacitors, and as a hole injecting layer in OLEDs.[56]Poly(3,4-ethylenedioxythiophene):poly(styrenesulfonate) (PEDOT:PSS) provides an interesting alternative to indium tin oxide (ITO), showing better mechanical properties, low surface roughness and more facile processing from aqueous dispersions. While it was used successfully in the fabrication of flexible, all-plastic electrochromic devices,[99] PEDOT:PSS has a relatively low conductivity compared to ITO (100-500 S cm^{-1} vs. 4000 S cm^{-1}).[8] It is desirable to synthesize easily oxidized, low band gap conjugated polymers with a high degree of order, useful processability and flexible mechanical properties.

In recent publications, both Ritter[100] and Roncali[101] introduced 3,4-phenylenedioxythiophene (PheDOT) as an attractive synthon for obtaining highly ordered polythiophenes. X-ray crystal structures of 2,5-dibromo-PheDOT show that the thiophene and phenylene rings are fully coplanar (Figure 6-1). This should provide a strong driving force for a high degree of ordering in the solid state. PheDOT, and more

recently its dimer and trimer, were electropolymerized to yield electroactive films.[101,102] As is common with electropolymerized materials, the resulting polymers are insoluble arising from strong π- stacking interactions, and therefore cannot be solution-processed.

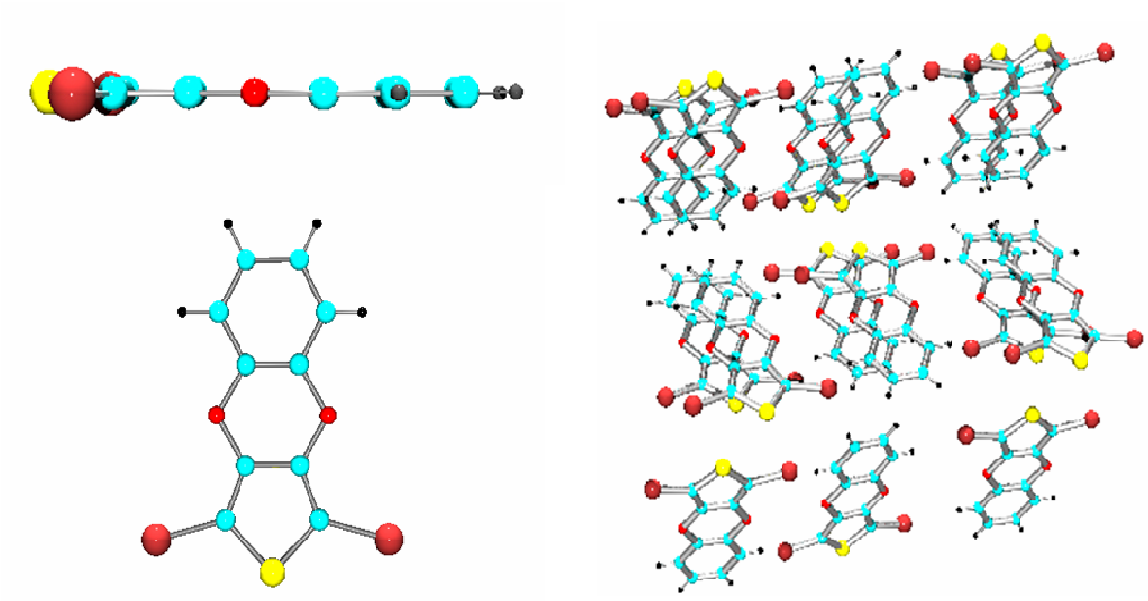

Figure 6-1. X-ray crystal structure of PheDOT-Br_2. Yellow spheres are sulfurs; blue spheres are carbons, black spheres are hydrogens, small red spheres are oxygens and large red spheres are bromides.

In this Chapter, the synthesis of the first soluble and processable PolyPheDOTs is introduced. Solubility is obtained by substitution at the 4- and 5- positions of the veratrole moiety with either dodecyl or ethylhexyl substituents (Figure 6-2). The side chains extend within the plane of the polythiophene backbone and are expected to have a strong effect on the polymers properties. Dodecyl side chains should provide a supplementary driving force for ordering, while the bulk of the ethylhexyl substituent should provide high solubility and strongly decrease interchain interactions.

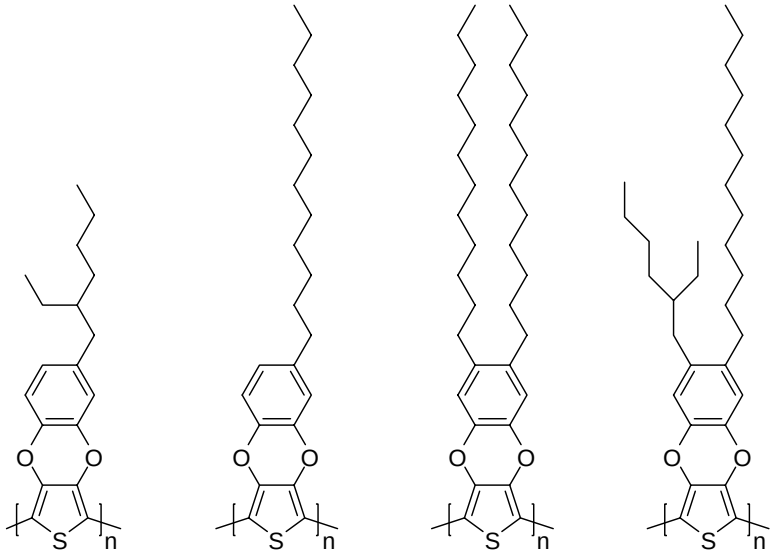

PPheDOTEtHx PPheDOTC$_{12}$ PPheDOT(C$_{12}$)$_2$ PPheDOTC$_{12}$EtHx

Figure 6-2. Family of Soluble Substituted PPheDOTs under study.

6.2 Synthesis of Soluble Substituted PheDOT

PheDOT-$(C_{12})_2$ was synthesized using a modified procedure outlined by Roncali et al. who synthesized PheDOT$(C_6)_2$ (Figure 6-3).[101] The synthesis starts with a Friedel-Crafts acylation of veratrole, followed by reduction of the ketone using $AlCl_3/LiAlH_4$. Dialkyl substituted veratroles are synthesized by repeating this two-steps procedure. The 4,5-bis(2-ethylhexyl)-veratrole derivative could not be obtained as the steric hindrance of the branched substituent in 4-(2-ethylhexyl)-veratrole prevented a second Friedel-Crafts reaction with 2-ethylhexanoyl chloride. On the other hand, 4,5-bis(2-ethylhexyl)-veratrole could react in a Friedel-Crafts reaction with lauroyl chloride to yield 4-dodecyl-5-(2-ethylhexyl)-veratrole after reduction. Interestingly, the Friedel-Crafts reaction between 4-dodecyl-veratrole and 2-ethylhexanoyl chloride was unsuccessful although it yields the same product after reduction.

The substituted veratroles are converted to the substituted catechols using boron tribromide. Transetherification between the substituted catechols and 3,4-

dimethoxythiophene yields the electropolymerizable monomers in 20-30% yield. The low yield arise from the lower nucleophilicity of the catechols compared to 1,3-propanediols that are used in the synthesis of substituted PProDOTs, as presented in Chapter 3,4 and 5.

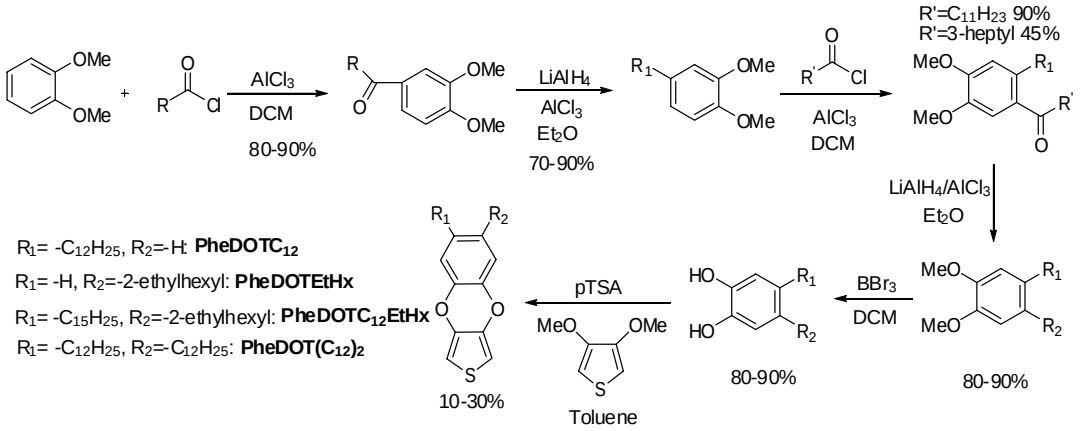

Figure 6-3. Synthesis of mono- and disubstituted PheDOTs. Substituents are either dodecyl or 2-ethylhexyl.

6.3. Electropolymerization of Substituted PheDOTs

6.3.1. Electrodeposition and Electronic Properties

After purification of the electropolymerizable monomers, polymer films were electrodeposited on a platinum button electrode. The electrodeposition by cyclic voltammetry was more difficult than for PProDOTs derivatives as evidenced by the slow growth (Figure 6-4a). This behavior can be explained by the increased stability of the PheDOT radical-cation, which is the reactive intermediate in electropolymerization.[27a] Roncali et al. carried out calculations demonstrating that the SOMO of the PheDOT radical cation has only little electron density on the 2- and 5- positions of the thiophene conversely to the EDOT radical-cation, having strong electronic density at these two positions.[101] As a result, EDOT polymerizes fast while PheDOT polymerizes slowly.

Another issue is that the dioxybenzene unit oxidizes irreversibly at potentials close to the monomer oxidation, as demonstrated for veratrole, which forms cyclic trimers

when oxidized electrochemically.[103] The electropolymerization must therefore be performed at a potential sufficiently high to have electrodeposition but low enough to limit side reactions. Another approach is to synthesize the dimer or trimer of PheDOT, which can be electropolymerized at potential well below the oxidation potential of the dioxybenzene unit.[102] Table 6-1 summarizes the electronic properties of the electropolymerizable monomers and polymers deposited by cyclic voltammetry. Substitution of PheDOT results in a decrease of the monomer oxidation due to a slight electron donation by the alkyl substituents into the benzene ring. In some cases, toluene was added to the acetonitrile monomer solution to achieve complete solubilization of the monomer. The amount of toluene must be as little as possible, as an excess toluene will cause delamination of the electrodeposited films.

Table 6-1. Electrochemical properties of substituted PheDOTs electropolymerizable monomers and electrodeposited disubstituted PPheDOTs films. Potentials are given vs. Fc/Fc^+ standard.

	E_{onset} **Monomer (mV)**[a]	E_{onset} **Polymer (mV)**[b]	$E_{1/2}$ **Polymer (mV)**	ΔE_p **(mV)**	I_a/I_c
PheDOT	980	N/A	N/A	N/A	N/A
PheDOTC$_{12}$	970[c]	139	520	80	1.23
PheDOTEtHx	920	8	465	76	1.07
PheDOTC$_{12}$EtHx	910[c]	395	607	260	1.22
PheDOT(C$_{12}$)$_2$	870[c]	330	629	320	1.65

(a) electrodeposition in 0.1M TBAP ACN; (b) determined by cyclic voltammetry; (c) Toluene added dropwise until full monomer dissolution

Overall, the polymer films oxidation is shifted to higher potentials with increasing steric bulk, with disubstituted PPheDOTs having the highest oxidation potentials. Figure 6-4a shows the slow electrodeposition by cyclic voltammetry of PheDOTC$_{12}$ on a platinum button electrode. In Figure 6-4b, cyclic voltammetry between -1V and 1.3V of an electrodeposited film of PPheDOTEtHx shows the presence of an irreversible

oxidation reaction, resulting in a strong decrease of electroactivity of the conjugated polymer. The degradation also occurs with other substituted or unsubstituted PPheDOT and is attributed to the degradation of the phenylene unit.

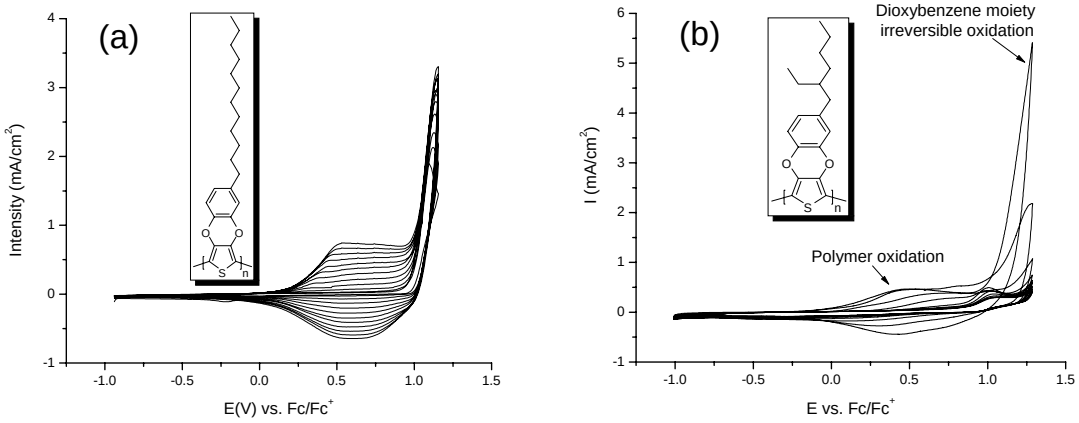

Figure 6-4. Electrodeposition and electrochemistry of substituted PPheDOTs films. (a) Electrodeposition of PPheDOT-C_{12} by cyclic voltammetry. Scan rate is 50mV s^{-1}. Every 5th cycle shown (out of 50 cycles); (b) PPheDOT-EtHx degradation of PPheDOTs at high potentials.

The disubstituted electropolymerizable monomers display unusual oxidation behavior. Figure 6-5 shows the monomer oxidation for PheDOT$(C_{12})_2$ at various scan rates.

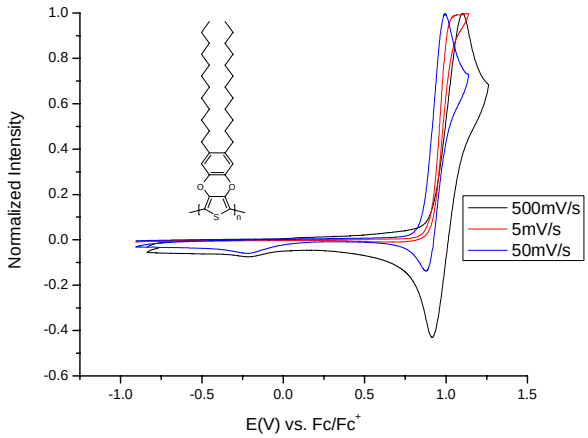

Figure 6-5. PheDOT$(C_{12})_2$ oxidation at various scan rates. Monomer concentration is 0.01M in 0.1M TBAP/(3:1 ACN/toluene).

At a scan rate of 50mV s^{-1}, the scan rate is partially reversible as a reduction peak for the oxidized monomer is observed. By increasing the scan rate to 500 mV s^{-1}, the oxidation wave becomes more reversible while decreasing the scan rate to 5 mV s^{-1} yields an irreversible wave. The reversibility arises from the increased stability of the disubstituted PheDOTs radical through electron donation by the alkyl groups, supported by theoretical calculations.[101] By decreasing the scan rate, the radical cations have more time to propagate and polymerize, and the oxidation peak become irreversible.

6.3.2. Spectroelectrochemical Characterization of Electrodeposited Films

Following electrodeposition of the polymers onto ITO-coated glass slides, the polymer films properties were probed by spectroelectrochemistry (Table 6-2). The results indicate that upon introducing linear dodecyl substituents, there are no significant changes of the optical bandgap. In the symmetrically substituted PPheDOT$(C_{12})_2$, the bandgap is even slightly decreased, possibly indicating an ordering effect of the dodecyl chains. It also shows that, as expected, the dodecyl offer little steric hindrance to interchain interactions. Introduction of 2-ethylhexyl substituents in PPheDOTEtHx leads to an increase of the optical bandgap by 50 meV compared to electrodeposited PPheDOT. In PPheDOTC12EtHx, the bandgap is 100meV higher showing a clear decrease of interchain interactions, due to introduction of the dodecyl chain in place of the smaller hydrogen present in PPheDOTEtHx.

Beside PPheDOT$(C_{12})_2$, all substituted monomers are unsymmetrical leading to regioirregular polymers, which could lead to intrachain torsion through steric repulsion between every other PheDOT repeat units. However, evidence that the chains remain planar despite the regioirregular distribution of the side chains will be presented later in this chapter.

Table 6-2. Optical properties of electrodeposited films onto ITO-coated glass slides. Polymers were deposited from 0.01M monomer solution in 0.1M TBAP in ACN. In the case where the monomer is not fully soluble, a minimal amount of toluene was added to obtain full solubility.

	λ_{max} (nm)	E_g (eV)[a]	Yxy Luminance Neutral film [c]	Yxy Luminance oxidized film
PPheDOT	560	1.82	N/A	N/A
PPheDOT [b]	623, 568	1.81	14%	45%
PPheDOTEtHx	609, 559	1.85	N/A	N/A
PPheDOTC_{12}	626, 572	1.80	30%, 0.314, 0.329	63%, 0.362, 0.398
PPheDOT$(C_{12})_2$	620, 567	1.78	31%, 0.333, 0.337	58%, 0.372, 0.392
PPheDOTC_{12}EtHx	608, 557, 518	1.92	18%, 0.329, 0.298	56%, 0.371, 0.407

(a) optical bandgap; (b) electropolymerized from PheDOT dimer; (c) Yxy CIE 1931 color coordinates, with Y being the relative luminance in %.

In Table 6-2, the optical properties of PPheDOT deposited from PheDOT or PheDOT dimer (BiPheDOT) are compared. BiPheDOT is electrodeposited at much lower potential, and the polymer films obtained have higher quality than the films obtained from PheDOT, with two well-resolved vibronic structures. Films electrodeposited from PheDOT have a broader absorption with no well-resolved vibronic features, indicating that the films morphology is changed, probably because of the side reactions involved with PheDOT, which are not occuring at the potential where BiPheDOT is electrodeposited.

Luminance studies carried on electrodeposited films of substituted PPheDOT show that the films switch from a purple absorptive color in the neutral state to a pale green color in the oxidized state. This color change corresponds to a luminance change of ca. 30%-40%, much lower than the luminance contrast observed in PProDOT polymers (50% to 80%). Given their poor stability in the fully oxidized state, it follows that these materials are not suited for electrochromic applications.

6.4 Synthesis of Soluble Substituted PPheDOT

Following bromination with N-bromosuccinimide at the 2- and 5- positions of the thiophene, the monomers were chemically polymerized using Grignard Metathesis (GriM) polymerization (Figure 6-6).[47,104]

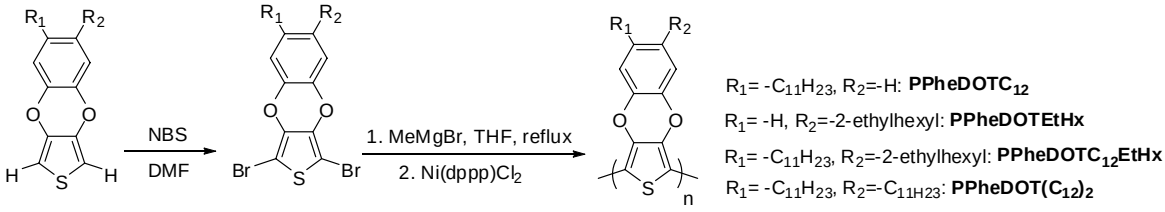

Figure 6-6. Synthesis of PPheDOT$(C_{12})_2$ by Grignard Metathesis.

Monosubstituted PPheDOTC_{12} and PPheDOTEtHx have poor solubility and form colloidal suspension in THF, toluene and chloroform. Heating the solution does not improve the solubility and does not yield significant optical changes (Figure 6-7). The lack of solubility is attributed to strong π-stacking interchain interactions, favored by the lower side chains density, possibly allowing significant interdigitation between polymer stacks.

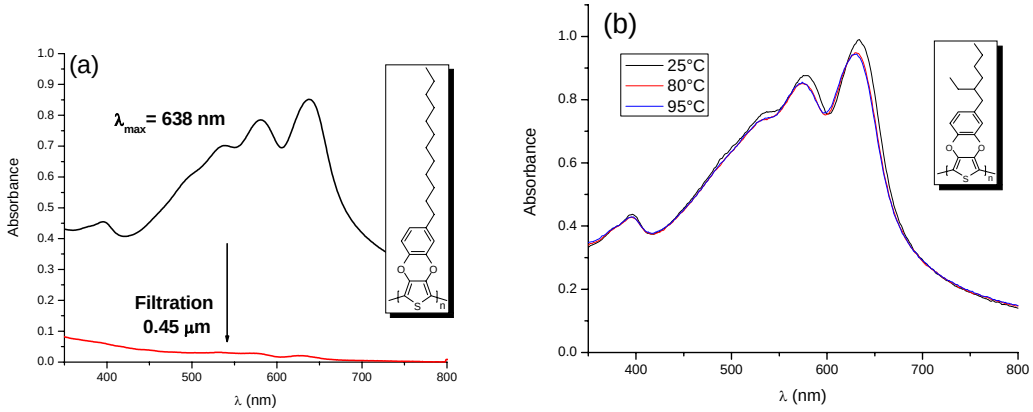

Figure 6-7. Solution optical properties of monosubstituted PPheDOTs. (a) PPheDOTC_{12} solution absorption spectrum in THF before and after 450nm filtration; (b) Absorption spectrum of PPheDOTEtHx xylenes solution at 25°C, 80°C, 95°C.

To obtain higher solubility, disubstituted PPheDOT(C_{12})$_2$ and PPheDOT(C_{12})EtHx were synthesized. The GPC results are given in Table 6-3. At room temperature, PPheDOT(C_{12})$_2$ also forms purple colloidal suspensions in toluene, tetrachloroethane, xylenes and THF, consistent with the presence of strong interchain interactions forcing aggregation. However, upon heating to ~80°C, PPheDOT(C_{12})$_2$ becomes readily soluble in a variety of aromatic or halogenated solvents. Solubility of the polymer is important, as it enables easy processing along with allowing full characterization of the polymer's structure, in particular molecular weight determination. High temperature GPC, carried at 140°C in trichlorobenzene, yields a number-average molecular weight M_n =14,800 g.mol^{-1} [1] and a polydispersity of 1.95, corresponding to a number-average molecular structure of ~30 number-average repeat units. A second polymerization yielded a higher molecular weight M_n= 29,400 g.mol^{-1} and PDI=2.42.

Table 6-3. GPC data for PPheDOTC_{12}EtHx and PPheDOT(C_{12})$_2$.

	M_n (g mol^{-1})	**M_w (g mol^{-1})**	**PDI**	**X_n**
PPheDOTC_{12}EtHx[a]	56, 200	82,700	1.5	110
PPheDOT(C_{12})$_2$[b] **#1**	14,800	28,900	1.95	30
PPheDOT(C_{12})$_2$[b] **#2**	29,400	71,300	2.42	60

[a] GPC determined at room temperature in THF; [b] molecular weight determined in 1,2,4-trichlorobenzene at 135°C; molecular weights are given for two different polymerization.

By substituting a dodecyl chain on the monomer by a more bulky 2-ethylhexyl side chains in PPheDOTC_{12}EtHx, solubility is dramatically improved. PPheDOTC_{12}EtHx is readily soluble at room temperature in most organic solvent such as hexanes, THF, chlorinated solvents and aromatic solvents. GPC, carried out in THF at room temperature yields a number-average molecular weight of M_n=56,200 g mol^{-1} and a polydispersity of 1.5, corresponding to a number-average molecular structure of 110 repeat units. The

increased solubility could be due either to a strong decrease in interchain π-stacking or a strong intrachain twisting of the PPheDOT backbone.

6.5 Solutions Properties

In solution, PPheDOT(C_{12})$_2$ displays a strong thermochromic effect changing from a dark purple color at low temperature to a red-orange color above 80°C. Figure 6-8 shows the UV-Vis spectrum of a polymer solution in xylenes as it is heated from 25 to 95 °C. The absorption maximum shifts by almost 70 nm from 614 nm to 546 nm as the temperature increases. The presence of vibronic features at high temperature indicates that the chains retain a planar (or highly conjugated) conformation. In poly(3-alkylthiophene)s, the absorption spectrum above the phase transition is broad and featureless, arising from intrachain twisting of the polythiophene backbone.[105] This difference is consistent with studies on short oligothiophenes with alkyl or alkoxy substituents showing that the presence of the oxygens induces planar conformations of the oligomers. This effect is attributed to the smaller steric demand of the oxygens, mesomeric effects, as well as sulfur-oxygen interactions.[57a,106] PPheDOTC_{12}EtHx displays a different behavior. At room temperature in xylenes solution, there is a strong hypsochromic shift, and the absorption spectrum resembles the spectrum of PPheDOT(C_{12})$_2$ above the phase transition. Thermochromism experiment on PPheDOTC_{12}EtHx dissolved in xylenes leads to a progressive bathochromic shift of the absorption. Comparing the solution absorption spectra of both polymers (λ_{max} and vibronic features) indicate that above the phase transition of PPheDOT(C_{12})$_2$, the absorption spectra of both polymers at equal temperatures are almost identical. This result confirms the observation made in Chapter 5 that intrachain twisting is also involved in the thermochromic changes below the phase transition. However, in

aggregated solutions, intrachain twisting induce only minor optical changes, and the breakup of the interchain interactions is responsible for the most optical changes observed.

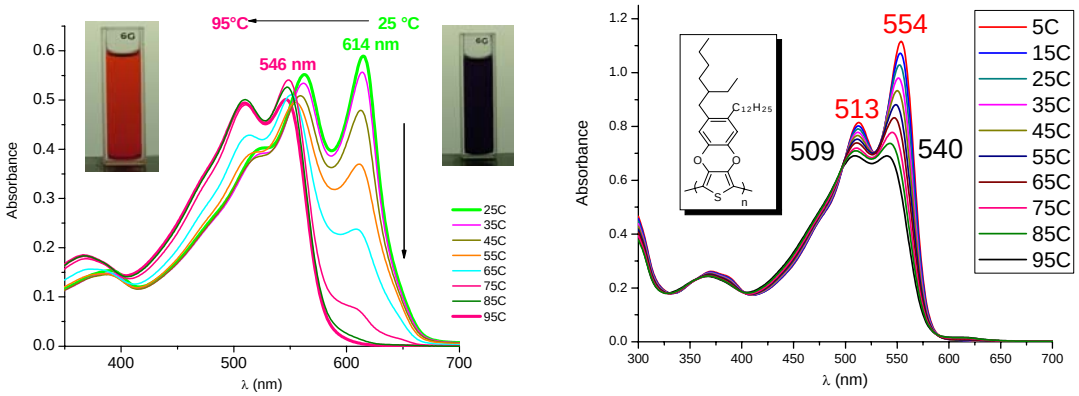

Figure 6-8. Solution thermochromism of Poly[PheDOT-(C12)2] in xylenes. Concentration is $6x10^{-5}$ M (relative to the repeat unit). Pictures show the solution at 25°C (right) and 95°C.

Due to aggregation, PPheDOT$(C_{12})_2$ is not fluorescent at room temperature. However, if heated above 80°C, temperature where the polymer chains become molecularly dissolved, the polymer becomes strongly fluorescent, emitting a bright orange color. PPheDOTC_{12}EtHx is fluorescent at room temperature, emitting the same bright orange color, shown in (Figure 6-9).

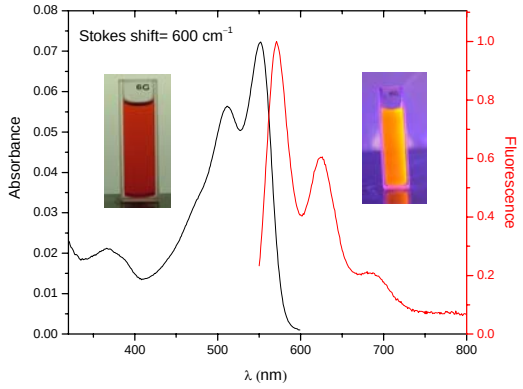

Figure 6-9. Absorption and Emission spectrum of PPheDOTC_{12}EtHx. Sample is excited at 550nm.

The fluorescence of PPheDOTC_{12}EtHx at room temperature or PPheDOT$(C_{12})_2$ above 80°C is further evidence that interchain interactions are broken and the chains molecularly dissolved. The small Stokes shift and the well-resolved vibronic coupling for PPheDOTC_{12}EtHx in xylenes solution indicate that the polymer chains are mostly planar.

6.6. PPheDOT$(C_{12})_2$: A Soluble, Ordered Polymer

Spray-coated films of Poly(PheDOT-$(C_{12})_2$) are electroactive, switching from a dark purple color to a transmissive green in the oxidized state. Cyclic voltammetry (Figure 6-10) shows a low onset of oxidation at -0.2V vs. Fc/Fc^+ for Poly(PheDOT-$(C_{12})_2$), corresponding to a HOMO level at 4.6 eV, which is substantially lower in energy (higher oxidation potential) than neutral PEDOT (4.1 eV).[107108]

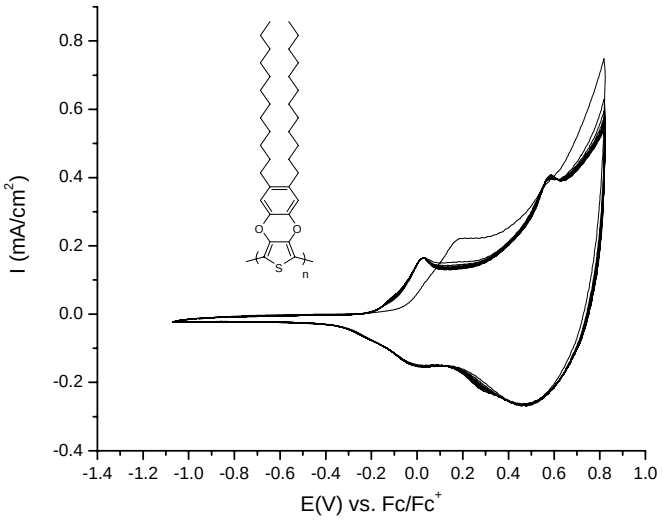

Figure 6-10. Cyclic voltammetry of disubstituted PPheDOT$(C_{12})_2$ in 0.1M TBAP in ACN at a scan rate of 50mV/s. Film was drop cast onto platinum button electrode from a 5mg/ mL toluene solution.

The higher oxidation potential is consistent with the trend reported recently, where theroretical and experimental studies on the PheDOT dimer and trimer showed that resonance of the oxygens with the phenylene ring induces a decrease in electron release of the oxygens into the thiophene.[102] Higher oxidation potential gives the neutral polymer

greater air stability and allows for long term storage without the need to keep the materials under inert atmosphere. Spectroelectrochemistry was carried out on films cast onto an ITO-coated glass slides. As PPheDOT(C_{12})$_2$ is not soluble at room temperature, spray-casting was not possible and drop-casting was used instead. As shown in Figure 6-11, as the potential applied to the PPheDOT(C_{12})$_2$ film is increased to 0.2V, the π-π^* transition is progressively bleached, while two near-infrared optical transitions appear, characteristic of the polaronic and bipolaronic states. The optical bandgap, determined from the onset of absorption is estimated at 1.88 eV, 0.25 eV higher than PEDOT (1.6 eV). The presence of vibronic features in the films absorption spectrum suggests planarity of the polymer chains.

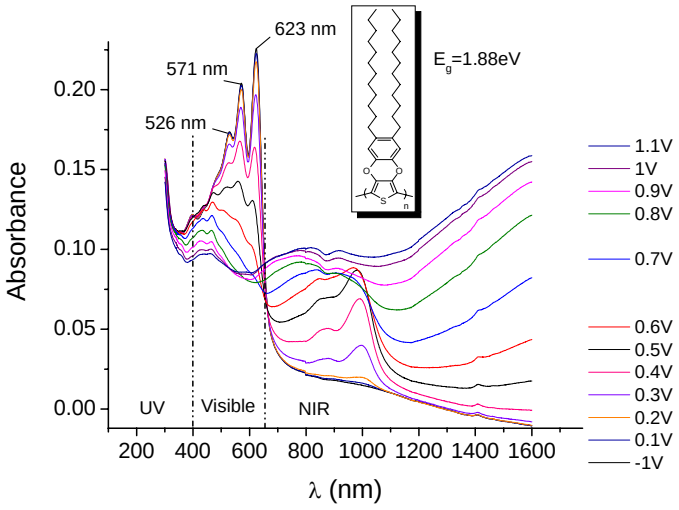

Figure 6-11. Spectroelectrochemistry of soluble disubstituted PPheDOT(C_{12})$_2$ film on ITO-coated glass slides. The film was drop-cast from 5mg/mL hot toluene solution (100°C). The film was electrochemically oxidized in 0.1M TBAP/propylene carbonate solution. A silver wire was used as a quasi-reference and was calibrated against Fc/Fc$^+$.

The conformation of the polymer chains in the processing solution (aggregated versus isolated chains) plays an important role in the solid state ordering. AFM imaging was carried out for films spin-coated onto mica from either hot (130°C) or cold (25°C)

ortho-dichlorobenzene (ODCB) solutions. As seen in Figure 6-12, the films spin-coated from the hot ODCB solution yield nano-fibrillar structures. The average height of the fibrils is 3 nm, a value slightly lower, but close to the polymer chain width for a conformation where the thiophenes are in a trans conformation and the dodecyl chains are extended. This lower value is not surprising given that at high temperature in ODCB the dodecyl chains are expected to be disordered. During spin-coating of the hot solution, the fast evaporation of the solvent does not allow the side chains to order properly. The fibrils are estimated to be about 10 nm in width (after correction for the lateral tip broadening effect[109]), which is consistent with the estimated length of the polymer chains in their fully extended conformation. From these data, the following model is proposed: the material forms nanoribbons of π-stacked polymer chains, with the polymer chains arranged perpendicular to the plane of the substrate (Figure 6-12).

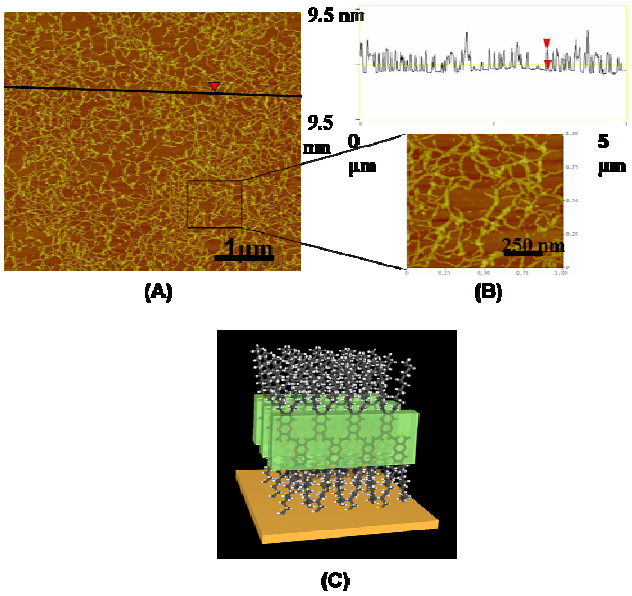

Figure 6-12. Self-assembly of PPheDOT$(C_{12})_2$ polymer chains in films spin-coated on mica from a hot ODCB solution (C= 0.2 mg.mL^{-1}). (A) AFM picture (5× 5µm^2) of PPheDOT$(C_{12})_2$; (B) cross section analysis and magnification (1× 1µm^2). The fibril marked by the red arrow in the surface profile has a height of 3.2 nm; (C) Proposed 3D-model of the nanoribbons arrangement on the mica surface.

Similar self-assembled nanostructures have been proposed for alkyl substituted poly(phenyleneethynylene) (PPE), polyfluorene copolymers and poly(3-alkylthiophenes).[110] For the films obtained by spin-coating from a cold ODCB solution, there is formation of heterogenous aggregates both in structure and size (Figure 6-13). This can be explained by comparison with the solution thermochromism results described earlier. Similar to the xylenes solution, the polymer chains in ODCB form stable colloidal suspensions of aggregates at room temperature. During the spin-coating of this solution, the solvent evaporates and the concentration of the aggregates increases, leading to their collapse into larger, ill-defined structures. This difference of morphology is an important result as order within crystalline domains, and order of the crystalline domains with respect to one another, have dramatic consequences on charge mobilities, as previously shown in regioregular poly(3-hexylthiophene).[17c]

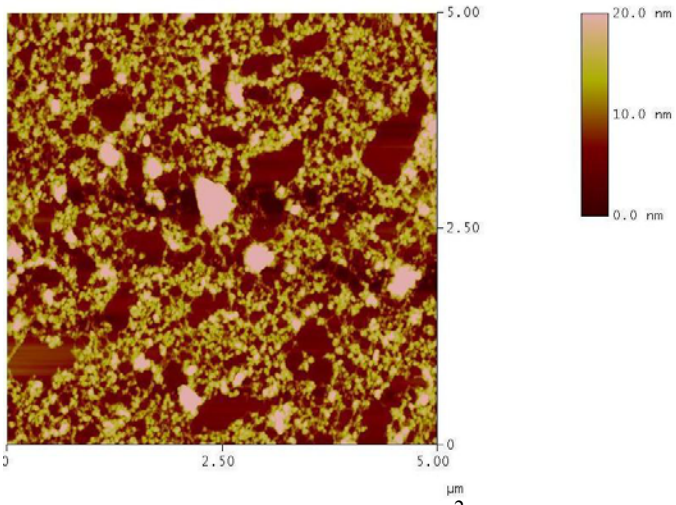

Figure 6-13. AFM picture ($5\times 5\mu m^2$) of PPheDOT-$(C_{12})_2$ spin-coated on mica from ODCB solution at room temperature (C= 0.2 mg mL^{-1})

The thermal behavior of PPheDOT$(C_{12})_2$ in the solid state was investigated. TGA analysis shows that the polymer is thermally stable up to 300°C, under both oxygen and nitrogen atmosphere. After conditioning with a ramp at 10°C per minute up to 220°C and

cooling to 0°C, the second DSC scan shows an endothermic transition at 132° C on heating and an exothermic transition at 110°C on cooling (Figure 6-14). The small phase transition enthalpy suggests that there is little structural rearrangement during the transition. This thermal transition is assigned to the melting and recrystallization of the side chains. No further transitions corresponding to a melting of the crystalline regions are observed. This confirms the presence of strong intermolecular π-π stacking interactions, as expected from the planarity of the monomer. As mentioned earlier, the presence of sulfur-oxygen interactions and mesomeric effects contributes to a rigidification of the planar conformation of the phenylene dioxythiophene backbone. As a result, only the transition corresponding to the melting of the side chains is observed.

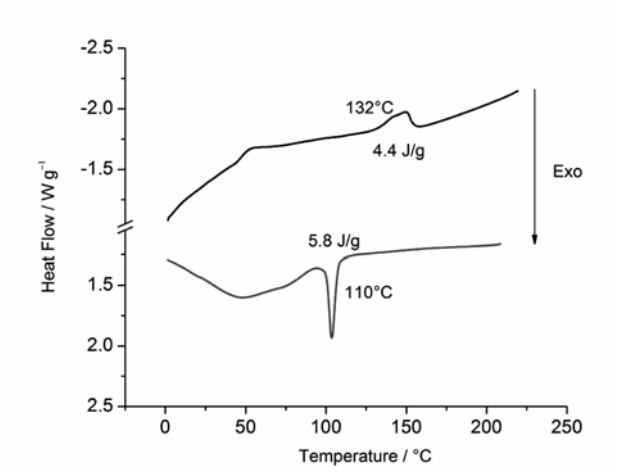

Figure 6-14. DSC (2nd scan) of PPheDOT-$(C_{12})_2$. Sample was heated and cooled at a rate of 10°C/min.

The organization of PPheDOT$(C_{12})_2$ in the solid-state has been investigated by using two-dimensional wide-angle X-ray scattering (2D-WAXS) measurements, carried out by Dr Wojciech Pisula at the Max Planck Institute for Polymer Science, Mainz, Germany. The samples were prepared by shear-alignment at 150 °C using a home-built mini-extruder.[50] At ambient temperatures, the 2D pattern displayed sharp and distinct

reflections indicating a well-ordered structure of the conjugated polymer with a pronounced alignment of the chains in the extrusion direction. (Figure 6-15a). The equatorial small-angle reflection was related to the lateral distance of 3.88 nm of the polymer chains. This relatively large distance is in good accordance with the polymer configuration, as illustrated in Figure 6-15b, in which the monomer units are arranged in one plane, forming a lamella structure of rigid stacked conjugated chains.

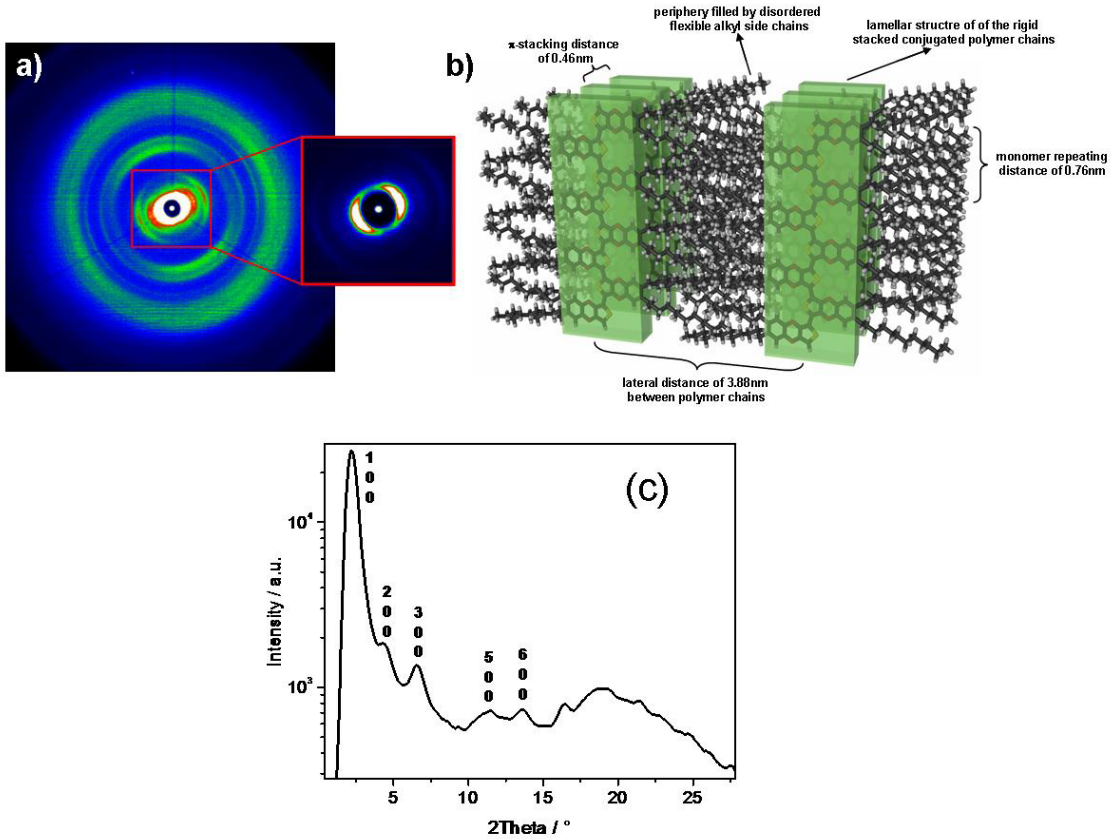

Figure 6-15. Ordering in mechanically aligned PPheDOT(C_{12})$_2$ fibers.(a) 2D-WAXS pattern at 30 °C (the inset displays the small-angle reflections at a lower contrast) and (b) packing of PPheDOT(C_{12})$_2$ as indicated by the X-ray results; (c) Equatorial reflection intensity distribution recorded at 30 °C as a function of the scattering angle. Reflections are indexed by the Miller's indexes.

Additional higher-order equatorial reflections, positioned at multiple angle values, confirmed the well-defined organization of the filament (Figure 6-15c). The wide-angle reflection, positioned also in the equatorial plane of the X-ray pattern, is assigned to the

π-stacking distance of 0.46 nm of the polymer chains, whereby the low-intensity anisotropic halo was assigned to the poorly ordered alkyl side chains, which filled the periphery between the rigid conjugated units. The meridional reflection corresponded to the period of 0.76 nm and therefore to every second monomer unit along the polymer backbone being in an identical arrangement as illustrated in Figure 6-15b.

The organization of the polymer changed slightly above the phase transition of 132 °C (Figure 6-16). The equatorial reflections showed an unchanged shape and intensity, but were shifted to lower angles indicating smaller lateral distances of 3.15 nm at the higher temperature phase. Such distance decrease between rigid well-packed polymer chains might be explained by the melting of the alkyl substituents. Indeed, the diffuse anisotropic halo was characteristic for the melting of the alkyl side chains. The change of the side chain dynamics did not affect the correlations between the repeat units along the polymer chain, but led to an increase of their steric demand and thus to a hindrance of the polymer stacking. This was reflected by the lowered reflection intensity corresponding to the stacking distance, whereas the full intensity was recovered by cooling the sample back to 30 °C.

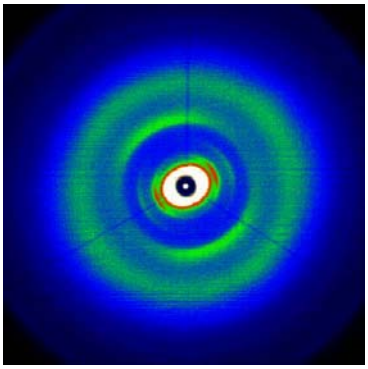

Figure 6-16. 2D-WAXS pattern of PPheDOT-$(C_{12})_2$ at 150°C.

The higher molecular weight fraction displays significantly different behavior. DSC analysis reveals that the melting and crystallization transitions of the side chains are

shifted to lower temperatures (T_m= 100°C, T_c= 70°C). The enthalpies of these transitions are also higher than for the lower molecular weight sample (10-20 J g^{-1} vs. 4-6 J g^{-1}). The 2D-WAXS profiles, shown in Figure 6-17, indicate similar packing as the lower molecular weight fraction.

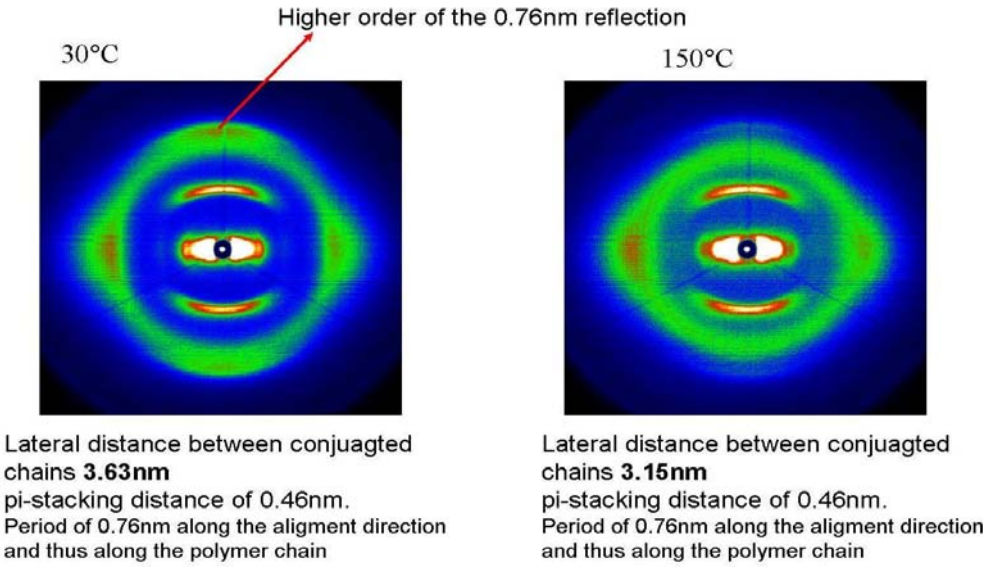

Figure 6-17. 2D-WAXS analysis of higher molecular weight PPheDOT(C_{12})$_2$ fraction. The diffraction profile is shown below and above DSC transition attributed to the melting of the side chains.

The reflections for the higher molecular weights are more intense and broader, indicating higher macroscopic order but lower crystallinity. The lower crystallinity also explains the lower melting and crystallization temperatures. Such increase of the longer order with increased molecular weight was also observed in alkyl polythiophenes and is believed to be the origin of the enhancement of the charge-carrier mobilities with increasing molecular weight.

6.7. PPheDOTC_{12}EtHx: a Disordered Polymer

As mentioned earlier, PPheDOTC_{12}EtHx polymer chains are molecularly dissolved in solution although having a planar conformation, as indicated by the presence of vibronic coupling and the small Stokes shift value. The absence of interchain interactions

in solution, at room temperature, indicates that asymmetric substitution of PheDOT with ethylhexyl and dodecyl substituents effectively hinders ordering, contrarily to PPheDOT(C_{12})$_2$, PPheDOTC_{12} and PPheDOTEtHx, all strongly aggregating at room temperature.

PPheDOTC_{12}EtHx was spray-cast from toluene onto ITO-coated glass slides and the cast films absorption spectra were examined. As observed in Figure 6-18, the cast films have almost identical maxima of absorption than the polymer in xylenes solution, showing that the polymer chains retain a "solution" conformation. The broader absorption may arise from some intrachain twisting of the chains in the solid state, or presence of a small amount of interchain interactions. When irradiated under 365nm UV lamp, the film show solid-state fluorescence, confirming that the polymer does not display strong interchain interactions. After several electrochemical doping/de-doping cycles between +0.9V and -0.5V, the absorption of the cast film is mostly unchanged.

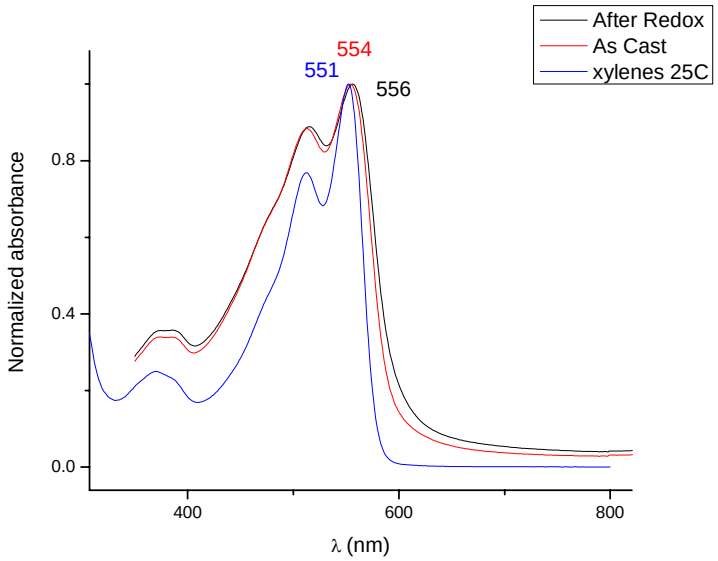

Figure 6-18. Absorption spectrum of PPheDOTC_{12}EtHx: in xylenes solution, film spray-cast from toluene and film spray-cast after electrochemical doping/reneutralization.

Electrochemistry was carried out on films drop-cast on a platinum button electrode (Figure 6-19). The onset of oxidation is similar to the electropolymerized film at 0.3V vs. Fc/Fc^+ (5.1eV HOMO[107]). The onset potential is much higher than PPheDOT$(C_{12})_2$, arising from the decreased interchain interactions. Spectroelectrochemistry experiment carried out on a spray-cast film of PPheDOTC_{12}EtHx yields significantly higher bandgap (2.1eV) than the electropolymerized film. Also, the neutral state optical spectrum of the electrodeposited films displays an additional vibronic feature at 608nm, not seen in the spray-cast film. As observed in PPheDOT$(C_{12})_2$ solution thermochromism, the transition at 608nm is characteristic of interchain aggregates, showing that electrodeposited films have higher interchain order, possibly arising from the side chain reactions at the oxidation potential used for the electrodeposition. Similarly to substituted PProDOTs, introduction of the bulky 2-ethylhexyl substituents also leads to large optical changes within a narrow potential window (300mV), explained by a more open morphology of the polymer film and decreased interchain interactions.

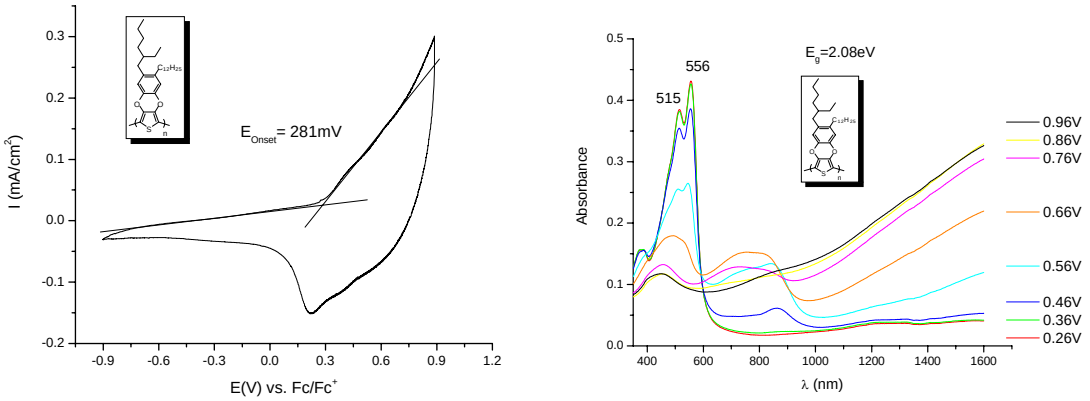

Figure 6-19. Electrochemistry and spectroelectrochemistry of PPheDOTC_{12}EtHx cast films. (left) Cyclic voltammetry in 0.1M TBAP/ACN electrolyte solution of a PPheDOTC_{12}EtHx drop-cast on a platinum button electrode; (right) Spectroelectrochemistry of a PPheDOTC_{12}EtHx spray-cast on an ITO-coated glass slide in 0.1M TBAP/propylene carbonate electrolyte. Potentials are vs. ferrocene.

The bulk polymer was analyzed by differential scan calorimetry (Figure 6-20). Small melting and crystallization peaks corresponding to the dodecyl substituents chains are observed, indicating some interchain ordering through the side chains. The enthalpy associated with these transitions is much lower than PPheDOT(C_{12})$_2$.

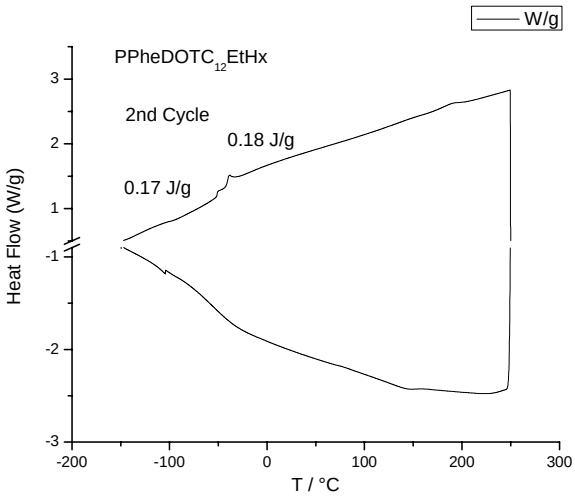

Figure 6-20. DSC (2nd scan) of PPheDOTC$_{12}$EtHx. Heat and cooling rate= 10°C/min.

Also, the melting and crystallization occur well below room temperature (ca. -50°C) contrarily to PPheDOT(C_{12})$_2$, displaying high temperature transitions (*ca.* 100°C). As a result, the polymer is highly amorphous at room temperature, which is confirmed by the observation of solid state fluorescence.

6.8. Conclusion

In conclusion, new electron rich, electroactive mono and di-substituted soluble polymers based on the (3,4-phenylenedioxythiophene) unit were synthesized by chemical polymerization. The monosubstituted polymers, as well as Poly(PheDOT(C_{12})$_2$), possess a high degree of intra- and inter-chain order, both in solution and solid state. At high temperature in ODCB or xylenes solutions, Poly(PheDOT(C_{12})$_2$) possesses a planar conformation, leading to aggregation at low temperature. Spin-coating of this polymer

from a hot ODCB solution leads to the formation of nanoribbons. Structural investigation by 2D-WAXS of mechanically aligned Poly(PheDOT(C_{12})$_2$) filaments revealed a pronounced 2D organization of the conjugated polymer. Strong correlations along the polymer backbone and between the polymer chains have been observed. PPheDOTC_{12}EtHx, on the other hand, although having a mostly planar chain conformation do not order strongly in the solid state, as steric hindrance of the side chains prevent interchain interactions. Since the order of conjugated polymers, as organic semiconductors, is an essential requirement for charge carrier transport, and thus for their implementation in electronics, this work has shown that PPheDOT(C_{12})$_2$ is a promising candidate for device applications. PPheDOTC_{12}EtHx, having little interchain order in the solid state, is not suitable for such applications, but is promising in light-emitting applications, where interchain interactions are undesirable.

6.9. Closing Statements

To be successfully applied commercially, solubility of the conducting polymers is required, allowing inexpensive and easy processing. Thanks to their unique synthetic versatility, conducting polymers can be tailored and modified to achieve that goal. One of the strategies is to introduce substituents on the conjugated backbone. However, it should be clear from Chapter 1 that the ultimate application must be taken into account when considering what substituents to use and where to place these substituents on the conjugated backbone.

In Chapter 3 and 4, bulky branched substituents were successfully used to increase the solubility of poly(3,4-propylenedioxythiophenes) (PProDOTs), which are promising materials for electrochromic applications. The bulkiness of the substituents induces a decrease of interchain interactions and leads to a more open morphology of the polymer

films. As a result, the branched polymers are better electrochromic materials, with higher contrasts, shorter switching times and higher coloration efficiencies. The alkyl substituted PProDOT-R_2 were found to spontaneously self-assemble during film casting, in contrast with the ether-linked PProDOT-$(CH_2OR)_2$ polymers that retain a solution conformation. This behavior was attributed to intrachain twisting of the PProDOT-$(CH_2OR)_2$ polymer chains preventing their self-assembly in the solid state, supported by the studies detailed in Chapter 5 on the chiral analogs of these polymers. Theoretical work should be carried out on branched PProDOTs oligomers substituted with either alkyl or alkoxymethyl side chains to gain more insight on the reason behind the more twisted conformation observed for the ether linked substituted PProDOTs. Such work would be helpful to design highly ordered polymers needed in high conductivity and high mobilities applications, or highly disordered polymers needed in light-emitting applications.

In Chapter 5, the synthesis of chiral equivalents of the PProDOTs investigated in Chapter 3 and 4 is described. The self-assembly of the chiral polymer chains were studied through thermochromism and solvatochromism experiments, probed by absorption, fluorescence and circular dichroism spectroscopy, leading to an unprecedented level of understanding on the structure-property relationships. Especially promising is the introduction of the chiral substituents synthesis, opening the door to new chiral polymers with unseen chiral ordering. Of particular interest for future work would be the synthesis of stackable chiral substituents, which should lead to stronger chiral ordering. The effect of side chain crystallization on the ordering of the PProDOT backbone is unknown. It is expected to be quite different from poly(3-alkylthiophenes) as the side chains do not

extend within the plane of the polythiophene backbone but rather above and below this plane.

The focus of Chapter 6 was to synthesize the first soluble conjugated poly(3,4-phenylenedioxythiophenes) (PPheDOTs). This objective was accomplished by attaching either dodecyl or ethylhexyl substituent at both the 4- and 5- positions of the benzene ring, as monosubstituted compounds were found to have poor solubility. Didodecyl substituted PPheDOT$(C_{12})_2$ has high solubility at temperatures above 80°C. The polymer has a high degree of order in the solid state and is a promising candidate for high conductivity and high mobility applications. Asymmetrically substituted PPheDOTC_{12}EtHx, on the other hand, is highly soluble at room temperature. The polymer is highly disordered in the solid state and is a promising material for light-emitting applications. The considerable differences between the two polymers' properties, although they differ little structurally, illustrates perfectly the importance the side chains in the ordering of polymer chains. Future work in PPheDOTs polymers should investigate the structure-properties relationships in PPheDOTs. An essential study would be to investigate the effect of the chain length on the properties of linear disubstituted PPheDOTs polymers. As described in Chapter one, the conductivity and mobility of substituted polythiophenes often go through an optimum with increasing side chains length. Also, the efficiency of the synthesis of disubstituted PPheDOT suffers greatly from a low yield in the transetherification step, a late step in the synthesis. This step of the synthesis will require significant improvement for these materials to become commercially interesting.

6.10. Synthetic Details

1-(3,4-dimethoxyphenyl)dodecan-1-one: In a 2L 3-neck flask equipped with an argon inlet and a pressure-equalizing addition funnel was dissolved aluminum trichloride (26g, 200 mmol, 1.1 eq.) in dry dichloromethane (700mL, distilled from CaH_2). The reaction was cooled at 0°C, and a solution of veratrole (25g, 180 mmol, 1 eq.) in dry dichloromethane (150 mL) was added dropwise followed by addition of a lauroyl chloride solution (40g, 180 mmol, 1eq.) in dry dichloromethane (150 mL). The mixture is refluxed for 24 hours, then cooled at 0°C. The excess aluminum chloride was quenched by slow addition of 6M HCl (100 mL). The aqueous phase is further extracted with dichloromethane (2×200 mL). The combined organic layers are washed with water (3×400 mL), and dried with magnesium sulfate. The solvent is removed under vacuum to yield a white solid, purified by recrystallization from toluene. The product is obtained as a white solid (52g, 90% yield); ^{1}H NMR (300MHz, $CDCl_3$) 0.83-0.93 (t, 3H), 1.18-1.43 (m, 16H), 1.64-1.8 (m, 2H), 2.88-2.95 (m, 2H), 3.94 (s, 3H), 3.95 (s, 3H), 6.88 (d, 1H, J_1=8.3Hz), 7.54 (d, 1H, J_2=1.9Hz), 7.59 (dd, 1H, J_1= 8.3Hz and J_2=1.9Hz) ; ^{13}C NMR (75 MHz, $CDCl_3$) 14.32, 22.90, 25.03, 29.55, 29.72, 29.84, 32.12, 38.38, 56.18, 110.16, 110.42, 122.84, 130.57, 149.2, 153.28, 199.44.

4-dodecyl-1,2-dimethoxybenzene: In a 3L 3-neck flask equipped with an argon inlet was dissolved LAH (12.6g, 331.4 mmol, 4.5eq) in dry diethyl ether (500 mL, distilled from Na/benzophenone). A solution of $AlCl_3$ (14.8g, 110.5 mmol, 1.5eq.) in dry diethylether (500 mL) was added via cannula to the LAH solution, cooled at 0°C. After 15 min, a solution of 1-(3,4-dimethoxyphenyl)dodecan-1-one (23.6g, 73.64 mmol, 1eq.) in diethylether (500 mL) was added dropwise to the reaction (maintained at 0°C). Upon completion of the addition, the mixture was allowed to warm up to room temperature.

After four hours, the reaction was cooled back to 0°C and quenched slowly by addition of 200 mL of 6M HCl. The organic layer was washed with water (3×400 mL) and dried with magnesium sulfate. The organic solvent was removed under vacuum, to yield a white solid purified by column chromatography on silica gel using 50/50 dichloromethane/hexanes as eluent. This yields the product as a white solid (14g, 62% yield). ^{1}H NMR (300MHz, $CDCl_3$) 0.83-0.92 (t, 3H), 1.2-1.38 (m, 18H), 1.52-1.65 (m, 2H), 2.5-2.58 (m, 2H), 3.86 (s, 3H), 3.88 (s, 3H), 6.68-6.82 (m, 3H); ^{13}C NMR (75 MHz, $CDCl_3$) 14.34, 22.92, 29.58, 29.77, 29.90, 31.95, 32.16, 35.82, 56.02, 56.16, 111.41, 112.01, 120.32, 135.87, 147.21.

4-dodecylbenzene-1,2-diol: In a 2L three-neck flask equipped with an argon inlet was added 1-dodecyl-4,5-dimethoxybenzene (4g, 13 mmol, 1eq.) in dry dichloromethane (500 mL, distilled from CaH_2). Boron tribromide (13 mL , 137mmol, 4eq.) was added dropwise using a pressure-equalizing addition funnel. After 12 hours, the mixture was poured in a 2L Erlenmeyer filled with 1L of ice. The aqueous phase was further extracted with dichloromethane (2×200 mL) and the combined organic layers were washed with water (3×300 mL). The organic phase is dried with magnesium sulfate and the solvent was evaporated under vacuum to yield the product as an off-white solid (2.8g, 77% yield). ^{1}H NMR (300MHz, $CDCl_3$) 0.84-0.92 (t, 3H), 1.2-1.36 (m, 20H), 1.47-1.62 (m, 2H), 2.42-2.52 (t, 2H), 4.91 (br s, 1H), 5.05 (br s, 1H), 6.58-6.62 (dd, 1H), 6.68-6.70 (d, 1H); 6.76 (d,1H); ^{13}C NMR (75 MHz, $CDCl_3$) 14.35, 22.93, 29.48, 29.59, 29.76, 29.91, 31.82, 32.16, 35.49, 115.45, 115.73, 121.03, 136.57, 141.35, 143.50;HRMS [M^+] calcd for $C_{18}H_{30}O_2$ 278.2246 amu Found 278.2242 amu.

PheDOT-C_{12}: In a 100 mL round bottom flask, 4-dodecylbenzene-1,2-diol (2g, 7.04 mmol,1eq) was dissolved in 60 mL of dry toluene (distilled from Na/benzophenone). To this solution was added 3,4-dimethoxythiophene (1g, 7.04 mmol, 1eq.) and p-toluenesulfonic acid (136 mg, 0.7mmol, 0.1eq). The flask was equipped with a soxhlet apparatus containing a thimble filled with $CaCl_2$. The mixture was refluxed for three days. Triethylamine (1 mL) and water (200 mL) were added and the product was extracted with diethylether (3×100 mL). After drying with sodium sulfate and removal of the solvent under reduced pressure, the resulting brown solid was purified by column chromatography on silica gel using pentane as eluent. The product was obtained as a white solid (0.4g, 15% yield). ^{1}H NMR (300MHz, $CDCl_3$) 0.82-0.94 (t, 3H), 1.2-1.37 (m, 18H), 1.46-1.52 (m, 2H), 2.44-2.57 (m, 2H), 6.38-6.42 (m, 2H), 6.67-6.74 (m, 2H), 6.79-6.83 (m, 1H); ^{13}C NMR (75 MHz, $CDCl_3$) 14.36, 22.92, 29.38, 29.88, 31.53, 32.16, 35.32, 100.96, 116.54, 116.67, 123.63, 138.96; HRMS [M^+] calcd for $C_{22}H_{30}O_2S$ 358.1967 amu Found 358.1973 amu.

PheDOT-C_{12}-Br_2: PheDOT-C_{12} (0.25g, 0.7 mmol) was dissolved in 100 mL of DMF. After the solution was bubbled with argon for one hour, N-bromosuccinimide (0.27g, 1.54 mmol, 2.2 eq.) was added in one portion. The solution was stirred overnight after which 200 mL of water was added. The product was extracted with ether, washed with water and the organic layer dried with magnesium sulfate. The solvent was evaporated under vacuum and the resulting yellowish white solid was purified by column chromatography on silica using pentane as eluent. The product was obtained as a white solid (0.245g, 70% yield). ^{1}H-NMR (300MHz, $CDCl_3$) δ 0.88 (t, J= 6.7Hz, 3H), 1.17-1.37 (bs, 36H), 1.5-1.65 (bs, 4H), 2.52 (t, J=7.6Hz, 4H), 6.83 (dd, J_1= 8.3Hz, J_2= 2.2Hz,

1H), 6.86 (d, J_2= 2Hz, 1H), 6.925 (d, J_1= 8.3Hz, 1H); ^{13}C-NMR (75MHz, CDCl3) 14.34, 22.91, 29.32, 29.57, 29.58, 29.67, 29.77, 29.84, 29.86, 29.89, 31.40, 32.14, 35.29, 86.88, 86.99, 116.75, 116.85,124.39 137.95, 139.64, 139.65, 139.83; HRMS [M^+] calcd for $C_{22}H_{28}O_2SBr_2$ 514.0177 amu Found 514.0223 amu; Elemental analysis Calcd. For $C_{22}H_{28}O_2SBr_2$ %C 51.18 %H 5.47, %S 6.21 Found %C 51.03, %H 5.41; %S 6.15.

PPheDOTC$_{12}$: To a solution of PheDOT-C_{12}-Br_2 (220 mg, 0.43 mmol) in 30 mL of freshly distilled THF (from Na/benzophenone), was added CH_3MgBr via syringe (solution freshly titrated, C=0.94M) (0.45 mL, 0.43 mmol). The solution was refluxed for 2 hours. Then Ni(dppp)Cl_2 (5mgs, 0.009 mmol) was added in one portion. The solution was refluxed for 24hrs. The polymer was then precipitated in 100 mL MeOH and filtered through a soxhlet thimble. The polymer was purified via soxhlet extraction with MeOH, hexanes and then extracted with toluene. The product was obtained as a dark purple solid (120mg, 79% yield).

1-(2-dodecyl-4,5-dimethoxyphenyl)dodecan-1-one: In a 1L 3-neck flask equipped with an argon inlet and a pressure-equalizing addition funnel was dissolved aluminum chloride (7.2g, 55 mmol, 1.1 eq.) in dry dichloromethane (300 mL, distilled from CaH_2). To the reaction cooled at 0°C, a solution of 4-dodecyl-1,2-dimethoxybenzene (15.2g, 50 mmol, 1 eq.) in dry dichloromethane (100 mL) was added dropwise followed by the addition of a solution of lauroyl chloride (10.82g, 50 mmol, 1eq.). The mixture is refluxed for 24 hours, then cooled at 0°C. The excess aluminum chloride was quenched by slow addition of 6M HCl (150 mL). The aqueous phase is further extracted with dichloromethane (2×200 mL). The combined organic layers are washed with water (3×200 mL), and dried with magnesium sulfate. The solvent is

removed under vacuum to yield a yellow-white solid, purified by column chromatography on silica gel (50/50 hexanes/dichloromethane as eluent). The product is obtained as a white solid (16.2g, 67% yield); ^{1}H NMR (300MHz, $CDCl_3$) 0.82-0.96 (t, 6H), 1.18-1.42 (m, 34H), 1.45-1.60 (m, 2H), 1.62-77 (m, 2H), 2.74-2.9 (m, 4H), 3.88 (s, 3H), 3.92 (s, 3H), 6.72 (s, 1H), 7.12 (s, 1H); ^{13}C NMR (75 MHz, $CDCl_3$) 14.33, 22.92, 24.98, 29.59, 29.76, 29.88, 30.03, 32.15, 32.4, 34.23, 41.99, 56.11, 56.41, 112.36, 113.88, 137.70, 146.45, 151.28, 203.53; HRMS [M^+] calcd for $C_{32}H_{56}O_3$ 488.4229 amu Found 488.4219 amu.

1,2-didodecyl-4,5-dimethoxybenzene: In a 2L 2-neck flask equipped with an argon inlet was dissolved LAH (8.76g, 230 mmol, 6eq) in dry diethyl ether (250 mL, distilled from Na/benzophenone). A solution of $AlCl_3$ (7.56g, 60 mmol, 2eq.) in dry diethylether (250 mL) was added via cannula to the LAH solution, cooled at 0°C. After 15 min, a solution of 1-(2-dodecyl-4,5-dimethoxyphenyl)dodecan-1-one (16.2g, 33mmol, 1eq.) in diethylether (200 mL) was added dropwise to the reaction (maintained at 0°C). Upon completion of the addition, the mixture was allowed to warm up to room temperature. After four hours, the reaction was cooled to 0°C and quenched slowly by addition of 100 mL of 6M HCl. The reaction mixture was poured in 500 mL water. The aqueous phase was further extracted with diethylether (2×200 mL) and the combined organic layers were washed with water (3×300 mL). After drying with magnesium sulfate, the organic solvent was removed under vacuum, to yield a white solid purified by column chromatography on silica gel using 50/50 dichloromethane/hexanes as eluent. This yields the product as a white solid (13g, 80% yield). ^{1}H NMR (300MHz, $CDCl_3$) 0.84-0.93 (t, 6H), 1.18-1.42 (m, 36H), 1.44-1.6 (m, 4H), 2.47-2.57 (m, 4H), 3.84 (s, 6H),

6.65 (s, 2H); ^{13}C NMR (75 MHz, $CDCl_3$) 14.36, 22.94, 29.91, 31.95, 32.17, 32.71, 56.17, 112.87, 132.86, 146.99.

4,5-didodecylbenzene-1,2-diol: In a 2L three-neck flask equipped with an argon inlet was added 1,2-didodecyl-4,5-dimethoxybenzene (13g, 27.4mmol, 1eq.) in dry dichloromethane (600 mL, distilled from CaH_2). Boron tribromide (10.5 mL, 110mmol, 4eq.) was added dropwise using a pressure-equalizing addition funnel. After 12 hours, the mixture was poured in a 2L Erlenmeyer filled with 1L of ice. The aqueous phase was further extracted with dichloromethane (2×200 mL) and the combined organic layers were washed with water (3×300 mL). The organic phase is dried with magnesium sulfate and the solvent was evaporated under vacuum to yield the product as an off-white solid (11g, 90% yield). ^{1}H NMR (300MHz, $CDCl_3$) 0.84-0.93 (t, 6H), 1.27-1.4 (m, 36H), 1.42-1.58 (m, 4H), 2.42-2.5 (m, 4H), 6.65 (s, 2H); ^{13}C NMR (75 MHz, $CDCl_3$) 14.35, 22.93, 29.60, 29.93, 31.68, 32.17, 32.29, 116.36, 133.66, 141.27; HRMS [M^+] calcd for $C_{30}H_{54}O_2S$ 446.4124 amu Found 446.4118 amu.

PheDOT-(C_{12})$_2$: In a 100 mL round bottom flask, 4,5-didodecylbenzene-1,2-diol (5g, 11.2 mmol,1eq) was dissolved in 60 mL of dry toluene (distilled from Na/benzophenone). To this solution was added 3,4-dimethoxythiophene (1.6g, 11.2 mmol, 1eq.) and p-toluenesulfonic acid (213 mg, 1.12mmol, 0.1eq). The flask was equipped with a soxhlet apparatus containing a thimble filled with $CaCl_2$. The mixture was refluxed for three days. Triethylamine (1 mL) and water (200 mL) were added and the product was extracted with diethylether (3×100 mL). After drying with sodium sulfate and removal of the solvent under reduced pressure, the resulting brown solid was purified by column chromatography on silica gel using pentane as eluent. The product

was obtained as a white solid (1.15g, 20% yield). ^{1}H NMR (300MHz, $CDCl_3$) 0.84-0.95 (t, 6H), 1.2-1.42 (m, 36H), 1.45-1.6 (m, 4H), 2.44-2.56 (m, 4H), 6.4 (s, 2H), 6.7 (s, 2H); ^{13}C NMR (75 MHz, $CDCl_3$) 14.35, 22.92, 29.59, 29.76, 29.79, 29.82, 29.88, 29.90, 29.92, 31.28, 32.16, 32.17, 100.74, 117.01, 136.36, 138.53, 139.66; HRMS [M^+] calcd for $C_{34}H_{54}O_2S$ 526.3845 amu Found 526.3863 amu.

PheDOT-(C_{12})$_2$-Br_2: PheDOT-(C_{12})$_2$ (0.5g, 0.95 mmol) was dissolved in 100 mL of DMF. After the solution was bubbled with argon for one hour, N-bromosuccinimide (0.42g, 2.37 mmol, 2.5 eq.) was added in one portion. The solution was stirred overnight after which 200 mL of water was added. The product was extracted with ether, washed with water and the organic layer dried with magnesium sulfate. The solvent was evaporated under vacuum and the resulting yellowish white solid was purified by column chromatography on silica using pentane as eluent. The product was obtained as a white solid (0.48g, 74% yield). ^{1}H-NMR (300MHz, $CDCl_3$) δ 0.87 (t, 6H), 0.97-1.4 (m, 36H), 1.4-1.6 (bs, 4H), 2.5 (t, 4H), 6.81 (s, 2H); ^{13}C-NMR (75MHz, CDCl3) 14.35, 22.92, 29.59, 29.76, 29.79, 29.81, 29.90, 31.14, 32.16, 32.18, 86.73, 117.13, 137.21, 137.53, 137.94; HRMS [M^+] calcd for $C_{34}H_{52}O_2SBr_2$ 682.2055 amu Found 682.2038 amu; Elemental analysis Calcd. For $C_{34}H_{52}O_2SBr_2$ %C 59.65, %H 7.66 Found %C 59.53, %H 7.43. MP 77-79°C.

PPheDOT(C_{12})$_2$: To a solution of PheDOT-(C_{12})$_2$-Br_2 (415 mg, 0.606 mmol) in 30 mL of freshly distilled THF (from Na/benzophenone), was added CH_3MgBr via syringe (solution freshly titrated, C=0.94M) (0.67 mL, 0.606 mmol). The solution was refluxed for 2 hours. Then Ni(dppp)Cl_2 (6.6mg, 0.012 mmol) was added in one portion. The solution was refluxed for 24hrs. The polymer was then precipitated in 100 mL

MeOH and filtered through a soxhlet thimble. The polymer was purified via soxhlet extraction with MeOH, hexanes and then extracted with toluene. The product was obtained as a dark purple solid (220mg, 69% yield). The product after toluene soxhlet extraction was a dark black-purple solid. ^{1}H NMR (300MHz, $C_2D_2Cl_4$, 120°C) δ 0.9-1.1 (bs, 6H), 1.25-1.6 (bs, 36H), 1.6-1.8 (bs, 4H), 2.6-2.8 (bs, 4H), 6.9-7.1 (bs, 2H); GPC (135ºC, trichlorobenzene) Mn= 14,800 g mol-1, Mw= 28,900 g mol-1, PDI= 1.95. Elemental analysis Calcd. For $C_{34}H_{52}O_2S$ (repeat unit) %C 77.51 %H 10.33 Found %C 74.82; %H 10.6.

1-(3,4-dimethoxyphenyl)-2-ethylhexan-1-one: In a 2L 3-neck flask equipped with an argon inlet and a pressure-equalizing addition funnel was dissolved aluminum trichloride (28.7g, 217 mmol, 1.3 eq.) in dry dichloromethane (700 mL, distilled from CaH_2). The reaction was cooled at 0°C, and a solution of veratrole (25g, 180 mmol, 1 eq.) in dry dichloromethane (150 mL) was added dropwise followed by addition of a 2-ethylhexanoyl chloride solution (32.3g, 200 mmol, 1.2 eq.) in dry dichloromethane (150 mL). The mixture is refluxed for 24 hours, then cooled at 0°C. The excess aluminum chloride was quenched by slow addition of 6M HCl (100 mL). The aqueous phase is further extracted with dichloromethane (2×200 mL). The combined organic layers are washed with water (3×400 mL), and dried with magnesium sulfate. The solvent is removed under vacuum to yield a yellow-orange oil, purified by column chromatography (SiO_2, 75/25 DCM/Hexanes The product is obtained as a clear oil (41g, 86% yield); ^{1}H NMR (300MHz, $CDCl_3$) 0.8-0.94 (m, 6H), 1.17-1.38 (m, 4H), 1.42-1.62 (m, 2H), 1.65-1.83 (m, 2H), 2.27-2.38 (m, 1H), 3.96 (s, 6H), 6.84-6.94 (d, 1H), 7.56-7.64 (m, 2H); ^{13}C NMR (75 MHz, $CDCl_3$) 12.27, 14.17, 23.16, 26.01, 30.07, 32.35, 47.31, 56.16, 56.26,

110.14, 110.59, 122.82, 131.29, 149.29, 153.32, 203.45; HRMS [M^+] calcd for $C_{16}H_{24}O_3$ 264.1725 amu Found 264.1734 amu.

4-(2-ethylhexyl)-1,2-dimethoxybenzene: In a 3L 3-neck flask equipped with an argon inlet was dissolved LAH (3.77g, 100 mmol, 1 eq) in dry diethyl ether (500 mL, distilled from Na/benzophenone). A solution of $AlCl_3$ (13.13g, 100 mmol, 1eq.) in dry diethylether (500 mL) was added via cannula to the LAH solution, cooled at 0°C. After 15 min, a solution of 1-(3,4-dimethoxyphenyl)-2-ethylhexan-1-one (26g, 100 mmol, 1eq.) in diethylether (500 mL) was added dropwise to the reaction (maintained at 0°C). Upon completion of the addition, the mixture was allowed to warm up to room temperature. After four hours, the reaction was cooled back to 0°C and quenched slowly by addition of 200 mL of 6M HCl. The organic layer was washed with water (3×400 mL) and dried with magnesium sulfate. The organic solvent was removed under vacuum, to yield a white solid purified by column chromatography on silica gel using 50/50 dichloromethane/hexanes as eluent. This yields the product as a clear oil (21g, 85% yield). ^{1}H NMR (300MHz, $CDCl_3$) 0.77-0.96 (m, 6H), 1.17-1.38 (m, 8H), 1.45-1.60 (m, 1H), 2.47 (d, J= 7Hz, 2H), 3.86 (s, 3H), 3.87 (s, 3H), 6.66-6.71 (m, 2H), 6.75-6.81 (m, 1H); ^{13}C NMR (75 MHz, $CDCl_3$) 11.02, 14.37, 23.31, 25.66, 29.07, 29.72, 32.52, 39.98, 41.36, 56.05, 56.12, 111.23, 112.70, 121.27, 134.68, 147.18, 148.82; HRMS [M^+] calcd for $C_{16}H_{26}O_2$ 250.1933 amu Found 250.1935 amu; Elemental analysis Calcd. For $C_{16}H_{26}O_2$ %C 76.75 %H 10.47 Found %C 77.05, %H 10.76.

4-(2-ethylhexyl)benzene-1,2-diol: In a 2L three-neck flask equipped with an argon inlet was added 1-(2-ethylhexyl)-4,5-dimethoxybenzene (16g, 64 mmol, 1eq.) in dry dichloromethane (500 mL, distilled from CaH_2). Boron tribromide (24 mL, 256

mmol, 4eq.) was added dropwise using a pressure-equalizing addition funnel. After 12 hours, the mixture was poured in a 2L Erlenmeyer filled with 1L of ice. The aqueous phase was further extracted with dichloromethane (2×200 mL) and the combined organic layers were washed with water (3×300 mL). The organic phase is dried with magnesium sulfate and the solvent was evaporated under vacuum to yield the product as a slightly yellow oil (12.2g, 86% yield). ^{1}H NMR (300MHz, $CDCl_3$) 0.88-0.94 (m, 6H), 1.14-1.35 (m, 8H), 1.47-1.55 (m, 1H), 2.35-2.42 (d, 2H), 5.18 (br s, 2H), 6.55-6.62 (d, 1H), 6.62-6.72 (s, 1H); 6.72-6.8 (d,1H); ^{13}C NMR (75 MHz, $CDCl_3$) 11.00, 14.37, 23.28, 25.56, 29.09, 32.52, 39.64, 41.34, 115.29, 116.42, 121.84, 135.37, 141.36, 143.41.

PheDOT-EtHx: In a 100 mL round bottom flask, 4-(2-ethylhexyl)-benzene-1,2-diol (5g, 22.5 mmol,1eq) was dissolved in 60 mL of dry toluene (distilled from Na/benzophenone). To this solution was added 3,4-dimethoxythiophene (3.2g, 22.5 mmol, 1eq.) and p-toluenesulfonic acid (427 mg, 2.25mmol, 0.1eq). The flask was equipped with a soxhlet apparatus containing a thimble filled with $CaCl_2$. The mixture was refluxed for three days. Triethylamine (1 mL) and water (200 mL) were added and the product was extracted with diethylether (3×100 mL). After drying with sodium sulfate and removal of the solvent under reduced pressure, the resulting brown solid was purified by column chromatography on silica gel using pentane as eluent. The product was obtained as a clear oil (0.76g, 11% yield). ^{1}H NMR (300MHz, $CDCl_3$) 0.82-0.93 (m, 6H), 1.14-1.37 (m, 8H), 1.42-1.55 (m, 1H), 2.38-2.45 (m, 2H), 6.42 (s, 2H), 6.67-6.74 (m, 2H), 6.78-6.84 (d, 1H); ^{13}C NMR (75 MHz, $CDCl_3$) 11.01, 14.36, 23.24, 25.60, 29.07, 32.51, 39.51, 41.25, 100.88, 100.97, 116.41, 117.37, 124.43, 137.94.

PheDOT-EtHx-Br_2: PheDOT-EtHx (0.5g, 1.99 mmol) was dissolved in 100 mL of DMF. After the solution was bubbled with argon for one hour, N-bromosuccinimide (0.78g, 4.4 mmol, 2.2 eq.) was added in one portion. The solution was stirred overnight after which 200 mL of water was added. The product was extracted with ether, washed with water and the organic layer dried with magnesium sulfate. The solvent was evaporated under vacuum and the resulting yellowish white solid was purified by column chromatography on silica using pentane as eluent. The product was obtained as a clear oil (0.78g, 85% yield). ^{1}H-NMR (300MHz, $CDCl_3$) δ 0.82-0.93 (m, 6H), 1.15-1.36 (m, 8H), 1.43-1.6 (m, 2H), 2.45 (d, J=7.1Hz, 2H), 6.76 (dd, J_1= 8.3Hz, J_2= 1.9Hz, 1H), 6.83 (d, J_2= 2.1Hz, 1H), 6.92 (d, J_1= 8.3Hz, 1H); ^{13}C-NMR (75MHz, CDCl3) 10.98, 14.34, 23.21, 25.57, 29.06, 32.49, 39.54, 41.25, 86.88, 86.99, 116.62, 117.52, 126.16, 137.94, 138.84, 139.56 ;HRMS [M^+] calcd for $C_{34}H_{52}O_2SBr_2$ 514.0177 amu Found 514.0223 amu; Elemental analysis Calcd. For $C_{18}H_{20}O_2SBr_2$ %C 46.98 %H 4.38, %S 6.97 Found %C 47.07, %H 4.11; %S 7.33.

PPheDOTEtHx: To a solution of PheDOT-EtHx-Br_2 (719 mg, 1.56 mmol) in 30 mL of freshly distilled THF (from Na/benzophenone), was added CH_3MgBr via syringe (solution freshly titrated, C=0.92M) (1.7 mL, 1.56 mmol). The solution was refluxed for 2 hours. Then Ni(dppp)Cl_2 (5mgs, 0.031 mmol) was added in one portion. The solution was refluxed for 24hrs. The polymer was then precipitated in 100 mL MeOH and filtered through a soxhlet thimble. The polymer was purified via soxhlet extraction with MeOH, hexanes and then extracted with toluene. The product was obtained as a shiny brown solid solid (350mgs,70% yield).

1-(2-(2-ethylhexyl)-4,5-dimethoxyphenyl)dodecan-1-one: In a 1L 3-neck flask equipped with an argon inlet and a pressure-equalizing addition funnel was dissolved aluminum chloride (14.45g, 110 mmol, 1.3 eq.) in dry dichloromethane (600 mL, distilled from CaH_2). To the reaction cooled at 0°C, a solution of 4-(2-ethylhexyl)-1,2-dimethoxybenzene (21g, 84 mmol, 1 eq.) in dry dichloromethane (200 mL) was added dropwise followed by the addition of a solution of lauroyl chloride in 200 mL (26.4g, 101 mmol, 1.2 eq.). The mixture is refluxed for 24 hours, then cooled at 0°C. The excess aluminum chloride was quenched by slow addition of 6M HCl (150 mL). The aqueous phase is further extracted with dichloromethane (2×200 mL). The combined organic layers are washed with water (3×200 mL), and dried with magnesium sulfate. The solvent is removed under vacuum to yield a yellow-white solid, purified by column chromatography on silica gel (50/50 hexanes/dichloromethane as eluent). The product is obtained as a clear oil (16g, 45% yield); ^{1}H NMR (300MHz, $CDCl_3$) 0.78-0.96 (m, 9H), 1.1-1.42 (m, 24H), 1.42-1.47 (m, 1H), 1.62-1.78 (m, 2H), 2.75-2.9 (m, 4H), 3.92 (s, 6H), 6.68 (s, 1H), 7.09(s, 1H); ^{13}C NMR (75 MHz, $CDCl_3$) 10.95, 14.34, 22.90, 23.34, 24.95, 25.69, 28.85, 29.56, 29.62, 29.72, 29.74, 29.85, 32.13, 32.53, 37.97, 41.19, 42.23, 56.09, 56.33, 112.15, 114.65, 131.43, 136.23, 146.43, 150.79, 204.03.

1-dodecyl-2-(2-ethylhexyl)-4,5-dimethoxybenzene: In a 2L 2-neck flask equipped with an argon inlet was dissolved LAH (4.11g, 108.3 mmol, 6eq) in dry diethyl ether (250 mL, distilled from Na/benzophenone). A solution of $AlCl_3$ (4.77g, 36.1 mmol, 2eq.) in dry diethylether (250 mL) was added via cannula to the LAH solution, cooled at 0°C. After 15 min, a solution of 1-(2-(2-ethylhexyl)-4,5-dimethoxyphenyl)dodecan-1-one (15.6g, 36.1 mmol, 1eq.) in diethylether (200 mL) was added dropwise to the reaction

(maintained at 0°C). Upon completion of the addition, the mixture was allowed to warm up to room temperature. After four hours, the reaction was cooled to 0°C and quenched slowly by addition of 100 mL of 6M HCl. The reaction mixture was poured in 500 mL water. The aqueous phase was further extracted with diethylether (2×200 mL) and the combined organic layers were washed with water (3×300 mL). After drying with magnesium sulfate, the organic solvent was removed under vacuum, to yield a white solid purified by column chromatography on silica gel using 50/50 dichloromethane/hexanes as eluent. This yields the product as a clear oil (14g, 93% yield). ^{1}H NMR (300MHz, $CDCl_3$) 0.8-0.95 (m, 12H), 1.18-1.42 (m, 26H), 1.42-1.6 (m, 3H), 2.43-2.57 (m, 4H), 3.83 (s, 3H), 3.84 (s, 3H), 6.6 (s, 1H), 6.65 (s, 1H).

4-dodecyl-5-(2-ethylhexyl)-benzene-1,2-diol: In a 2L three-neck flask equipped with an argon inlet was added 1-dodecyl-2-(2-ethylhexyl)-4,5-dimethoxybenzene (14g, 33.4mmol, 1eq.) in dry dichloromethane (500 mL, distilled from CaH_2). Boron tribromide (12.64 mL, 134mmol, 4eq.) was added dropwise using a pressure-equalizing addition funnel. After 12 hours, the mixture was poured in a 2L Erlenmeyer filled with 1L of ice. The aqueous phase was further extracted with dichloromethane (2×200 mL) and the combined organic layers were washed with water (3×300 mL). The organic phase is dried with magnesium sulfate and the solvent was evaporated under vacuum to yield the product as a viscous, brown oil (11.7g, 90% yield). ^{1}H NMR (300MHz, $CDCl_3$) 0.8-0.92 (m, 6H), 1.14-1.39 (m, 26H), 1.40-1.58 (m, 3H), 2.36-2.51 (m, 4H), 4.83-4.93 (bs, 2H), 6.61 (s, 1H), 6.65 (s,1H); ^{13}C NMR (75 MHz, $CDCl_3$) 11.12, 14.34, 14.37, 22.91, 23.33, 25.77, 29.17, 29.58, 29.80, 29.85, 29.87, 29.91, 31.71, 32.15, 32.27, 32.76, 36.71,

40.88, 116.33, 117.41, 132.54134.28, 140.99, 141.31; HRMS [M^+] calcd for $C_{26}H_{46}O_2$ 446.4124 amu Found 446.4118 amu.

PheDOTC$_{12}$EtHx: In a 100 mL round bottom flask, 4,5-didodecylbenzene-1,2-diol (5g, 12.8 mmol,1eq) was dissolved in 60 mL of dry toluene (distilled from Na/benzophenone). To this solution was added 3,4-dimethoxythiophene (1.82g, 12.8 mmol, 1eq.) and p-toluenesulfonic acid (250 mg, 1.3mmol, 0.1eq). The flask was equipped with a soxhlet apparatus containing a thimble filled with $CaCl_2$. The mixture was refluxed for three days. Triethylamine (1 mL) and water (200 mL) were added and the product was extracted with diethylether (3×100 mL). After drying with sodium sulfate and removal of the solvent under reduced pressure, the resulting brown solid was purified by column chromatography on silica gel using pentane as eluent. The product was obtained as a clear oil (1.4g, 23% yield). ^{1}H NMR (300MHz, $CDCl_3$) 0.77-0.97 (m, 9H), 1.15-1.41 (m, 26H), 1.41-1.59 (m, 3H), 2.27-2.58 (m, 4H), 6.39 (s, 2H), 6.66 (s, 1H), 6.70 (s,1H); ^{13}C NMR (75 MHz, $CDCl_3$) 11.11, 14.36, 22.92, 23.29, 25.79, 29.15, 29.58, 29.75, 29.82, 29.88, 29.91, 31.34, 32.15, 32.19, 32.74, 36.66, 40.71, 100.75, 117.00, 118.02, 135.28, 136.91, 138.28, 138.59, 139.67; HRMS [M^+] calcd. for $C_{30}H_{42}O_2S$ 470.3219 amu Found 470.3214 amu; Elemental analysis Calcd. For $C_{30}H_{42}O_2S$ %C 76.54, %H 9.85, %S 6.80 Found %C 76.57, %H 10.05, %S 6.65.

PheDOT-(C_{12})$_2$-Br$_2$: PheDOT-(C_{12})$_2$ (1.15g, 2.44 mmol) was dissolved in 100 mL of DMF. After the solution was bubbled with argon for one hour, N-bromosuccinimide (1.09g, 6.2 mmol, 2.5 eq.) was added in one portion. The solution was stirred overnight after which 200 mL of water was added. The product was extracted with ether, washed with water and the organic layer dried with magnesium sulfate. The solvent

was evaporated under vacuum and the resulting yellowish white solid was purified by column chromatography on silica using pentane as eluent. The product was obtained as a clear oil (1.4g, 91% yield). ^{1}H-NMR (300MHz, $CDCl_3$) δ 0.82-0.93 (m, 9H), 1.16-1.41 (m, 26H), 1.42-1.61(m, 3H), 2.38-2.54 (m, 4H), 6.77 (s, 1H), 6.82 (s, 1H); ^{13}C-NMR (75MHz, CDCl3) 11.12, 14.35, 22.92, 23.28, 25.79, 29.18, 29.58, 29.75, 29.80, 29.88, 31.23, 32.15, 32.21, 32.76, 36.71, 40.73, 86.73, 117.14, 118.13, 136.18, 137.29, 137.59, 137.77, 137.95; HRMS [M^+] calcd for $C_{30}H_{40}O_2SBr_2$ 626.1429 amu Found 626.1476 amu; Elemental analysis Calcd. For $C_{30}H_{40}O_2SBr_2$ %C 57.33, %H 7.06, %S 5.10 Found %C 57.41, %H 6.86, %S 5.09.

PPheDOTC$_{12}$EtHx: To a solution of PheDOT-C_{12}EtHx-Br_2 (1.37g, 2.18 mmol) in 75 mL of freshly distilled THF (from Na/benzophenone), was added CH_3MgBr via syringe (solution freshly titrated, C=0.99M) (2.21 mL, 2.18 mmol). The solution was refluxed for 2 hours. Then Ni(dppp)Cl_2 (23.6mg, 0.435 mmol) was added in one portion. The solution was refluxed for 24hrs. The polymer was then precipitated in 100 mL MeOH and filtered through a soxhlet thimble. The polymer was purified via soxhlet extraction with MeOH, hexanes and then extracted with toluene. The product was obtained as a dark purple solid (220mg, 69% yield). The product after toluene soxhlet extraction was a shiny brown solid. ^{1}H NMR (300MHz, CDCl3) δ 0.34-0.98 (bs, 12H), 0.98-1.50 (bs, 26H), 1.50-1.87 (bs, 3H), 1.88-2.96 (bs, 4H), 6.45-7.11 (bs, 2H); ^{13}C NMR (75MHz, CDCl3) δ 11.31, 14.31, 22.92, 23.40, 25.93, 29.64, 29.98, 32.18, 40.84, 107.43, 110.56, 117.34, 134.75, 136.73, 138.30; GPC (THF, RT) M_n= 58,900 g mol^{-1}, M_w= 87,700 g mol^{-1}, PDI= 1.5.

LIST OF REFERENCES

1. Heeger, A. J. *Ang. Chem.- Int. Ed.* **2001**, *40*, 2591-2611.

2. Salzner, U., Lagowski, J. B., Pickup, P. G., Poirier, R. A. *Synth. Met.* **1998**, *96*, 177-189.

3. Bredas, J. L. *J. Chem. Phys.* **1985**, *82*, 3808-3811.

4. Heeger, A. J., Kivelson, S., Schrieffer, J. R., Su, W. P. *Reviews of Modern Physics* **1988**, *60*, 781-850.

5. Bredas, J. L., Street, G. B. *Acc. Chem. Res.* **1985**, *18*, 309-315.

6. Bredas, J. L., Themans, B., Fripiat, J. G., Andre, J. M., Chance, R. R. *Phys. Rev. B.* **1984**, *29*, 6761-6773.

7. Welsh, D. M., Kumar, A., Meijer, E. W., Reynolds, J. R. *Adv. Mater.* **1999**, *11*, 1379-1382.

8. Ouyang, J., Chu, C.-W., Chen, F.-C., Xu, Q., Yang, Y. *Adv. Funct. Mater.* **2005**, *15*, 203-208.

9. Carpi, F., De Rossi, D. *Optics and Laser Technology* **2006**, *38*, 292-305.

10. Schwendeman, I., Hickman, R., Soenmez, G., Schottland, P., Zong, K., Welsh, D. M., Reynolds, J. R. *Chem. Mater.* **2002**, *14*, 3118-3122.

11. Pei, Q. B., Yu, G., Zhang, C., Yang, Y., Heeger, A. J. *Science* **1995**, *269*, 1086-1088

12. Karl, N. *Synth. Met.* **2003**, *133*, 649-657.

13. (a) Sirringhaus, H., Brown, P. J., Friend, R. H., Nielsen, M. M., Bechgaard, K., Langeveld-Voss, B. M. W., Spiering, A. J. H., Janssen, R. A. J., Meijer, E. W. *Synth. Met.* **2000**, *111*, 129-132.; (b) Sirringhaus, H., Brown, P. J., Friend, R. H., Nielsen, M. M., Bechgaard, K., Langeveld-Voss, B. M. W., Spiering, A. J. H., Janssen, R. A. J., Meijer, E. W., Herwig, P., de Leeuw, D. M. *Nature* **1999**, *401*, 685-688; (c) Wang, G. M., Swensen, J., Moses, D., Heeger, A. J. *J. Appl. Phys.* **2003**, *93*, 6137-6141.

14. Mcculloch, I., Heeney, M., Bailey, C., Genevicius, K., Macdonald, I., Shkunov, M., Sparrowe, D., Tierney, S., Wagner, R., Zhang, W. M., Chabinyc, M. L., Kline, R. J., Mcgehee, M. D., Toney, M. F. *Nat. Mater.* **2006**, *5*, 328-333..

15. (a) Chang, J. F., Sun, B. Q., Breiby, D. W., Nielsen, M. M., Solling, T. I., Giles, M., McCulloch, I., Sirringhaus, H. *Chem. Mater.* **2004**, *16*, 4772-4776.

16. Zen, A., Pflaum, J., Hirschmann, S., Zhuang, W., Jaiser, F., Asawapirom, U., Rabe, J. P., Scherf, U., Neher, D. *Adv. Funct. Mater.* **2004**, *14*, 757-764.

17. (a) Kline, R. J., McGehee, M. D., Kadnikova, E. N., Liu, J. S., Frechet, J. M. J., Toney, M. F. *Macromolecules* **2005**, *38*, 3312-3319; (b) Kline, R. J., McGehee, M. D., Kadnikova, E. N., Liu, J. S., Frechet, J. M. J. *Adv. Mater.* **2003**, *15*, 1519; (c) Yang, H. C., Shin, T. J., Yang, L., Cho, K., Ryu, C. Y., Bao, Z. N. *Adv. Funct. Mater.* **2005**, *15*, 671-676; (d) Verilhac, J.-M., Pokrop, R., LeBlevennec, G., Kulszewicz-Bajer, I., Buga, K., Zagorska, M., Sadki, S., Pron, A. *J. Phys. Chem. B* **2006**, *110*, 13305-13309; (e) Zen, A., Saphiannikova, M., Neher, D., Grenzer, J., Grigorian, S., Pietsch, U., Asawapirom, U., Janietz, S., Scherf, U., Lieberwirth, I., Wegner, G. *Macromolecules* **2006**, *39*, 2162-2171.

18. Scharber, M. C., Wuhlbacher, D., Koppe, M., Denk, P., Waldauf, C., Heeger, A. J., Brabec, C. L. *Adv. Mater.* **2006**, *18*, 789-794.

19. Li, G., Shrotriya, V., Huang, J. S., Yao, Y., Moriarty, T., Emery, K., Yang, Y. *Nat. Mater.* **2005**, *4*, 864-868.

20. Thompson, B. C., Kim, Y.-G, Reynolds, J. R. *Macromolecules* **2005**, *38*, 5359-5362.

21. (a) Yu, G., Gao, J., Hummelen, J. C., Wudl, F., Heeger, A. J. *Science* **1995**, *270*, 1789-1791.; (b) Halls, J. J. M., Walsh, C. A., Greenham, N. C., Marseglia, E. A., Friend, R. H., Moratti, S. C., Holmes, A. B. *Nature* **1995**, *376*, 498-500.

22. Bredas, J. L., Beljonne, D., Coropceanu, V., Cornil, J. *Chem. Rev.* **2004**, *104*, 4971-5003.

23. Rowley, N. M., Mortimer, R. J., *Science Progress* **2002**, *85*, 243-262.

24. Gaupp, C. L., Welsh, D. M., Rauh, R. D., Reynolds, J. R. *Chem. Mater.* **2002**, *14*, 3964-3970.

25. Argun, A. A., Aubert, P. H., Thompson, B. C., Schwendeman, I., Gaupp, C. L., Hwang, J., Pinto, N. J., Tanner, D. B., MacDiarmid, A. G., Reynolds, J. R. *Chem. Mater.* **2004**, *16*, 4401-4412..

26. Roncali, J. *Chemical Reviews* **1997**, *97*, 173-205.

27. (a) Thomas, C.A. *Donor-Acceptor Methods For Band Gap Reduction in Conjugated Polymers: The Role of Electron Rich Donor Heterocyles*, University of Florida, Ph. D. Dissertation, **2001**; (b) Dubois, C. J., *Donor-Acceptor Methods for Band Gap Control in Conjugated Polymers*, University of Florida, Ph. D. Dissertation, **2003**.; (c) Thompson, B. C. *Variable Band-Gap Poly(3,4-Alkylenedioxythiophene)-Based Polymers for Photovoltaic and Electrochromic Applications*, University of Florida, Ph. D. Dissertation, **2005**.

28. Lemaire, M., Garreau, R., Roncali, J., Delabouglise, D., Youssoufi, H. K., Garnier, F. *New J. Chem.* **1989**, *13*, 863-871.

29. Bredas, J. L., Street, G. B., Themans, B., Andre, J. M. *J. Chem. Phys.* **1985**, *83*, 1323-1329.

30. Kobayashi, N., Sasaki, S., Abe, M., Watanabe, S., Fukumoto, H., Yamamoto, T. *Macromolecules* **2004**, *37*, 7986-7991.

31. (a) Morin, J. F., Leclerc, M., Ades, D., Siove, A. *Macromol. Rapid Commun.* **2005**, *26*, 761-778; (b) Scherf, U., List, E. J. W. *Adv. Mater.* **2002**, *14*, 477-487.

32. (a) Mccullough, R. D., Lowe, R. D., *J. Chem. Soc., Chem. Commun.* **1992**, 70-72; (b) Mccullough, R. D., Lowe, R. D., Jayaraman, M., Anderson D. L., *J. Org. Chem.* **1993**, *58*, 904-912; (c) Chen, T. A., Wu, X. M., Rieke, R. D. *J. Am. Chem. Soc.* **1995**, *117*, 233-244.

33. Mccullough, R. D., Tristramnagle, S., Williams, S. P., Lowe, R. D., Jayaraman, M. *J. Am. Chem. Soc.* **1993**, *115*, 4910-4911.

34. Rughooputh, S. D. D. V., Hotta, S., Heeger, A. J., Wudl, F. *J. Polym. Sci., Part B: Polym. Phys.* **1987**, *25*, 1071-1078.

35. Rodriguez-Parada, J. M. Duran, R. S., Wegner, G. *Macromolecules* **1989**, *22*, 2507-2516.

36. (a) Prosa, T. J., Winokur, M. J., Moulton, J, Smith, P., Heeger, A. J. *Macromolecules* **1992**, *25*, 4364-4372; (b) Prosa, T. J., Winokur, M. J., Moulton, J., Smith, P., Heeger, A. J. *Synth. Met.* **1993**, *55*, 370-377; (c) Prosa, T. J., Winokur, M. J., McCullough, R. D. *Macromolecules* **1996**, *29*, 3654-3656.

37. Bao, Z. N., Lovinger, A. J. *Chem. Mater.* **1999**, *11*, 2607-2612.

38. (a) Kraabel, B., Moses, D., Heeger, A. J. *J. Chem. Phys.* **1995**, *103*, 5102-5108; (b) Beljonne, D., Shuai, Z., Pourtois, G., Bredas, J. L. *J. Phys. Chem. A* **2001**, *105*, 3899-3907.

39. Andersson, M. R., Thomas, O., Mammo, W., Svensson, M., Theander, M., Inganas, O. *J. Mater. Chem.* **1999**, *9*, 1933-1940.

40. Siddiqui, S., Spano, F. C. *Chem. Phys. Lett.* **1999**, *308*, 99-105; Cornil, J., Beljonne, D., Calbert, J. P., Bredas, J. L. *Adv. Mater.* **2001**, *13*, 1053-1067.

41. Kasha, M., Rawls, H. R., El-Bayoumi, M. A. *Pure Appl. Chem.* **1965**, *11*, 371-92.

42. (a) Cornil, J., dos Santos, D. A., Crispin, X., Silbey, R., Bredas, J. L. *J. Am. Chem. Soc.* **1998**, *120*, 1289-1299; (b) Bredas, J. L., Cornil, J., Beljonne, D., dos Santos, D., Shuai, Z. G. *Acc. Chem. Res.* **1999**, *32*, 267-276; (c) Cornil, J., dos Santos, D. A., Silbey, R., Bredas, J. L. *Synthetic Metals* **1999**, *101*, 492-495.

43. Wurthner, F., Thalacker, C., Diele, S., Tschierske, C. *Chem.-Eur. J.* **2001**, *7*, 2245-2253.

44. Zahn, S., Swager, T. M. *Ang. Chem.- Int. Ed.* **2002**, *41*, 4225-4230.

45. Pinto, M. R., Schanze, K. S. *Synthesis-Stuttgart* **2002**, 1293-1309.

46. McCullough, R. D. *Adv. Mater.* **1998**, *10*, 93-116.

47. (a) Hou, J. H., Huo, L. J., He, C., Yang, C. H., Li, Y. F. *Macromolecules* **2006**, *39*, 594-603; (b) Hiorns, R. C., Khoukh, A., Gourdet, B., Dagron-Lartigau, C. *Polym. Int.* **2006**, *55*, 608-620; (c) Iovu, M. C., Jeffries-El, M., Sheina, E. E., Cooper, J. R., McCullough, R. D. *Polymer* **2005**, *46*, 8582-8586; (d) Jeffries-El, M., Sauve, G., McCullough, R. D. *Macromolecules* **2005**, *38*, 10346-10352; (e) Jeffries-El, M., Sauve, G., McCullough, R. D. *Adv. Mater.* **2004**, *16*, 1017; (f) Mao, Y. X., Wang, Y., Lucht, B. L. *J. Polym. Sci., Part A: Polym. Chem.* **2004**, *42*, 5538-5547; (g) Zhai, L., Pilston, R. L., Zaiger, K. L., Stokes, K. K., McCullough, R. D. *Macromolecules* **2003**, *36*, 61-64; (h) Endo, T., Takeoka, Y., Rikukawa, M., Sanui, K. *Synth. Met.* **2003**, *135*, 333-334; (i) Liu, J. S., McCullough, R. D. *Macromolecules* **2002**, *35*, 9882-9889; (j) Loewe, R. S., Ewbank, P. C., Liu, J. S., Zhai, L., McCullough, R. D. *Macromolecules* **2001**, *34*, 4324-4333; (k) Loewe, R. S., Khersonsky, S. M., McCullough, R. D. *Adv. Mater.* **1999**, *11*, 250; (l) Liu, J. S., Loewe, R. S., McCullough, R. D. *Macromolecules* **1999**, *32*, 5777-5785.

48. Sheina, E. E., Liu, J. S., Iovu, M. C., Laird, D. W., McCullough, R. D. *Macromolecules* **2004**, *37*, 3526-3528.

49. Liu, J. S., Sheina, E., Kowalewski, T., McCullough, R. D. *Ang. Chem.- Int. Ed.* **2002**, *41*, 329-332.

50. Pisula, W., Tomovic, Z., Simpson, C., Kastler, M., Pakula, T., Mullen, K. *Chem. Mater.* **2005**, *17*, 4296-4303.

51. Carbonnier, B., Egbe, D. A. M., Birckner, E., Grummt, U. W., Pakula, T. *Macromolecules* **2005**, *38*, 7546-7554.

52. http://omlc.ogi.edu/spectra/PhotochemCAD/html/alpha.html. Last accessed on 11/08/2006.

53. Palsson, L. O., Monkman, A. P. *Adv. Mater.* **2002**, *14*, 757-758.

54. (a) Thompson, B. C., Schottland, P., Zong, K. W., Reynolds, J. R. *Chem. Mater.* **2000**, *12*, 1563-1571.; (b) Billmeyer, F. *Appl. Opt.* **1969**, 8, 737.

55. Uhlir, A. *Bell System Technical Journal* **1955**, *34*, 105-128.

56. (a) Kirchmeyer, S., Reuter, K. *J. Mater. Chem.* **2005**, *15*, 2077-2088; (b) Groenendaal, B. L., Jonas, F., Freitag, D., Pielartzik, H., Reynolds, J. R. *Adv. Mater.* **2000**, *12*, 481-494.

57. (a) Turbiez, M., Frere, P., Allain, M., Videlot, C., Ackermann, J., Roncali, J. *Chem.-Eur. J.* **2005**, *11*, 3742-3752.; (b) Apperloo, J. J., Groenendaal, L., Verheyen, H., Jayakannan, M., Janssen, R. A. J., Dkhissi, A., Beljonne, D., Lazzaroni, R., Bredas, J. L. *Chem.-Eur. J.* **2002**, *8*, 2384-2396.

58. Spencer, H. J., Skabara, P. J., Giles, M., McCulloch, L., Coles, S. J., Hursthouse, M. B. *J. Mater. Chem.* **2005**, *15*, 4783-4792.

59. Daoust, G., Leclerc, M. *Macromolecules* **1991**, *24*, 455-459.

60. Kumar, A., Reynolds, J. R. *Macromolecules* **1996**, *29*, 7629-7630.

61. Aubert, P. H., Groenendaal, L., Louwet, F., Lutsen, L., Vanderzande, D., Zotti, G. *Synth. Met.* **2002**, *126*, 193-198..

62. Groenendaal, L., Zotti, G., Jonas, F. *Synth. Met.* **2001**, *118*, 105-109.

63. (a) Welsh, D. M., Kloeppner, L. J., Madrigal, L., Pinto, M. R., Thompson, B. C., Schanze, K. S., Abboud, K. A., Powell, D., Reynolds, J. R. *Macromolecules* **2002**, *35*, 6517-6525; (b) Reeves, B. D., Thompson, B. C., Abboud, K. A., Smart, B. E., Reynolds, J. R. *Adv. Mater.* **2002**, *14*, 717; (c) Kumar, A., Welsh, D. M., Morvant, M. C., Piroux, F., Abboud, K. A., Reynolds, J. R. *Chem. Mater.* **1998**, *10*, 896-902.

64. Gaupp, C. L., Welsh, D. M., Reynolds, J. R. *Macromol. Rapid Commun.* **2002**, *23*, 885-889.

65. Joshi V. M., Bhide B. V., **S**ir Parashurambhau Coll. P. *J. Indian Chem. Soc.* **1960**, *37*, 461-464

66. B. E. Love, E. G. Jones *J. Org. Chem.* **1999**, *64*, 3755-3756.

67. I. Schwendeman *Optical and Transport Properties of Conjugated Polymers and their Application to Electrochromic Devices*, University of Florida, Ph. D. Dissertation, **2002**.

68. Hofkens, J., Vosch, T., Maus, M., Kohn, F., Cotlet, M., Weil, T., Herrmann, A., Mullen, K., De Schryver, F. C. *Chem. Phys. Lett.* **2001**, *333*, 255-263.

69. J. L. Bredas, J. Cornil, F. Meyers, D. Beljonne *Handbook of Conducting Polymers (2nd Edition)* **2000**, p. 1-22.

70. Kasha, M. *Discussions of the Faraday Society* **1950**, 14-19.

71. Perepichka, I. F., Perepichka, D. F., Meng, H., Wudl, F. *Adv. Mater.* **2005**, *17*, 2281-2305.

72. Hill, M. G., Mann, K. R., Miller, L. L., Penneau, J. F. *J. Am. Chem. Soc.* **1992**, *114*, 2728-2730.

73. Reeves, B. D. *Processable Disubstituted Poly(propylenedioxythiophenes)*, University of Florida, Ph. D. Dissertation, **2005**.

74. Hoeben, F. J. M., Jonkheijm, P., Meijer, E. W., Schenning, A. P. H. J. *Chem. Rev.* **2005**, *105*, 1491-1546.

75. Fasman, G. D. *Circular dichroism and the conformational analysis of biomolecules;* Plenum Press: New York, **1996**.

76. http://www.enzim.hu/~szia/cddemo/edemo1.htm Last accessed on 11/13/06

77. Lighthner, D. A., Gurst J. E.. *Organic Conformational Analysis and Stereochemistry from Circular Dichroism Spectroscopy*; Wiley-VCH; New York, **2000**.

78. Oda, M., Nothofer, H. G., Lieser, G., Scherf, U., Meskers, S. C. J., Neher, D. *Adv. Mater.* **2000**, *12*, 362.

79. (a) Verbiest, T., Sioncke, S., Koeckelberghs, G., Samyn, C., Persoons, A., Botek, E., Andre, J. M., Champagne, B. *Chem. Phys. Lett.* **2005**, *404*, 112-115.; (b) Samyn, C., Verbiest, T., Persoons, A. Macromol. *Rapid Commun.* **2000**, *21*, 1-15; (c) Ochiai, K., Rikukawa, M., Sanui, K., Ogata, N., Ueno, Y., Ema, K. *Synth. Met.* **1999**, *101*, 84-85.

80. (a) Huang, J. X., Egan, V. M., Guo, H. L., Yoon, J. Y., Briseno, A. L., Rauda, I. E., Garrell, R. L., Knobler, C. M., Zhou, F. M., Kaner, R. B. *Adv. Mater.* **2003**, *15*, 1158-1161; (b) Tigelaar, D. M., Lee, W., Bates, K. A., Saprigin, A., Prigodin, V. N., Cao, X. L., Nafie, L. A., Platz, M. S., Epstein, A. *J. Chem. Mater.* **2002**, *14*, 1430-1438.

81. Schwartz, B. J. *Annu. Rev. Phys. Chem.* **2003**, *54*, 141-172.

82. Zahn, S., Swager, T. M. *Ang. Chem.- Int. Ed.* **2002**, *41*, 4225-4230.

83. (a) Satrijo, A., Meskers, S. C. J., Swager, T. M. *J. Am. Chem. Soc.* **2006**, *128*, 9030-9031; (b) Satrijo, A., Swager, T. M. *Macromolecules* **2005**, *38*, 4054-4057.

84. (a) Rughooputh, S. D. D. V., Hotta, S., Heeger, A. J., Wudl, F. *J. Polym. Sci., Part B: Polym. Phys.* **1987**, *25*, 1071-1078; (b) Faid, K., Frechette, M., Ranger, M., Mazerolle, L., Levesque, I., Leclerc, M., Chen, T. A., Rieke, R. D. *Chem. Mater.* **1995**, *7*, 1390-1396.

85. Yue, S., Berry, G. C., McCullough, R. D. *Macromolecules* **1996**, *29*, 933-939.

86. Apperloo, J. J., Janssen, R. A. J., Malenfant, P. R. L., Frechet, J. M. J. *Macromolecules* **2000**, *33*, 7038-7043.

87. (a) Bouman, M. M., Havinga, E. E., Janssen, R. A. J., Meijer, E. W. Mol. Cryst. Liq. Cryst. Sci. Technol., Sect. A **1994**, *256*, 439-448; (b) Langeveld-Voss, B. M. W., Janssen, R. A. J., Meijer, E. W. *J. Mol. Struct.* **2000**, *521*, 285-301.

88. (a) Hoppe, H., Glatzel, T., Niggemann, M., Schwinger, W., Schaeffler, F., Hinsch, A., Lux-Steiner, M. C., Sariciftci, N. S. *Thin Solid Films* **2006**, *511-512*, 587-592; (b) Friend, R. H., Gymer, R. W., Holmes, A. B., Burroughes, J. H., Marks, R. N., Taliani, C., Bradley, D. D. C., Dos Santos, D. A., Bredas, J. L., Logdlund, M., Salaneck, W. R. *Nature* **1999**, *397*, 121-128; (c) Sirringhaus, H., Tessler, N., Friend, R. H. *Science* **1998**, *280*, 1741-1744; Kraft, A., Grimsdale, A. C., Holmes, A. B. *Ang. Chem.- Int. Ed.* **1998**, *37*, 402-428.

89. Oda, M., Nothofer, H. G., Scherf, U., Sunjic, V., Richter, D., Regenstein, W., Neher, D. *Macromolecules* **2002**, *35*, 6792-6798.

90. (a) Myers, A. G., Yang, B. H., Chen, H., Gleason, J. L. *J. Am. Chem. Soc.* **1994**, *116*, 9361-9362; (b) Myers, A. G., Yang, B. H., Chen, H., McKinstry, L., Kopecky, D. J., Gleason, J. L. *J. Am. Chem. Soc.* **1997**, *119*, 6496-6511; (c) Myers, A. G., Yang, B. H., Chen, H. *Org. Synth.* **2000**, *77*, 29-44; Myers, A. G., Yang, B. H. *Org. Synth.* **2000**, *77*, 22-28.

91. Knox, R. S. *J. Phys. Chem.* **1994**, *98*, 7270-7273.

92. Langeveld-Voss, B. M. W., Christiaans, M. P. T., Janssen, R. A. J., Meijer, E. W. *Macromolecules* **1998**, *31*, 6702-6704.

93. Schenning, A. P. H. J., Kilbinger, A. F. M., Biscarini, F., Cavallini, M., Cooper, H. J., Derrick, P. J., Feast, W. J., Lazzaroni, R., Leclere, P., McDonell, L. A., Meijer, E. W., Meskers, S. C. J. *J. Am. Chem. Soc.* **2002**, *124*, 1269-1275.

94. Koeckelberghs, G., De Cremer, L., Vanormelingen, W., Verbiest, T., Persoons, A., Samyn, C. *Macromolecules* **2005**, *38*, 4545-4547.

95. Zhang, Z. B., Fujiki, M., Motonaga, M., McKenna, C. E. *J. Am. Chem. Soc.* **2003**, *125*, 7878-7881.

96. Koeckelberghs, G., Vangheluwe, M., Samyn, C., Persoons, A., Verbiest, T. *Macromolecules* **2005**, *38*, 5554-5559.

97. (a) Tanase, C., Meijer, E. J., Blom, P. W. M., de Leeuw, D. M. *Phys. Rev. Lett.* **2003**, *91*, 216601/1-216601/4; (b) Kaneto, K. *Thin Solid Films* **2001**, *393*, 249-258.

98. (a) Padinger, F., Rittberger, R. S., Sariciftci, N. S. *Adv. Funct. Mater.* **2003**, *13*, 85-88; (b) Yang, X. N., Loos, J., Veenstra, S. C., Verhees, W. J. H., Wienk, M. M., Kroon, J. M., Michels, M. A. J., Janssen, R. A. J. *Nano Lett.* **2005**, *5*, 579-583 (c) Reyes-Reyes, M., Kim, K., Carroll, D. L. *Appl. Phys. Lett.* **2005**, *87*, 083506/1-083506/3; (d) Ma, W. L., Yang, C. Y., Gong, X., Lee, K., Heeger, A. J. *Adv. Funct. Mater.* **2005**, *15*, 1617-1622.

99. (a) Argun, A. A., Cirpan, A., Reynolds, J.R. *Adv. Mat.* **2003**, *15*, 1338-1341; (b) P. Andersson, P., Nilsson, D., Svensson, P. O., Chen, M. X., Malmstrom, A., Remonen, T., Kugler, T., Berggren, M. *Adv. Mater.* **2002**, *14*, 1460.

100. Storsberg, J., Schollmeyer, D., Ritter, H. *Chem. Lett.* **2003,** *32*, 140-141.

101. Roquet, S., Leriche, P., Perepichka, I., Jousselme, B., Levillain, E., Frere, P., Roncali, J. *J. Mater. Chem.* **2004**, *14*, 1396-1400.

102. Perepichka, I. F., Roquet, S., Leriche, P., Raimundo, J. M., Frere, P., Roncali, J. *Chem.-Eur. J.* **2006**, *12*, 2960-2966.

103. Lagrost, C., Carrie, D., Vaultier, M., Hapiot, P. *J. Phys. Chem. A* **2003**, *107*, 745-752.

104. Reeves, B. D., Grenier, C. R. G., Argun, A. A., Cirpan, A., McCarley, T. D., Reynolds, J. R. *Macromolecules* **2004**, *37*, 7559-7569.

105. Leclerc, M., Frechette, M., Bergeron, J. Y., Ranger, M., Levesque, I., Faid, K. *Macromol. Chem. Phys.* **1996**, *197*, 2077-2087.

106. (a) DiCesare, N., Belletete, M., Durocher, G., Leclerc, M. *Chem. Phys. Lett.* **1997**, *275*, 533-539; (b) Roux, C., Bergeron, J.-Y., Leclerc, M. *Makromol. Chem.* **1993**, *194*, 869-877.

107. HOMO level was estimated using E_{HOMO}= Eonset (vs. Fc/Fc+) + 4.8eV

108. Sotzing, G. A., Reynolds, J. R., Steel, P. J. *Adv. Mater.* **1997**, *9*, 795-796.

109. Samori, P., Francke, V., Mangel, T., Mullen, K., Rabe, J. P. *Optical Materials* **1998**, *9*, 390-393.

110. (a) Samori, P., Francke, V., Mullen, K., Rabe, J. P. *Thin Solid Films* **1998**, *336*, 13-15; (b) Kim, D. H., Park, Y. D., Jang, Y., Kim, S., Cho, K. *Macromol. Rapid Commun.* **2005**, *26*, 834-839; (c) Surin, M., Marsitzky, D., Grimsdale, A. C., Mullen, K., Lazzaroni, R., Leclere, P. *Adv. Funct. Mater.* **2004**, *14*, 708-715; (d) Leclere, P., Surin, M., Jonkheijm, P., Henze, O., Schenning, A. P. H. J., Biscarini, F., Grimsdale, A. C., Feast, W. J., Meijer, E. W., Mullen, K., Bredas, J. L., Lazzaroni, R. *Eur. Polym. J.* **2004**, *40*, 885-892.

BIOGRAPHICAL SKETCH

Christophe Grenier was born in Lille, France, on November 10th, 1979. He spent his childhood in Nieppe until 1990 where he went to high school in Armentieres. In 1997, he graduated from high school and went on to attend his undergraduate studies in Lycee Faidherbe in Lille until 1999. He developed there a strong interest in organic chemistry and later joined l'Ecole Nationale Supérieure de Chimie de Montpellier (ENSCM) until 2001. There, he progressively specialized in polymer chemistry until he was convinced by the international studies center staff, along with Professor Bruno Améduri to spend his last undergraduate year in the Chemistry Department of the University of Florida. After receiving his undergraduate degree, he decided to pursue his Ph.D. in organic chemistry at the University of Florida under the supervision of Professor John Reynolds in the area of conjugated polymer synthesis. Upon graduation, he will head Eindhoven, The Netherlands, for a postdoctoral position under the supervision of Professor "Bert" Meijer and Professor Albert Schenning.